UNIVERSITY OF SOUTHAMPTON

FACULTY OF NATURAL AND ENVIRONMENTAL SCIENCES

School of Ocean and Earth Sciences

PROCESSES AND DEPOSITS OF SUBMARINE SEDIMENT DENSITY FLOWS WITHIN THE MOROCCAN TURBIDITE SYSTEM, OFFSHORE NW AFRICA

by

Christopher John Stevenson

Thesis for the degree of Doctor of Philosophy

July 2012

Graduate School of the National Oceanography Centre, Southampton

This Ph.D. thesis is by

Christopher John Stevenson

And has been produced under the supervision of the following persons:

Peter J. Talling

Russell B. Wynn

Douglas Masson

Chair of advisory panel

Jon Bull

UNIVERSITY OF SOUTHAMPTON
FACULTY OF NATURAL AND ENVIRONMENTAL SCIENCES
SCHOOL OF OCEAN AND EARTH SCIENCES

Doctor of Philosophy

PROCESSES AND DEPOSITS OF SUBMARINE SEDIMENT DENSITY FLOWS WITHIN THE MOROCCAN TURBIDITE SYSTEM, OFFSHORE NW AFRICA

By **Christopher John Stevenson**

ABSTRACT

Submarine sediment density flows are a major process for transporting sediment from the continental shelf to the deep-ocean. Understanding submarine flow dynamics relies upon analysis of their deposits (beds) because monitoring them directly is difficult. However, it is rare to be able to correlate individual beds for long distances. This limits our understanding to 'idealized' models based on field data with limited lateral extent. Validation of these models requires individual beds to be mapped out. Using > 100 shallow sediment cores this thesis correlates individual beds across their depositional extent (over 2000 km), within the Late Quaternary Moroccan Turbidite System, offshore NW Africa. The vertical and spatial distributions of facies and grain size are examined in each bed to understand the dynamics of the parent flows. The height to which deposits drape up topography is used to infer flow thicknesses.

Proximally, synchronous flows passed into the system from multiple disparate entry points. Earthquakes could have triggered these flows. However, it is not possible to determine if these beds were related to earthquakes, highlighting the difficulties faced extending turbidite palaeoseismology beyond the historical earthquake record.

Across the central parts of the system flows are interpreted to have been relatively thin and slow moving, yet able to run out for hundreds of kilometers on slopes of < 0.02º. Current, models cannot explain how this is possible.

Distally, channels develop and connect two basins. Examination of these channels reveals they are purely constructional features. Flows were able to bypass > 100 km^3 of sediment through the channel axes without eroding. Channel relief was built and maintained by deposition along the channel margins and no erosion.

The distribution of grain-size breaks is examined within individual beds across the entire system. Grain-size breaks between sand and mud occur almost everywhere. This is attributed to fluid mud layers bypassing intermediate grain sizes down slope. Such a process should (almost) always occur; hence this type of grain-size break should be recognized as a typical feature rather than an exception.

The ability to map out individual beds over such distances provides a rare and valuable opportunity to validate models; developed from laterally restricted outcrops, laboratory experiments and theory. Results from this thesis demonstrate current models are limited and that we still have much to learn about the dynamics of submarine flows and how they transport sediment across vast swathes of the seafloor.

Contents

List of figures

List of Tables

DECLARATION OF AUTHORSHIP

I, Christopher John Stevenson declare that the thesis entitled:

"Processes operating within submarine sediment density flows within the Moroccan Turbidite System, offshore NW Africa"

and the work presented in the thesis are both my own, and have been generated by me as the result of my own original research. I confirm that:

- this work was done wholly or mainly while in candidature for a research degree at this University;
- where any part of this thesis has previously been submitted for a degree or any other qualification at this University or any other institution, this has been clearly stated;
- where I have consulted the published work of others, this is always clearly attributed;
- where I have quoted from the work of others, the source is always given. With the exception of such quotations, this thesis is entirely my own work;
- I have acknowledged all main sources of help;
- where the thesis is based on work done by myself jointly with others, I have made clear exactly what was done by others and what I have contributed myself;
- parts of this work have been published. Chapter 5 is published as:

STEVENSON, C. J., TALLING, P. J., WYNN, R. B., MASSON, D. G., HUNT, J. E., FRENZ, M., AKHMETZHANOV, A. & CRONIN, B. T. (2012) The flows that left no trace: very large-volume turbidity currents that bypassed sediment through submarine channels without eroding the seafloor. *Marine and Petroleum Geology***,** In Press. doi.org/10.1016/j.marpetgeo.2012.02.008

Signed: ……..

Date:……

Acknowledgements

First and foremost I would like to thank my three official supervisors: Dr. Peter Talling, Dr. Russell Wynn and Prof. Douglas Masson. Their guidance and support throughout the duration of my PhD studies has been invaluable. Special thanks goes to Dr. Esther Sumner who listened to and argued through my ideas throughout the course of my studies, so much so that she became my unofficial supervisor. Thanks go to the staff at the British Ocean Sediment Core Research Facility (BOSCORF), who provided access to the cores used in this thesis. Particularly, Dr. Suzanne MacLachlan and Dr. Guy Rothwell are thanked for their continued technical support whilst using the BOSCORF facilities. I would also like to thank the following colleagues at the National Oceanography Centre who have helped me in my work: Tim Le Bas, Veerle Huvenne and Rose Edwards. Over the past 40 years the tireless efforts of the masters, officers and crew aboard numerous scientific cruises, around the NW African Margin, have recovered one of the most impressive core data sets in the world. Their dedication and commitment shown at sea makes this work possible, and they are all gratefully thanked. The officemates James Hunt, Giuseppe Malgesini, and Hector Marin-Moreno have been a source of countless hours discussing all manner of things. I will miss the intense white-board arguments/discussions. I would like to acknowledge the Natural Environment Research Council (NERC) and the UK-TAPS Consortium (Conoco Phillips, Shell, Exxon Mobil, BHP Bilton and Norsk Hydro) as the sources of funding for my PhD.

I would also like to thank Michal Janocko and Simon Barker for their constructive reviews on Chapter 5, which improved the manuscript considerably for publication.

Outside work I would like to say a big thank you to my family who have been a source of constant support an encouragement. Natalie, my girlfriend, has been heroic in her ability to help me through the challenges of PhD life. Without her I would not be where I am today. Finally, I would like to say a thank you to the boys of NOC FLOP for much needed breaks from writing.

1 Introduction

Submarine sediment density flows (including turbidity currents) are a major process for transporting sediment from the continental shelf to the deep-ocean. Volumetrically, individual events can be extremely large (> 100 km^3), 5 – 10 times the annual supply of sediment to the oceans from all of the rivers on earth ~ 10 – 20 km^3 (Mulder and Syvitski, 1995; Syvitski, 2003; Syvitski et al., 2003). Therefore, understanding the processes operating within these flows is fundamental if we are to better understand how sediment is transported around the planet. From an applied perspective, submarine flows pose a significant geohazard for sea floor infrastructure, such as communication cables (Piper et al., 1999; Hsu et al., 2008; Mosher et al., 2010) and oil and gas pipelines (Zakeri, 2008). They are also economically important, as their ancient deposits host large subsurface oil and gas reserves (Stow and Mayall, 2000).

As catastrophic and unpredictable processes, submarine flows are difficult to monitor directly (Hay, 1987; Piper and Savoye, 1993 ; Kripounoff et al., 2003; Xu et al., 2004; Vangriesheim et al., 2009). Therefore, most of our understanding is derived from careful analysis of their deposits, coupled with scaled physical experiments and numerical modelling (Kneller and Buckee, 2000). It is rare to be able to correlate individual beds for significant distances (see review Amy and Talling, 2006). Therefore, idealized facies models (Bouma, 1962; Stow and Shanmugam, 1980; Lowe, 1982; Mutti, 1992; Haughton et al., 2009), the most widely used being the Bouma and Lowe Sequences, are important for predicting down flow changes in depositional architecture (Sumner et al., 2012). Alongside field observations, experiments have provided valuable insights into the structure and dynamics of submarine flows (see reviews by Middleton, 1993; Kneller and Buckee, 2000; and more recent studies by McCaffrey et al., 2003; Choux et al., 2005; Felix et al., 2005; Gray et al., 2005; Baas et al., 2009; Sumner et al., 2009; Baas et al., 2011). From both experimental and field data, numerical models have attempted to simulate turbidity currents, ranging from 1-D depth averaged models (Pantin, 1979; Parker, 1982; Parker et al., 1986) to more computationally demanding 3-D fully resolved models (Felix, 2002; Blanchette et al., 2005; Cleary, 2010; Cantero et al., 2012). These numerical simulations have provided insights into the physics

operating within these flows, and have been important in predicting the behaviour of natural submarine flows. However, validation of these experimental and numerical models is difficult due to a paucity of in-situ measurements and the limited lateral extent of beds documented in outcrop. What is required is an extensive and detailed field data set, documenting individual beds across their depositional extent. From such data it will be possible to validate the experimental and numerical models, and interpret with more confidence the dynamics of submarine flows.

1.1 The Moroccan Turbidite System

The Moroccan Turbidite System is situated offshore NW Africa (Figure 1-1). It consists of three interconnected deep-water basins (Wynn et al., 2002b): the Seine Abyssal Plain in the northeast, the Agadir Basin situated in the central part of the system, and the Madeira Abyssal Plain in the west. The system is fed by: 1) Organic-rich flows, sourced from the Moroccan Margin, 2) Volcanoclastic flows sourced from the Canary Islands and Madeira, and 3) Carbonate-rich flows, sourced from local seamount collapse (Figure 1-1; Wynn et al., 2002b). Over the past 40 years a robust geochemical and chronostratigraphic framework has been established across the system (Weaver and Kuijpers, 1983; de Lange et al., 1987; Weaver, 1991; Pearce and Jarvis, 1992; Rothwell et al., 1992; Weaver et al., 1992; Pearce and Jarvis, 1995; Davies et al., 1997; Wynn et al., 2002b). This enables individual beds to be correlated over large distances (Wynn et al., 2002b; Wynn et al., 2010). Excellent core recovery throughout the Moroccan Turbidite System means that individual beds can be mapped out, in considerable detail, in both down flow and across flow directions. These beds present a rare opportunity to examine the architectures of natural beds over their depositional extent. The deposits are unconsolidated allowing quantification of grain size. Most importantly, analysis of deposits on the modern sea floor allows the relationships between bed architecture and seafloor gradient to be established. This is arguably the most detailed and extensive correlative framework for individual flows in any turbidite system.

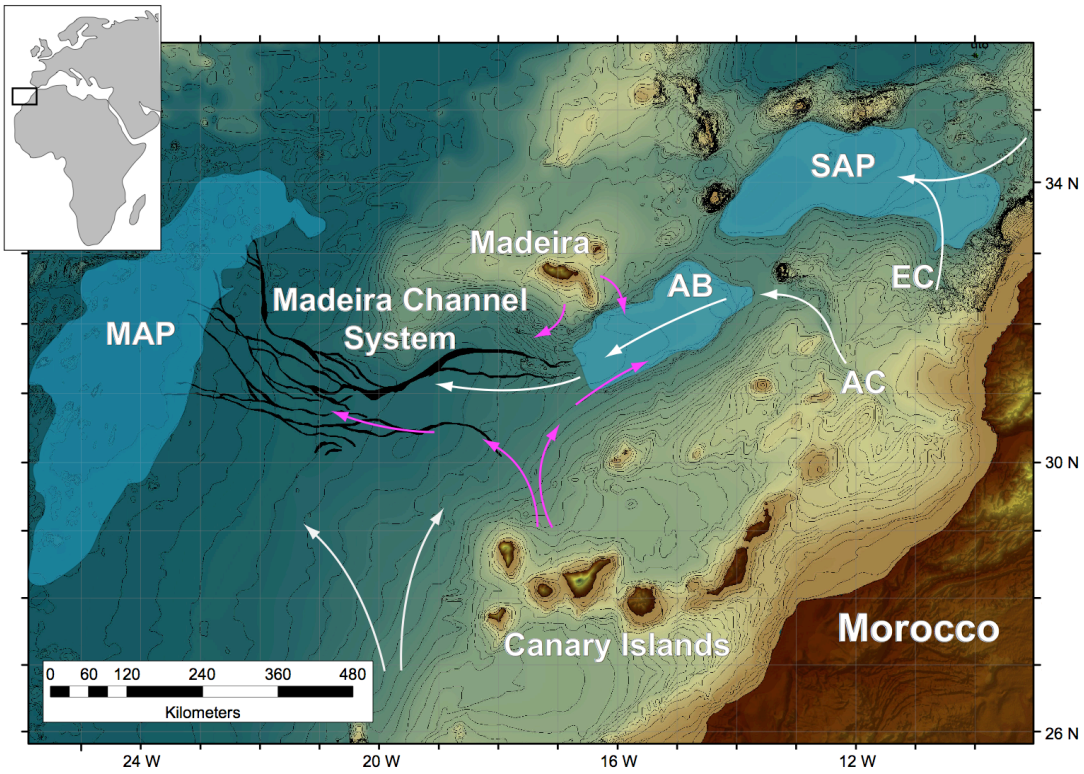

Figure 1-1: Map of the Moroccan Turbidite System. Insert map shows global location of the system, situated offshore NW Africa. The system comprises three inter-connected basins: the Seine Abyssal Plain (SAP), Agadir Basin (AB), and Madeira Abyssal Plain (MAP). Flows are primarily sourced from: the Moroccan Margin (white arrows) and pass through the system from east to west; the Canary Islands (purple arrows) and spread out across the system from the south. An additional flow pathway is marked sourced from the Sahara Headwall to the south of the study area. Important features include the Agadir Canyon (AC) and El Jadida Canyon (AC), which supply the Agadir Basin and Seine Abyssal Plain, and the Madeira Channel System, which connects the Agadir Basin to the Madeira Abyssal Plain.

1.2 Aims

The broad approach of this thesis is to use individual bed correlations to better understand flow processes within turbidity currents. By mapping out individual beds across their depositional extent predictive facies and numerical models can be validated against the field data. Such an approach has proved valuable in the Marnoso Arenacea, where turbidite architectures differ significantly from established models, which has provided new insights into flow processes (Amy and Talling, 2006; Talling et al., 2007a, b; Sumner et al., 2012). This thesis aims to better understand flow processes through consideration of the following fundamental questions:

1. *Can turbidite deposits situated across a basin floor allude to the origins and trigger mechanisms of the parent slope failure? (Chapter 3)*

2. *How thick were the flows that deposited each turbidite bed? (Chapter 4)*

3. *What are the processes that allow flows to run-out for hundreds (even thousands) of kilometres across essentially flat seafloor? (Chapter 4)*

4. *How do flows respond to changes in slope and confinement (i.e. channelization)? (Chapter 5)*

5. *How do flows build and maintain submarine channels: Is erosion essential in the life of a submarine channel? (Chapter 5)*

6. *What processes generate grain-size breaks within turbidites and what can they tell us about changing processes over the life of a flow? (Chapter 6)*

1.3 Thesis outline

The thesis opens with this introduction, which outlines the theme and rationale of the project, the study area, and general aims of the thesis. Chapter 2 contains a description of the materials and methods used within Chapters 3 – 6. Chapters 3 – 6 investigate different areas of the Moroccan Turbidite System. First, separate areas of the system are examined in detail, building and extending individual bed correlations and interpreting flow processes from deposits. As such, Chapters 3, 4, 5 and 6 are ordered geographically with areas closest to the Moroccan Margin examined first, followed by areas progressively further from the margin (respectively). Each area represents a section along extensive flow pathways across the system with each chapter examining an aspect of deep-water flow processes operating within that area (outlined below).

Chapter 3 examines flow pathways across the Seine Abyssal Plain, which is situated adjacent to the Moroccan Margin. This chapter shows multiple flows entering the basin simultaneously from disparate locations. The discussion centres on the origins of the flows, and whether specific trigger mechanisms can be attributed to the slope failures that produced them. Chapter 4 examines individual flow deposits across the Agadir Basin, which forms the central part of the Moroccan Turbidite System (Figure 1-1). Discussion centres on flow processes; specifically how the flows were able to run-out for hundreds of kilometres across an essentially flat seafloor and produce beds that did not appreciably thin or fine down slope. Chapter 5 documents how individual bed architectures change from the Agadir Basin into the Madeira Channel System (Figure 1-1). The discussion explores the flow processes operating across the channel system and how flows transform from bypassing to depositional with changes in slope. Chapter 6 encompasses data from the entire Moroccan Turbidite System (Figure 1-1). Analysis from Chapters 3, 4, and 5 are used to develop a more complete picture of flow processes operating across the entire Moroccan Turbidite System. The discussion focuses on understanding how grain-size breaks form within individual beds, and how these phenomena can be used to interpret flow processes over the entire life of a flow.

Combined, Chapters 3 – 6 examine how individual flows change and evolve along their flow pathways, and how these changes relate to subtle changes in slope and confining topography. Such field data is a rare and valuable contribution, providing much needed data for numerical modellers to incorporate into future simulations.

1.4 Authorship

All papers in this thesis were written by myself, as the first named author, with contributions from my four supervisors: Peter Talling, Russell Wynn, Doug Masson and Esther Sumner. Grain-size data was contributed by Micha Frenz in Chapters 4 – 6. James Hunt contributed geochemical data to Chapters 3 and 5. Samantha Gibbs contributed to Chapter 3. Bryan Cronin and Andrey Akhmetzhanhov contributed to Chapter 5.

2. Materials and methods

This chapter documents materials and methods used throughout this thesis, i.e. common to chapters 3 – 6. Methods that are specific to individual chapters are described within the relevant chapter. For example, the analysis of grain size is a method used across Chapters 3 – 6 and therefore is described here. In contrast, stable oxygen isotope analysis is only used within Chapter 3; hence the method is described separately in Chapter 3.

2.1 Sea floor bathymetry and slope maps

Modern seafloor topography is determined using the General Bathymetric Chart of the Oceans (GEBCO). This data provides bathymetry across the entire Moroccan Turbidite System with a pixel size of ~900m^2 (horizontal resolution ~5km). In addition, hull mounted EM12 swath bathymetry is used in conjunction with GEBCO data across the Madeira Channel System (see Chapter 5), providing a vertical and horizontal resolution of ~0.02m and ~350m respectively.

Slope maps are constructed from the GEBCO data. Seafloor gradients are calculated from GEBCO spot heights with a pixel size of ~900m^2, which are then smoothed within a ~3km^2 grid. 2D slope profiles are taken from the GEBCO slope maps described above. These 2D slope profiles are subject to a 3-point rolling average to reduce 'noise' along the profile. Slope maps and 2D slope profiles calculated from GEBCO data were then validated against slopes calculated between core sites. Water depths of core sites were obtained on site, during the coring process, from hull mounted echo sounding. Using trigonometry the average slope between core sites was calculated. Slopes calculated from GEBCO data and between core sites show good agreement.

It is important to understand whether modern bathymetry was similar to that of palaeobathymetry. Two main factors are examined that could have significantly changed bathymetry over the past 200ka. First, active tectonics could raise and/or lower areas of the seafloor, producing significant changes to seafloor gradients. Between 26 and 34N the Moroccan Margin is classified as a passive margin (e.g. Davison, 2005). Therefore, tectonic uplift/subsidence over the past 200ka is likely to be insignificant and not affected bathymetry across the Moroccan Turbidite System. However, the Seine Abyssal Plain is situated relatively close to the Gulf of Cadiz Africa-Eurasia Plate boundary, which has 2 – 4mm per year oblique NW – SE convergence (Argus, 1989). Structures associated with this convergence zone extend into the NE parts of the Seine Abyssal Plain (Medialdea et al., 2004). Therefore, bathymetry across parts of the Seine Abyssal Plain may have been altered via tectonic movement. However, there is relatively little information on shallow subsurface structures in this area and no estimates of rates of movement. Therefore, it is difficult to assess how the bathymetry might have changed over the past 200ka. Second, spatial variability in turbidity current deposition over the past 200ka could alter bathymetry, which would significantly change the calculated slopes across the Moroccan Turbidite System. To assess the impact turbidites might have had on bathymetry over the past 200ka, individual beds were sequentially removed from the stratigraphy, and the resulting palaeobathymetry and slopes were calculated (Figure 2-1; see Chapter 4 for bed correlations). This analysis shows that most turbidites did not change the bathymetry of the seafloor and slopes remained similar over the past 200ka. However, in certain areas across the Agadir Basin Bed A5 (documented in detail through Chapter 4) generated differences in slope of ~0.005º (Figure 2-1). At the distal end of the Agadir Basin cumulative turbidites produced changes in slope of ~0.007º. These changes in slope are considered insignificant. Therefore, modern bathymetry is considered similar to palaeobathymetry across the Moroccan Turbidite System over the past 200ka.

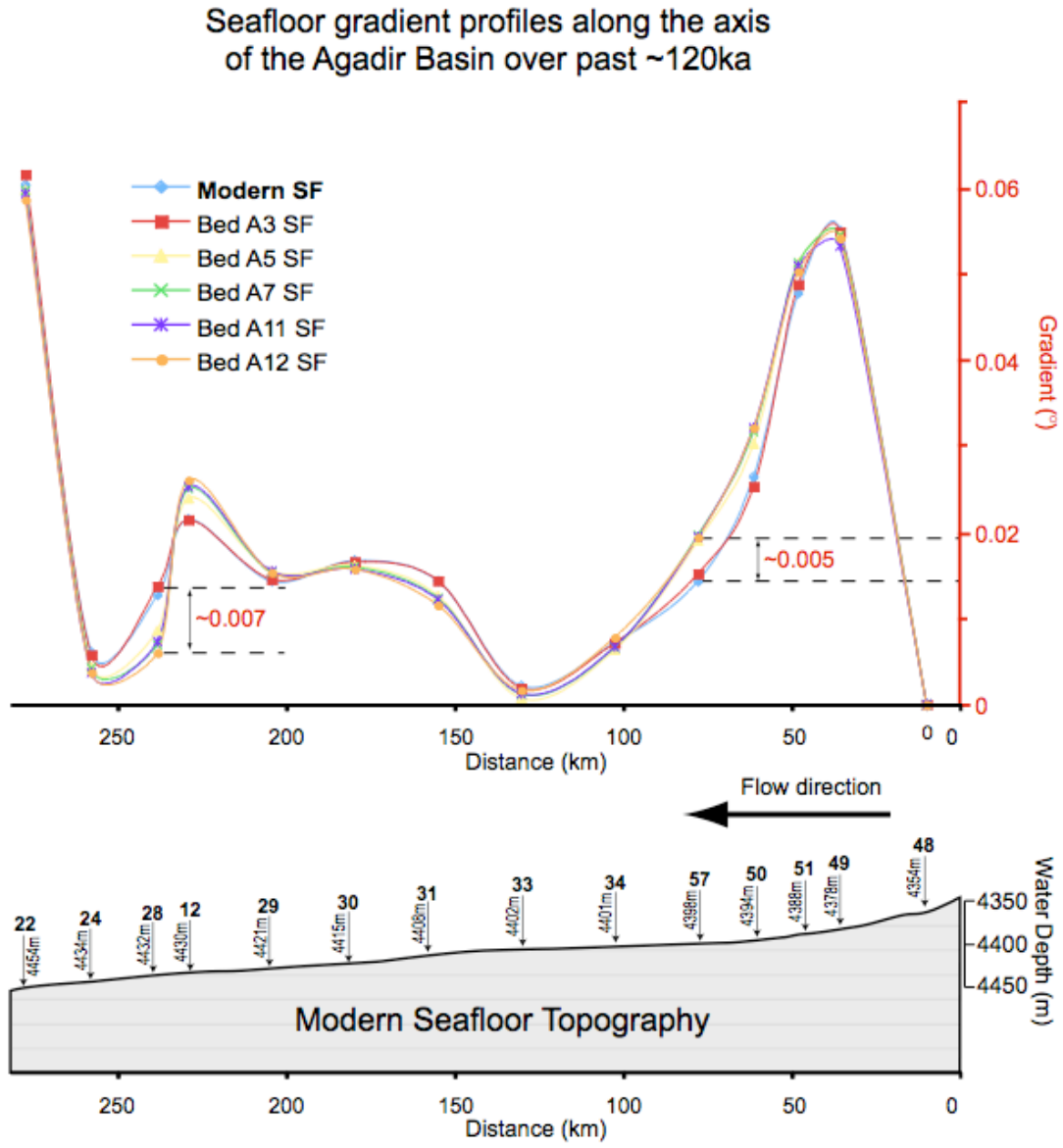

Figure 2-1: Effects of turbidites on the bathymetry of the Agadir Basin. Graph illustrates the calculated slopes along the axis of the Agadir Basin after sequential removal of Beds A3, A5, A7, A11 and A12 from the stratigraphy. Note that most of the beds do not alter the slope profile along the axis of the Agadir Basin. Only Bed A5 impacts on the palaeobathymetry of the basin.

2.2 Cores

The cores used in this study were taken from many cruises over the past 40 years. Cores are situated throughout the Moroccan Turbidite System. Cores have an average length of ~ 10 m and most were in good condition and were visually logged in detail (Figure 2-3). Grain size was initially established from visual examination with a 10x hand lens and comparison to a grain-size comparator card. However, the oldest cores, labeled 'VM' (taken in 1969; see Chapter 3) were not in sufficiently good condition to log. Therefore, sedimentary logs of 'VM' cores were constructed using original core photographs and core descriptions.

2.3 Facies scheme

Deposits of turbidity currents are described and interpreted within a facies scheme. Chapters 3 – 6 use this scheme to describe and interpret turbidites. In this section, facies found across the Moroccan Turbidite System is described. For interpretations of facies the reader is referred to the discussion section of Chapter 4 (see Table 4-1 for summary). Many of the features observed in turbidites across the Moroccan Turbidite System are analogous to facies depicted in existing schemes (Bouma, 1962; Stow and Shamugam, 1980; Lowe, 1982; Haughton et al., 2009).

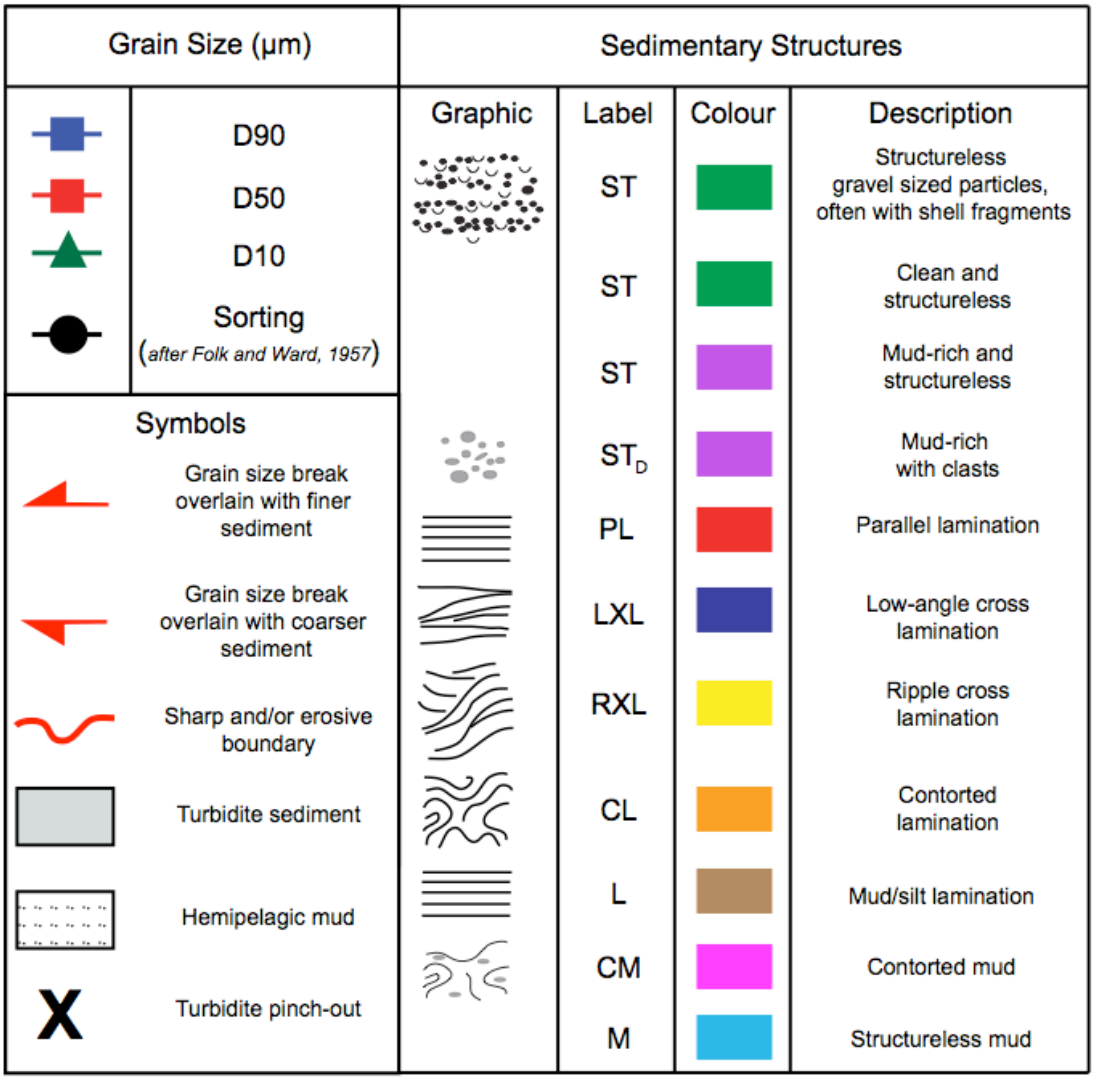

Figure 2-2: Key to all figures that use graphic logs. Figure includes symbology for graphic logs, key to vertical grain-size profiles, and colours and abbreviations for interpreted facies within turbidites. This key is also included within Chapter 4, for ease of reference.

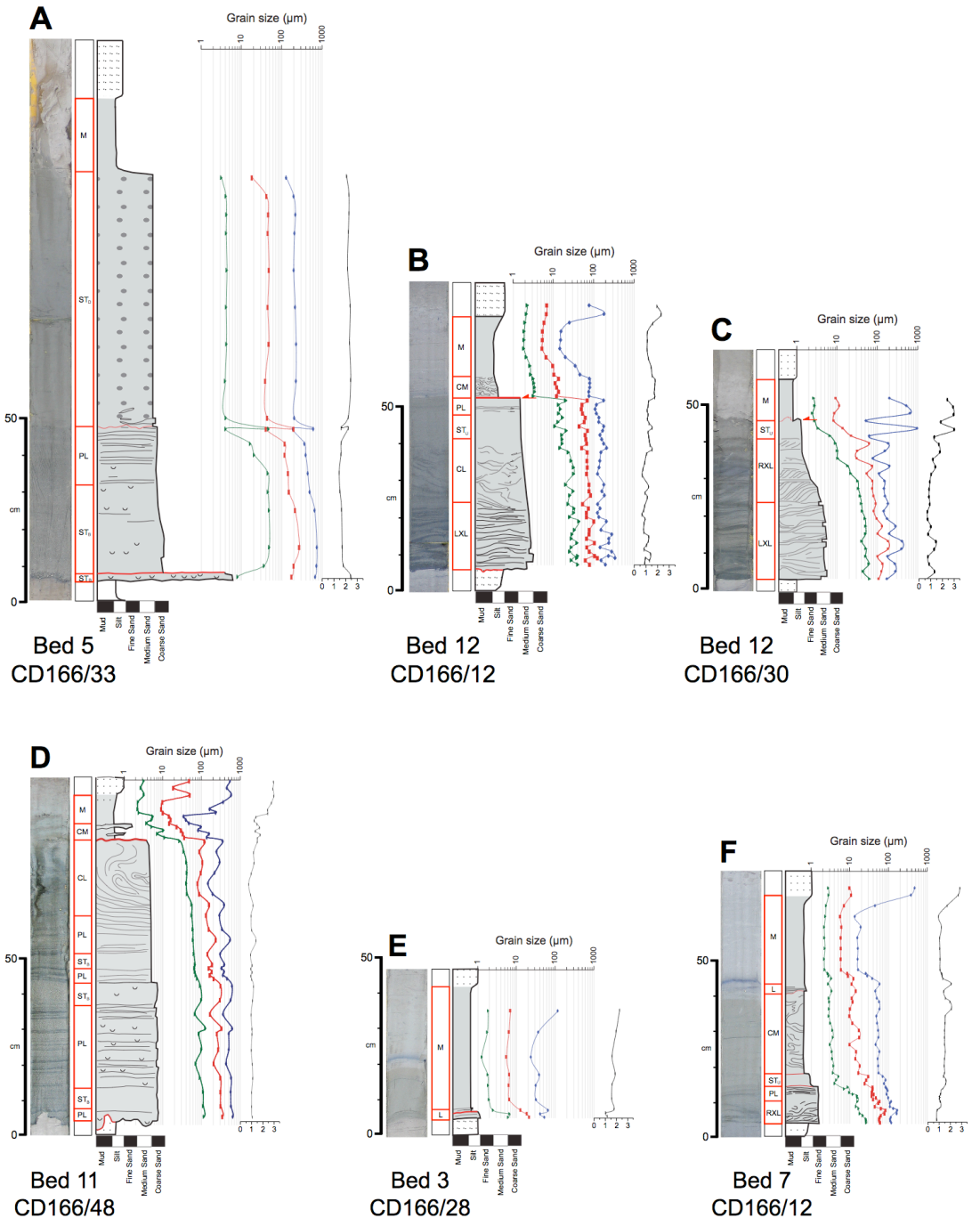

Figure 2-3: Examples of turbidite facies across the Moroccan turbidite System. Each deposit is illustrated with a visual log (shaded in grey), interpretation of facies (red column) and a core photograph. Grain-size analyses are shown vertically through each deposit including values for D10 (green), D50 (red), D90 (blue), and sorting (black).

Structureless Clean Sand (ST, Bouma T_A)

Structureless clean sand comprises sand displaying no sedimentary structures with mud contents < 20 %. The term 'clean' is used in a relative sense to distinguish this facies from mud-rich structureless sand, which has significantly higher mud contents (30 – 40 %). Two types of clean structureless sand are observed, distinguished by their position in the deposit. Intervals of structureless sand that occur at the base of the deposit are classified as basal structureless sand (ST_B; Figure 2-3A). Conversely, intervals of structureless sand occurring within upper parts of the deposit are termed upper structureless sand (ST_U; Figure 2-3B). When the core was split intervals of upper structureless sand appeared 'wobbly' indicating increased water content compared with the overlying and underlying sandy facies. This facies often contains significant amounts of carbonaceous matter, homogeneously distributed within the sediment. Upper structureless sand is typically overlain by planar or ripple cross-laminated sand then a sharp grain-size break and turbidite mud.

Mud-Rich Structureless Sand (ST_D)

Distinctive intervals of mud-rich (30 – 40 % mud), structureless sand are found within the middle to upper parts of the Bed 5 deposit (Figure 2-3A). One core location contains chaotic mud clasts (Talling et al., 2007c). The intervals are mostly ungraded but proximally the upper parts of the deposits are normally graded. Across the rest of the basin the interval is sharply overlain by either planar laminated sand or turbidite mud.

Planar Laminated Sand (PL, Bouma T_B)

Planar laminated, clean sand is the most common type of facies within sandy deposits, particularly in proximal locations (Figure 2-3D). Laminae are typically < 3 mm thick with low mud contents between 5-10%. Grain size and composition can vary between individual

laminae, switching between finer grained quartz and glauconite-dominated lamina to foraminifera-rich lamina. This facies has inverse-to-normal grading in proximal areas and develops weak normal grading distally.

Low angle cross-laminated sand (LXL, Bouma T_C)

This facies comprises clean sand (< 5 % mud) with laminations set at relatively low angles to each other (< 10º) and to the base of the turbidite (Figure 2-3C). Laminations are sub-parallel but are not observed to truncate each other. This facies occurs proximally within the upper parts of sand deposits, overlying parallel laminated sands. In distal localities this facies is found towards the base of deposits overlain by ripple cross-laminated sands (Figure 2-3B and C). It is normally graded.

Ripple cross-laminated sand (RXL, Bouma T_C)

This facies comprises clean sand (< 5 % mud) with relatively steeply dipping laminations (Figure 2-3C and F). The angles of laminae are steeper (> 10º) than those of low-angle cross-laminae and are often observed to truncate each other. Normally graded ripple cross-laminated sands are found proximally within the upper parts of deposits, overlain by turbidite silt and mud. In distal areas this facies is also normally graded but found towards the base of the deposits, overlain by turbidite silt and mud.

Contorted sand (CL, Bouma T_C)

Contorted lamination within clean sand intervals (5 – 10 % mud) occurs proximally in the basal parts of deposits and in the middle to upper parts of deposits distally (Figure 2-3B and D). Contorted intervals can be ungraded or normally graded.

Turbidite Mud (L, CM and, M, Bouma T_D and T_E)

A fine-grained turbidite mud cap overlies all sandy turbidite deposits across the Moroccan Turbidite System. Generally the turbidite mud is thin, structureless and ungraded (M; Figure 2-3A and C). However, occasionally the basal parts of the mud cap have thin inter-laminated silts and muds (L; Figure 2-3E), which normally grade into structureless mud. Some parts of the mud cap, particularly in Bed 7, have intervals of contorted silty laminae, often with clasts of silt (CM; Figure 2-3F). Contorted muds are typically ungraded but can have weak normal grading.

Grain-size breaks (GSB)

Abrupt vertical changes in grain size (grain-size breaks) occur within all turbidite beds throughout the Moroccan Turbidite System (Figure 2-3). These grain-size breaks are examined in detail within Chapter 6 and are only briefly described here. Five different types of grain-size break are found: *Type I* – occurred proximally between gravel and finer grained structureless sand, *Type II* – occurred proximally between inversely graded sand overlain by coarser sand, *Type III* – occurred proximally between sand overlain by ripple cross-laminated finer sand, *Type IV* – occurred almost everywhere between clean sand and mud, and *Type V* – occurred only in relatively distal areas between mud-rich (debrite) sand and mud.

2.4 Grain-size analysis

Grain-size samples were taken approximately every 1 cm vertically through turbidite beds (Figure 2-3). Samples were mixed with 60 ml of 1% deflocculent (sodium hexametaphosphate) solution then shaken for at least 5 hours to break up any aggregates of sediment. Samples were analyzed using a 'Malvern Mastersizer 2000' in combination with a 'Malvern Hydro G' accessory unit and a 36-pot autosampler. For the analyses, a laser target obscuration of 10 – 20 % was obtained for each sample. Particle refractive index was set to 1.52 with an absorption value of 0.1, providing average parameters for a mixed mineral assemblage as expected for marine sediments. Three measurements were carried out on each sample for which average particle-size distributions were calculated. Sorting was calculated for each grain-size sample using the inclusive graphic standard deviation (Folk and Ward, 1957).

3 Topographically complex flow pathways into the Seine Abyssal Plain, offshore NW Africa: Implications for the interpretation of synchronously emplaced turbidites

Stevenson C.J., Talling P.J., Masson D.G., Sumner, E.J., Hunt, J.E., Gibbs, S.J., and Wynn R.B.

3.1 Abstract

Turbidites found in deep-water basins are derived from sediment from adjacent continental margins. In seismically active areas earthquakes can trigger submarine flows, which are potentially recorded within the basin turbidite sequence. Thus a basin turbidite sequence can potentially be used as a record of palaeoseismicity. Here we present a robust correlation of individual turbidite beds across the Seine Abyssal Plain, offshore NW Africa. Three turbidites have fining trends (in grain size) that originate from disparate areas of the basin. The flows that deposited these beds are interpreted to have passed into the basin synchronously from multiple disparate entry points. Two hypotheses are proposed to explain the origins of the synchronous events: 1) multiple disparate slope failures occurring simultaneously across the Moroccan Margin or, 2) a single slope failure that was subsequently split along its flow pathway into the basin. Multiple slope failures occurring simultaneously requires a regional trigger, most likely an earthquake. However, a single slope failure could be produced via a number of different mechanisms. In this case, it is not possible to categorically determine which model is most likely, thus, an earthquake-trigger is not certain. This study highlights the problems facing turbidite palaeoseismology when examining prehistoric sequences. Even with spatially extensive, synchronous turbidite emplacement across disparate areas of seafloor, a careful approach must be employed when interpreting palaeoseismicity from the ancient turbidite record.

3.2 Introduction

The Moroccan turbidite System, offshore NW Africa, has been the subject of intensive research over the past 30 years (Weaver and Kuijpers, 1983; Weaver and Kuijpers, 1986; de Lange et al., 1987; Weaver and Rothwell, 1987; Weaver, 1991; Jones et al., 1992; Pearce and Jarvis, 1992; Rothwell et al., 1992; Weaver et al., 1992; Weaver and Thomson, 1993; Pearce and Jarvis, 1995; Davies et al., 1997; Weaver et al., 1999; Weaver et al., 2000; Wynn et al., 2000; Wynn et al., 2002a; Wynn et al., 2002b; Talling et al., 2007; Macdonald et al., 2011). It is one of the largest documented turbidite systems on earth with run-out distances > 2000 km (Wynn et al., 2002b; Wynn et al., 2010). Unlike other turbidite systems, it has been cored extensively along its length (> 300 shallow piston cores). Excellent core coverage coupled with a robust geochemical and chronostratigraphic framework enables individual turbidite beds to be correlated for vast distances across the seafloor (> 2000km; Wynn et al., 2002b; Wynn et al., 2010). The rare opportunity to examine individual beds over such distances has provided unique insights into deep-water flow processes and resulting depositional architectures.

Despite this substantial body of work, the Seine Abyssal Plain, situated in the NE part of the Moroccan Turbidite System, is poorly studied. This area is important, as it forms the most proximal basin within the Moroccan Turbidite System, adjacent to the African continental margin. Studying the most proximal basin is integral in understanding flow pathways across this very large turbidite system and how flows evolve as they travel from their source to distal areas of the seafloor. In addition, the Seine Abyssal Plain is situated close to the African-Eurasian Plate Boundary, which is a slow convergent margin (4 – 5 mm/yr) and subject to significant seismic activity (Argus et al., 1989; Roca et al., 2004). Turbidite sequences found in basins that are situated close to seismically active regions can potentially be used to determine a long-term record of palaeoseismicity in the region.

3.2.1 Turbidite palaeoseismology

The basic principle of turbidite palaeoseismology is that earthquakes can trigger turbidity currents, and the resulting turbidites can be distinguished in the marine record from turbidites produced via other triggers (Adams, 1990; Goldfinger et al., 2003; Goldfinger, 2011). In this way turbidite sequences within basin sediments can provide a long-term record of nearby continental margin palaeoseismic activity. This approach has been widely applied over the past 20 years, in many locations around the world (Goldfinger, 2011).

However, the assertion that earthquake-generated turbidites are distinguishable from turbidites generated via other mechanisms is not straightforward. In addition to earthquakes, turbidity currents can also be triggered via: loading by sedimentation, storm waves, volcanic activity and flank collapse, low sea-level exposing and failing sediments, tilting due to tectonic activity or salt movement, changes in methane hydrate stability, or river-derived hyperpycnal flows (Coleman et al., 1983; Wright, 1985; Sparks et al., 1993; Mulder and Syvitski, 1995; Masson et al., 2010; Hunt et al., 2011; Masson et al., 2011). Indeed, it is questionable whether a specific trigger mechanism that generates a turbidity current would have any affect on the resulting turbidite (Gorsline et al., 2000; Masson et al., 2011). Criteria that have been used to interpret earthquake-generated turbidites includes: multiple fining upward sequences (and mineralogical differences) within individual turbidite beds, interpreted as a product of multiple flows converging within the basin; unusually coarse grain sizes within turbidite deposits compared with other beds in the basin, interpreted to be sourced from earthquakes destabilizing different parts of the continental margin; spatially extensive deposits correlated between a number of core sites, interpreted to represent larger than normal failures, i.e. a large earthquake; synchronous events occurring in disparate geographical areas, interpreted to be multiple events generated by a regional trigger, i.e. an earthquake (Adams, 1990; Gorsline et al., 2000; Goldfinger et al., 2003; Gracia et al., 2010; Goldfinger, 2011). However, it is difficult to determine to what extent individual criteria are affected by the local sedimentary environment (e.g. sediment supply, flow processes, basin morphology, and slope stability factors). For example, Masson et al., (2011) correlated synchronous turbidites within the Setubal and Cascais Canyons, offshore Portugal, with the

huge 1755 Lisbon earthquake (magnitude > 8.5). Despite the large magnitude earthquake, the turbidite associated with it was relatively small-volume, which is interpreted to be a consequence of low sedimentation rates along the continental margin prior to the earthquake.

Considering these complexities imposed by local factors, there is only one diagnostic criterion that is widely applied to interpret earthquake-generated turbidites, and that is synchronous emplacement of multiple turbidites across disparate areas of a basin. Indeed, advocates of turbidite palaeoseismology argue that virtually all studies use the synchronous triggering criterion, even when additional sedimentological arguments for seismic triggering are present (Goldfinger, 2011).

3.2.2 Aims

This contribution presents a suite of shallow sediment cores recovered across the Seine Abyssal Plain, offshore NW Africa. Previous work is limited in the area (Davies et al., 1997; Wynn et al., 2002), meaning there is not a robust individual bed correlation framework that extends across the entire basin. Hence, the first objective of this chapter is to construct an individual bed correlation framework across the Seine Abyssal Plain, which can be integrated into the established Moroccan Turbidite System stratigraphy. Using the turbidite stratigraphy developed across the Seine Abyssal Plain, the chapter then examines: 1) the recurrence times of turbidite events through time and whether external forcing (i.e. sea-level) is an important control on event frequency and; 2) How multiple simultaneous flows could enter the basin from disparate locations, potentially recording earthquake triggered slope failures. Specific objectives include:

1. To extend individual bed correlations across the entire Seine Abyssal Plain. This will involve dating and sedimentological analysis of shallow sediment cores recovered within the basin.

2. To establish an inter-connected turbidite stratigraphy across the Seine Abyssal Plain and the adjacent Agadir Basin. This framework will show which turbidite beds are local to each basin and which beds extend across both.

3. To determine likely source areas and flow pathways into the Seine Abyssal Plain and Agadir Basin. This will involve mineralogical and grain-size analysis, and analysis of coccolith assemblages within individual beds across both basins.

4. To investigate the frequency of turbidite events over the past ~ 250 ka across the Seine Abyssal Plain and Agadir Basin. This will involve statistical analysis of turbidite recurrence times, which shows clustering of turbidite events during periods of sea-level high-stand.

5. To investigate how spatially extensive turbidites could be emplaced synchronously across both the Seine Abyssal Plain and Agadir Basin. This will involve discussion as to whether the flows originated from a single slope failure or multiple disparate slope failures and, what triggers (if any) can be confidently interpreted as the cause of the parent slope failures.

3.2.3 Seine Abyssal Plain

The Seine Abyssal Plain is one of three interconnected basins that make up the Moroccan Turbidite System, situated offshore NW Africa (Figure 3-1A). It covers an area ~ 54,000 km^2 and occupies water depths of between 4300 m and 4450 m. To the west, the Seine Abyssal Plain is bounded by the Madeira Tore Rise, a series of volcanic seamounts trending NE – SW. To the east, it is bounded against the African continental margin. The northwestern boundary is defined by the Unicorn, Ampere, and Coral Patch seamounts trending E – W (Figure 3-1A). The southern boundary is defined by a spur projecting SE – NW from the continental margin, the Casablanca seamount, and a low relief sill that separates the Agadir Basin from the Seine Abyssal Plain. Initially, the southern basin margin comprises a relatively steep slope followed by the Safi Plateau. Then it sharply rises again to the crest of

the Agadir Canyon, ~ 850 m from the basin floor. The Seine Abyssal Plain has significant topographic complexity with low points situated to the west and central parts of the basin (Figure 3-1A).

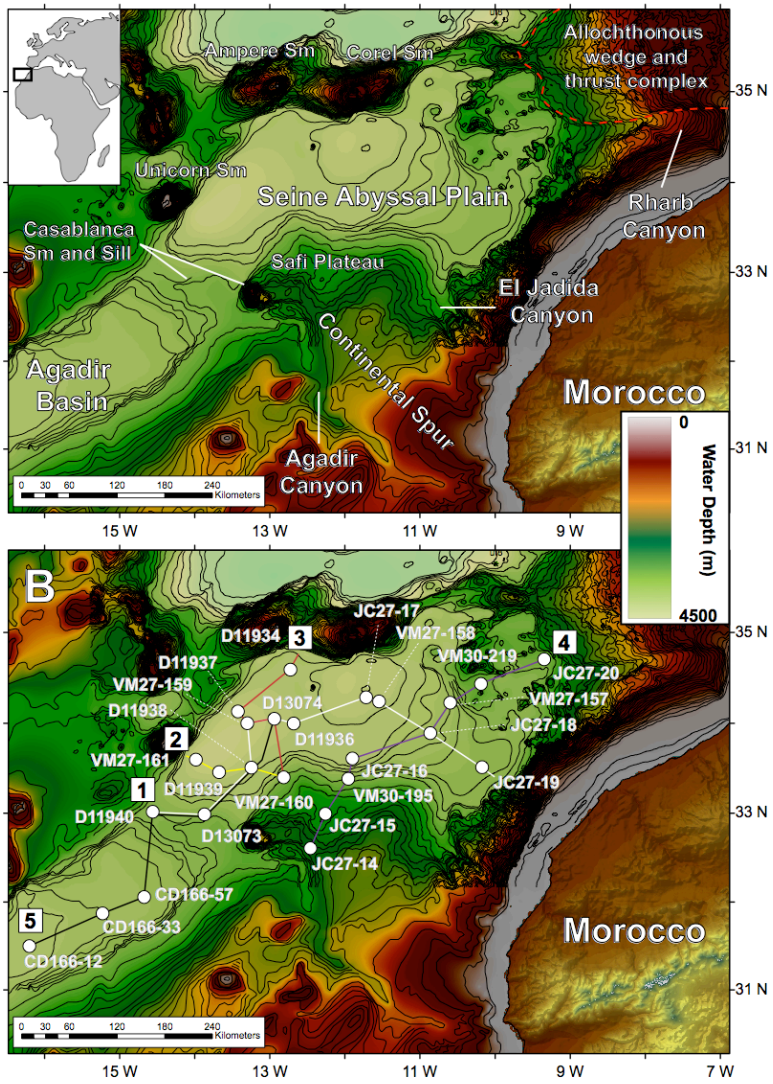

Figure 3-1: Map of the Seine Abyssal Plain and interconnected Agadir Basin. Black and white inset map shows regional situation, offshore NW Africa. (A) Highlights a number of topographic features in and around the two basins (Sm – seamount). Note the two topographic low points; one just east of the Unicorn Sm and, another situated centrally within the Seine Abyssal Plain. Major thrust faults penetrating deep into the oceanic crust are related to the 'Gulf of Cadiz Olistrosome' and marked with red dashed lines (Medialdea et al., 2004). (B) Shows locations of cores used in this study across both basins. Core Transects 1 – 5 are labelled and marked with solid coloured lines.

3.3 Materials and methods

3.3.1 Sea floor bathymetry and slope

GEBCO data is used to map seafloor bathymetry and generate slope maps across the Seine Abyssal Plain (as discussed in Chapter 2). GEBCO data provides bathymetry across the Seine Abyssal Plain and surrounding area with sufficient resolution to define large-scale topographic features such as canyons, seamounts and topographic low points within the basin.

3.3.2 Cores and grain-size analysis

The 23 cores used in this study were taken from many cruises over the past 40 years. Cores are situated across the entire Seine Abyssal Plain and along its margins (Figure 3-1B). Cores have an average length of 7 metres and most were in good condition and were visually logged in detail. Grain size was initially established from visual examination with a 10x hand lens and comparison to a grain-size comparator card. After visual logging the grain size of turbidite sediments was analyzed using a 'Malvern Mastersizer 2000' (see Chapter 2). However, the oldest cores, labelled 'VM' (taken in 1969) were not in sufficiently good condition to log or sample. Therefore, sedimentary logs of 'VM' cores were constructed using original core photographs and core descriptions. For a key to graphic logs refer to Figure 2-2 (Chapter 2).

3.3.3 Smear slides and coccolith analysis

High-resolution coccolith biostratigraphy was conducted from analyses of smear slides taken from cores D11940, D13074, D11936, JC27-14, JC27-15, JC27-16, JC27-19, and JC27-20. Smear slides were taken from hemipelagic sediment approximately every 3 cm vertically within the core. Smear slides were also taken from individual mud caps approximately every 10 cm vertically. The abundance of six coccolith species was analyzed in each smear slide following the method of Weaver and Kuijpers (1983).

To quantify error in coccolith species identification, three repeat counts were conducted for samples within a turbidite mud cap (Bed 5; see results; e.g. Figure 3-14 for detail) at core sites CD166-12 and CD166-57 from the Agadir Basin and, D11936 and JC27-19 from the Seine Abyssal Plain (Figure 3-2). The error between repeat counts is typically between 1 – 5 %.

3.3.4 Oxygen isotope analysis

Samples of hemipelagic sediment were taken from core D13074 for bulk oxygen isotope analysis. Samples were dried in an oven at 50º C then ground into a powder. Approximately 2000 μg of each sample was used for isotope analysis using a gas source mass spectrometer (Europa GEO 20–20) equipped with an automatic carbonate preparation system. Results are presented in the delta notation as ‰ relative to Vienna Pee Dee Belemnite. Replicate analyses of in-house standards, which are calibrated to NBS–19, yield a routine external reproducibility of 0.065 ‰ for $\delta^{18}O$ and 0.031 ‰ for $\delta^{13}C$.

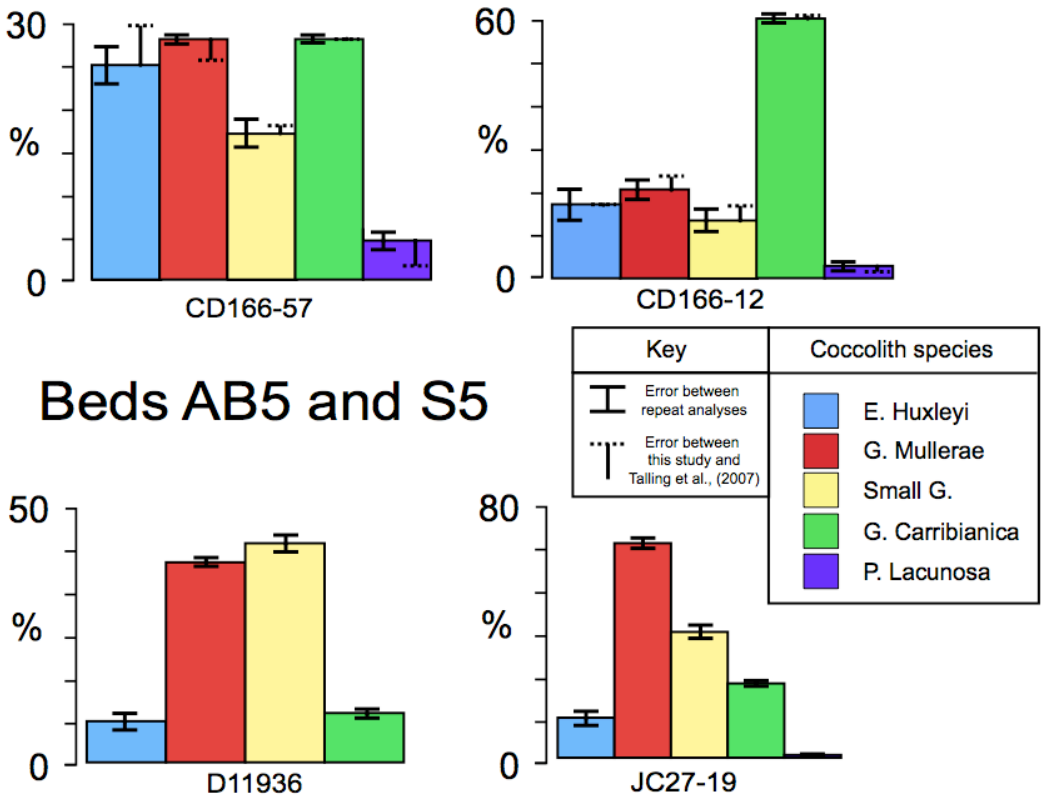

Figure 3-2: Histograms of coccolith assemblages within the mud caps of Beds AB5 and S5. Samples from cores CD166-57 and 12 were taken at 245 cm and 143 cm from the base of the bed respectively, identical positions to coccolith samples analyzed by Talling et al. (2007c). Solid black error bars represent variation in counts between three separate analyses of the same smear slide with variation typically between 1 – 5 %. Dashed black error bars represent coccolith counts obtained by Talling et al. (2007c). Their results show good agreement with coccolith counts obtained in this study.

3.3.5 Radiocarbon dating

Samples of hemipelagic sediment were taken from the upper parts of cores JC27-19 and 20 for radiocarbon dating. Each sample, ~ 1 – 4 cm^3, was washed through a 63 µm sieve. 10 – 20 mg of mixed planktonic foraminifera were picked under a binocular microscope. The main planktonic species present were *Globigerina bulloides*, *Globorotalia scitula*, *Neogloboquadrina pachyderma*, *Globorotalia truncatulinoides*, *Globigerinoides ruber*, *Globorotalia inflata*, *Globoritalia hirsuta* and *Orbulina universa*. The samples were analysed using an AMS (Accelerator Mass Spectrometry) (Beta Analytic, Florida) and conventional

radiocarbon ages were converted to calibrated radiocarbon ages using (Reimer et al., 2004) and the MARINE04 (Hughen et al., 2004) calibration curve, which both use a reservoir age of 400 yr. Samples younger than 21,786 Cal yr BP assume a 400-year reservoir age, whereas older samples assume a reservoir correction of 255 yr (Fairbanks et al., 2005).

3.4 Results

3.4.1 Sediments in cores

Two distinct sediment types are found in the cores: (1) hemipelagic mud, and (2) turbidite sand/mud (Figure 3-3). Hemipelagic sediments comprise two end member lithologies. In interglacial periods, the sediments are cream coloured carbonate oozes, comprising foraminifera tests, smaller coccolithophores and some fine terrigenous clay (Weaver and Kuijpers, 1983; Weaver and Rothwell, 1987; Rothwell et al., 1992; Weaver et al., 1992). In glacial periods, increased rates of carbonate dissolution in the bottom waters dissolve most of the foraminifera tests and coccolithophores, which produces grey coloured marl (Crowley, 1983; Weaver et al., 1992). Turbidite sediments are distinguished from hemipelagic sediment via changes in grain size and colour. The base of a turbidite is sharp and often relatively coarse-grained (i.e. sandy). This coarse material ranges in colour from dark olive green to brick red and is easily distinguished from the pale cream-coloured hemipelagic sediment. Typically, turbidite deposits fine upwards into silt and mud. The upper contact with the hemipelagic sediment is gradational due to bioturbation of hemipelagic sediment into the turbidite mud cap. Turbidite beds are labelled sequentially down core, and where correlated into the Agadir Basin take the nomenclature of Wynn et al. (2002b). Individual bed correlations are presented later in the results (e.g. Figure 3-10).

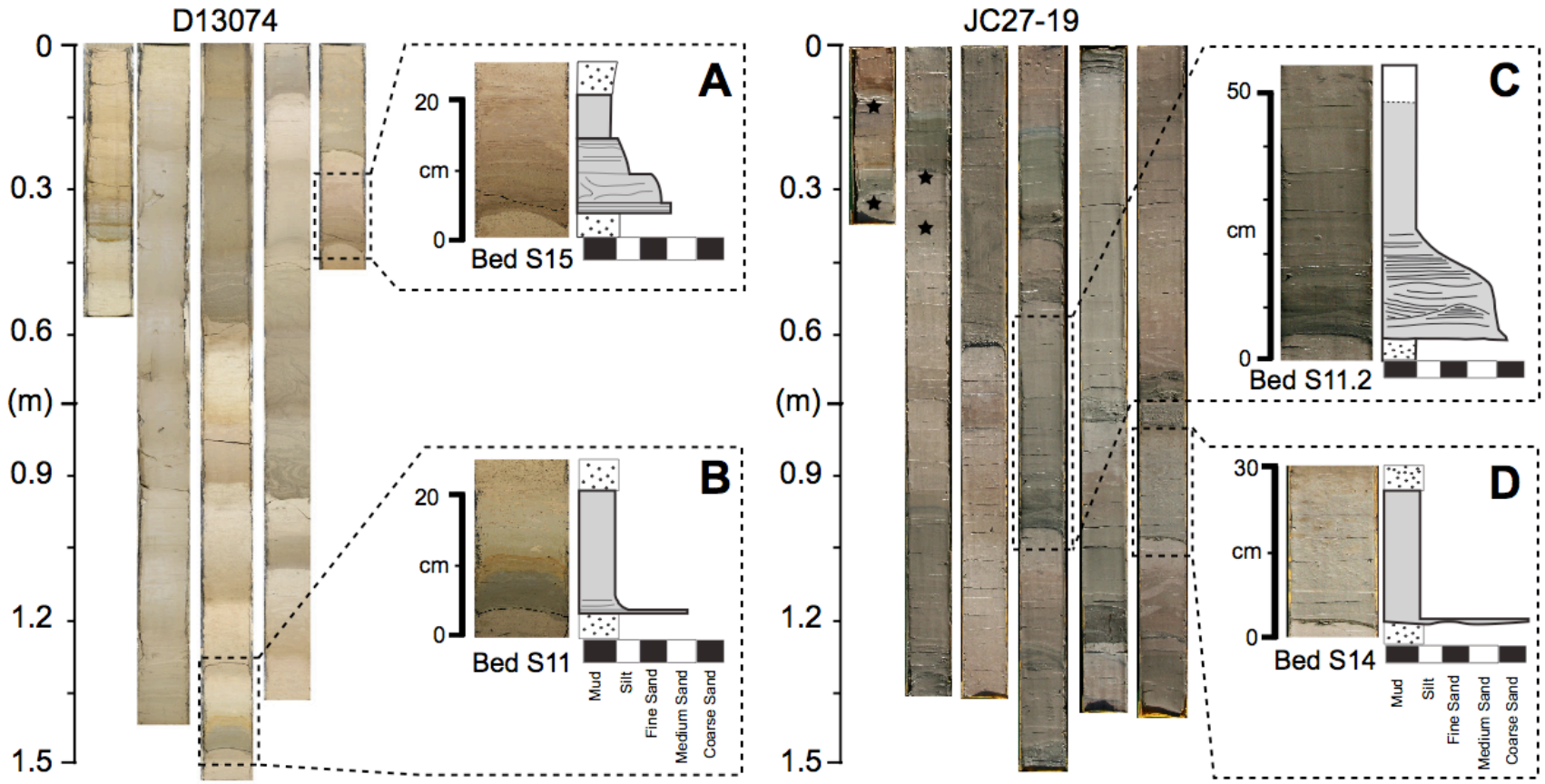

Figure 3-3: Examples of core photographs for D13074 and JC27-19. Top of cores is top left and sections follow in sequence down core, from left to right. Cores are ~ 10 cm in diameter. Hemipelagic sediments are paler (light grey to pinkish brown) and turbidites are darker (olive-green, red-brown). Black stars indicate where radiocarbon samples were taken from core JC27-19. Different types of turbidite are highlighted including: red-brown (A), mint-green (B) and olive-green (C) organic-rich turbidites, and volcanoclastic Bed S14 (D). Each example is accompanied by a visual log, which highlights features within each type of deposit.

3.4.2 Composition of turbidites

Four main types of turbidite are identified: organic-rich, volcanoclastic, carbonate-rich, and pyrite-rich (Figure 3-4). The provenance of different types of turbidite forms part of the discussion.

Organic-rich turbidites - Organic-rich turbidites are the most common type of turbidite found in the Seine Abyssal Plain. They have mud caps that are coloured either dark brick red or olive-green (Figure 3-3A and Figure 3-3C). An exception is turbidite S11, which exhibits a distinct bright mint-green mud cap (Figure 3-3B). The distinctive colour of this turbidite enables it to be used as a marker bed across the basin. Organic-rich turbidites have a sand fraction mineralogy dominated by quartz, glauconite and sandstone lithics with minor amounts of pyrite and mica (Figure 3-4). Biogenic constituents include: pelagic and benthic foraminifera, sponge spicules, fish teeth, echinoid spines, and shallow-water bivalves. This is consistent with turbidite compositions previously reported for organic-rich turbidites from the Agadir Basin and the southwestern Seine Abyssal Plain (Wynn et al., 2002b).

Volcanoclastic turbidites - Only one volcanoclastic turbidite, Bed S14, is identified across the Seine Abyssal Plain. It has a grey mud cap with dark grey/black silt sized sediment. The bed comprises almost 100 % phonolitic glass with a small amount of mafic lithics (Figure 3-4; Hunt et al., 2011; this study). In contrast to organic and carbonate-rich turbidites, it has high magnetic susceptibility values (Wynn et al., 2002b). The distinct colour, geochemistry and high magnetic susceptibility values make this turbidite an excellent marker bed across the basin.

Carbonate-rich turbidites - Carbonate-rich turbidites are cream coloured, and similar in colour to the hemipelagic sediment. Composition is strongly bimodal, and comprises large foraminifera tests and fine-grained mud with minor amounts of quartz (Figure 3-4).

Carbonate-rich turbidites are identified apart from hemipelagic sediment by a lack of randomly distributed foraminifera within their mud caps, i.e. smooth turbidite mud. Carbonate-rich turbidites found in the southern parts of the basin contain small amounts of sponge spicules, fish teeth and echinoid spines. In contrast, the carbonate-rich turbidite found in the northwest of the basin contains only foraminifera and fine-grained mud.

Pyrite-rich turbidites - Pyrite-rich turbidites are cream or olive-green in colour and similar in appearance to the organic-rich turbidites described above. The sand fraction is dominated by pyrite grains (> 30 %) but also can have significant amounts of quartz, mica, glauconite, and clastic lithics (Figure 3-4). In Bed 16 pyrite comprises almost 100 % of the sand fraction mineralogy. Biogenic material includes abundant pelagic and benthic foraminifera, sponge spicules and echinoid spines. Pyrite-rich turbidites are generally restricted to the northeastern parts of the basin, close to the mouth of the Rharb Canyon. However, relatively thin fine-grained deposits are found occasionally in the eastern parts of the basin.

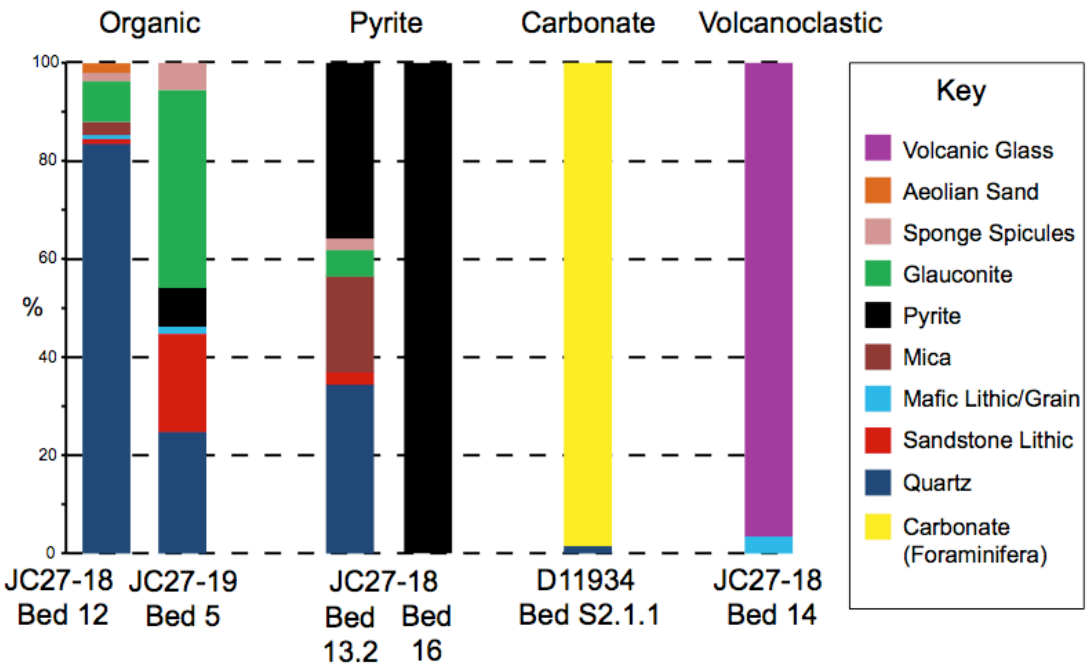

Figure 3-4: Bulk compositions of turbidites across the Seine Abyssal Plain. Point counts of minerals under a binocular microscope identified four types of turbidite: (1) organic-rich, (2) pyrite-rich, (3) carbonate-rich and, (4) volcanoclastic. Note that pyrite-rich beds are turbidites with > 30 % pyrite within their sand fraction.

3.4.3 Turbidite facies

Sedimentary textures found within turbidite beds are described within a facies scheme (Figure 3-5). Many of the facies described in this study are common to deep-water turbidite systems and have been thoroughly described elsewhere (Bouma, 1962; Lowe, 1982; Sumner et al., 2012). For clarity a brief description of each facies is provided below.

Structureless Clean Sand (ST_B; Bouma T_a)

Structureless clean sand comprises sand displaying no sedimentary structures with mud contents up to ~ 20 % (Figure 3-5B). The term 'clean' is used in a relative sense to distinguish this facies from mud-rich structureless sand, which has higher (30 – 40 %) mud contents.

Mud-Rich Structureless Sand (linked-debrite; ST_D)

A distinctive interval of mud-rich (30 – 40 % mud), structureless sand is found within the middle to upper parts of Bed S5 in the eastern parts of the Seine Abyssal Plain (Figure 3-5B). Mud-rich sand is mostly ungraded but can have normal grading within the upper parts of some deposits. This facies is referred to as 'linked-debrite' deposits.

Laminated Sand (PL, RXL, CL; Bouma T_b and T_c)

Planar laminated sand (PL) is found towards the base of turbidite deposits (Figure 3-5B). Laminae are relatively thin (< 2 mm thick) with low mud contents between 5 – 10 %. This facies can be inverse-to-normal graded and/or normally graded. Ripple cross-laminated sand (RXL) occurs towards the upper parts of deposits, or at the base of relatively thin-bedded turbidites (Figure 3-5A). This facies is normally graded and has low mud content (< 5 %). Contorted lamination (CL) within sand intervals is common through the basin (Figure 3-5B). This facies typically occurs in the middle parts of the turbidite deposits and has a

relatively low mud content (5 – 10 %). Contorted intervals can have inverse and/or normal grading.

Turbidite Mud (L, CM and, M; Bouma T_d and T_e)

Volumetrically, turbidite mud is the most abundant type of deposit within the Seine Abyssal Plain. All sandy turbidites have a relatively thick overlying mud cap (Figure 3-5) and many turbidites are composed only of fine-grained sediment. Often, basal parts of the mud cap have thin inter-laminated silts and muds (L). This facies normally grades into ungraded, structureless mud (M). Some parts of the mud cap have intervals of contorted silty laminae, some with clasts of silt. These intervals can have multiple fining upward sequences.

Grain-size breaks (GSB)

Abrupt vertical changes in grain size (grain-size breaks) occur within turbidite beds throughout the Seine Abyssal Plain. Three types of grain-size break can be identified: (1) fine sand to coarse sand, (2) coarse sand to fine sand and, (3) sand to mud. Types 1 and 2 are restricted to areas proximal to the mouth of the Agadir Canyon, whereas Type 3 grain-size breaks are found almost everywhere across the basin.

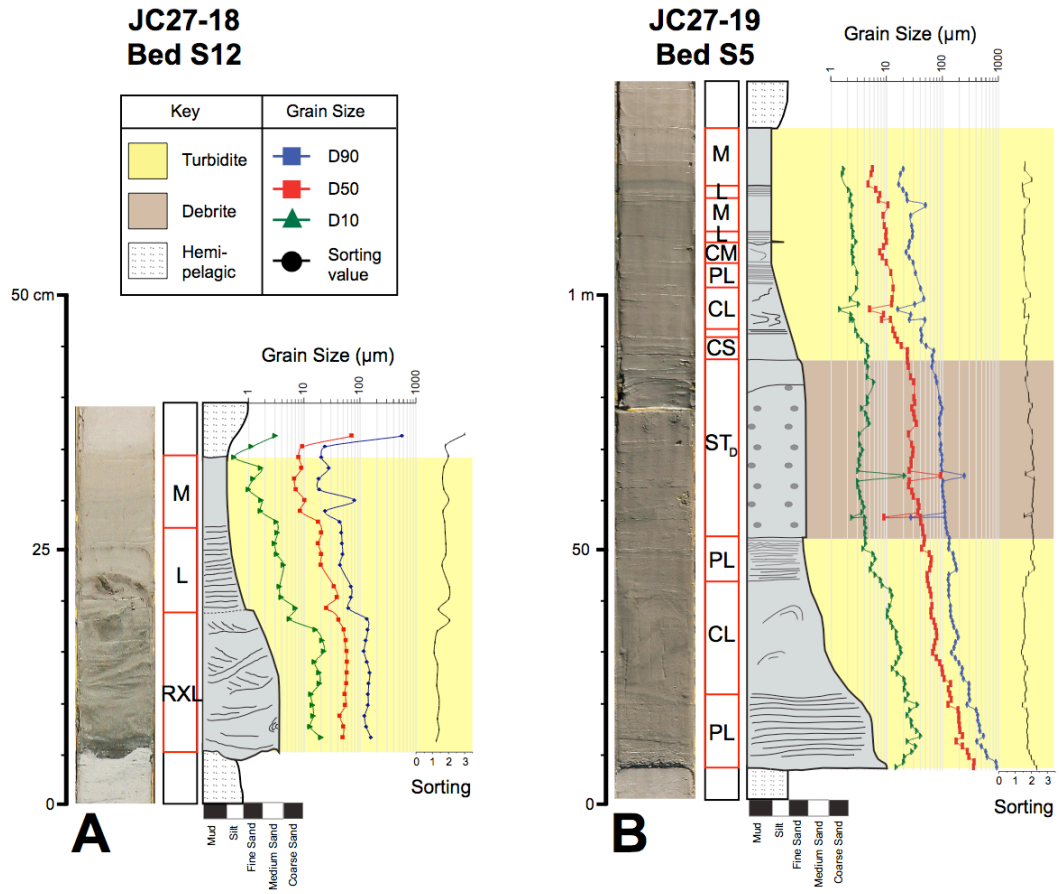

Figure 3-5: Examples of facies found within turbidite beds across the Seine Abyssal Plain. Each bed has a detailed visual log (light grey) accompanied by: a core photograph, facies interpretation, and quantitative grain-size analysis ~ every 1 cm through the deposit. Refer to Figure 2-2 for Key to facies codes. Note 'clean sand' and 'turbidite mud' deposits are highlighted in yellow whilst 'mud-rich sand' deposits are highlighted in brown.

3.4.4 Dating and correlation of hemipelagic sediment

Coccolith biolithostratigraphy was used to date hemipelagic sediments within the cores. In addition, cores CD166-12, D11940 and D13074 were also dated using bulk oxygen isotope analysis, providing a means to link coccolith biolithostratigraphy to ages of oxygen isotope stage boundaries (Weaver and Kuijpers, 1983). To validate this method, radiocarbon ages were obtained from hemipelagic sediments found within the upper parts of cores JC27-19 and 20. Radiocarbon ages show good agreement with ages determined from coccolith biostratigraphy and oxygen isotope analysis (Figure 3-6). By dating lithological changes in

hemipelagic sediment up to nine chronostratigraphic horizons can be identified between oxygen isotope stages 1 – 10 (i.e. ~ 350 ka; Lisiecki and Raymo, 2005). These horizons are correlated between core sites producing a high-resolution, chronostratigraphic framework that is extended across the Agadir Basin, Casablanca Sill and Seine Abyssal Plain (Figure 3-7 and Figure 3-8). However, not all cores record the same changes in hemipelagic lithology over the past 350 ka. Indeed, some cores proximal to the African Shelf do not show significant changes in hemipelagic sediment at all (e.g. JC27-20; Figure 3-8). Without distinct lithological changes, coccolith biostratigraphy alone only provides 4 chronostratigraphic horizons in these areas. Hence, the resolution of the age model is reduced in certain parts of the basin.

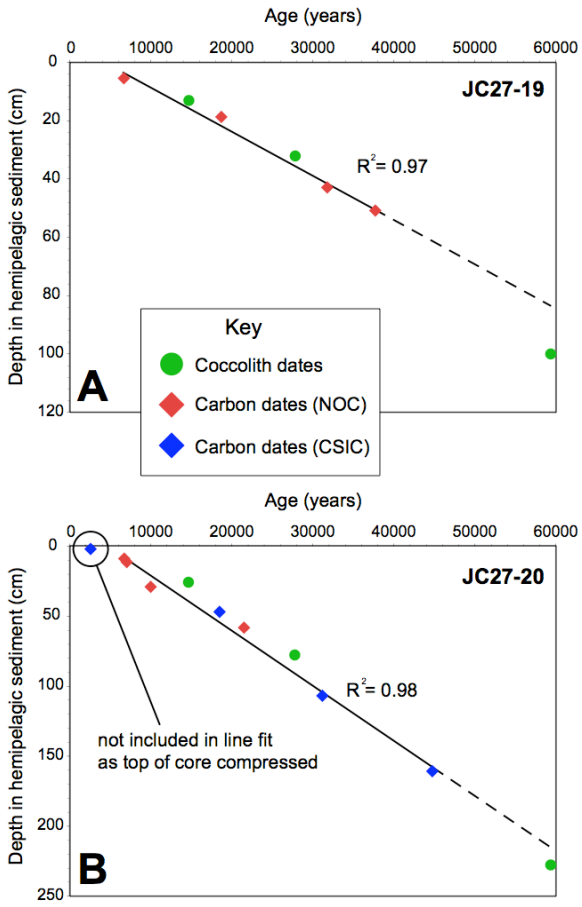

Figure 3-6: Radiocarbon ages down core for sites JC27-19 (A) and JC27-20 (B). Lines of best fit are shown through this data and projected sedimentation rates are extended with dashed black lines. Note the lines of best fit do not intercept at 0. This is because the tops of the cores are compressed, e.g. (B). Dates determined via coccolith biolithostratigraphy are overlain on the radiocarbon data. These data are not included in the regression but show good agreement with ages obtained from radiocarbon dating methods.

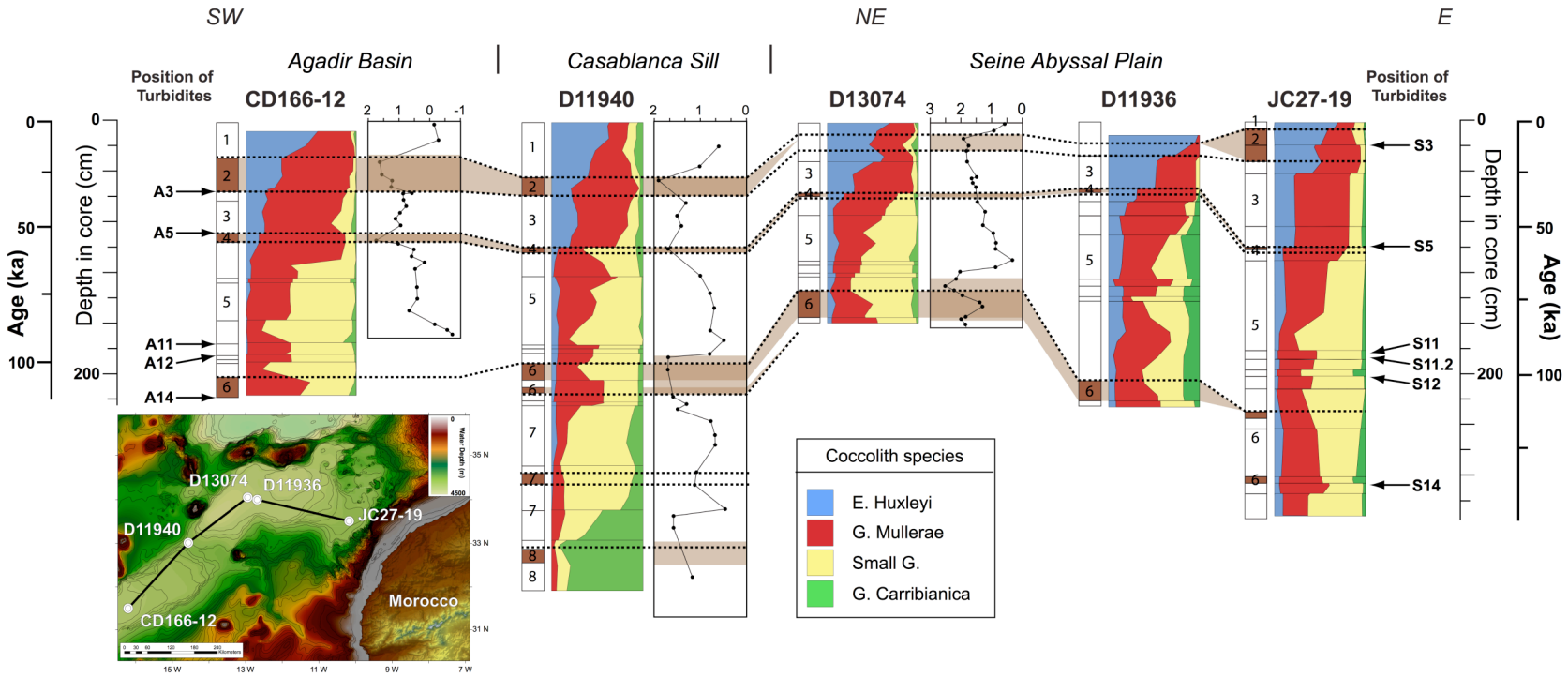

Figure 3-7: Chronostratigraphic framework of hemipelagic sediments across the Agadir Basin, Casablanca Sill and Seine Abyssal Plain. Inset map shows position of cores along the transect. Each core site has turbidite sediments removed leaving just hemipelagic material that is highlighted white for carbonate ooze (interglacial) and brown for marl (glacial). Coccolith biostratigraphy is illustrated for each core by the coloured columns. In addition, cores CD166-12, D11940 and D13074 show down core bulk oxygen isotope profiles. Black dashed lines denote correlated horizons of the same age. The stratigraphic positions of basin-wide turbidites are highlighted on cores CD166-12 (Agadir Basin) and JC27-19 (Seine Abyssal Plain).

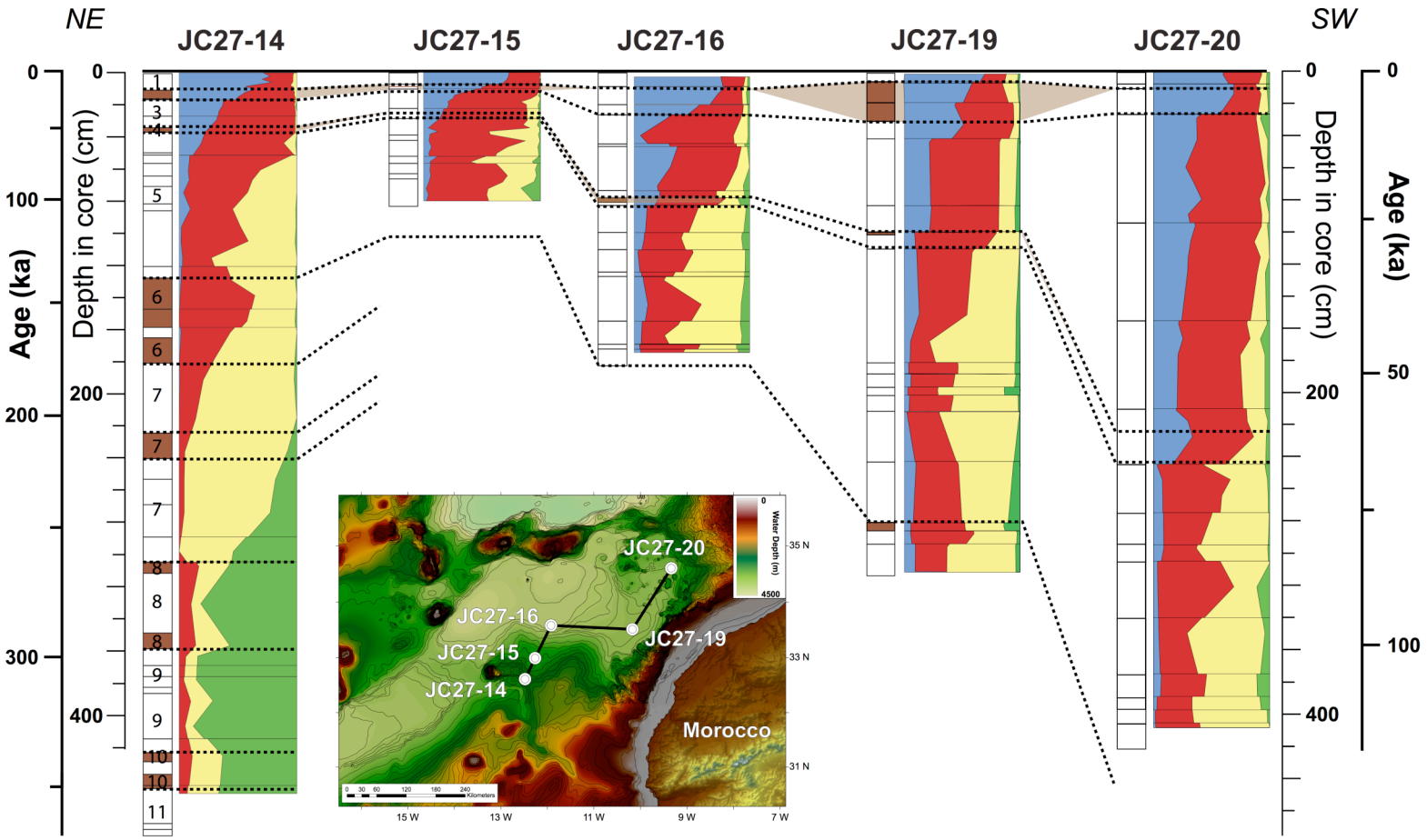

Figure 3-8: Chronostratigraphic framework of hemipelagic sediments across the Seine Abyssal Plain, from the crest of the Agadir Canyon to the mouth of the Rharb Canyon. Inset map shows the position of the cores and transect. Each core site has turbidite sediments removed, leaving just hemipelagic material that is highlighted white for carbonate ooze (interglacial) and brown for marl (glacial). Coccolith biostratigraphy is illustrated for each core by the coloured columns. Black dashed lines denote correlated horizons of the same age.

The chronostratigraphic framework reveals variation in hemipelagic sedimentation rates spatially and temporally (down core) across the Seine Abyssal Plain (Figure 3-9). Down core sedimentation rates are stepped with significantly reduced sedimentation within glacial intervals. This trend is not as strong proximal to the African margin, which has relatively constant rates of sedimentation over the past ~ 100 ka (e.g. JC27-20; Figure 3-9A). Sedimentation rates are also spatially variable across the Seine Abyssal Plain. Within the western-central parts of the basin sedimentation rates are relatively low (~ 8 cm per 10 ka). East, towards the continental margin, sedimentation rates progressively increase up to 2.7 cm/kyr. Hemipelagic sedimentation rates are high at the southern and western margins of the basin (1.4 cm/kyr), when compared to the centre of the basin.

Distinguishing horizons between hemipelagic sediments is difficult because changes in lithology are gradational; this introduces error into the biolithostratigraphic method. This effect causes a maximum error of ± 4800 years based on the range in potential positions of the most gradational contact and the minimum measured sedimentation rate (0.8 cm/kyr; Figure 3-9B).

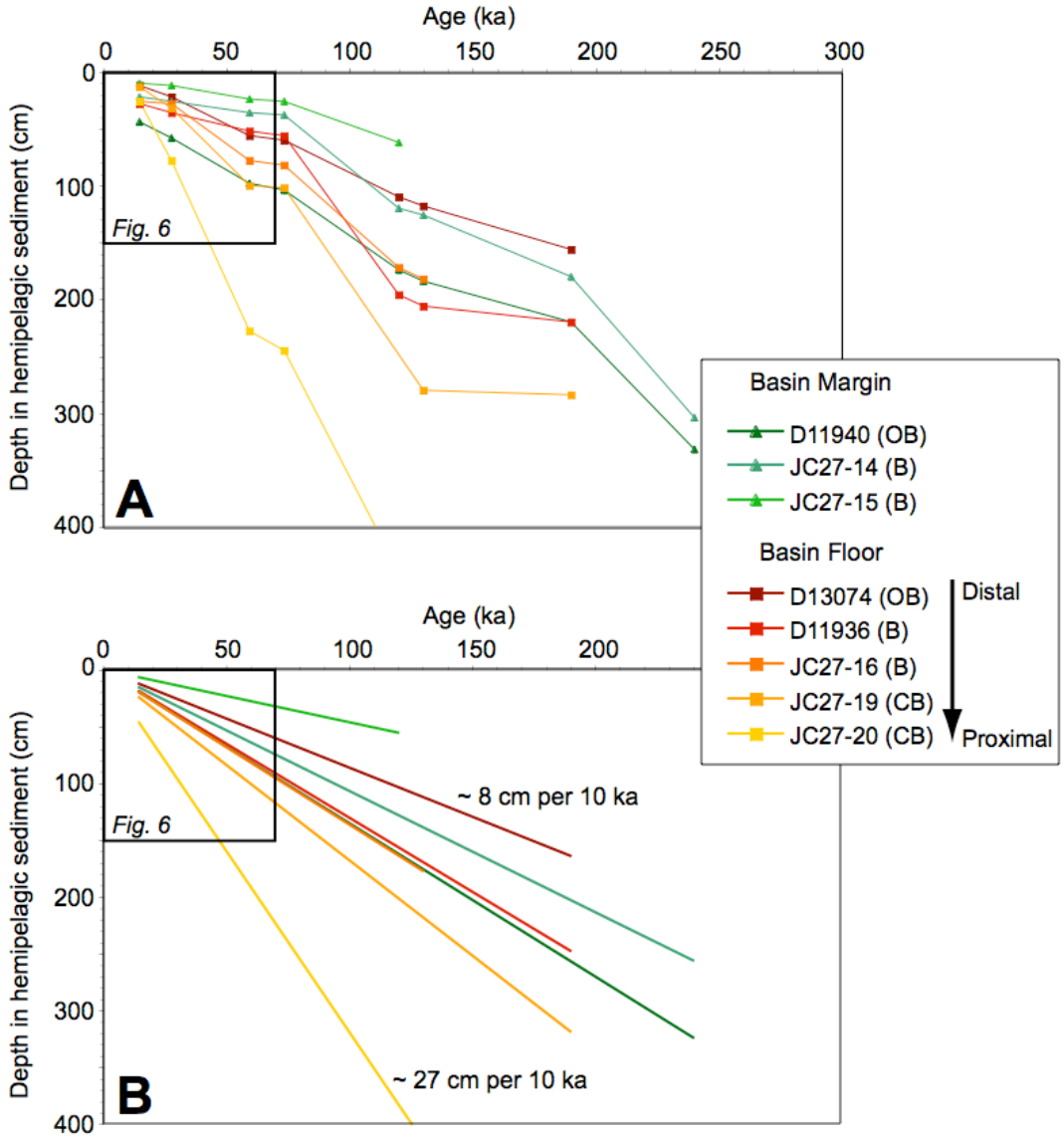

Figure 3-9: Sedimentation rates as determined via high-resolution coccolith biolithostratigraphy for cores across the Seine Abyssal Plain. Core sites are coloured according to their position across the basin; greens represent basin margin sites whilst reds represent sites within the centre of the basin. Within these colour schemes dark and light tones highlight whether a site is relatively distal or proximal to the continental margin, respectively. (B) Shows lines of best fit through the data. The inset shows dating methods applied to each core site: (O) for bulk oxygen isotope analysis, (B) for coccolith biostratigraphy, and (C) for radiocarbon dating. (A) Shows horizons dated down core across the basin. Note the stepped sedimentation rates in every down core profile and the significant increase in sedimentation rates towards the continental margin.

3.4.5 Individual turbidite bed correlation

A robust geochemical and chronostratigraphic framework has been established across the Moroccan Turbidite System from:

- High-resolution coccolith biostratigraphy and down core oxygen isotope analysis of hemipelagic sediment, which provides an age model to ~ 400 ka (Weaver and Kuijpers, 1983; Davies et al., 1997; Wynn et al., 2002b).
- Detailed geochemical analysis of large-volume volcanoclastic turbidites, which provides aerially extensive marker beds (de Lange et al., 1987; Pearce and Jarvis, 1992; Pearce and Jarvis, 1995; Wynn et al., 2002b; Hunt et al., 2011).
- Analysis of coccolith assemblages within turbidite mud caps, which provides a biological fingerprint of individual turbidite events and their erosional history (Weaver and Thomson, 1993; Weaver, 1994; Wynn et al., 2002b).
- The colour and relative position of turbidite beds within the stratigraphy

The above methods have been used to correlate individual turbidite beds across the Seine Abyssal Plain (Figure 3-10, Figure 3-11, Figure 3-12, and Figure 3-13), and also between the Seine Abyssal Plain and the Agadir Basin (Figure 3-14). Turbidites are numbered sequentially down core, using the nomenclature adopted by Wynn et al. (2002b) for the Agadir Basin. Prefixes are used to denote in which basin the beds occur: ‘A’ for Agadir Basin and ‘S’ for Seine Abyssal Plain. The prefix ‘R’ is used for beds that are restricted to the northeastern parts of the Seine Abyssal Plain, close to the mouth of the Rharb Canyon. Integrating turbidite stratigraphy across these three areas of seafloor provides a total of 58 individual beds, of which only five extend across both the Seine Abyssal Plain and Agadir Basin (Table 3-1).

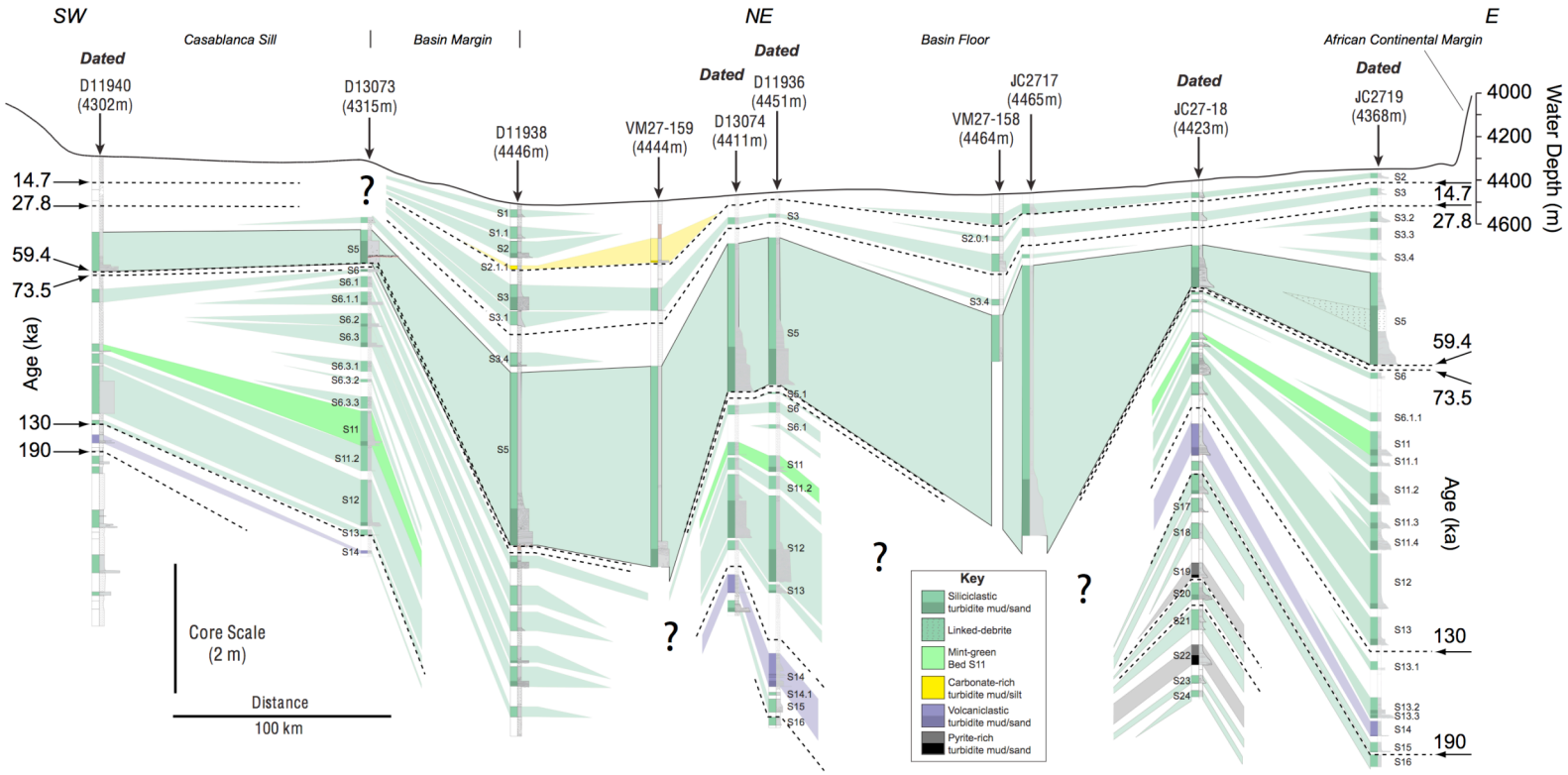

Figure 3-10: Core correlation (Transect 1) through the axis of the Seine Abyssal Plain, extending from the Casablanca Sill to the base of the continental margin (see Fig. 1B for location of transect). Cores are hung from vertically exaggerated seafloor topography (~ 125 times) and comprise a lithological column and visual log. Datums are marked between cores with dashed black lines and dated cores are labelled. Key marker beds comprise: volcanoclastic Bed S14 (purple shading), mint-green organic-rich Bed S11 (bright green shading), and the largest volume event Bed S5 (heavy black outline). Note the increased thickness of turbidite muds within the topographic low points across the basin.

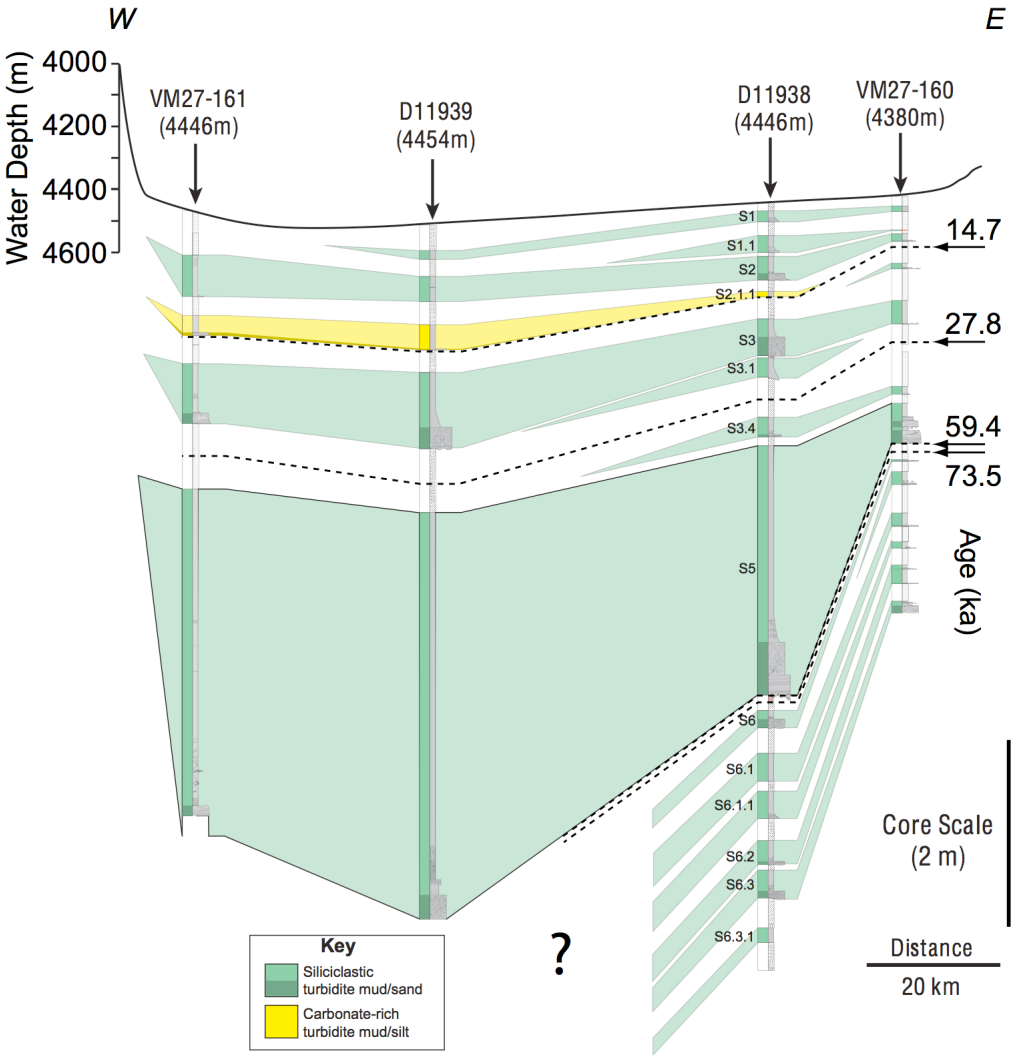

Figure 3-11: Core correlation (Transect 2), across the southwestern part of the Seine Abyssal Plain, extending from the Unicorn Seamount up the southern basin margin (see Fig. 1B for location of transect). Cores are hung from exaggerated seafloor topography (~ 50 times) and comprise a lithological column and visual log. Datums are marked between cores with dashed black lines and dated cores are labelled. The largest volume event, Bed S5, is highlighted with a heavy black outline. Note the increased thickness of turbidite mud in the topographic low point.

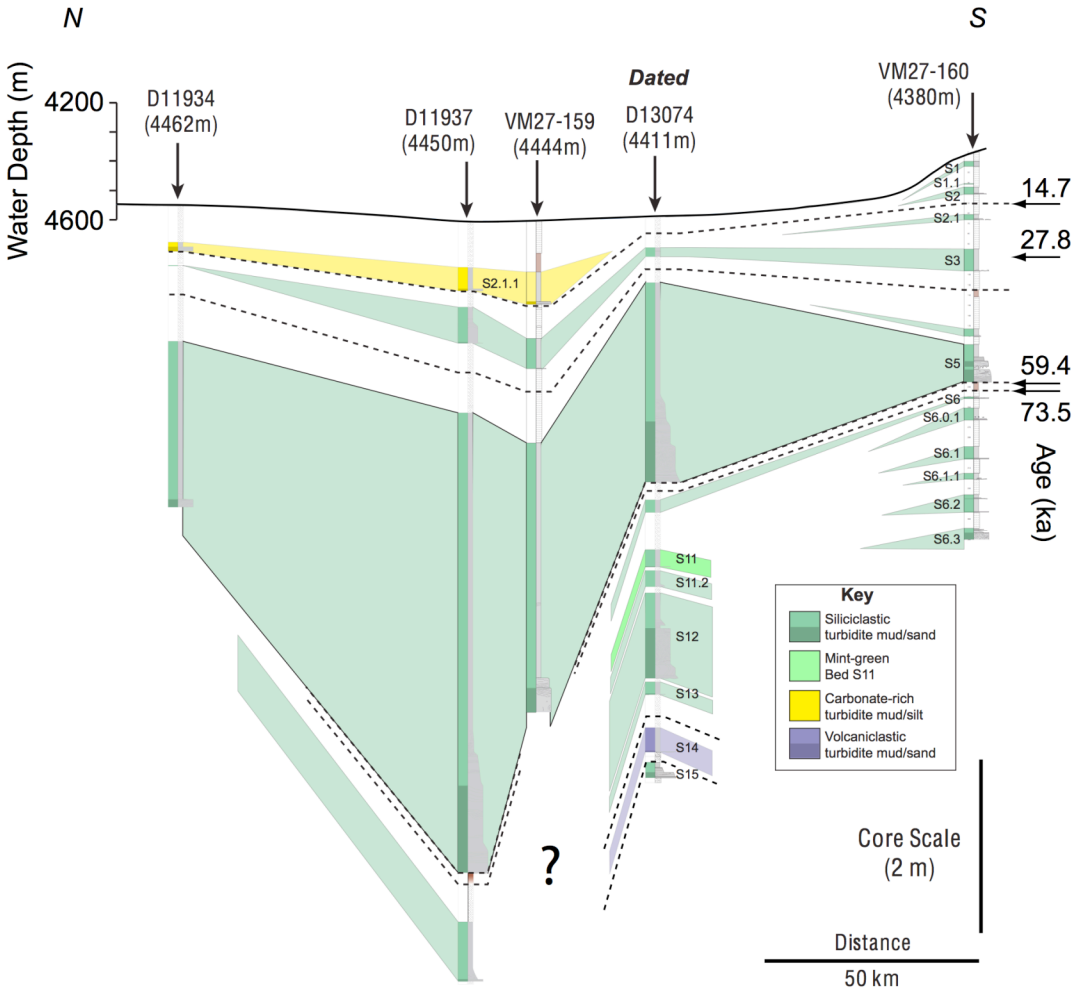

Figure 3-12: Core correlation (Transect 3), across the western part of the Seine Abyssal Plain, extending from the Ampere Seamount to the southern basin margin (see Fig. 1B for location of transect). Cores are hung from exaggerated seafloor topography and comprise a lithological column and visual log. Datums are marked between cores with dashed black lines and dated cores are labelled. Key marker beds comprise: volcanoclastic Bed S14 (purple shading), mint-green organic-rich Bed S11 (bright green shading), and the largest volume event Bed S5 (heavy black outline). Note the increased thickness of turbidite muds within the topographic low points across the basin.

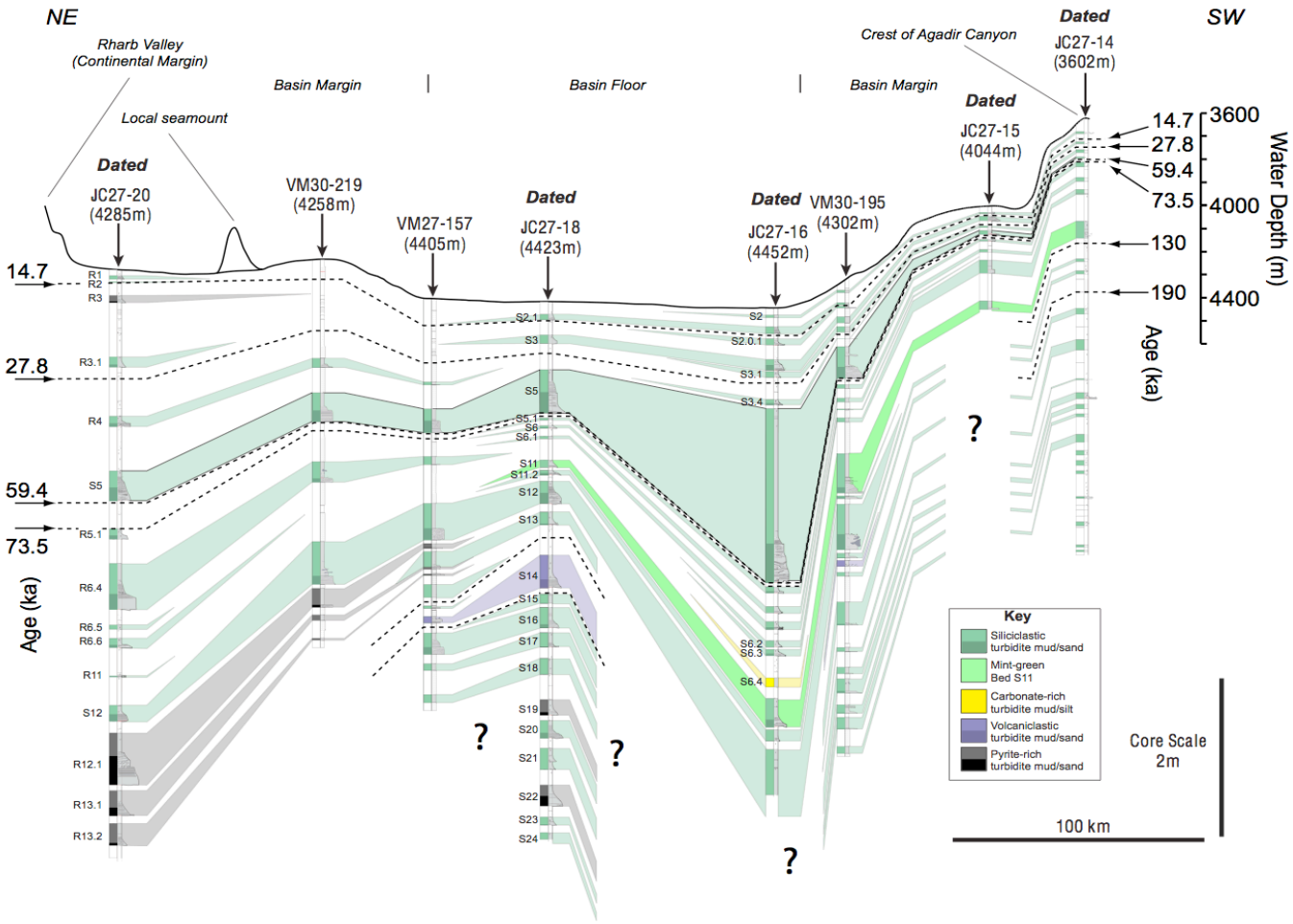
NE
SW
Rharb Valley
(Continental Margin)
Local seamount
Basin Margin
Basin Floor
Basin Margin
Crest of Agadir Canyon
Dated
JC27-20
(4285m)
VM30-219
(4258m)
VM27-157
(4405m)
Dated
JC27-18
(4423m)
Dated
JC27-16
(4452m)
VM30-195
(4302m)
Dated
JC27-15
(4044m)
Dated
JC27-14
(3602m)
14.7
27.8
59.4
73.5
130
190
3600
4000
4400
Water Depth (m)
Age (ka)
Key
Siliciclastic turbidite mud/sand
Mint-green Bed S11
Carbonate-rich turbidite mud/silt
Volcaniclastic turbidite mud/sand
Pyrite-rich turbidite mud/sand
Core Scale
2m
100 km

Figure 3-13: Core correlation (Transect 4), across the central part of the Seine Abyssal Plain, extending from the crest of the Agadir Canyon to the mouth of the Rharb Canyon (see Fig. 1B for location of transect). Cores are hung from exaggerated seafloor topography and comprise a lithological column and visual log. Datums are marked between cores with dashed black lines and dated cores are labelled. Key marker beds comprise: volcanoclastic Bed S14 (purple shading), mint-green organic-rich Bed S11 (bright green shading), and the largest volume event Bed S5 (heavy black outline). Note the increased thickness of turbidite muds within the topographic low points across the basin.

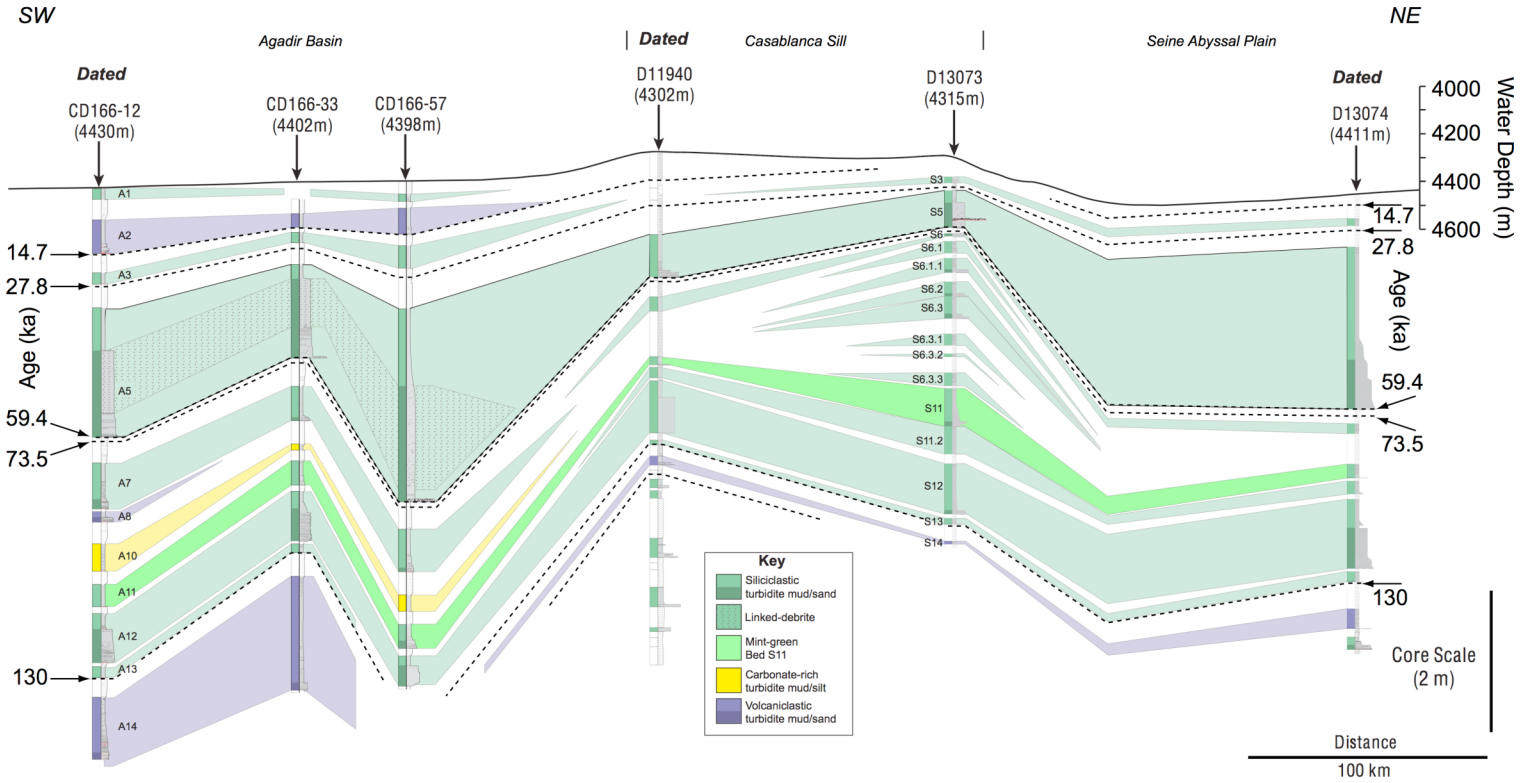

Figure 3-14: Core correlation (Transect 5), between the Agadir Basin and Seine Abyssal Plain, extending from the SW Agadir Basin across the Casablanca Sill and into the western part of the Seine Abyssal Plain (see Fig. 1B for location of transect). Cores are hung from exaggerated seafloor topography and comprise a lithological column and visual log. Datums are marked between cores with dashed black lines and dated cores are labelled. Key marker beds comprise: volcanoclastic Beds A2, A8 and A14/S14 (purple shading), mint-green organic-rich Bed S11 (bright green shading), and the largest volume event Bed S5 (heavy black outline). Note the interconnected stratigraphy with some turbidite beds extending across both basins.

Agadir Basin				Seine Abyssal Plain				Rharb Canyon (NE Seine Abyssal Plain)						
Bed	Volume (km^3)	Max thickness (cm)	Max grain size (D90 µm)	Bed	Volume (km^3)	Max thickness (cm)	Max grain size (D90 µm)	Bed	Volume (km^3)	Max thickness (cm)	Max grain size (D90 µm)	Type	Provenance	Age ± 5000 years (ka)
A1	< 1	60	47									Siliciclastic	Sahara slide headwall	1
				S1	0.5	10	71					Siliciclastic	African Margin	2.8
				S1.1	0.5	16	(63)					Siliciclastic	African Margin	5.5
				S2	1	22	210					Siliciclastic	African Margin	6.7 (C)
								R1	< 0.5	5	(80)	Siliciclastic	African Margin, Rharb Canyon	6.8 (C)
								R2	<< 0.5	2	(< 63)	Siliciclastic	African Margin, Rharb Canyon	7.1 (C)
								R3	< 0.5	9	125	Pyrite-rich	African Margin, Rharb Canyon	10 (C)
				S2.1	1	6	(63)					Siliciclastic	African Margin	13

				S2.1.1	2.5	23	(187)					Carbonate-rich	Local seamount	14.7
A2	5	49	330									Volcanoclastic	El Hierro, Canary Islands	14.7
A3	4.5	62	468	S3	8	33	167					Siliciclastic	African Margin	18.7 (C)
				3.1	1	13	(63)					Siliciclastic	African Margin	23.9
								R3.1	< 0.5	12	(63)	Siliciclastic	African Margin, Rharb Canyon	28
				S3.2	< 1	34	300					Siliciclastic	African Margin	31.8 (C)
				S3.3	< 1	13	(< 63)					Siliciclastic	African Margin	41.8
								R4	< 3	14	(187)	Siliciclastic	African Margin, Rharb Canyon	44 (C)
				S3.4	1.5	18	(187)					Siliciclastic	African Margin	54.4
A5	21.6	327	1000	S5	100	452	920					Siliciclastic	African Margin	59.4
				S5.1	0.1	8	(130)					Siliciclastic	African Margin	74
								R5.1	?	14	(130)	Siliciclastic	African Margin, Rharb Canyon	74

				S6	5	17	(187)					Siliciclastic	African Margin	75
				S6.1	1	19	(125)					Siliciclastic	African Margin	78
				S6.1.1	1	18	(250)					Siliciclastic	African Margin	81
								R6.4	2	58	814	Siliciclastic	African Margin, Rharb Canyon	82
A7	9.5	71	210									Siliciclastic	African Margin/SE Agadir Margin	85.7
								R6.5	<< 0.5	5	(< 63)	Siliciclastic	African Margin, Rharb Canyon	87
A8	> 2.5	> 54	380									Volcanoclastic	Madeira Archipelago	88
				S6.2	1	16	(250)					Siliciclastic	African Margin	88
				S6.3	1	25	(250)					Siliciclastic	African Margin	89
								R6.6	< 1	13	(210)	Siliciclastic	African Margin, Rharb Canyon	90
								R11	<< 0.5	1	(125)	Siliciclastic	African Margin, Rharb Canyon	100
				S6.3.1	< 0.5	14	(<63)					Siliciclastic	African Margin	100

				S6.3.2	< 0.5	4	(<63)					Siliciclastic	African Margin	106
A10	4.5	43	143									Carbonate-rich	SE Agadir Margin	108
				S6.3.3	< 0.5	16	(<63)					Siliciclastic	African Margin	119
A11	7.5	87	760	S11	8	46	403					Siliciclastic	African Margin	120
				S11.1	0.5	14	(360)					Siliciclastic	African Margin	120
				S11.2	5	45	632					Siliciclastic	African Margin	122
				S11.3	0.5	23	(200)					Siliciclastic	African Margin	124
				S11.4	0.5	29	(230)					Siliciclastic	African Margin	124
A12	9.1	> 69	378	S12	30	113	324					Siliciclastic	African Margin	126
								R12.1	< 3	65	750	Pyrite-rich	African Margin, Rharb Canyon	128
								R13.1	< 3	31	154	Pyrite-rich	African Margin, Rharb Canyon	129
								R13.2	< 3	28	(130)	Pyrite-rich	African Margin, Rharb Canyon	129
A13	> 2	17	(< 63)	S13	11	37	632					Siliciclastic	African Margin	130

				S13.1	<< 0.5	1	(125)					Siliciclastic	African Margin	147
				S13.2	0.5	22	(140)					Siliciclastic	African Margin	165
				S13.3	0.5	5	(280)					Siliciclastic	African Margin	165
A14	35.8	> 165	330	S14	15	44	208					Volcanoclastic	Tenerife, Canary Islands	168
				S15	4	15	(250)					Siliciclastic	African Margin	180
				S16	4	25	(130)					Siliciclastic	African Margin	190
				S17	?	17	(130)					Siliciclastic	African Margin	192
				S18	?	20	(< 63)					Siliciclastic	African Margin	200
				S19	?	18	(135)					Pyrite-rich	African Margin, Rharb Canyon	216
				S20	?	23	(210)					Siliciclastic	African Margin	223
				S21	?	26	(80)					Siliciclastic	African Margin	240
				S22	?	26	(220)					Pyrite-rich	African Margin, Rharb Canyon	248
				S23	?	10	(125)					Siliciclastic	African Margin	253

Table 3-1: Table listing all turbidite beds found within the Agadir Basin, Seine Abyssal Plain and NE parts of the Seine Abyssal Plain. Each area has an individual turbidite stratigraphy. However, some beds correlate across multiple areas, highlighted in light grey. The maximum thickness, grain size and estimated volume is listed for each area in which a bed is found. Grain size was measured quantitatively using a Malvern Mastersizer (see methods) or determined visually by comparison with a grain-size comparator card. Grain sizes determined visually are in brackets. Bed volumes are revised from previous estimates by Wynn et al. (2002b) and Frenz et al. (2008). All turbidite beds are ordered sequentially by age from ~ 1 to 260 ka. Ages are determined via coccolith biolithostratigraphy and have errors of ~ ±5000 years. Relatively young turbidite beds whose age of emplacement was determined from radiocarbon dating are marked with (C).

3.4.6 Frequency of turbidite events

The margins of the Seine Abyssal Plain have the highest frequency of events (with a mean of 1 turbidite every 9000 years), whilst the central parts of the basin have a lower frequency of events (with a mean of 1 turbidite every 15, 000 years; Figure 3-15A). Integrating turbidite stratigraphy from all areas of the Seine Abyssal Plain and Agadir Basin provides 58 dated beds occurring over the past ~ 260, 000 years (Figure 3-15B). This area integrated stratigraphy has three periods that have a higher frequency of turbidite events compared to the average: ~ 0 – 15 ka, ~ 70 – 90 ka and, ~ 115 – 130 ka (Figure 3-16).

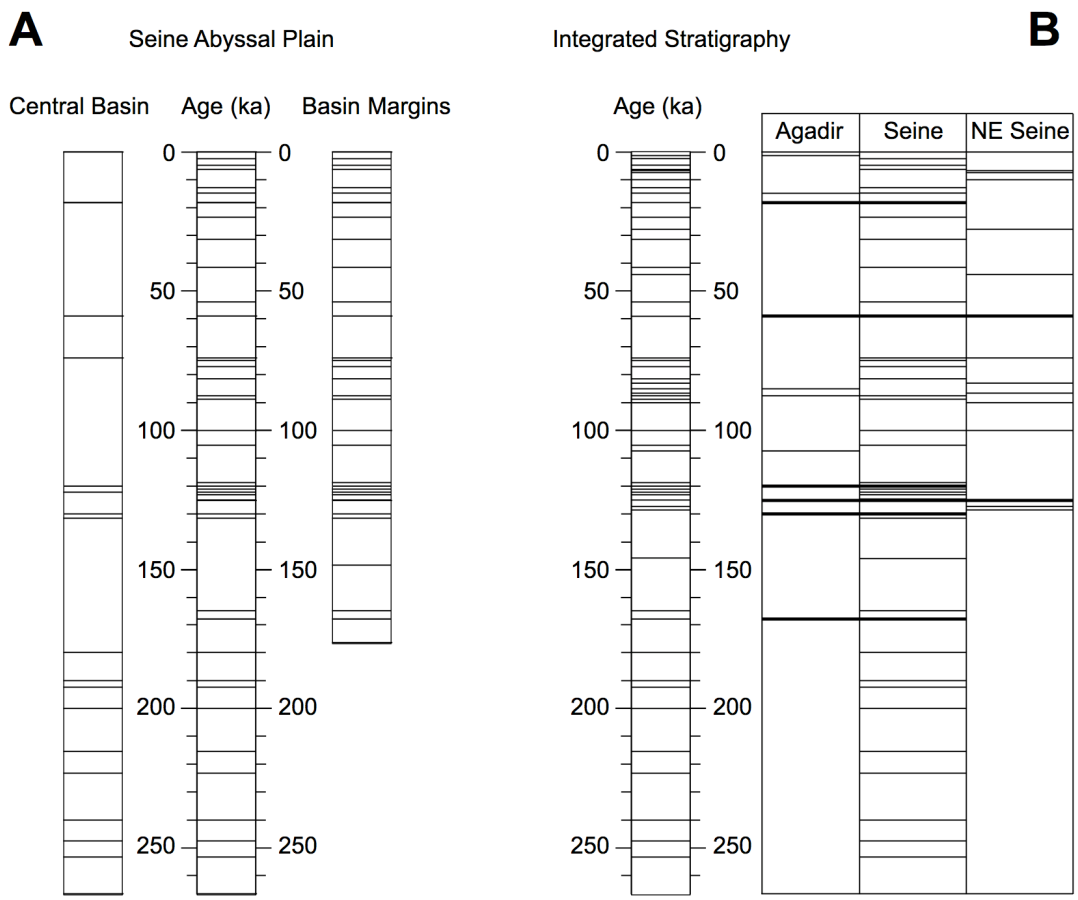

Figure 3-15: Turbidite stratigraphy in different areas of the Seine Abyssal Plain and Agadir Basin. Vertical columns represent dated hemipelagic sequences with turbidite beds removed. The stratigraphic position where turbidites occur is marked on the hemipelagic sequences as horizontal black lines. (A) Shows turbidite stratigraphy within different parts of the Seine Abyssal Plain, central parts of the basin (left) and basin margins (right). An area integrated pseudo core site combines both of these turbidite stratigraphies (centre). (B) Shows an area integrated pseudo core site (left) combining turbidite stratigraphy from: the Agadir Basin, Seine Abyssal Plain, and Rharb Canyon (NE Seine Abyssal Plain). Beds that correlate across multiple areas are marked with thick black lines.

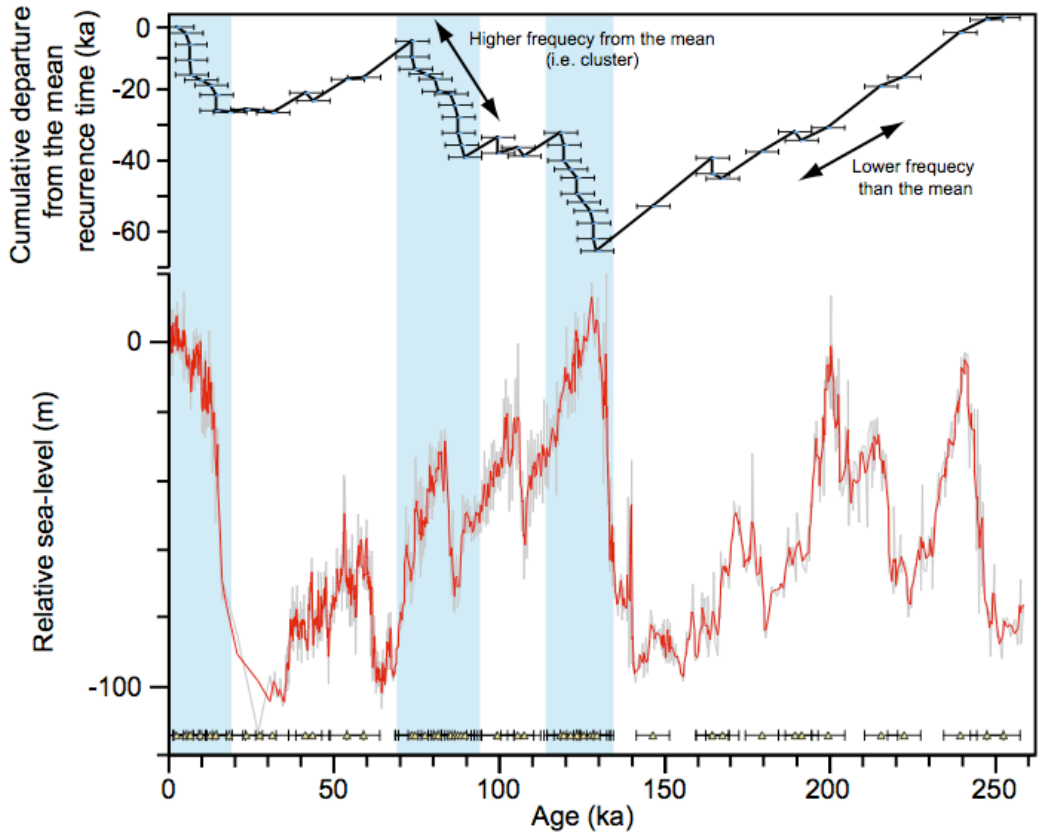

Figure 3-16: Composite graph showing frequency of turbidite events over the past ~260ka. Turbidite events are marked at the bottom of the graph with yellow triangles, errors are ~ ± 5000 years. Relative sea-level changes over the past ~ 260 ka are shown with a red line (Rohling et al., 2009). Recurrence times of each turbidite are plotted successively as a cumulative departure from the mean recurrence time (black line). The slope of this graph shows whether successive beds have recurrence times higher than the mean (i.e. clustering) or lower than the mean. Three clusters of turbidite beds are highlighted in blue (including error).

3.4.7 Bed geometries and facies of turbidites across the Seine Abyssal Plain

Correlations of individual turbidite beds are shown in (Figure 3-10, Figure 3-11, Figure 3-12, Figure 3-13, and Figure 3-14). In general, two types of turbidite are identified: (1) large-volume beds > 5 km^3 that extend across the entire basin, and (2) small-volume beds < 5 km^3 that are restricted to the basin margins. The geometries and facies of turbidite beds vary significantly across the basin.

Turbidites in the southwestern parts of the Seine Abyssal Plain are generally thin with structureless basal sands (~ 5 – 10 cm thick), overlain by a sharp grain-size break, in turn overlain by ungraded, structureless mud (~ 5 – 20 cm thick). A large proportion of these beds are small-volume and pinch out over relatively short (< 50 km) distances. Larger volume beds extend into the central parts of the basin.

Turbidite stratigraphy within the central parts of the Seine Abyssal Plain comprises: relatively thick (~ 45 – 80 cm) sandy beds overlain by thick mud caps (~ 35 – 115 cm), and fine-grained thin beds (~ 5 – 20 cm thick). Turbidite mud caps are thickest in topographic low points, particularly at site JC27-17 (Figure 3-10). These thick ponded mud caps have normally graded bases, often with contorted lamination, and progress upwards into ungraded, structureless mud (e.g. core D11939; Figure 3-11).

The southern basin margin is described in four zones: (1) the margin of the Agadir Canyon, (2) the Safi Plateau, (3) the basin margin, and (4) the basin floor (Figure 3-13). Turbidites situated upon the margin of the Agadir Canyon are all strongly bioturbated, ~ 1 – 10 cm thick traces of turbidite mud. Turbidites located on the Safi Plateau are mostly thin (3 – 7 cm) sand deposits, occasionally overlain by thin (1 – 10 cm) strongly bioturbated turbidite muds. Turbidites situated at the base of the southern margin are similar, with thin sand overlain by thin mud (~ 5 – 20 cm thick). However, Bed S5 is significantly thicker and coarser, comprising ~ 45 cm of ripple cross-laminated sand overlain by 170 cm of structureless turbidite mud. The thin beds found on the margin generally pinch out to the north, away from the basin margin, whilst thicker deposits (e.g. Bed S5) typically extend across the entire basin.

3.4.8 Spatial grain-size trends of individual turbidites

Relatively small volume turbidites (< 5 km^3) have deposits that fine away from the basin margins and pinch out before reaching the central parts of the basin. However, large-volume turbidites (> 5 km^3) that extend across the entire basin have a range of fining patterns. Indeed, most of the large-volume events have more than one fining pattern (laterally) across the basin. The spatial distribution of grain sizes within basal sands is described below for individual beds, in order of increasing complexity.

Bed S11.2 has a relatively simple fining trend in grain size from east to west (Figure 3-17A). The coarsest deposits found are ~ 600 μm situated in the eastern parts of the basin. The bed progressively fines to the west and ultimately terminates as a silty mud (~ 20 μm) on the Casablanca Sill.

Bed S12 has relatively coarse deposits of ~ 400 μm sands, situated around the mouth of the Agadir Canyon (Figure 3-17B). These deposits fine (~ 140 μm) to the north across the Casablanca Sill, before reaching the Seine Abyssal Plain. Poor core penetration of this bed within the southwestern and southern parts of the basin means that grain-size distributions are unknown in these areas. Within central/western parts of the Seine Abyssal Plain Bed 12 has coarser deposits (~ 320 μm), compared to those found on the Casablanca Sill. Deposits in the central parts of the basin fine in a radial fashion to the north and the east.

Beds S3, S5 and S11 have three fining trends. One fining trend is from south to north but originates in two separate areas: the mouth of the Agadir Canyon fining (to the north) across the Casablanca Sill, and the Safi Plateau fining (to the north) across the southern basin margin. The second fining trend is from east to west and originates from the mouth of the El Jadida Canyon (Figure 3-17C, Figure 3-17D, and Figure 3-17E). This fining trend is similar to that found in Bed 11.2 (Figure 3-17A). These three fining trends from the Safi Plateau, and

mouths of the Agadir and El Jadida Canyons are combined across central and western parts of the basin floor.

Beds S3 and S11 have deposits across the Safi Plataeu that fine from south to the north. However, the deposits of Bed S5 situated on the Safi Plateau do not have a strong fining trend from south to north (Figure 3-17E). Rather, deposits are considerably finer grained (~ 160 μm) than those found across the basin floor (> 350 μm).

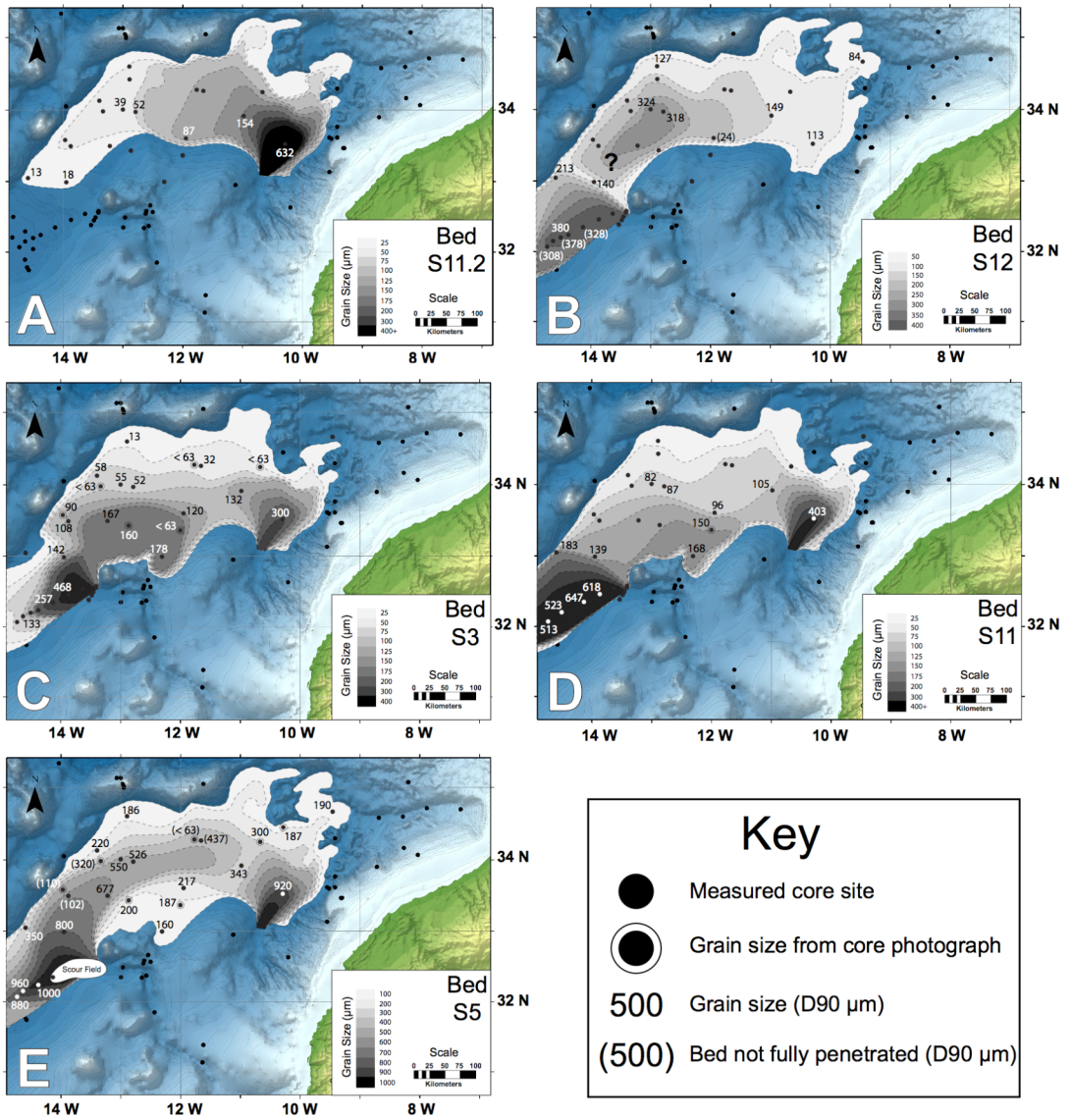

Figure 3-17: Isograms for individual turbidites across the Seine Abyssal Plain and NE parts of the Agadir Basin: (A) = Bed S11.2, (B) = Bed S12, (C) = Bed S3, (D) = Bed S11, and (E) = Bed S5. Note the variable grain-size scale between A, B, C, D and E. Black circles are core sites with adjacent numbers indicating the measured grain size (D90) for the basal sediment of a particular turbidite. Numbers with brackets denote sites where the core does not penetrate the base of the bed, thus the measured grain size is not the true basal part of the deposit and is likely to be coarser than that measured. Core sites where grain size was estimated from core photographs are shown as double ringed black circles. Isograms for Bed S12 (B) are difficult to interpret across the southwestern parts of the Seine abyssal Plain. This is due to poor core penetration into the bed within the southwestern parts of the basin and southern basin margin.

3.4.9 Coccolith mixtures within individual turbidites

Analyzing the assemblages of coccolith species within the mud caps of turbidites provides a means by which individual beds can be characterized. The mixture of coccoliths also provides insights into the erosional history of the parent flows. Here the mixture of coccoliths within individual beds is examined to understand the erosive history of the parent flows and whether they originated from single or multiple slope failures. Coccolith species were analyzed within the mud caps of large-volume (> 5km^3) organic-rich turbidites from the Seine Abyssal Plain and NE parts of the Agadir Basin. Overall, Beds S5, S11 and S11.2 have similar proportions of coccolith species, whereas Beds S3 and S12 have different abundances of these species (Figure 3-18). However, the proportions of coccoliths from the mud caps of individual beds can display considerable variability across the basins (Figure 3-19).

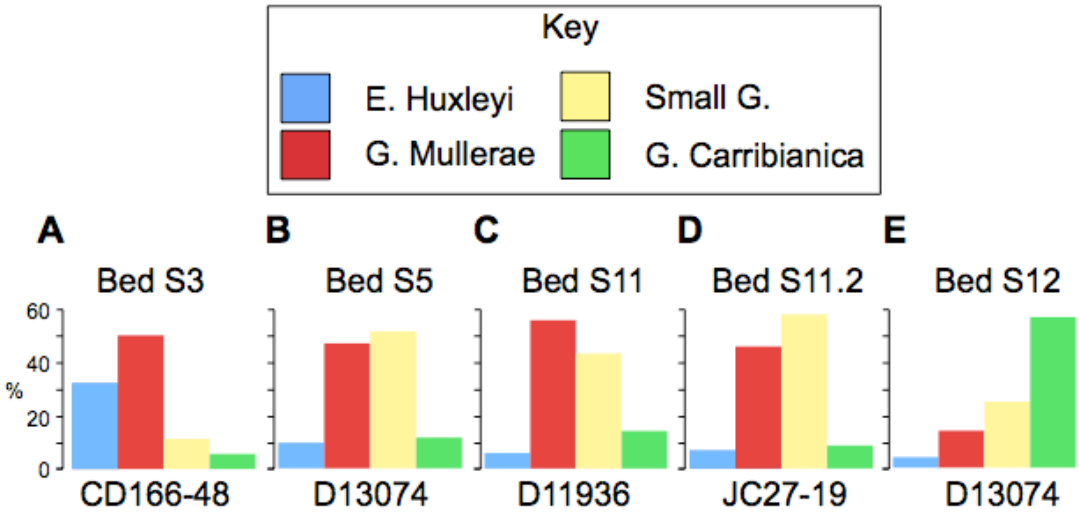

Figure 3-18: Histograms of different mixtures of coccoliths found in turbidites: Beds (A) S3, (B) S5, (C), S11, (D) S11.2 and (E) S12. Refer to Figure 3-1B for locations of cores. Note, Beds S5, S11 and S11.2 have similar mixtures of coccoliths, which are different from the mixtures of coccoliths found in Beds S3 and S12.

Bed S11.2 is the only large-volume turbidite in this study that has a consistent mixture of coccoliths across the depositional extent of the turbidite, i.e. within the Seine Abyssal Plain (Figure 3-19A). All other large-volume turbidites display spatial variability in their coccolith

mixtures across the basin. Bed S12 shows the least variability, with coccolith mixtures remaining similar across the NE Agadir Basin and western parts of the Seine Abyssal Plain (Figure 3-19B). The exception to this is a subtle change in the mixture of coccoliths along the south-central basin margin, where there is an increase in the abundance of both *Gephyrocapsa mullerae* and s*mall Gephyrocapsas*; and a decrease in the abundance of *Gephyrocapsa mullerae* in eastern parts of the basin .The mixtures of coccoliths found in Bed S11 show more spatial variability than Bed S12 (Figure 3-19C). Across the NE parts of the Agadir Basin and western parts of the Seine Abyssal Plain, the mixture of coccoliths in Bed S11 remains similar. However, within the eastern parts of the Seine Abyssal Plain there is a higher abundance of s*mall Gephyrocapsas* and *Gephyrocapsa carabianica*, compared with western parts of the basin. Deposits found across the Safi Plateau are different from those found across both western and eastern parts of the Seine Abyssal Plain. Here, mixtures of coccoliths are dominated by *Gephyrocapsa mullerae* and have very low abundances of *Emiliani huxleyi, small Gephyrocapsas* and *Gephyrocapsa carabianica* species.

The mixtures of coccoliths found in Bed S5 show the most spatial variability. The NE Agadir Basin has different mixtures of coccoliths to deposits situated on the Casablanca Sill with increased abundances of *Emiliani huxleyi, Gephyrocapsa carabianica* and *Pseudoemiliania lacunosa* (Figure 3-19D). Across the western parts of the Seine Abyssal Plain the mixture of coccoliths remains similar before changing in the eastern parts of the basin with *Gephyrocapsa mullerae* dominating the assemblage. Bed S5 is correlated beyond the southern basin margin onto the Safi Plateau. Deposits here (e.g. JC27-15) have significantly different mixtures of coccoliths compared to deposits found in other parts of the basin, comprising almost exclusively *Gephyrocapsa mullerae* (Figure 3-19D).

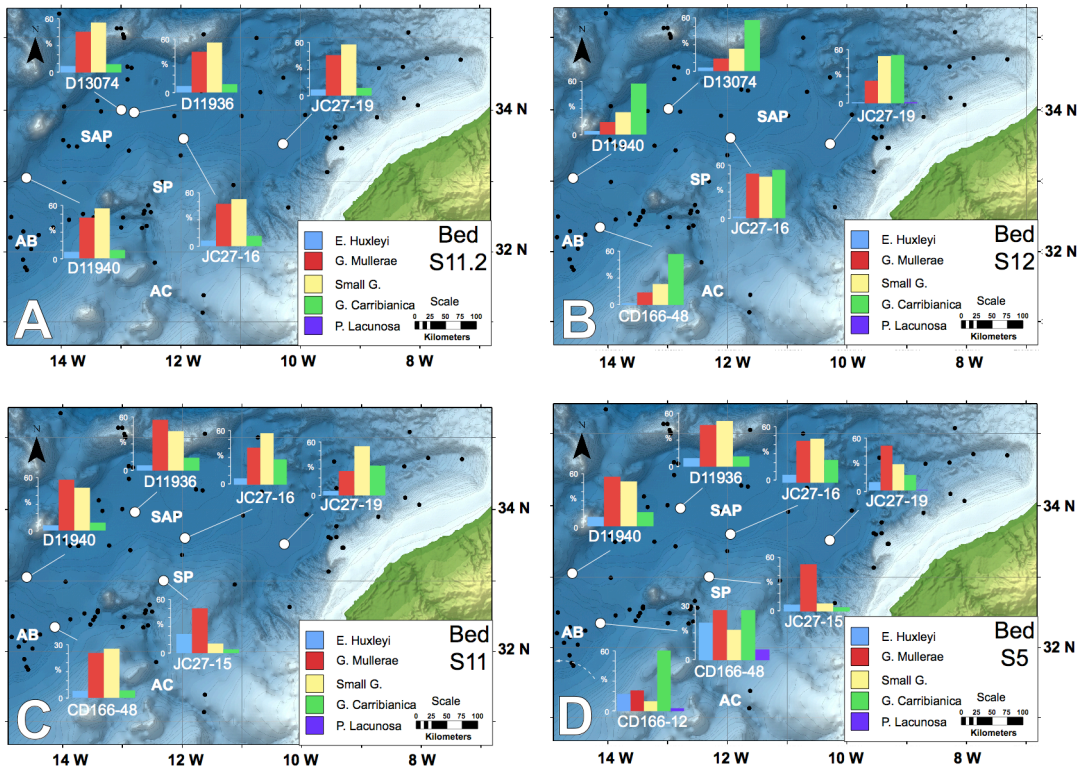

Figure 3-19: Spatial variability of coccolith mixtures within individual turbidite beds across the Seine Abyssal Plain and NE Agadir Basin. Histograms show mixtures of coccolith species at specific core sites, which are indicated via a white line and circle. Note that Bed S11.2 (A) is the only turbidite to have similar mixtures of coccolith species within its mud cap across its depositional extent (Seine Abyssal Plain). 'AC' = Agadir Canyon, 'AB' = Agadir Basin, 'SAP' = Seine Abyssal Plain and 'SP' = the Safi Plateau.

3.5 Interpretation of results

3.5.1 Provenance of turbidites within the Seine Abyssal Plain

Organic-rich turbidites - Significant amounts of glauconite and abundant shallow-water bivalves and benthic foraminifera suggest that organic-rich turbidites have a shallow-water, shelf source (Wynn et al., 2002b). However, it has been argued that the majority of glauconite and pyrite found on the continental shelf originates from Miocene age strata, which crops out along the outer shelf (Summerhayes et al., 1976). Miocene age strata that crop out on the outer shelf could also account for the significant proportion of sandstone lithics found in the turbidite beds. The evidence could be interpreted in two ways: 1) turbidites could have been sourced from greater water depths along the outer shelf, although this would not explain the abundance of shallow-water benthic species; 2) that turbidites were sourced from relatively shallow water and the parent flows were strongly erosive as they passed over the outer shelf, entraining Miocene age strata.

Volcanoclastic turbidites - Bed S14 has been linked to the Icod landslide, originating off Tenerife ~ 170 ka ago (Hunt et al., 2011). This is based on: 1) dating onshore landslide scarps via Kr-Ar and $^{40}Ar/^{39}Ar$ methods (~ 173 – 183 ka; Marti et al., 1994); 2) calculating the time for a 10 m hemipelagic sediment drape to accumulate over the Icod debris flow (170 ka; (Watts and Masson, 1995); 3) constraining the age of the distal turbidite from its position in oxygen isotope stage 6 using coccolith biolithostratigraphy and stable oxygen isotope analysis (~ 165 – 170 ka; Wynn et al., 2002b; Frenz et al., 2008; Stevenson et al., 2012); and 4) demonstrating that the phonolitic composition within Bed 14 is characteristic of Tenerife, and distinct from other volcanoclastic turbidites sourced from different volcanic islands in this region (de Lange et al., 1987; Pearce and Jarvis, 1992; Pearce and Jarvis, 1995; Hunt et al., 2011).

Carbonate-rich turbidites - Carbonate-rich turbidites are typically localized deposits, situated close to the basin margins and at the base of volcanic seamounts. Pelagic sediment draping

the relatively steep slopes of the Casablanca, Unicorn, Ampere and Corel Seamounts can become unstable and generate relatively small-scale slope failures. This explains the dominance of biogenic material within carbonate-rich turbidites, their small-volume and restricted area of deposition proximal to the base of the Casablanca and Ampere Seamounts.

Pyrite-rich turbidites - As with organic-rich turbidites, abundant shallow-water fauna and significant amounts of glauconite suggest a shallow-water, shelf source. However, significant amounts of pyrite, and indeed rare beds comprising almost 100 % pyrite, indicate an additional source that is distinct from other parts of the shelf. Pyrite is formed by the movement of oxidized, iron-bearing fluids across a reduction front. The reducing conditions result in the precipitation of iron sulphides from solution and the generation of pyrite. The Rharb Canyon is situated on a large thrust fault, which forms the southern boundary of the "Gulf of Cadiz Accretionary Wedge" (Medialdea et al., 2004). This major structure has the potential to facilitate and focus fluid flow, resulting in mineralization along the fault and/or precipitation of pyrite directly onto the seafloor (Moore et al., 1986). Pyrite deposits situated along the fault (i.e. along the northern wall of the Rharb Canyon) are likely to have been eroded by flows passing through the canyon. This is the most likely source of pyrite within pyrite-rich turbidites found across the northeastern parts of the Seine Abyssal Plain. This interpretation has similarities with the 'Red Dog' zinc-lead-silver deposit within the Western Brookes range, Alaska, where metal-bearing fluids are interpreted to have been focused along faults and vented directly onto the seafloor (Moore et al., 1986).

3.5.2 Flow pathways into the Seine Abyssal Plain

The grain-size distributions of organic-rich, carbonate-rich, pyrite-rich and volcanoclastic turbidites show five distinct fining trends across the Seine Abyssal Plain, originating from: (1) the southwest, (2) south, (3) the southeast, (4) the northeast, and (5) the northwest. From these fining trends and interpretation of provenance, we interpret five distinct flow pathways into and across the Seine Abyssal Plain (Figure 3-20).

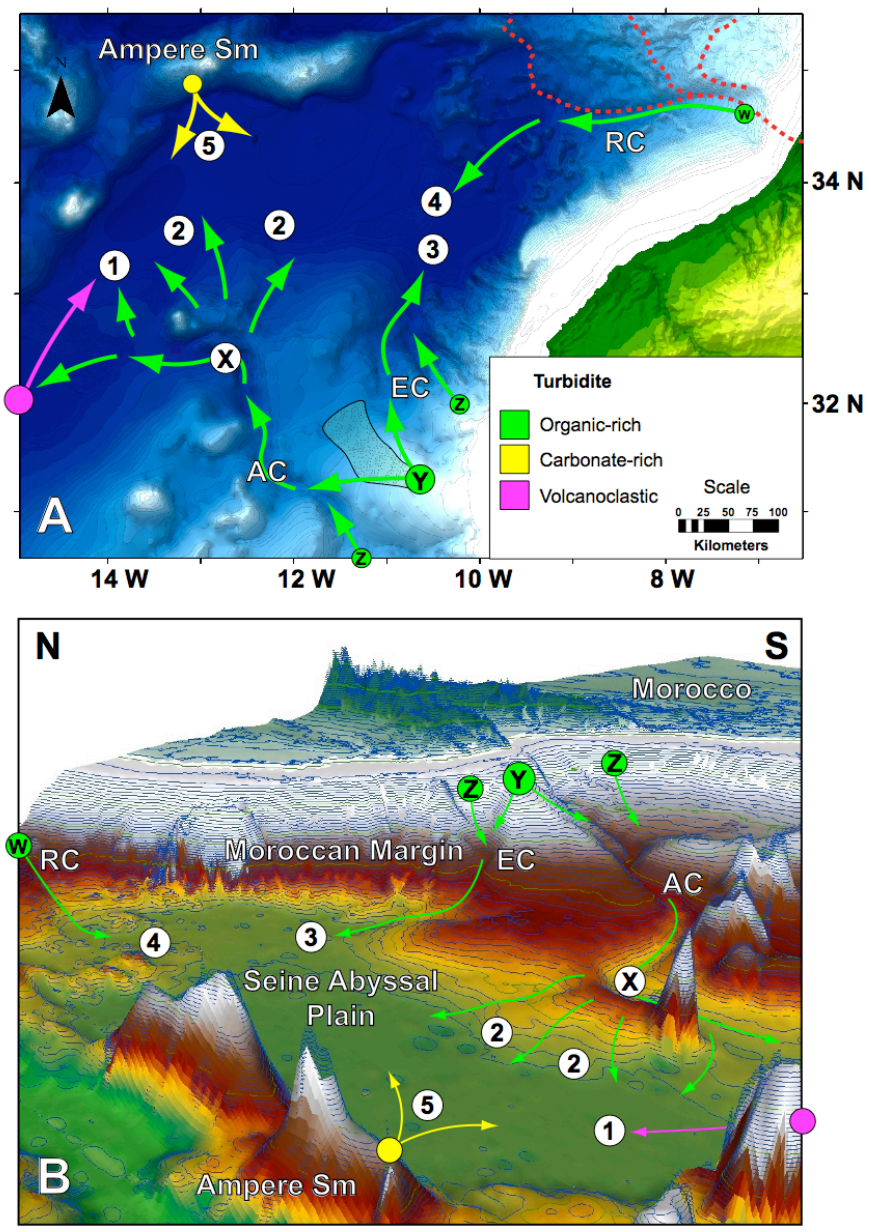

Figure 3-20: (A) 2D and (B) 3D maps showing inferred flow pathways into the Seine Abyssal Plain. Coloured arrows indicate the various flow pathways and associated entry points into the basin are labelled 1 – 5, described further in the main text. Letters denote areas of specific interest. 'X' shows the point where flows passing through the Agadir Basin overspill to the north and enter the basin from the southern margin. 'Y' shows the likely source area for flows originating from single slope failures, which then pass into the basin via three entry points. 'Z' shows alternative source areas for flows originating from simultaneous, multiple slope failures, which then pass into the basin from three entry points. 'W' highlights the source area for organic- and pyrite-rich flows entering the basin from the NE via the Rharb Canyon. 'RC' = Rharb Canyon, 'EC' = El Jadida Canyon and 'AC' = Agadir Canyon.

1. Organic-rich flows were able to enter the Seine Abyssal Plain from the southwest, via the Agadir Canyon (Point 1; Figure 3-20). Previously, this has been proposed as the main pathway for large-volume flows entering the Seine Abyssal Plain (Wynn et al., 2002b; Talling et al., 2007; Frenz et al., 2008). However, individual bed isograms show that relatively coarse-grained deposits found in the NE parts of the Agadir Basin quickly fine to the north, across the Casablanca Sill (e.g. Beds S11 and S12; Figure 3-17B and 1-17D). The same beds have relatively coarse-grained deposits that extend further to the SW, down the length of the Agadir basin. This suggests that the majority of the flows passed SW along the Agadir Basin with only a small proportion spilling over into the Seine Abyssal Plain. In the case of volcanoclastic Bed S14 that originated from the island of Tenerife, the parent flow passed NE up the Agadir Basin, before surmounting the Casablanca Sill and spreading across the Seine Abyssal Plain (Point 1; Figure 3-20).

2. Organic-rich flows were able to enter the Seine Abyssal Plain directly from the south, via the Agadir Canyon (Point 2; Figure 3-20). Correlation of turbidite beds above the confines of the basin (~ 850 m), on the Safi Plateau and the margin of the Agadir Canyon, demonstrate that parts of the flows were able to overspill on the outer bend of a sharp meander in the Agadir canyon (Point X; Figure 3-20). The unconfined flows were then able to pass into the Seine Abyssal Plain along its southern margin, most likely mixing with the primary flow contained within the Agadir Canyon, entering the basin from the southwest. Beds S3, S5 and S11 comprise thin sands overlain by a sharp grain-size break, immediately overlain by thin turbidite mud. Bed S5 has deposits that are considerably finer grained than those found on the basin floor. The thin bedded deposits with sharp grain-size breaks and the finer grained deposition of Bed S5 on the southern margin suggests overspilling flows were bypassing a high proportion of their sediment load across the Safi Plateau into the Seine Abyssal Plain. The bypassing sediment was likely mixed with the primary flow, still confined by the Agadir Canyon, entering the basin from the southwest. Therefore, it is difficult to assess the volume of sediment delivered into the basin from flow overspill.

3. Organic-rich flows were able to enter the Seine Abyssal Plain from the southeast, potentially via a number of canyons that cut back directly into the Moroccan Shelf,

the largest of these being the El Jadida Canyon (Point 3; Figure 3-20). Deposits found in the eastern parts of the Seine Abyssal Plain are often very coarse and have fining trends to the north and west. Persistent coarse-grained deposition in this area indicates the El Jadida Canyon is a major pathway for sediment into the Seine Abyssal Plain.

4. Organic-rich and pyrite-rich flows entered the basin from the northeast via the Rharb Canyon, which cuts back directly into the Moroccan Shelf (Point 4; Figure 3-20). In general, the area around the mouth of the Rharb Canyon has a relatively high frequency of small-volume beds. In this respect, the Rharb Canyon is not a volumetrically significant pathway into the basin over the past ~ 200 ka.

5. Carbonate-rich turbidites are coarsest and their deposits restricted to the NW parts of the basin (Figure 3-12). This indicates flows originated from the NW, most likely from flank collapses on the Ampere seamount (e.g. Point 5; Figure 3-20).

3.5.3 Turbidites with multiple entry points into the Seine Abyssal Plain

Beds S3, S5 and S11 have multiple fining trends across the Seine Abyssal Plain originating from the mouth of the Agadir Canyon, the Safi Plateau, and El Jadida Canyon. Hence, the flows that deposited these beds are interpreted to have: 1) traveled along the Agadir Canyon, passing into the Seine Abyssal Plain via flow overspill and directly from the mouth of the Agadir Canyon; and 2) traveled along the El Jadida Canyon, passing directly into the basin from the east.

3.6 Discussion

3.6.1 Controls on turbidite event frequency

Three intervals show a higher frequency of turbidite events from the average: ~ 0 – 15 ka, ~ 70 – 90 ka and, ~ 115 – 130 ka (Figure 3-16). Using the cross-correlation function in the software package 'R', the clustering of turbidites is positively correlated (with a confidence value of 0.6) to relatively high sea-level conditions after rapid sea-level rise (Figure 3-21). This correlation is the product of turbidite clusters between ~ 0 – 15 ka and ~ 115 – 130 ka situated at sea-level high-stands. This correlation indicates an increased sediment supply to the heads of the Agadir, El Jadida, and Rharb Canyons during periods of high sea-level. Between 30ºN – 34ºN the Moroccan Margin has little riverine input, and as a result sediments across the Shelf and Upper Slope are primarily reworked biogenic material, glauconite and, quartz. In addition, strong upwelling in this region means marine productivity is relatively high and contributes a significant proportion of sediment to the margin (Summerhayes et al., 1972; Summerhayes et al., 1976). Increased turbidite activity during high-stand conditions could be the product of littoral drift transporting sediment into the heads of the canyons, similar to the La Jolla Fan, offshore California (Covault et al., 2007). Furthermore, increased marine productivity along the margin during periods of high sea-level could increase sediment supply to the canyons, in turn increasing the frequency of turbidite events. However, there is also a negative correlation between turbidite frequency and sea-level generated by the turbidite cluster between 70 – 90 ka, which occurs at relatively low sea-level. The largest turbidite event (Bed 5 with a volume ~160 km^3) occurs within this cluster. The negative correlation suggests that sea-level is not the only factor influencing turbidite frequency within the Moroccan Turbidite System. As suggested by Covault and Graham (2010), climatic changes onshore coupled with the tectono-morphologic character of the shelf will dictate the response of a turbidite system to changes in sea-level. The Moroccan Turbidite System is another example of a turbidite system that does not conform to the classic sequence stratigraphic model, whereby turbidite systems are active during lowstands and inactive during highstands (e.g. Vail et al., 1977).

A general decrease in the frequency of turbidite beds is observed in sediments older than ~ 180 ka, irrespective of sea-level. This is likely to be a product of spatial and temporal bias in the data due to limited core coverage from ~ 180 ka to 260 ka.

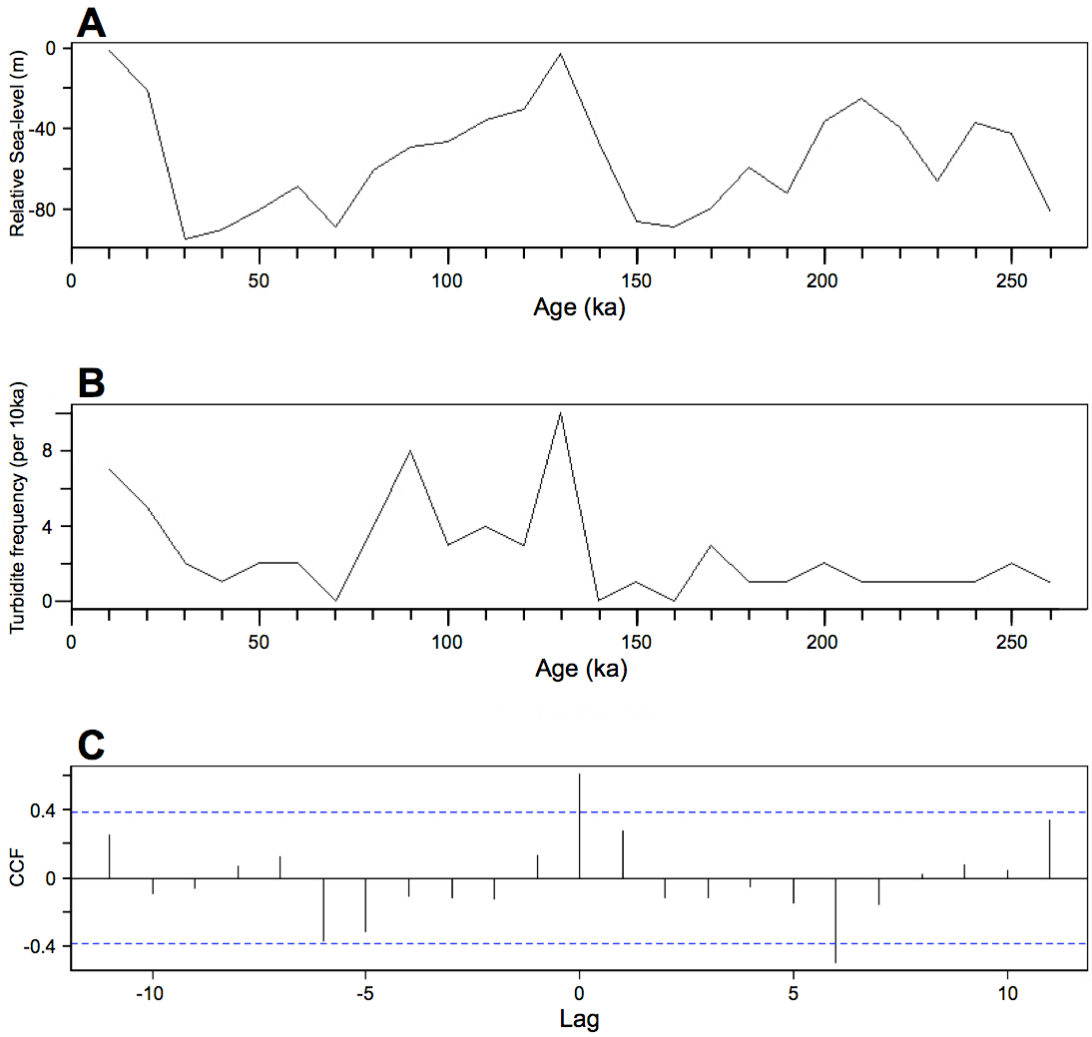

Figure 3-21: Cross-correlation analysis of (A) relative sea-level and (B) turbidite frequency over the past ~ 260 ka. Turbidite frequency was calculated within 10 ka bins and compared with relative sea-level values, averaged across each bin. (C) Shows the output of the cross-correlation function (CCF) from (A) and (B). Dashed horizontal lines indicate the threshold for a statistically significant correlation. Note the significant positive correlation of 0.6 at time lag 0 between turbidite frequency and sea-level.

3.6.2 Turbidites with three entry points into the basin

Three hypotheses are proposed to explain turbidites with three entry points into the Seine Abyssal Plain. First, individual flows passing into the basin were not synchronous but occurred at very similar times (i.e. within the resolution of the dating techniques used - tens to hundreds of years of each other). Second, multiple disparate slope failures occurred simultaneously across the margin, generating separate flows that synchronously entered the basin from the Agadir and El Jadida Canyons. Third, a single slope failure occurred that was split early along its flow pathway, generating flows that passed into the Agadir and El Jadida Canyon Systems, which then synchronously entered the Seine Abyssal Plain.

3.6.2.1 Are the turbidites synchronous?

From oxygen isotope analysis and coccolith biolithostratigraphy it is not possible to determine the ages of turbidite beds past an accuracy of ~ ± 5000 years. Therefore, correlated beds could have been emplaced hundreds of years apart but are not possible to distinguish from these methods. However, the relative timing between correlated deposits, situated across different parts of the Seine Abyssal Plain, can be established from sedimentological characteristics. Ideally, a single turbidity current produces a turbidite that has a sharp, relatively coarse-grained base, which then progressively fines upwards from sand into silt and mud. Such deposits are found within Bed 11.2 (Figure 3-3C), which is interpreted to have been deposited by a single flow entering the basin from one point. If multiple turbidity currents occur within a relatively short period of time, their deposits will likely amalgamate with no intervening hemipelagic sediments. Amalgamated deposits, composed of a discrete number of separate events, are likely to comprise multiple fining upward sequences (Rothwell et al., 1992; Hunt et al., 2011). If flows passing into the Seine Abyssal Plain from three entry points were not synchronous but separated by a relatively short period of time, it would be expected that one turbidite bed would overlie another. The resulting amalgamated deposit should contain at least two fining upward sequences. However, Beds S3, S5 and S11 all comprise deposits that have a single fining upward trend (Figure 3-22), albeit some

deposits have abrupt reductions in grain size from sand into turbidite mud (see Chapter 6; Figure 6-6A and 6-9A). This indicates that the parent flows entered the Seine Abyssal Plain synchronously and merged as they travelled across the basin.

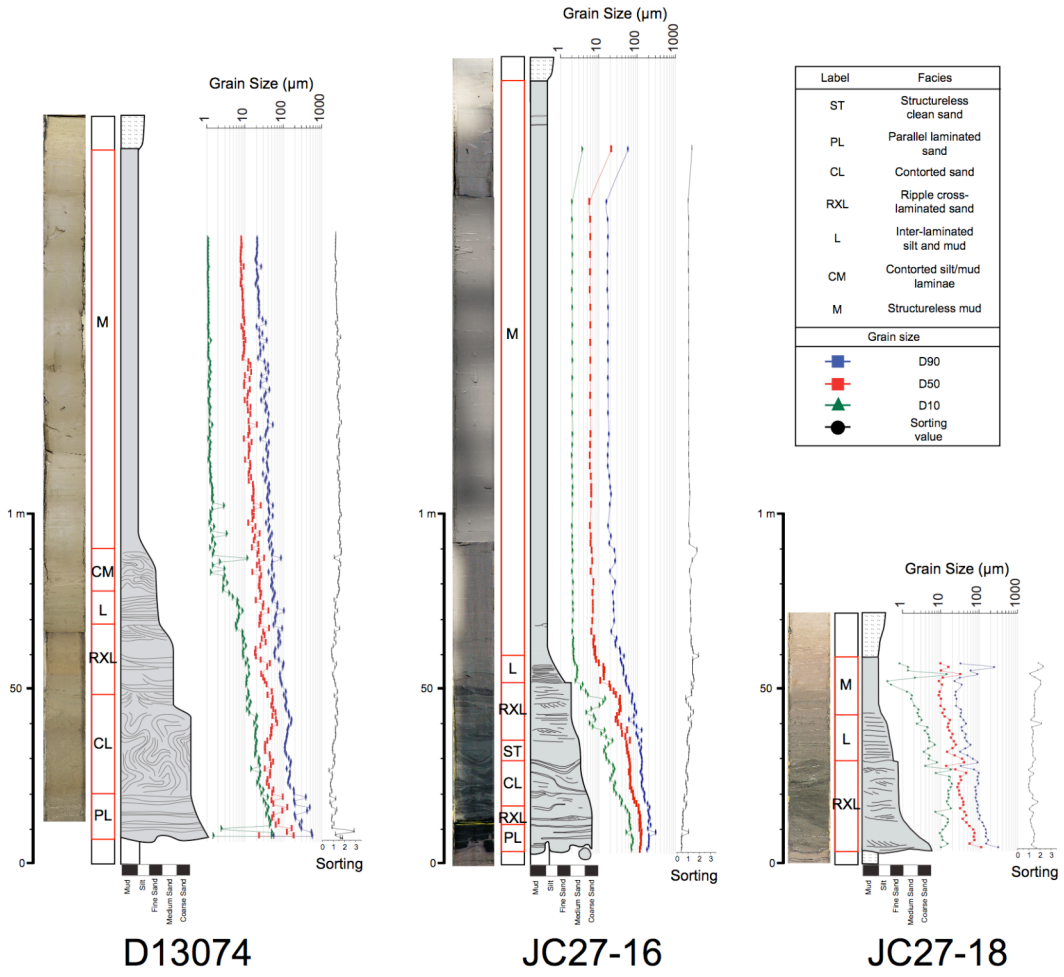

Figure 3-22: Vertical grain-size profiles through Bed S5 at different sites across the Seine Abyssal Plain. Core sites are selected from: eastern parts of the basin (JC27-18), central/southern parts of the basin (JC27-16), and western parts of the basin (D13074). Generally, deposits have a single fining upward trend from sand at the base, which is overlain by progressively finer sands, silts and ultimately turbidite mud. Deposits do not have distinctive multiple fining upward trends.

3.6.2.2 Were synchronous flows produced from a single or multiple slope failures?

Bed S5 is the largest volume turbidite within the Seine Abyssal Plain. It is penetrated in all cores recovered from the basin and is correlated with Bed AB5 in the Agadir Basin (Wynn et al., 2002b; Wynn et al., 2010). We consider the characteristics of these synchronously emplaced beds in detail and discuss whether they originated from a single or multiple disparate slope failures. Two lines of evidence are evaluated: (1) the sedimentological characteristics of the beds and, (2) the variation in the mixtures of coccolith species found in different parts of the NE Agadir Basin and Seine Abyssal Plain.

3.6.2.2.1 Sedimentological character of Bed AB5 and S5

The composition of sediments on the African shelf and upper slope, from 31°N to 34°N are relatively homogeneous, comprising similar grain sizes of sands, silts and clays composed of biogenic material, quartz and glauconite (McMaster and Lachance, 1969; Summerhayes et al., 1972). Therefore, disparate slope failures, occurring either separately or synchronously, along this area of the African margin are likely to produce turbidites that are similar in composition and grain size. The similar composition of sediments across a large area of the Moroccan Margin explains why most of the turbidites found across the Seine Abyssal plain are organic rich and comprise a narrow range of maximum grain sizes (~ 100 – 500 μm; Table 3-1). Although similar in composition, Beds S5 and AB5 are exceptionally coarse-grained compared to all other organic-rich turbidites across the Seine Abyssal Plain and Agadir Basin (max grain sizes ~ 920 – 1000 μm; Table 3-1). This suggests Beds S5 and AB5 originated either from an exceptionally coarse-grained area of the Moroccan Margin (not currently documented), or that an earthquake has destabilized sediments that would otherwise be stable across the Moroccan Margin. If Beds S5 and AB5 were sourced from multiple disparate slope failures, each event must have failed a similar, unusually coarse-grained stratigraphic interval on the Moroccan Margin. This scenario requires a regional trigger, i.e. an earthquake, to synchronously destabilize the unusually coarse-grained sediments across disparate areas of the margin.

3.6.2.2.2 Coccolith mixtures in Beds AB5 and S5

The mixture of coccolith species found in turbidite beds is a product of the initial slope failure and subsequent erosion along the flow pathway (Weaver and Thomson, 1993; Weaver, 1994). A flow that does not erode will have a coccolith mixture determined by the abundances of species present in the original slope failure. This will produce a turbidite with a characteristic mixture of coccoliths, which remains consistent across its depositional extent (Weaver, 1994). However, an erosive event will entrain new coccolith mixtures along its flow pathway. In this case, the characteristic mixture of coccoliths changes spatially across the deposit.

Coccolith mixtures in Beds A5 and S5 within the Agadir Basin and Seine Abyssal Plain are different (Figure 3-19). If the flows that deposited Beds AB5 and S5 were not erosive this would mean they were sourced from disparate slope failures, which were likely triggered by an earthquake (Points Z; Figure 3-20). However, Bed AB5 directly overlies 1 – 4 m deep erosional hiatuses within the Agadir Canyon and up to 25 m deep, kilometer-scale scours at its mouth (Wynn et al., 2002a; Talling et al., 2007c; Huvenne et al., 2009; Macdonald et al., 2011). This indicates the flow that deposited Bed AB5 was significantly erosive through the Agadir Canyon. Indeed, benthic foraminifera found in Bed AB5 indicate large volumes of sediment were entrained into the flow from water depths > 400 m, and a significant proportion from water depths > 2500 m (Talling et al., 2007c). Such large-scale erosion would significantly change the coccolith mixtures found in the turbidite compared with those from the original slope failure.

When a flow erodes and entrains hemipelagic sediment, coccolith mixtures from a number of different acme zones are combined, producing a synthetic mixture of coccoliths within the resulting turbidite (Weaver and Thomson, 1993). Following the method of Weaver and Thompson (1993) it is possible to calculate the synthetic mixtures of coccoliths added to flows via erosion along their pathways to the basin (Figure 3-23). Beds AB5 and S5 have coccolith mixtures that are similar to synthetic coccolith mixtures derived from erosion of

oxygen isotope stages 4 – 13 (~ 59 – 490 ka) and 4 – 8 (~ 59 – 252 ka) respectively (ages from Lisiecki and Raymo, 2005). Assuming a sedimentation rate of ~ 0.0014 cm per year (Figure 3-9), the coccolith mixtures found in Beds AB5 and S5 yield estimated erosional depths of ~ 690 cm and ~ 350 cm respectively. Assuming the flows that deposited Beds AB5 and S5 were initially composed of similar mixtures of coccoliths, different erosional pathways through the Agadir and El Jadida Canyons can explain: 1) the spatial variability in coccoliths across the Seine Abyssal Plain, and 2) the differences in coccolith mixtures between the Agadir Basin and the Seine Abyssal Plain.

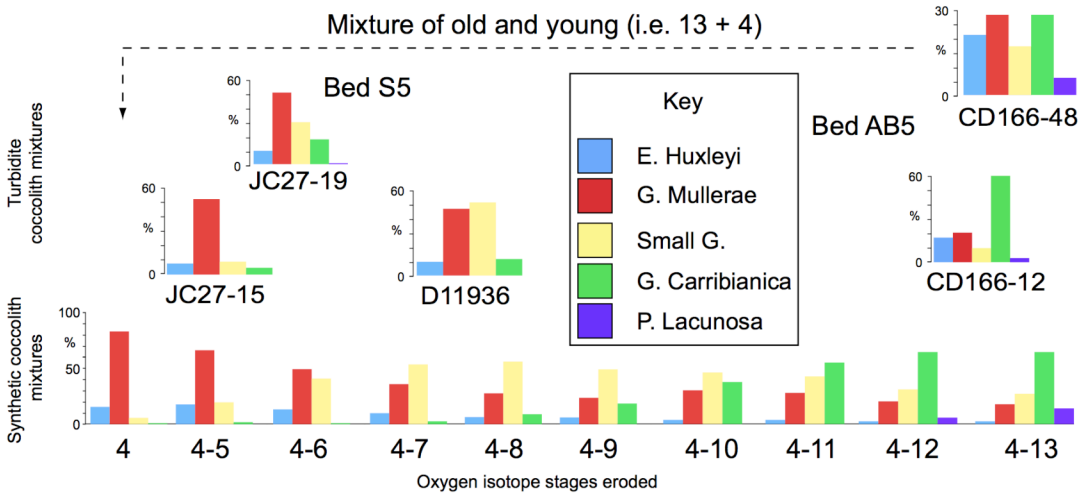

Figure 3-23: Synthetic coccolith mixtures (along the bottom) constructed from oxygen isotope stage 4 to 13. Synthetic mixtures were derived from sequentially adding coccolith assemblages from hemipelagic sediments down core. Coccolith biostratigraphy from two sites was used comprising: D11940 for oxygen isotope stages 4 – 9 (after Davies et al., 1997; this study), and the longer record of Weaver (1994) for stages 10 – 13. Mixtures of coccoliths found in Bed AB5 and S5 at various sites across the Agadir and Seine Abyssal Plain are each placed above the most similar synthetic coccolith mixture. Note the similar mixtures of coccoliths across the Seine Abyssal Plain (Bed S5) and different mixtures within the Agadir Basin (Bed AB5).

3.6.2.3 Summary of the evidence for single versus multiple slope failures

It is not possible to categorically determine whether the flows that deposited Beds AB5 and S5 originated from a single or multiple slope failures. Differences in the mixture of coccoliths within the Agadir Basin and across the Seine Abyssal Plain can be explained from: 1) a single slope failure being split along its flow pathway producing separate flows that eroded to different depths along the seafloor, which generated different coccolith assemblages in different parts of the basins; 2) multiple disparate slope failures that each failed a different depth of seafloor, which produced separate flows with different coccolith assemblages. The unusually coarse-grained nature of both beds can also be explained from: 1) a single slope failure failing an unusually coarse-grained area of the African Margin; or 2) multiple slope failures failing a similar stratigraphic horizon across disparate areas of the African Margin.

3.7 Conclusions

This contribution presents a suite of shallow sediment cores recovered within the Seine Abyssal Plain, situated offshore NW Africa. A robust chronostratigraphic framework is extended across the basin from high-resolution coccolith biolithostratigraphy, bulk stable-oxygen isotope and radiocarbon dating. This provides a framework by which individual turbidite beds are correlated across the basin for over 500 km. Turbidites, primarily sourced from the African Margin, passed into the basin via the Agadir, El Jadida and Rharb Canyons.

The frequency of turbidite events found within the Agadir Basin and Seine Abyssal Plain changes during the past ~ 260 ka. Two periods of high turbidite frequency are positively correlated with high sea-level conditions. This is attributed to canyon heads being supplied large volumes of sediment via littoral drift and increased in marine upwelling, across the flooded Moroccan Shelf. However, an interval of high turbidite frequency is also found at relatively low sea-level. This indicates other factors are important in dictating the response of

this turbidite system to changes in sea-level, such as onshore climate and the tectono-morphologic character of the shelf.

Some correlated beds have grain-size distributions that indicate they were emplaced by synchronous flows passing into the basin from multiple entry points. Two hypotheses are proposed to explain this phenomenon. First, multiple disparate slope failures occurred simultaneously across the Moroccan Margin. This produced synchronous yet separate flows that passed into the Seine Abyssal Plain from disparate entry points. Second, a single slope failure was split multiple times along its flow pathway. This produced separate flows that passed synchronously into the Seine Abyssal Plain via multiple disparate entry points. Assuming the beds originated from multiple disparate slope failures, then a regional trigger is required, i.e. a large earthquake. However, if the beds were sourced from a single slope failure, then a number of potential triggers are possible, including: loading by sedimentation, storm waves, sea-level fluctuations and earthquakes.

4 Flow thickness and processes of five large-volume, long run-out submarine gravity flows across a simple basin plain

Stevenson C.J., Talling P.J., Masson D.G., Sumner, E.J., Frenz M., Wynn R.B

4.1 Abstract

Turbidity currents operating within the deep-ocean are notoriously difficult to directly monitor. Therefore, much of our understanding of deep-water flow processes is derived from careful analysis of their deposits. This contribution presents individual bed correlations of five turbidites across the Agadir Basin, offshore NW Africa. The height to which deposits drape up the basin margins is interpreted to be a proxy for flow thickness. Generally, the flows depositing across the Agadir Basin were surprisingly thin (< 5 – 24 m thick). Flow thickness does not correlate with sand:mud volumes, grain size or total sediment volume within the beds. Examination of the vertical and spatial distribution of facies, grain size and bed thickness for each bed shows the parent flows were all different, each evolving differently down slope. Large-volume beds (A5, A7 and A12) have tabular bed shapes with no significant fining in grain size for hundreds of kilometres down slope. To achieve this flows must have been primarily bypassing (autosuspending), only depositing a small proportion of their sediment load per square kilometre along their pathway. The flows were non-erosive with near bed shear stresses below the erosional threshold of the seafloor. However, shear stresses required to bypass sands found in the beds exceed this threshold. Two conceptual models are proposed to explain this disparity. 1) Reduced particle settling velocities allowed flows to travel relatively slowly and still suspend most of their sediment loads. 2) The head of the flows was strongly depositional and armoured the seafloor before the faster moving (bypassing) body passed overhead, allowing near bed flow shear stresses to exceed the erosional threshold of the seafloor without eroding seafloor sediment. Examination of individual turbidites within a simple basin-plain setting reveals significant

complexity in facies, grain size and bed shape. Reproducing the key field observations here will be a challenge for future numerical and experimental models.

4.2 Introduction

4.2.1 Direct measurement of submarine flows

Submarine flows that reach the deep ocean are notoriously difficult to monitor directly because of their location, unpredictable and often infrequent occurrence, and most importantly because they tend to destroy equipment placed in their path. Few studies have measured natural submarine flows in-situ, and these are typically restricted to submarine channel environments situated on (or close to) the continental shelf (Hay, 1987; Xu et al., 2004). Only five locations in the world have directly measured turbidite flow speeds beyond the continental slope: the 1929 Grand Banks earthquake event offshore Newfoundland (Heezen and Ewing, 1952); events generating cable breaks on the Algerian Margin (Heezen et al., 1955); events associated with the 2006 Pingtung earthquake off SW Taiwan (Hsu et al., 2008); turbidity current activity within the Var (Piper and Savoye, 1993), and Zaire Fan (Kripounoff et al., 2003; Vangriesheim et al., 2009). It is these longer run-out flows that build the extensive submarine fan sequences observed in the rock record and are often host to large oil and gas reserves (Stow and Mayall, 2000).

4.2.2 Understanding flow processes

Due the paucity of in-situ flow measurements we derive much of our understanding of submarine flow processes from analyzing their deposits. Therefore, to understand how flows evolve along their pathways, we must examine the deposits of individual events. However, outcrop is usually limited in extent (tens to hundreds of meters across), making lateral correlation of individual beds extremely difficult. Only rarely have event beds been correlated for significant distances along their flow pathways (van Tassell, 1981; Bowen et

al., 1984; Wynn et al., 2002b; Amy and Talling, 2006; Talling et al., 2007a; Talling et al., 2007b; Talling et al., 2007c; Wynn et al., 2010; Hunt et al., 2011). In addition to these difficulties, outcrop studies have a poor control on seascape topography (i.e. slope, level of flow confinement etc). Indeed, it is only recently that studies on the modern seafloor have provided detailed morphological analysis of deep-water fan systems (Wynn et al., 2007 and references therein). Because of these difficulties in the field, our understanding of flow evolution has largely relied on scaled physical experiments and numerical modelling (Middleton, 1993; Kneller and Buckee, 2000).

4.2.3 Ignition theory

It has been proposed that submarine flows tend to one of three states. First, flows that erode sediment increase their buoyancy discharge and become faster, causing them to become more erosive. This has been termed ignition or self-acceleration (Pantin, 1979; Parker, 1982; Parker et al., 1986; Eidsvik and Brors, 1989; Fukushima and Parker, 1990). Experiments have demonstrated flows capable of entraining sediment from an erodable bed (Parker et al., 1987; Garcia and Parker, 1991; Garcia and Parker, 1993) in some cases producing self-acceleration (Pantin, 2001; Naruse et al., 2008; Pantin and Franklin, 2011). Second, flows that are powerful enough to suspend their entire sediment load yet unable to entrain more sediment into the flow reach equilibrium. This state has been termed ‘autosuspension’ and in theory can last indefinitely if the slope remains constant (Parker et al., 1986; Sequeiros et al., 2009). However, indefinite run-out is not physically possible due to entrainment of ambient fluid across the upper surface of the flow, causing it decelerate and ultimately deposit its sediment load. Autosuspension can arise if an igniting flow passes onto a non-erodable substrate or if a flow is fast enough to suspend its sediment load yet not fast enough to erode the sea-floor. Third, flows that deposit sediment will lose buoyancy discharge and become slower as they progress along their flow path, leading to more sedimentation from the flow. This state has been termed ‘subsiding’ by Parker et al. (1986). Herein, ‘subsiding’ flows are termed ‘depositional’ for clarity.

4.2.4 Modelling depositional turbidity currents

Depositional turbidity currents have been modelled via scaled physical experiments and numerical simulations. In both cases the modelled flows are typically considered to have low-concentrations of suspended sediment. Depositional flows modelled in experimental flume tanks are characterized by monotonic decay in velocity and quasi-exponential thinning of deposits away from source. Such behaviour includes 'surge' type flows from lock exchange experiments (Garcia and Parker, 1993; Middleton, 1993; Bonnecaze et al., 1996; Woods et al., 1998; Kubo, 2004) and sustained flows from continued supply of a sediment-fluid mixture into an ambient fluid (Garcia, 1994; Gray et al., 2005). Numerical simulations of depositional flows yield similar results, despite a wide range of approaches, including 'box-models' (Harris et al., 2002) and 'depth-averaged' models (Parker, 1982; Parker et al., 1986; Zeng and Lowe, 1997; Salaheldin et al., 2000; Kubo, 2004) and more computationally demanding simulations (Felix, 2002; Blanchette et al., 2005; Cantero et al., 2012).

However, increased sediment concentrations change the dynamics and depositional products of flows. Experiments have modelled high concentration flows, primarily examining the deposits they leave behind (Marr et al., 2001; Mohrig et al., 2003; Ilstad et al., 2004). Such experiments produce bed shapes that are very different from the quasi-exponential thinning generated by dilute flow experiments, which maintain thickness and pinch out/thin abruptly. With recent increases in computing power, direct numerical simulation of particles within a flow is possible, providing fully 3-D and depth resolved models that can simulate higher concentration flows (Cantero et al., 2012; Cleary, 2010 and references therein). Despite these major advances in our ability to model low and high-concentration turbidity currents, field data is lacking by which the models can be validated, in particular the correlation of turbidite facies with realistic seafloor topography.

4.2.5 Why is flow thickness important?

Flow thickness, together with sediment concentration and the vertical distribution of sediment within the flow, is a first order control on flow processes. It will have a profound affect on the range and mobility of submarine flows, and govern how they interact with topography (Kneller and Branney, 1995; Kneller et al., 1997; Kneller and McCaffrey, 1999). Hence, understanding flow thickness is crucial in determining the basic character of turbidity currents (both high- and low-density) and to what extent topography governs the distribution of their deposits. Constraining flow thickness also has direct practical applications in assessing the risk of submarine flows to seafloor infrastructure.

4.2.6 Calculating flow thickness from deposits

An alternative approach to documenting flow thickness by direct observation is to investigate the height to which flow deposits drape up basin-margin or channel-margin topography. The height to which flows extend up these margins is a combination of the thickness, vertical density profile and forward velocity of the flow (Kneller and Buckee, 2000). Velocity driven run-up effects increase the extent to which a deposit will drape up obstructing topography (Kneller and McCaffrey, 1999). However, in some circumstances topography will not obstruct the flow, for example when a flow moves parallel to a basin margin. In this case the heights to which deposits extend up the marginal slopes provide an estimate of the maximum thickness of the flow.

Only a limited number of studies have used the height that deposits drape up marginal slopes to estimate turbidity current thickness. Bowen et al. (1984) mapped out two individual turbidites over the Navy Fan, analyzing volume, grain-size distribution and the maximum height the deposits draped up basin topography. Their mud-rich Turbidite I (~ 3 % sand) was estimated as 15-75 m thick whilst their higher concentration, sand-rich Turbidite II (~ 42 %

sand) was calculated to be much thinner (< 10 m). Other studies are largely restricted to using submarine channel topography and analysis of overbank deposits to estimate flow thicknesses. These calculations typically yield much thicker flows, such as the Monterey Canyon (~ 100 m thick; Komar, 1969) Northwest Atlantic Mid-Ocean Channel (120-280 m thick; Klaucke, 1997) and the Amazon Channel (30-280 m thick; Hiscott, 1997; Pirmez and Imran, 2003).

4.2.7 Aims

This contribution documents five individual turbidite beds in unprecedented detail over exceptional distances across the Agadir Basin (~ 250 km; Figure 4-1). Excellent core coverage enables detailed sedimentological analysis of individual beds both in down flow and across flow directions. This contribution aims to provide a better understanding of submarine flow processes through consideration of the following four fundamental questions:

1. *How thick were the flows that deposited each turbidite bed?* Documenting the height to which deposits drape up basin margin topography allows the thickness of the parent flows to be constrained. Specific examination of the height to which different grain sizes (e.g. sand and mud) drape up topography provides an estimate of the relative thicknesses of the basal and upper parts of the flows.

2. *How did the five flows evolve with distance down slope?* Detailed sedimentological analysis of facies, grain-size distributions, and the shape of the beds, provides insights into the character of the parent flows.

3. *What controls govern flow evolution?* Examination of individual beds provides a rare opportunity to compare turbidites deposited by flows that travelled over a similar sea-floor gradient, and also to compare these deposits with numerical and experimental models. Differences between the five turbidites, and between turbidites

and models, are discussed in terms of observed deposit volume, grain size and mud fraction.

4. *How do these deposits inform us about more generalized flow processes?* Simple calculations are used to examine how the flows might transport their sediment loads over significant distances, yet not cause significant erosion of the underlying hemipelagic sediment. Competing generalized models for the behaviour of these flows are presented and critiqued.

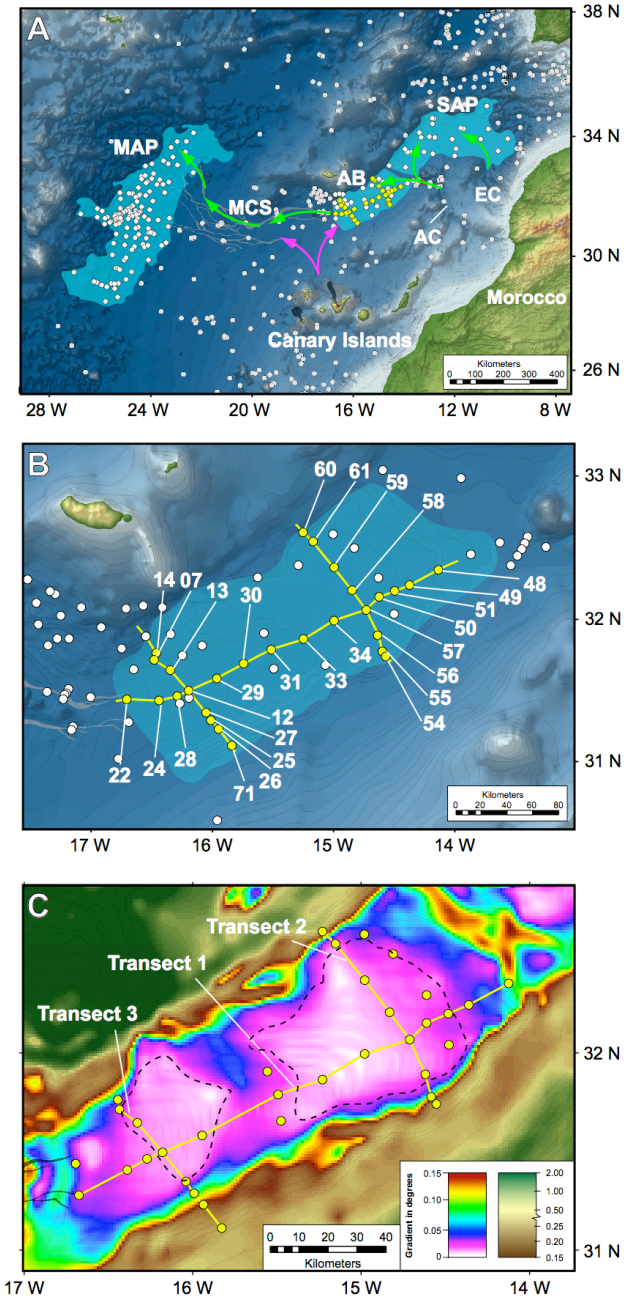

Figure 4-1: Map of the Moroccan Turbidite System, offshore NW Africa. (A) Regional map showing the entire Moroccan Turbidite System extending across: the Seine Abyssal Plain (SAP), the Agadir Basin (AB), the Madeira Channel System (MCS), and the Madeira Abyssal Plain. All cores that have been recovered from the area are shown with white circles. Cores used in this study are highlighted in yellow. Major flow pathways are highlighted for organic-rich flows sourced from the Moroccan Margin (green arrows), and volcanoclastic flows sourced from the Canary Islands (purple arrows). (B) Map of the Agadir Basin showing names and locations of cores used in this study (yellow circles). (C) Slope map of the Agadir Basin. Core transects 1 – 3 are labelled. Note the two flatter areas within the Agadir Basin (~0.01º) that are separated by a steeper ramp (~0.03º).

4.2.8 Study Area: The Agadir Basin

The Agadir Basin is one of three interconnected basins that make up the Moroccan Turbidite System, situated offshore NW Africa (Figure 4-1A and Figure 4-1B). Over the past 200 ka, this system has been host to a series of large volume (some > 100 km^3) turbidity currents, that have exceptionally long run-out distances (Wynn et al., 2002b; Talling et al., 2007c; Wynn et al., 2010). The Agadir Basin covers an area ~ 35, 000 km^2 and occupies water depths of between 4300 m and 4500 m. The basin slopes towards the southwest and comprises two particularly flat areas (< 0.01º) separated by a slightly steeper ramp (~ 0.02º; Figure 4-1C). To the north the basin is bounded by the Casablanca Seamount and a low-relief sill. Its southern margin opens out onto the continental rise, marked by an increase in slope from ~0.02º – 0.06º (Stevenson et al., 2012). Flows entering the system are primarily from three distinct sources: volcanoclastic flows rich in heavy minerals and basaltic glass from the Canary Islands; organic-rich flows from the Moroccan Margin containing a high fraction of biogenic material, quartz and glauconite; and carbonate-rich flows sourced from localized seamount collapses comprising clay and foraminifera tests (Weaver et al., 1992; Wynn et al., 2002b; Frenz et al., 2008). Previous work has established a robust geochemical, biological and chronostratigraphic framework allowing individual turbidite beds to be correlated across all three sub-basins (Weaver and Kuijpers, 1983; Weaver and Rothwell, 1987; Weaver, 1991; Rothwell et al., 1992; Weaver et al., 1992; Weaver and Thomson, 1993; Weaver, 1994; Davies et al., 1997; Wynn et al., 2002b; Talling et al., 2007c; Wynn et al., 2010).

4.3 Methods

4.3.1 Sea floor bathymetry and slope

GEBCO data is used to map seafloor bathymetry and generate slope maps across the Agadir Basin (as discussed in Chapter 2). GEBCO data provides bathymetry with sufficient resolution to define large-scale topographic features such as canyons, seamounts and topographic low points within the basin.

Heights to which deposits drape basin topography are calculated from the deepest core sites recovered from transects 2 and 3 (Figure 4-1B): sites 57 and 13 situated at 4398 m and 4431 m water depth respectively. For example, core site 54 is situated at 4374 m water depth, which is + 24 m above core site 57. The same bed found at both core sites is considered draping > 24 m up the basin margin.

4.3.2 Cores and grain-size analysis

The 29 sediment cores used in this study were collected during *RRS Charles Darwin cruise CD166* (core locations are shown in Figure 4-1B). Cores were recovered using a short (~ 12 m) piston corer. On average, spacing between cores is ~ 15 km with each core recovering ~ 8 m of sediment. Each core was visually logged in detail and with turbidites analyzed for grain size using a 'Malvern Mastersizer 2000' (see Chapter 2).

4.4 Results

4.4.1 Sedimentary Facies

Two distinct sediment types are found in the cores: (1) Background hemipelagic mud and, (2) turbidite sand/mud. Hemipelagic sediments comprise two end member lithologies. In interglacial periods, the sediments are cream coloured carbonate oozes, comprising foraminifera tests, coccolithophores and some fine terrigenous clay (Weaver and Kuijpers, 1983; Weaver and Rothwell, 1987; Rothwell et al., 1992; Weaver et al., 1992). In glacial periods, increased rates of carbonate dissolution in the bottom waters has dissolved most of the foraminifera tests and coccolithophores, leaving a smooth dark brown clay (Crowley, 1983; Weaver et al., 1992). Turbidite sediments are distinguished from hemipelagic sediment via a sharp change in grain size and a distinct change in colour.

4.4.2 Bed correlation

A robust geochemical and chronostratigraphic framework has been established across the Moroccan Turbidite System from:

- High-resolution coccolith biostratigraphy and down core oxygen isotope analysis of hemipelagic sediment, which provides an age model to ~ 400 ka (Weaver and Kuijpers, 1983; Davies et al., 1997; Wynn et al., 2002b).
- Detailed geochemical analysis of large-volume volcanoclastic turbidites, which provides aerially extensive marker beds (de Lange et al., 1987; Pearce and Jarvis, 1992; Pearce and Jarvis, 1995; Wynn et al., 2002b; Hunt et al., 2011).
- Analysis of coccolith assemblages within turbidite mud caps, which provides a biological fingerprint of individual turbidite events and their erosional history (Weaver and Thomson, 1993; Weaver, 1994; Wynn et al., 2002b).
- The colour and relative position of turbidite beds within the stratigraphy

Using the above methods this study combines additional cores with previous work, and extends individual turbidite bed correlations within the Agadir Basin. Approximately 11 turbidites are correlated across the Agadir Basin in both down flow (Figure 4-2) and across flow directions (Figure 4-3 and Figure 4-4). Turbidite Beds A3, A5, A7, A11 and A12 are the focus of this study. These beds were chosen because: (1) they are all organic-rich turbidites with similar sediment compositions, and (2) they have similar flow pathways, each inferred to have originated from the Moroccan Margin, passing into the Agadir Canyon, before spreading across the Agadir Basin from NE to SW (Wynn et al., 2002b; Frenz et al., 2008).

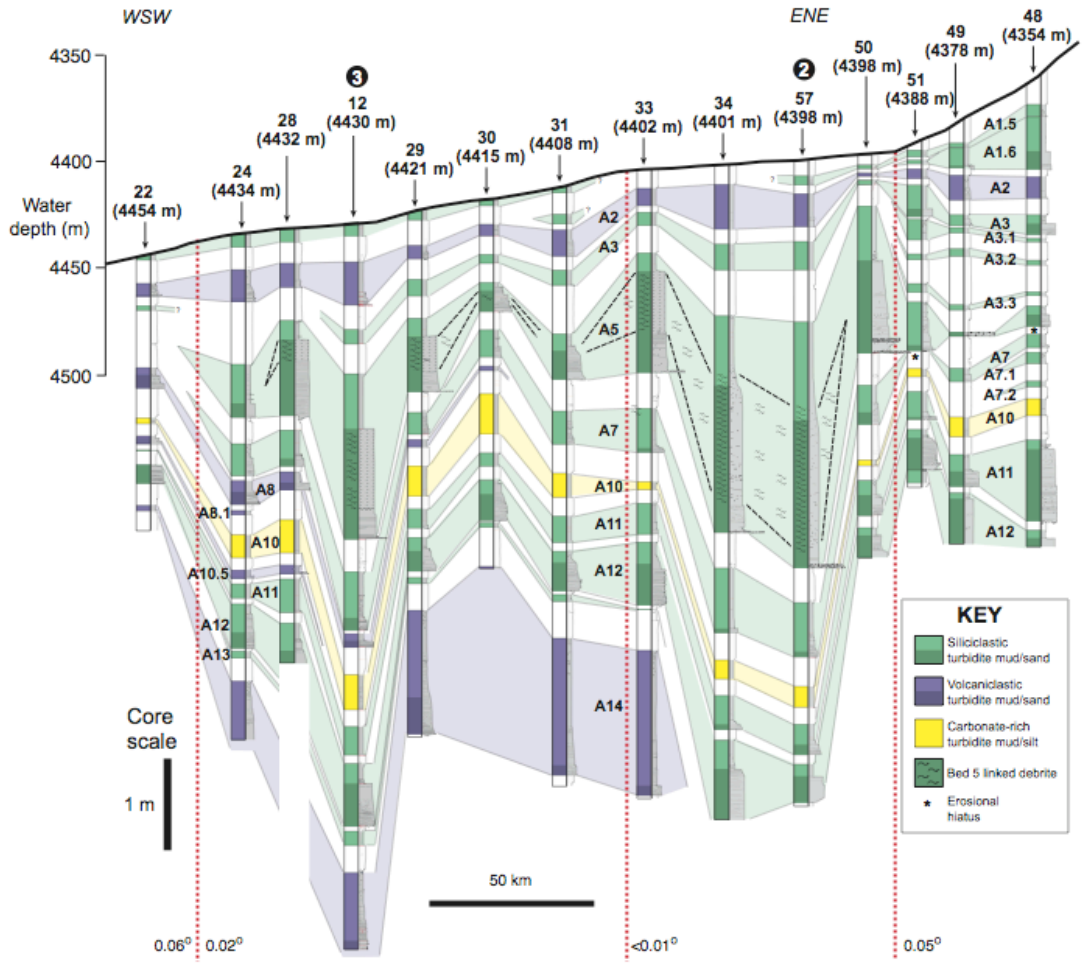

Figure 4-2: Transect 1 showing the turbidite stratigraphy along the axis of the Agadir Basin (Figure 4-1; adapted from Talling et al. (2007c) and Frenz et al. (2008). Position of cross cutting transects 2 and 3 are marked (black circles) Cores are hung off exaggerated sea floor topography (~ 650 times). Turbidites are shaded with colour whilst intervening hemipelagic sediment is white. Turbidites are labelled A1 – A14 (after Wynn et al., 2002b). Average gradient is highlighted along the transect (dashed red lines). Beds A3, A5, A7, A11 and A12 are the focus of this study.

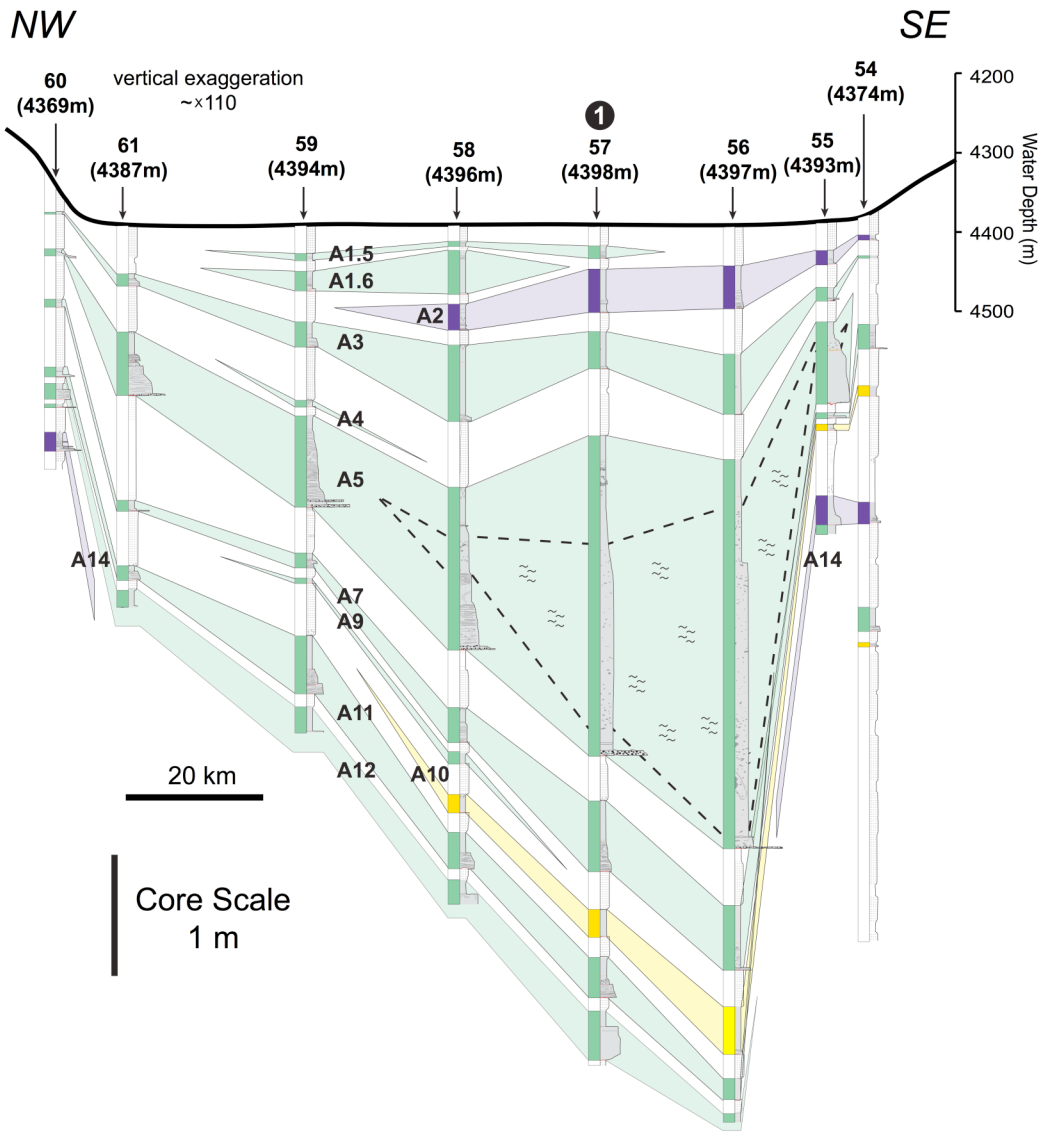

Figure 4-3: Transect 2 showing the turbidite stratigraphy from NW to SE across the northeastern part of the Agadir Basin (Figure 4-1). Cores are hung off exaggerated sea floor topography (~ 110 times). Position of cross cutting transect 1 is marked (black circle). Turbidites are shaded with colour whilst intervening hemipelagic sediment is white. Turbidites are labelled A1 – A14 (Wynn et al., 2002b). Beds A3, A5, A7, A11 and A12 are the focus of this study.

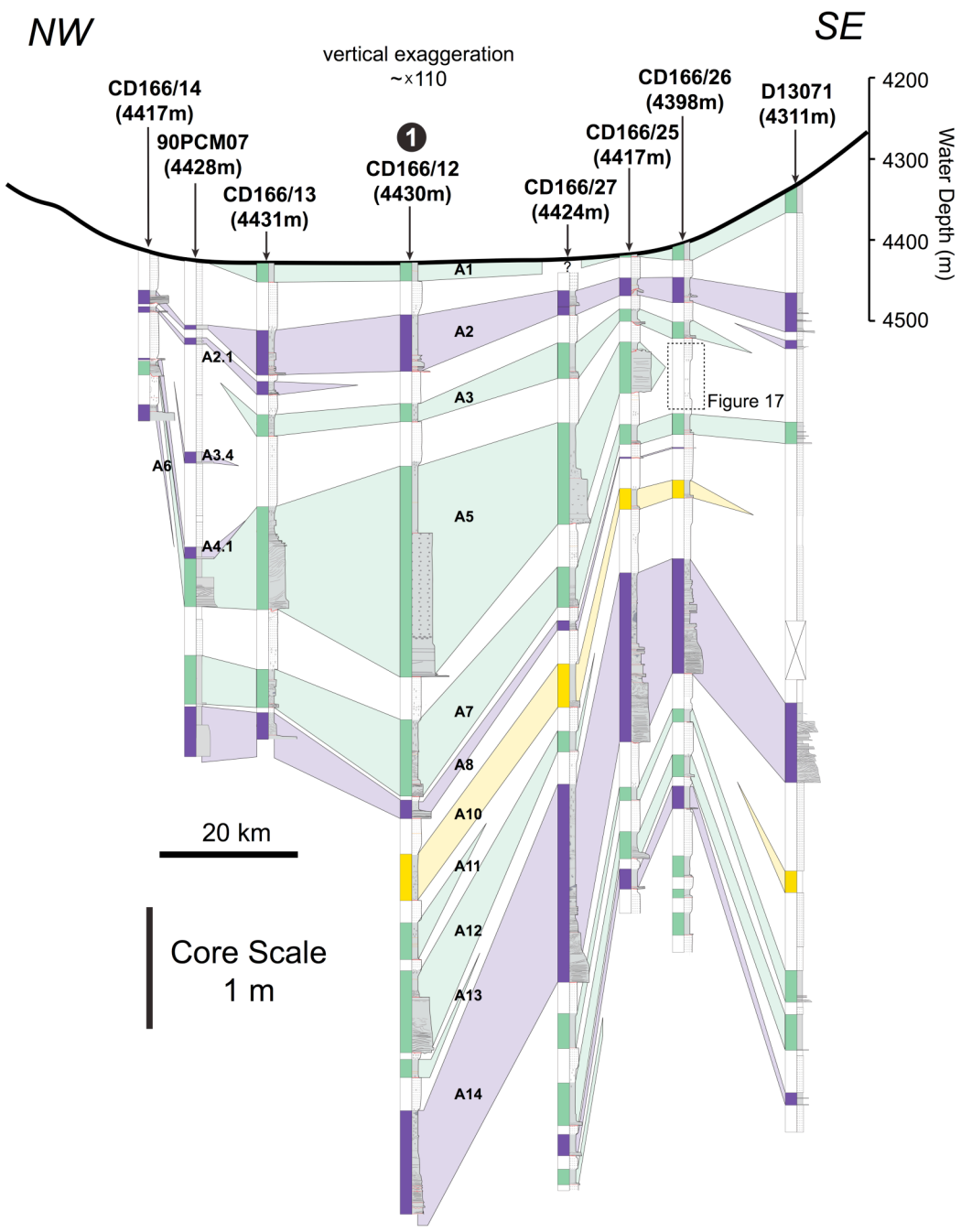

Figure 4-4: Transect 3 showing the turbidite stratigraphy from NW to SE across the southwestern part of the Agadir Basin (Figure 4-1). Cores are hung off exaggerated sea floor topography (~ 110 times). Position of cross cutting transect 1 is marked (black circle). Turbidites are shaded with colour whilst intervening hemipelagic sediment is white. Turbidites are labelled A1 – A14 (Wynn et al., 2002b). Beds A3, A5, A7, A11 and A12 are the focus of this study. Intervals of poor core recovery are marked with a cross. Note interval of detailed analysis in core 26, where Bed A5 pinches out.

4.4.3 Turbidite facies

Beds A3, A5, A7, A11 and A12 are described and interpreted within a facies scheme adopted from Sumner et al. (2012) and developed for this study (Table 4-1). Examples of turbidite deposits (facies) are illustrated in Figure 4-6 (see Figure 4-5 for key). Many of the features observed in deposits from the Agadir Basin are analogous to facies depicted in existing schemes (Bouma, 1962; Stow and Shamugam, 1980; Lowe, 1982; Haughton et al., 2009) and therefore are only briefly described here.

Structureless Clean Sand (ST, Bouma T_A)

Structureless clean sand comprises sand displaying no sedimentary structures with mud contents < 20 %. The term 'clean' is used in a relative sense to distinguish this facies from mud-rich structureless sand, which has significantly higher mud contents (30 – 40 %). Two types of clean structureless sand are observed, distinguished by their position in the deposit. Intervals of structureless sand that occur at the base of the deposit are classified as basal structureless sand (ST_B; Figure 4-6C). Conversely, intervals of structureless sand occurring within upper parts of the deposit are termed upper structureless sand (ST_U; Figure 4-6A). When the core was split intervals of upper structureless sand appeared 'wobbly' indicating increased water content compared with the overlying and underlying sandy facies. This facies often contains significant amounts of carbonaceous matter, homogeneously distributed within the sediment. Upper structureless sand is typically overlain by planar or ripple cross-laminated sand then a sharp grain-size break and turbidite mud.

Mud-Rich Structureless Sand (ST_D)

Distinctive intervals of mud-rich (30 – 40 % mud), structureless sand are found within the middle to upper parts of the Bed 5 deposit (Figure 4-6C). One core location contains chaotic mud clasts (Talling et al., 2007c). The intervals are mostly ungraded but proximally the upper parts of the deposits are normally graded. Across the rest of the basin the interval is sharply overlain by either planar laminated sand or turbidite mud.

Planar Laminated Sand (PL, Bouma T_B)

Planar laminated, clean sand is the most common type of facies within sandy deposits, particularly in proximal locations (Figure 4-6D). Laminae are typically < 3 mm thick with low mud contents between 5-10%. Grain size and composition can vary between individual laminae, switching between finer grained quartz and glauconite dominated lamina to foraminifera-rich lamina. This facies has inverse-to-normal grading in proximal areas and develops weak normal grading distally.

Low angle cross-laminated sand (LXL, Bouma T_C)

This facies comprises clean sand (< 5 % mud) with laminations set at relatively low angles (< 10º), to each other and to the base of the turbidite (Figure 4-6B). Laminations are sub-parallel but are not observed to truncate each other. This facies occurs proximally within the upper parts of sand deposits, overlying parallel laminated sands. In distal localities this facies is found towards the base of deposits overlain by ripple cross-laminated sands. It is normally graded.

Ripple cross-laminated sand (RXL, Bouma T_C)

This facies comprises clean sand (< 5 % mud) with relatively steeply dipping laminations (Figure 4-6B). The angles of laminae are steeper (> 10º) than those of low-angle cross-laminae and are often observed to truncate each other. Normally graded ripple cross-laminated sands are found proximally within the upper parts of deposits, overlain by turbidite silt and mud. In distal areas this facies is also normally graded but found towards the base of the deposits, overlain by turbidite silt and mud.

Contorted sand (CL, Bouma T_C)

Contorted lamination within clean sand intervals (5 – 10 % mud) occurs proximally in the basal parts of deposits and in the middle to upper parts of deposits distally (Figure 4-6A and Figure 4-6D). Contorted intervals can be ungraded or normally graded.

Turbidite Mud (L, CM and, M, Bouma T_D and T_E)

A fine-grained turbidite mud cap overlies all the sandy turbidite deposits across the basin. Generally the turbidite mud is thin, structureless and ungraded (M; Figure 4-6B). However, occasionally the basal parts of the mud cap have thin inter-laminated silts and muds (L), which normally grade into structureless mud. Some parts of the mud cap, particularly in Bed 7, have intervals of contorted silty laminae, often with clasts of silt (CM; Figure 4-6A). Contorted muds are typically ungraded but can have weak normal grading.

Grain-size breaks (GSB)

Abrupt vertical changes in grain size (grain-size breaks) occur within turbidite beds throughout the Agadir Basin (Figure 4-6). Three types of grain-size break can be identified; (1) fine sand to coarse sand, (2) coarse sand to fine sand, and (3) sand to mud. Types 1 and 2 are restricted to areas proximal to the mouth of the Agadir Canyon, whereas Type 3 grain-size breaks are ubiquitous across the basin.

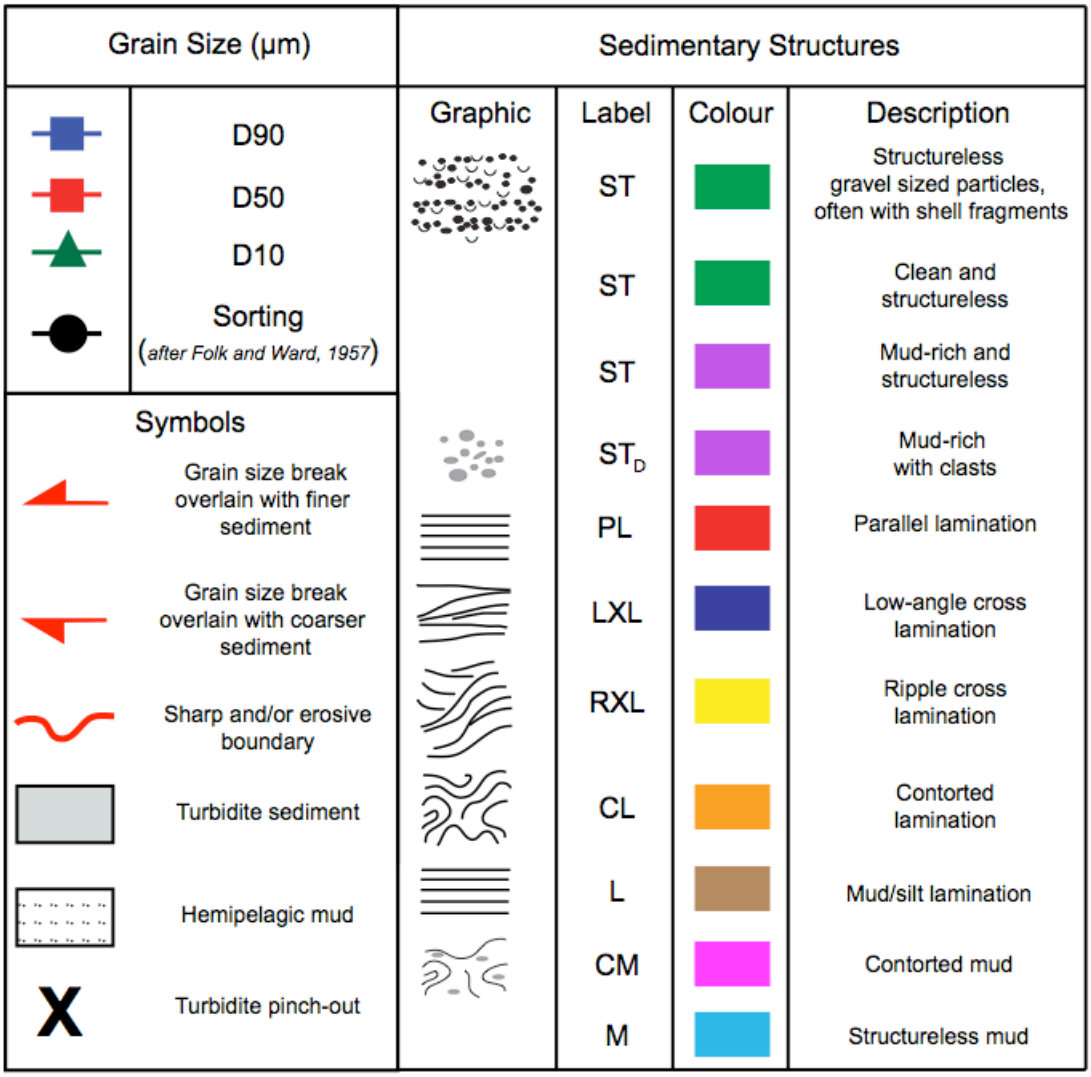

Figure 4-5: Key to all figures using graphic logs. Figure includes: symbology for graphic logs and vertical grain-size profiles, and colours and abbreviations for interpreted facies.

Facies		Description	Grain Size			Thickness	Grading	Position	Associated Facies				Interpretation	Equivalent Facies
			Range (μm)	Mode (μm)	Sorting	Range			Vertical		Lateral			
									Above	Below	Upstream	Downstream		
Clean Structureless Sand (Lower and Upper)	ST_B	Clean sand with no sedimentary structures	82 – 200	~ 600	1.5 – 2.5	10 – 63	Mostly ungraded, Normal and Inverse	Proximal, Basal parts of deposit	PL CL ST_D M	PL	ST_B PL	PL	Rapid deposition from a high-density turbidity current (Lowe, 1982; Kneller and Branny, 1995; Sumner et al., 2008)	T_A (Bouma, 1962) S_3 (Lowe, 1982)
	ST_U	Clean sand with no sedimentary structures	44 – 72	~ 177	1.5 – 2	6 – 13	Weak normal grading, Multiple grading sequences	Distal, Upper parts of deposit	PL RXL M	PL LXL CL RXL	CL LXL	LXL RXL	Capacity-induced collapse of sediment from the rear part of a turbidity current*	N/A

Mud-Rich Structureless Sand	ST_D	Mud-rich (30 – 40 %) structureless sand, mud clasts can be present (See Talling et al., 2007c)	72 – 320	~ 250	2.4 – 3	5 – 138	Weak normal grading proximal, Ungraded distal	Proximal, central parts of deposit. Distal progressively higher in deposit	GSB M	ST_B PL	ST_U PL	PL	En masse deposition from a mud-rich debris flow developed toward the rear of a turbidity current (Talling et al., 2007c)	H_3 (Haughton et al., 2009)
Planar Laminated Sand	PL	Clean sand with parallel lamination, most common deposit type	62 – 250	~ 250	~ 1	5 – 58	Proximal, Inverse to Normal grading. Distal, Weak normal grading	Middle and lower parts of deposit	GSB LXL ST_D M	ST_B ST_U (Rarely)	ST_B CL ST_D	LXL RXL ST_D	1. Collapsing laminar sheared layers at the base of a high-density turbidity current (Vrolijk and Southard, 1996; Sumner et al., 2008) 2. Migration of low amplitude bedwaves along the base of a dilute flow	T_B (Bouma, 1962) H_4 (Haughton et al., 2009)

												(Allen, 1982)	
Low-Angle Cross-Laminated Sand	LXL	Clean sand with low angle (< 10º), non-parallel lamination	177 – 350	~ 200	~ 1	5 – 20	Inverse and Normal grading	Middle and upper parts of deposit	GSB RXL ST_U	PL	PL	RXL CL	Tractional reworking of sediment along the bed from a dilute, decelerating turbidity current (Allen, 1982)	T_C (Bouma, 1962) H_4 (Haughton et al., 2009)
Ripple Cross-Laminated Sand	RXL	Clean sand with high angle (> 10º) cross-lamination. Laminae often truncated	62 – 190	~ 150	0.6 – 1	5 – 13	Normal grading. Rare inverse grading	Distal, upper parts of deposit	ST_U CL GSB M	LXL	CL LXL PL	CL	Tractional reworking of sediment along the bed from a dilute, decelerating turbidity current (Allen, 1982)	T_C (Bouma, 1962) H_4 (Haughton et al., 2009)
Convolute/ Contorted	CL	Sand with contorted laminations	110 – 350	~ 150	1 – 2.3	7 – 45	Normal grading	Proximal and distal, Middle and	ST_U GSB	RXL LXL	RXL	PL RXL	Excess pore pressure re-suspends	T_C (Bouma, 1962)

Laminated Sand								upper parts of deposit	M	ST_B			sediment resulting in contortion of existing sedimentary structures (Allen, 1977)	
Laminated Silt and Mud	L	Fine-grained mud with silt laminations	15 – 62	~ 20	1.2 – 1.4	3 – 21	Normal grading	Upper parts of deposit. Basal parts of mud cap	GSB CM M	ST_U PL RXL	CM M	M	Alternating near bed boundary conditions, from granular to cohesive, within a dilute decelerating turbidity current (Piper, 1972; Stow and Bowen, 1978)	T_D (Bouma, 1962) T_{2-3} (Stow and Shanmugam, 1980) E_1 (Piper, 1978)
Contorted Mud	CM	Fine-grained mud matrix with contorted silt laminations	10 – 70	~ 20	1.8 – 3	5 – 23	Ungraded, Rare weak normal grading	Upper parts of deposits. Middle and lower parts of mud cap	M	GSB L M PL	L M	L M	Collapse of muddy suspension, in tail end of a dilute turbidity current, into a cohesive fluid	T_{4-6} (Stow and Shanmugam, 1980)

		and silt/sand clasts								ST_U			mud layer (Kneller and McCaffrey, 2003)	
Mud	M	Fine-grained structureless mud	2 – 32	~ 18	1.5 – 3	8 – 44	Ungraded, Normal grading at base	Upper parts of deposit	CM	GSB CM LXL RXL ST_U	L CM	L CM	1. Slow settling of fine silt and hydraulically equivalent clay flocs from a dilute turbidity current 2. Cohesive fluid mud layer develops near to bed and freezes 'En masse' (McCave and Jones, 1988)	T_E (Bouma, 1962) E_3 (Piper, 1978) T_{7-8} (Stow and Shanmugam, 1980)

Table 4-1: Summary of facies found in the Agadir Basin.Synonomous facies from existing facies schemes are compared to those described in this study. Interpretation of facies is discussed in the main text and summarized within this table.

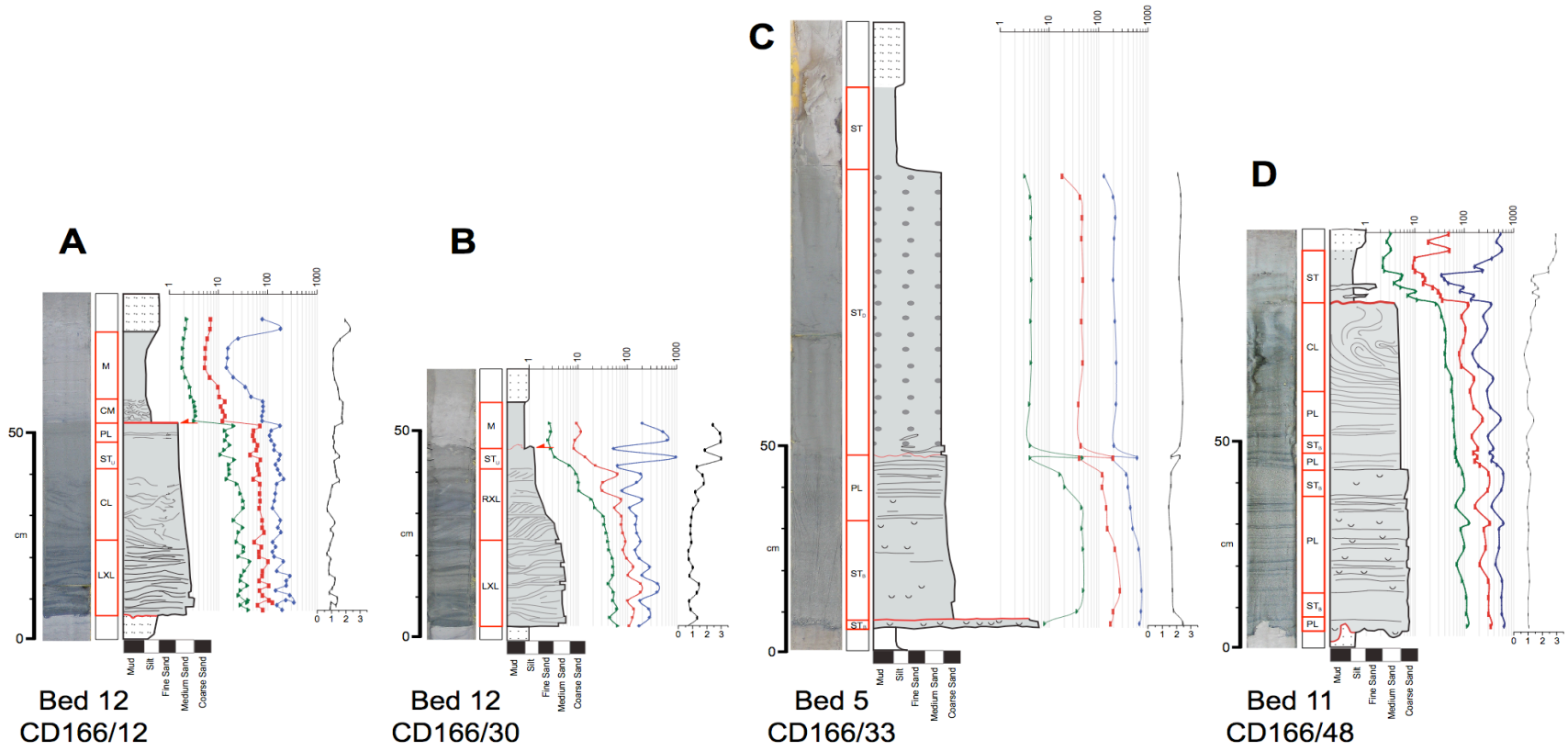

Figure 4-6: Examples of turbidite deposits within the Agadir Basin. Each deposit is illustrated with a visual log, interpretation of facies and a core photograph. Grain-size analyses are shown vertically through each deposit including values for D10 (green), D50 (red), D90 (blue) and sorting (black).

4.4.4 Bed geometries

Bed geometries, grain-size profiles and the distribution of facies for Beds A3, A5, A7, A11 and A12 are illustrated in (Figure 4-7 to 4-16), in both across flow and down flow directions.

4.4.5 Vertical and spatial grain-size trends

Sand to mud ratios were calculated for each bed, averaged over the Agadir Basin and Madeira Abyssal Plain (Table 4-2). Generally the turbidites are mud-rich with between ~ 10 – 25 % sand. However, Bed 5 has significantly more sand than the other beds (~ 40 %). The sand deposits for Beds A3, A5, A7, A11 and A12 are mostly restricted to the Agadir Basin. Typically, the sands have fining upward grain-size trends, ranging from sand to silt and mud (Figures 4-7 to 4-16). However, superimposed on this general fining upward trend individual turbidite beds can contain multiple fining upward sequences, particularly within the northeastern parts of the Agadir Basin, close to the mouth of the Agadir Canyon (e.g. Bed A5; Figure 4-9A). The spatial distribution of grain size varies markedly between turbidite beds.

4.4.6 Height to which deposits drape up topography

Lateral patterns of deposition, and the height to which different lithologies, facies and grain size drape up the basin margins was/is established using ‘across flow’ transects 2 and 3 (Figure 4-8, Figure 4-10, Figure 4-12, Figure 4-14, and Figure 4-16). The complete thickness of the oldest deposit in this study (Bed A12) was not always recovered. This limits description of the basal part of Bed A12 in across flow directions, however, in general sufficient sediment was recovered to establish the height to which both the sand and mud within the flow draped marginal topography. The exception to this is within the distal

northwest part of the basin where there is insufficient core recovery to establish flow thickness for Beds A11 and A12.

Beds A11 and A12 have sandy deposits pinching out laterally over elevations of < 5 m and mud pinching out over elevations of < 14 m (Figure 4-14 and Figure 4-16). Bed A5 extends further up the basin margins with deposits of sand and mud pinching out laterally over elevations of < 24 m (Figure 4-10). In contrast, Beds A3 and A7 both have deposits that extend relatively far up the basin margins, beyond the coverage of the cores (> 33 m; Figure 4-8 and Figure 4-12). Further details of the maximum heights to which turbidite sand and mud drape up basin margin topography are provided in Table 4-2.

Bed	Volume AB/MAP/Total (Km^3)	Total Sand/ Mud	Maximum height to which deposits drape up basin margins (m)					Maximum grain size (D 90)	Interpreted flow concentration		Bed shape	Agreement with models	Reasons for discrepancy
			Sediment	Proximal		Distal			Proximal	Distal			
				NW	SE	NW	SE						
3	5/0/5	10/90	*Sand*	< 29	N/A	< 3	> 33	470 µm	High	Low	Tabular abruptly thinning	No	High sediment concentrations
			Mud	> 29	> 24	< 3	> 33						
5	22/30/52	40/60	*Sand*	> 29	< 24	< 89	< 33	960 µm	High	High	Tabular abruptly thinning	No	High sediment concentrations + Cohesive effects of mud
			Mud	> 29	< 24	< 89	< 33						
7	10/110/ 120	10/90	*Sand*	< 29	> 24	< 3	< 33	150 µm	Low	Low	Tabular	No	High flow efficiency
			Mud	> 29	> 24	> 3	> 33						

11	8/0/8	25/75	*Sand*	> 29	< 1	?	N/A	640 µm	High	Low	Quasi-exponential	Yes	
			Mud	> 29	< 5	N/A	< 7						
12	9/190/200	15/85	*Sand*	> 29	< 5	?	< 6	391 µm	High	Low	Slowly thinning to tabular	No	Increasing flow efficiency from source
			Mud	> 29	< 5	?	< 14						

Table 4-2: Summary of various measured and interpreted aspects of Beds A3 – A12. Note that estimates for total bed volumes include the Agadir Basin (AB) and Madeira Abyssal Plain (MAP). Bed volumes are taken from Frenz et al. (2008). Sand/mud ratios are estimated from the total sand and mud volumes in the AB and MAP. Height to which deposits drape up the basin margins is derived from figures 8, 10, 12, 14 and 16. Maximum measured grain sizes are taken from figures 4-7C, 4-9C, 4-11C, 4-13C and 4-15C. The right side of the table summarizes interpretation of flow concentration and bed shape, which is discussed further within the main text.

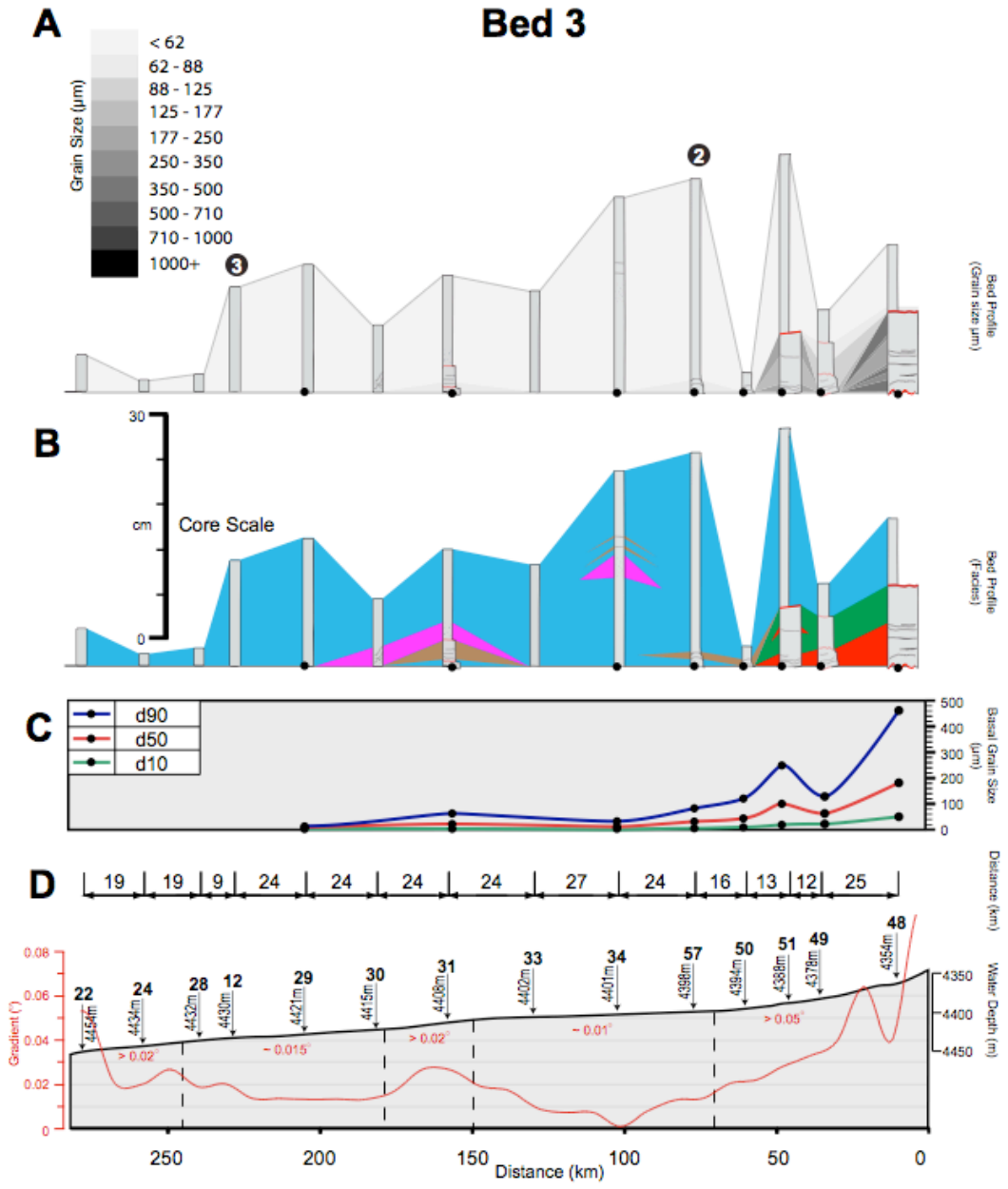

Figure 4-7: Bed A3 transect 1 along the axis of the Agadir Basin. Graphic logs are anchored onto a horizontal surface to highlight changes in bed thickness. Refer to Figure 4-5 for key. (A) Vertical and spatial distribution of grain size. Position of across flow transects 2 and 3 are marked. (B) Colour denotes interpreted facies. (C) Basal grain size at each core site. (D) Sea floor topography (grey shaded area) overlain with sea floor gradient (red line) along the axis of the Agadir Basin.

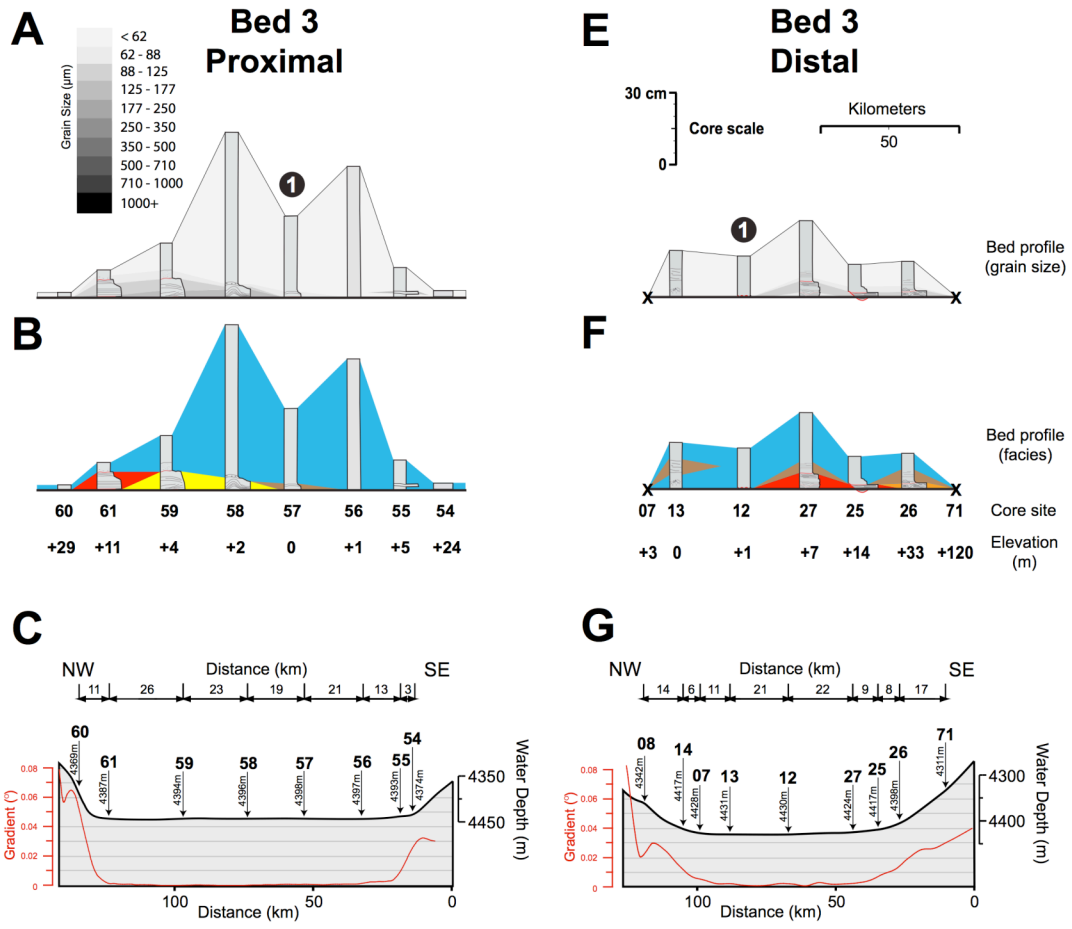

Figure 4-8: Bed A3 transects 2 (proximal) and 3 (Distal) from NW to SE across the Agadir Basin. Graphic logs are anchored onto a horizontal surface to highlight changes in bed thickness. (A and D) Vertical and spatial distribution of grain size. Position of transect 1 is marked. (B and E) Colour donotes interpreted facies. (C and F) Sea floor topography (grey shaded area) overlain by sea floor gradient (red line). Vertical exaggeration ~ 160 times.

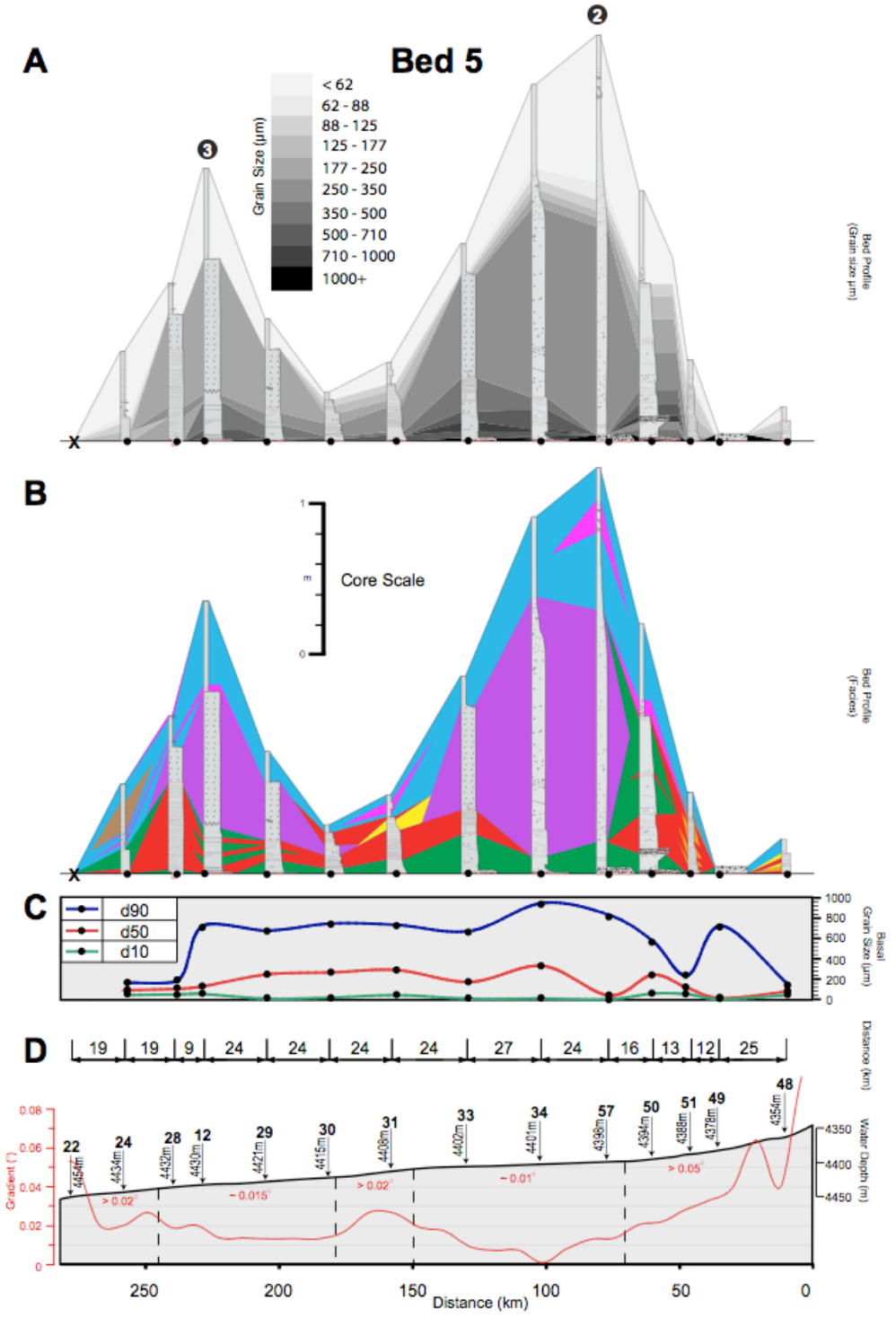

Figure 4-9: Bed A5 transect 1 along the axis of the Agadir Basin. Graphic logs are anchored onto a horizontal surface to highlight changes in bed thickness. Refer to Figure 4-5 for key. (A) Vertical and spatial distribution of grain size. Position of across flow transects 2 and 3 are marked. (B) Colour denotes interpreted facies. (C) Basal grain size at each core site. (D) Sea floor topography (grey shaded area) overlain with sea floor gradient (red line) along the axis of the Agadir Basin.

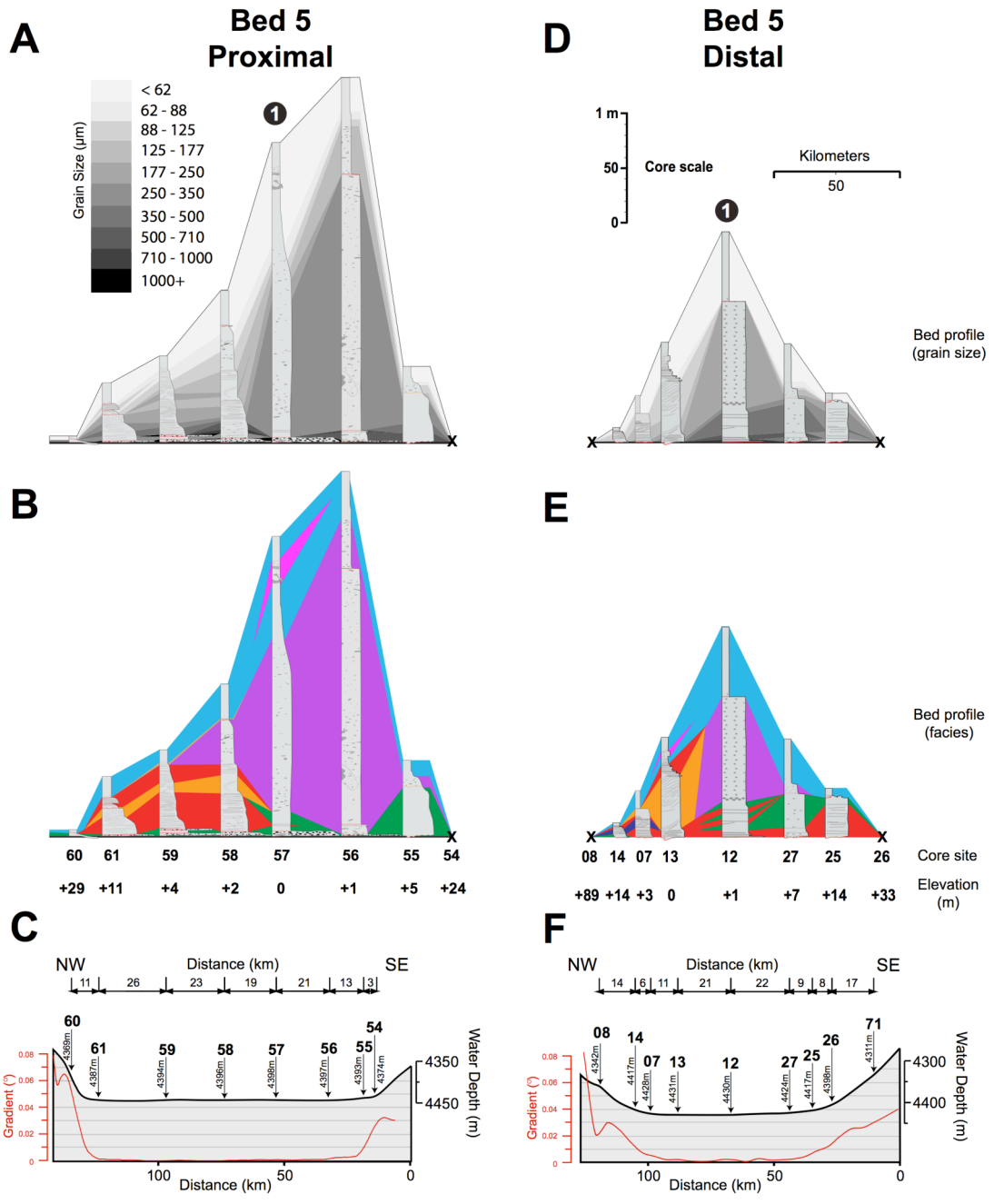

Figure 4-10: Bed A5 transects 2 (proximal) and 3 (Distal) from NW to SE across the Agadir Basin. Graphic logs are anchored onto a horizontal surface to highlight changes in bed thickness. (A and D) Vertical and spatial distribution of grain size. Position of transect 1 is marked. (B and E) Colour donotes interpreted facies. (C and F) Sea floor topography (grey shaded area) overlain by sea floor gradient (red line). Vertical exaggeration ~ 160 times.

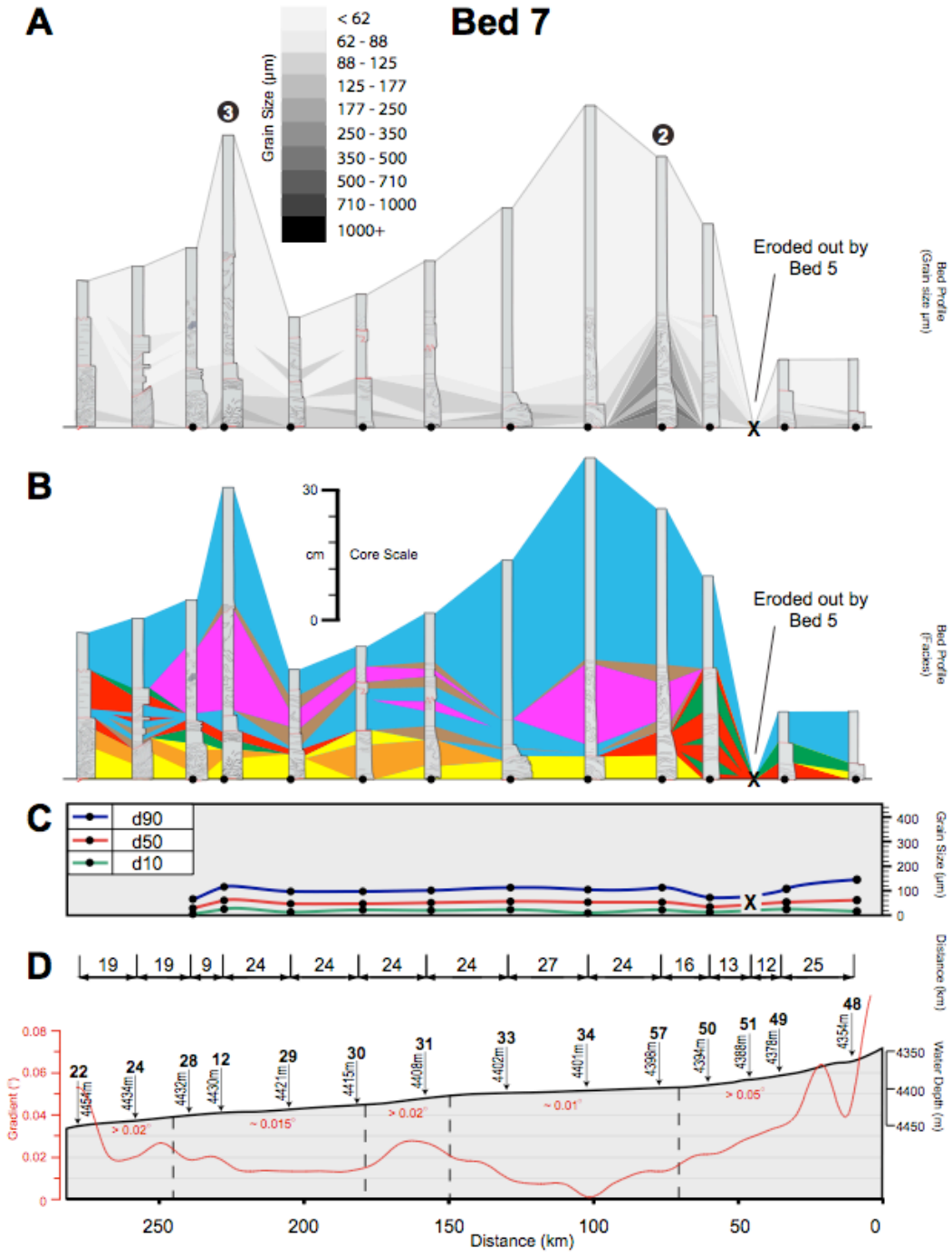

Figure 4-11: Bed A7 transect 1 along the axis of the Agadir Basin. Graphic logs are anchored onto a horizontal surface to highlight changes in bed thickness. Refer to Figure 4-5 for key. (A) Vertical and spatial distribution of grain size. Position of across flow transects 2 and 3 are marked. (B) Colour denotes interpreted facies. (C) Basal grain size at each core site. (D) Sea floor topography (grey shaded area) overlain with sea floor gradient (red line) along the axis of the Agadir Basin.

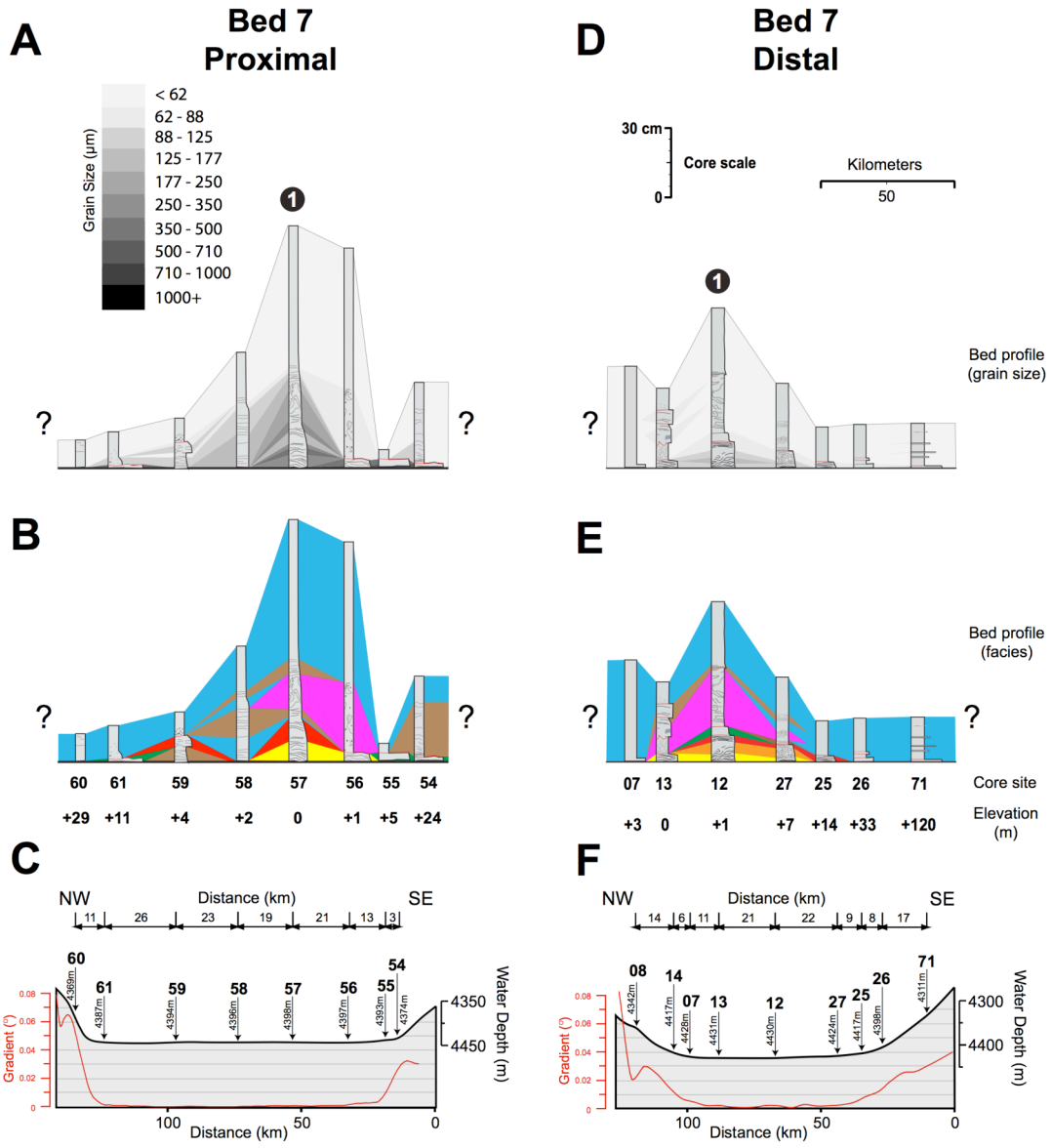

Figure 4-12: Bed A7 transects 2 (proximal) and 3 (Distal) from NW to SE across the Agadir Basin. Graphic logs are anchored onto a horizontal surface to highlight changes in bed thickness. (A and D) Vertical and spatial distribution of grain size. Position of transect 1 is marked. (B and E) Colour denotes interpreted facies. (C and F) Sea floor topography (grey shaded area) overlain by sea floor gradient (red line). Vertical exaggeration ~ 160 times.

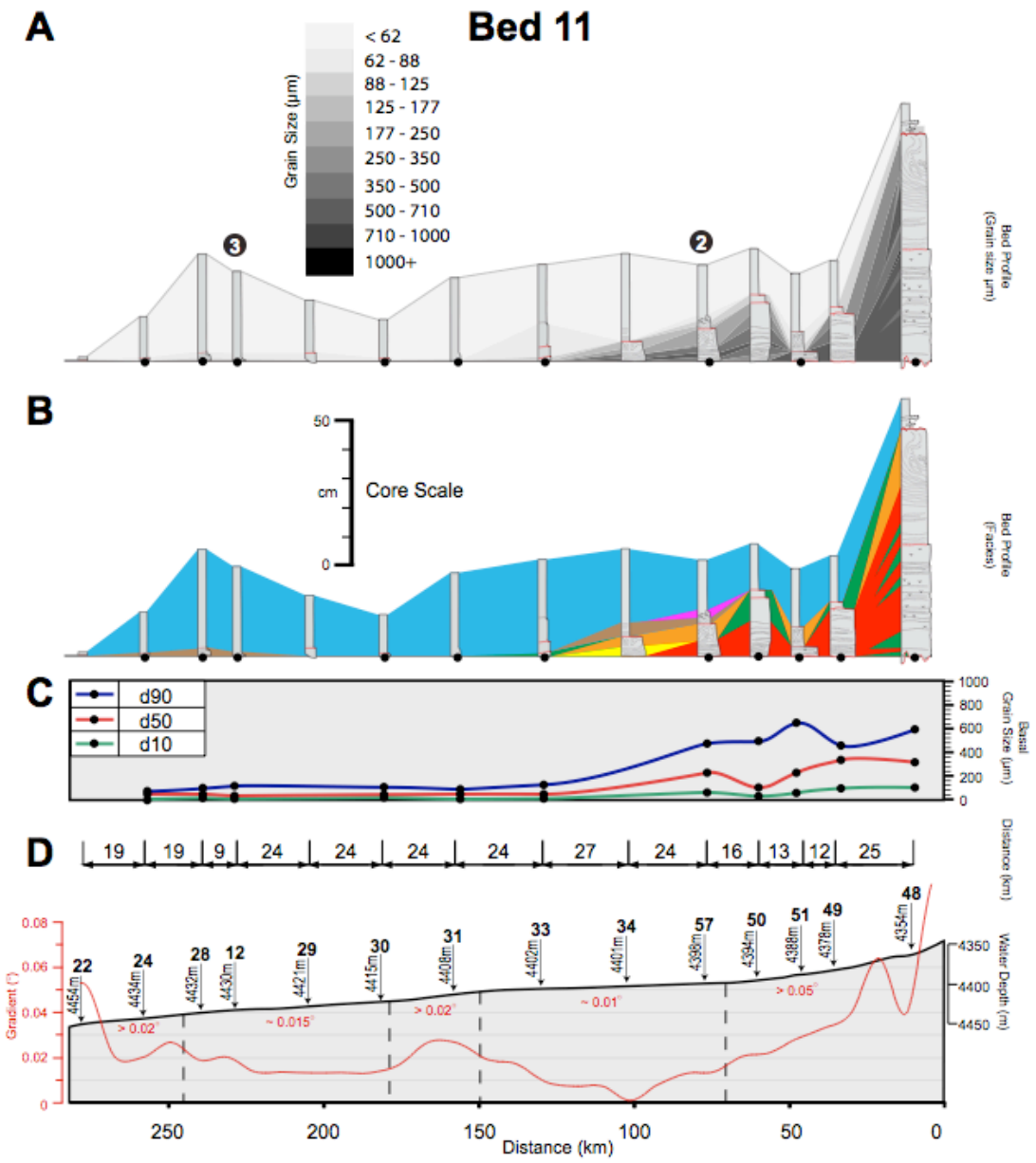

Figure 4-13: Bed A11 transect 1 along the axis of the Agadir Basin. Graphic logs are anchored onto a horizontal surface to highlight changes in bed thickness. Refer to Figure 4-5 for key. (A) Vertical and spatial distribution of grain size. Position of across flow transects 2 and 3 are marked. (B) Colour denotes interpreted facies. (C) Basal grain size at each core site. (D) Sea floor topography (grey shaded area) overlain with sea floor gradient (red line) along the axis of the Agadir Basin.

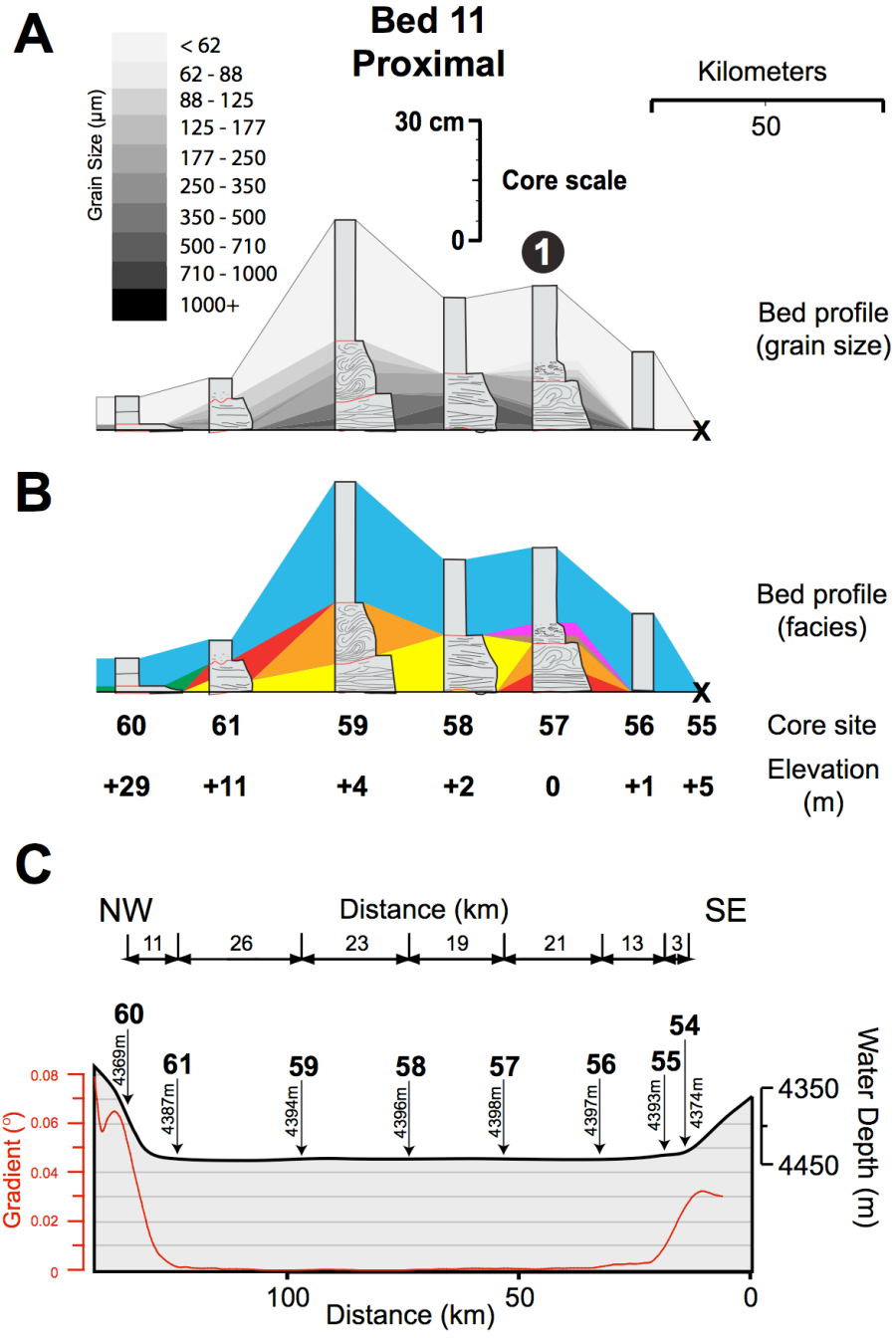

Figure 4-14: Bed A11 transect 2 (proximal) from NW to SE across the Agadir Basin. Graphic logs are anchored onto a horizontal surface to highlight changes in bed thickness. (A) Vertical and spatial distribution of grain size. Position of transect 1 is marked. (B) Colour donotes interpreted facies. (C) Sea floor topography (grey shaded area) overlain by sea floor gradient (red line). Vertical exaggeration ~ 160 times.

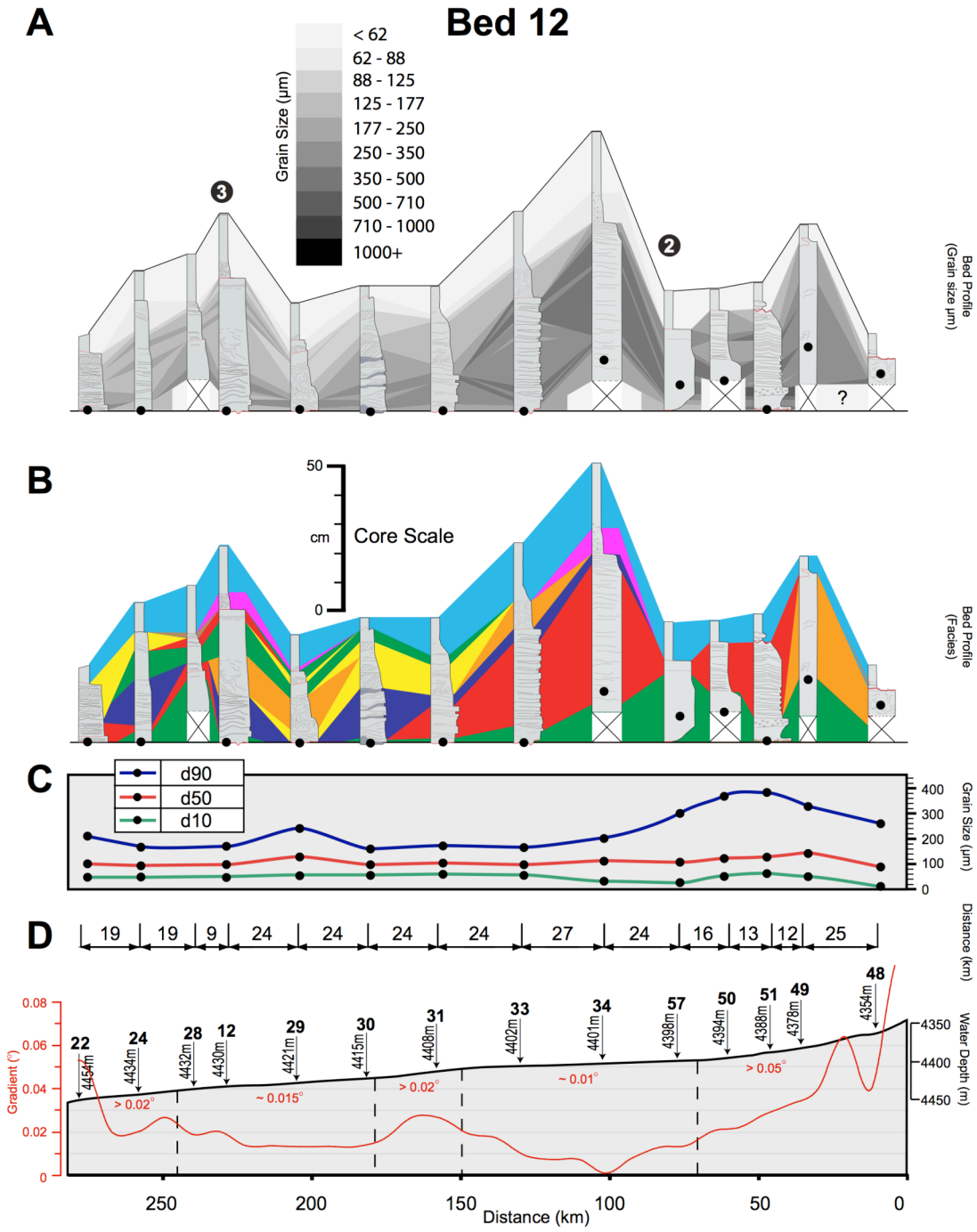

Figure 4-15: Bed A12 transect 1 along the axis of the Agadir Basin. Graphic logs are anchored onto a horizontal surface to highlight changes in bed thickness. Refer to Figure 4-5 for key. (A) Vertical and spatial distribution of grain size. Position of across flow transects 2 and 3 are marked. (B) Colour denotes interpreted facies. (C) Basal grain size at each core site. (D) Sea floor topography (grey shaded area) overlain with sea floor gradient (red line) along the axis of the Agadir Basin.

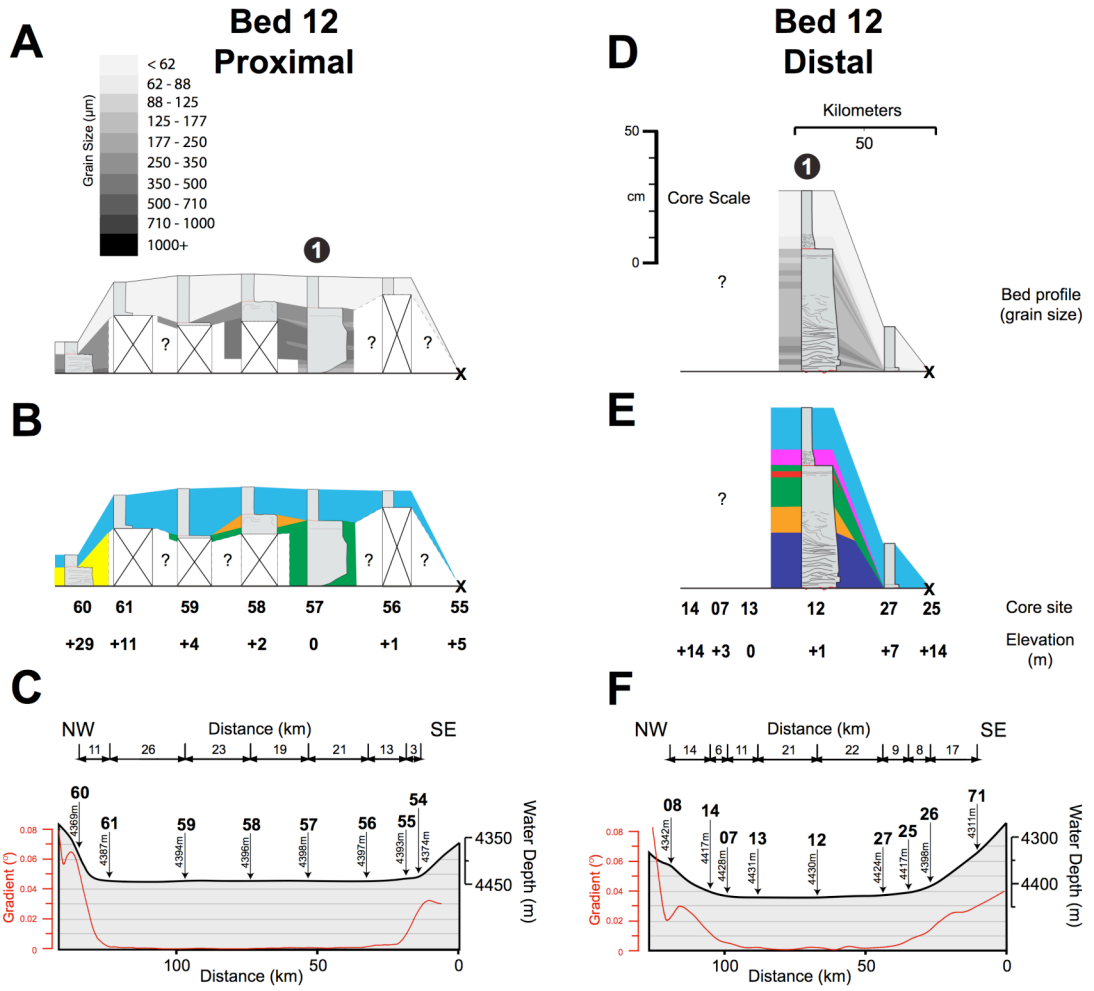

Figure 4-16: Bed A12 transects 2 (proximal) and 3 (Distal) from NW to SE across the Agadir Basin. Graphic logs are anchored onto a horizontal surface to highlight changes in bed thickness. White crossed areas indicate poor core recovery. (A and D) Vertical and spatial distribution of grain size. Position of transect 1 is marked. (B and E) Colour donotes interpreted facies. (C and F) Sea floor topography (grey shaded area) overlain by sea floor gradient (red line). Vertical exaggeration ~ 160 times.

4.4.7 Identifying traces of deposition from turbidity currents

Key core sites 25, 26, 54 and 55 are located along the margins of the Agadir Basin (Figure 4-1). These sites mark the boundary at which specific beds did not deposit sediment, i.e. the lateral pinch out of individual beds. Turbidite mud, silt and sand is easily distinguished from background hemipelagic sediment by visual logging for beds thicker than ~ 5 cm. However, if deposits are very thin (< 1 cm) fine-grained and/or strongly bioturbated they can be visually challenging to recognise. Hence, in key core sites 25, 26, 54 and 55, where turbidite beds pinch out, differences in the detailed grain-size characteristics of turbidite versus hemipelagic sediment were used to establish whether any turbidite deposition has occurred (Figure 4-17).

Hemipelagic carbonate ooze (interglacial) has a bimodal grain-size distribution with modes of ~ 5 and ~ 250 μm, representing clay and foraminifera tests respectively (Figure 4-17C; modes A and C). In glacial periods the tests are dissolved leaving just the fine clay mode (~ 5 μm). Both interglacial and glacial hemipelagic sediments have grain-size distributions with a low frequency of grain sizes between ~ 35 μm to ~ 70 μm (Figure 4-17C; mode B). Traces of turbidite sediment will change the signature of the hemipelagic grain-size distribution. Traces of very fine silt/mud (~ 20 μm) will either significantly broaden the ~ 5 μm mode or increase the modal grain size to higher values. Traces of coarser grained turbidite sediment (~ 35 μm to ~ 70 μm) will generate anomalously high frequencies within what would otherwise be the lowest frequency grain-size range. None of the key core sites (25, 26, 54 and 55) contained grain-size distributions suggestive of small amounts of turbidite sediment being deposited in these locations

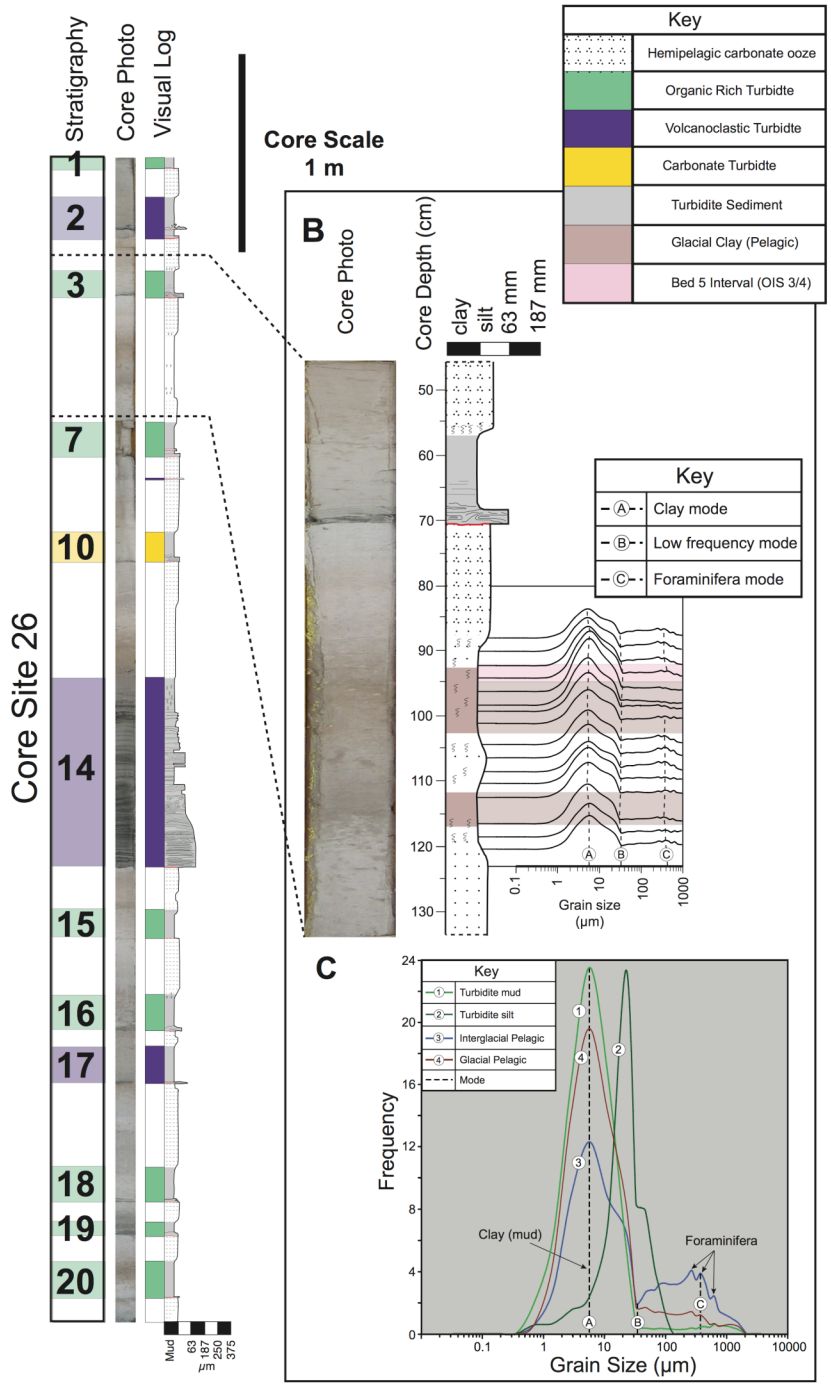

Figure 4-17: (A) Examination of basin margin core site 26, illustrating turbidite stratigraphy down core. Note the absence of Bed A5 in the stratigraphy, marked with a black dashed box (see Figure 4-4). (B) Grain-size analysis every 1 cm through the interval where Bed 5 should appear. Position where Bed A5 appears in other core sites is shaded pink. Grain size does not change through the interval, indicating no turbidite deposition. (C) Grain-size distributions sampled from Core 12. Bed A5 turbidite mud (1) and silt (2) are shown against interglacial (3) and glacial (4) hemipelagic sediments. Note the low frequency mode in the hemipelagic sediments of ~ 35 μm, similar grain-size distributions as seen above through in Core 26 (B).

4.5 Interpretation of results

This section presents interpretations of across flow (lateral) pinch outs of turbidite beds and how they reflect flow thickness, lithofacies and how it records the character of the flows that deposited them, and bed shapes and how they record the evolution of the flows that produced them.

4.5.1 Estimating flow thicknesses: What do lateral pinch outs represent?

Having established the lateral extent of turbidite deposition along the basin margins it is now important to understand the processes governing how far deposits can drape up topography. Close to the mouth of the Agadir Canyon, Beds A5, A11 and A12 drape higher up the northwest basin margin than along the southeast basin margin. The entry point of turbidity currents was slightly oblique to the basin axis (Figure 4-1A). Therefore, close to the mouth of the Agadir Canyon, the flows are likely to have run up the north-west basin margin, increasing the height that deposits drape up the slope (Kneller and McCaffrey, 1999). In contrast, the southeast basin margin has not blocked the flows and onlap along this margin more closely records the true thickness of the turbidity currents. In terms of flow thickness, the height to which deposits drape along the southeast basin margin can be interpreted in two ways. First, the height provides a maximum estimate of flow thickness (Figure 4-18A). Second, the height at which the deposits drape represents the maximum thickness of the depositional part of the flow. In this case the upper parts of the flow, which onlap higher up the margins, are erosional and/or bypassing (Figure 4-18B; Time 1 and Time 2). This upper layer is likely to be fine-grained and dilute (Kneller et al., 1999; Kneller and Buckee, 2000; Duitt et al., 2002; Gladstone and Sparks, 2002). Hence, only very low flow velocities would be needed to keep the sediment in suspension. In this scenario the upper parts of the flow were capable of efficiently transporting fine-grained sediment, and able to bypass these grain sizes for hundreds of kilometers down slope. Indeed, the majority of the silt and mud from these flows is found ~ 700 km down slope in the Madeira Abyssal Plain (McCave and Jones, 1988; Jones et al., 1992; Rothwell et al., 1992; Weaver et al., 1992). Despite this, some silt

and mud was deposited in the Agadir Basin. These deposits were most likely generated from the tail of the flow, where flow speeds would be sufficiently slow to allow the finer grains to settle from suspension. These fine-grained deposits pinch out abruptly, at similar or slightly higher elevations to the sandy deposits (e.g. Bed A5; Figure 4-10). This indicates the flow tails were also thin, and comparable in thickness to the main body of the flow (Figure 4-18B; Time 3 and Time 4). However, in Bed A11 fine-grained silts and muds drape higher up the basin margins (< 5 m) than coarser grained sands (< 1 m; Table 4-2), indicating the upper parts of the flow was thicker (i.e. up to ~ 4 m thicker) than the underlying sand-laden parts of the flow (Figure 4-18C). Bed A12 shows a similar trend in the southwestern parts of the Agadir Basin (Figure 4-16). Here, sand deposits drape < 6 m up the basin margins, whilst silt and mud drape < 14 m, indicating the tail of the parent flow was up to ~ 8 m thicker than the sand-laden basal part of the flow.

4.5.2 How do individual lithofacies record flow character?

This section explores how individual lithofacies found within turbidites record the character of the flow that deposited them.

4.5.2.1 Origins of structureless clean sand (ST)

Structureless clean sand can potentially be deposited in several different ways including rapid sediment fallout beneath high density turbidity currents (Kuenen, 1966; Sumner et al., 2008), which may generate sustained liquefied zones (Kneller and Branney, 1995; Johansson et al., 1998), or by en-masse deposition from sandy debris flows (Shanmugam, 1996; Shanmugam, 2000). Post-depositional processes such as fluidization and liquefaction can also produce structureless sands (Duranti and Hurst, 2004).

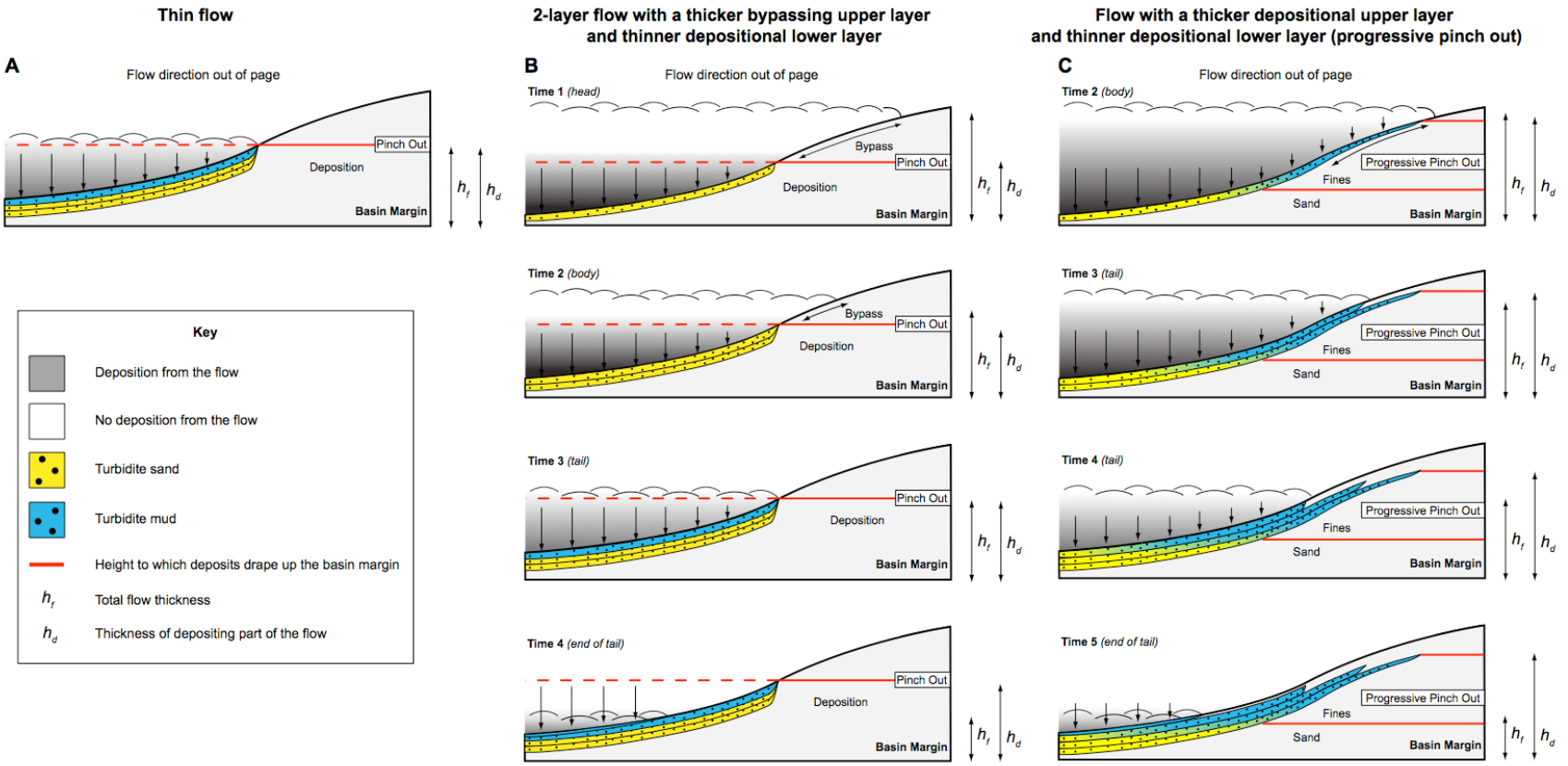

Figure 4-18: An across flow schematic illustrating two models. (A) A 2-layer stratified flow with a high-concentration basal layer and a dilute upper layer. Deposition is restricted to the basal zone with the upper layer bypassing. The flow is thicker than the height the deposit drapes up the margin. (B) A single layer high-concentration flow. Here the depositional thickness is the same as the total thickness of the flow.

Rapid aggradation beneath high-concentration turbidity currents best explains the range of features observed in the basal and upper structureless clean sands found in Beds 3, 5, 7, 11 and 12. They include inverse and normally graded intervals and interbedded with or laterally grading into parallel laminated sands (e.g. Bed A11; Figure 4-13). Basal structureless sands are overlain and in some cases interbedded with undisturbed planar laminated sand, indicating that liquefaction did not generate the structureless texture (e.g. Core 12; Figure 4-9B). Similarly, upper structureless sand found distally in Bed 12 is immediately overlain by undisturbed laminated sand (Core 12; Figure 4-15B). This again, suggests that liquefaction was not the cause for the structureless texture.

4.5.2.2 Origins of planar laminated sand (PL)

Planar lamination within the upper-stage plane bed regime can be produced by the migration of low amplitude bedwaves at the base of a dilute flow with low rates of aggradation (Allen, 1982; Best and Bridge, 1992), and the repeated collapse of near bed laminar-sheared layers at the base of a high-concentration flow with high rates of aggradation (Vrolijik and Southard, 1997; Sumner et al., 2008). Indeed, these two mechanisms need not be mutually exclusive within a single deposit. The experiments of Sumner et al. (2008) demonstrate that initially high-concentration flows are able to produce planar lamination. First, under high rates of aggradation by the repeated collapse of laminar-sheared layers. Then, as the flow becomes more dilute, under low rates of aggradation by the migration of low amplitude bedwaves (Sumner et al., 2008). Distinguishing the two mechanisms from deposits alone is problematic. However, lateral and vertical associations with well-understood facies provide a means to assess which was more likely.

Planar laminated sands found proximally in turbidites across the Agadir Basin typically occupy the basal parts of the deposits, and often laterally grade or are interbedded with basal structureless sands (e.g. Bed A5; Figure 4-9B). Structureless sands are most likely produced beneath a high-density turbidity current. Hence, these facies associations suggest planar

lamination was formed via the repeated collapse of laminar-sheared layers beneath a high-concentration flow. In contrast, planar lamination found in the upper parts of the turbidites and also in distal areas of the basin, is associated with cross-laminated sands (e.g. Bed 12; Figure 4-15B). Such facies can only be produced beneath dilute flows. In this case, planar laminated sands were most likely being deposited beneath a dilute flow via the migration of low amplitude bedwaves.

4.5.2.3 Syn/Post depositional liquefaction (CL)

The inability of pore fluid to escape during or immediately after deposition can liquefy a bed, especially where sedimentation rates are high (Allen, 1982). In this mechanism pore pressure is high enough that the grains become fluid supported (i.e. liquefied) and settle over time (Allen, 1977). This results in the disruption and/or complete destruction of existing sedimentary structures, producing deposits with convolute laminations and/or structureless textures.

Syn-depositional liquefaction best explains the association of contorted sand intervals with rapidly deposited structureless and planar laminated sands (e.g. Core 49; Figure 4-15B), and distally with ripple cross-laminated sands (e.g. Bed 7; Figure 4-11B), and the occurrence of contorted intervals at various heights in deposits.

4.5.2.4 Origins of mud-rich structureless sand (ST_D)

The occurrence of a chaotic, mud-rich facies within an otherwise clean turbidite sand can be produced from a flow containing both turbulent and laminar (cohesive) flow rheologies (Haughton et al., 2003; Talling et al., 2004; Talling et al., 2007c; Haughton et al., 2009). Within the turbulent part of the flow particles can be sedimented in a grain-by-grain fashion, and produce deposits that are graded and may have sedimentary structures. Within the

laminar part of the flow particles are unable to settle onto the bed individually and are deposited 'en masse' by frictional freezing. This produces deposits that are poorly sorted (chaotic), ungraded and often overlain by a sharp grain-size break. Experiments have demonstrated that mud content is a fundamental control on flow rheology (i.e. whether a flow is turbulent or laminar; Baas et al., 2009). Further experiments have shown that this style of deposit can be produced from the deceleration of an initially turbulent suspension that contains sufficient volume of cohesive mud (Sumner et al., 2009). As the turbulent flow decelerates, shear stresses decrease allowing the mud to form yield strength (laminar plug) and support grains within the flow. When a critical velocity is reached the laminar plug deposits 'en masse' (Sumner et al., 2009).

The mud-rich structureless sand bounded by 'clean' turbidite sand in Bed 5 has been interpreted by Talling et al. (2007c) to be a hybrid bed, with a mud-rich laminar plug (debris flow) forming towards the rear of an otherwise turbulent flow. The subtle changes in sea floor gradient along the axis of the basin control the velocity and in turn the rheology of the flow, meaning the plug is best developed on flatter areas of sea floor (Figure 4-9).

4.5.2.5 Origin of cross-laminated turbidite sand (LXL and RXL)

Ripple cross-laminated sand is produced beneath dilute flows with very low rates of aggradation. Near-bed turbulence systematically reworks sediment along the bed, generating ripple bedforms (Allen, 1982). Experiments have demonstrated that increasing the concentration of mud within the overriding flow radically changes ripple development (Baas et al., 2011). As mud concentration increases within the flow, ripple height and wavelength increase until high mud concentrations stop ripple formation. The increase in wavelength is attributed to increased near-bed turbulence, which leads to increased erosion on the lee side of the ripples (Baas et al., 2011). Ripples with extended wavelengths produce deposits of low-angle cross-laminated sand (Baas et al., 2011).

The event beds in this study are mud-rich containing large volumes of mud, either deposited separately from the sand, i.e. bypassed down slope in the Madeira Abyssal Plain (Wynn et al., 2002b), or with the sand as linked-debrite facies (Talling et al., 2007c). This suggests the parent flows had significant concentrations of mud. Ripple formation beneath a muddy flow best explains the low-angle cross-laminated sands in this study, and their association with ripple cross-laminated sands.

Sumner et al. (2012) have made similar interpretations for dune-scale cross-laminated sands found within individually correlated turbidite beds in the Marnoso Arenacea Formation, Italy. They proposed that flows with elevated mud contents preferentially developed dune-scale cross-laminae, which explains why dune-scale cross-laminae were common throughout some beds but entirely absent in others. This appears similar for turbidites in the Agadir Basin with low-angle cross-laminae common in Bed A12, yet rare in Beds A3, A5, A7 and A11.

4.5.2.6 Origin of turbidite mud (L, CM, M)

The processes surrounding the transport and emplacement of fine-grained turbidite mud/silt are complex. Clay particles are cohesive, meaning they can aggregate to form larger particles called flocs as they settle out from a suspension. These flocs can have a similar settling velocity (0.1 to 1 mm/s) to that of non-cohesive silt sized particles (Whitehouse et al., 2000). With increasing clay concentration these flocs can aggregate further to form a gel (Torfs et al., 1996; Cuthbertson et al., 2008a; Dankers et al., 2008), which causes the suspension to have a yield strength that must be overcome in order for particles to settle out. A similar phenomenon, in which fluid muds develop is well documented in estuarine and coastal settings (Trowbridge and Kineke, 1994; Kineke and Sternberg, 1995; McAnally et al., 2007a; McAnally et al., 2007b).

It has been proposed that the deposition of silt/mud laminae (L) is the product of alternating granular and cohesive bed conditions (Piper, 1972; Stow and Bowen, 1980). Due to

flocculation of clay particles, silt and mud within turbidity currents will initially settle towards the bed at similar shear velocities. However, near to the bed increased shear stresses will break up the flocs and prevent the mud from settling. Non-cohesive silt grains are able to settle through the boundary layer and deposit onto the bed via tractional processes (Piper, 1972). Continued sediment fallout from the overlying suspension will increase clay concentration near to the bed, which hinders the settling of both silt grains and mud flocs. Eventually the concentration of clay is sufficient to develop a fluid mud layer, which is deposited 'en masse' via frictional freezing onto the bed. Adhesion of the mud layer to the bed decreases clay concentration, once again allowing silt to settle onto the bed (Piper, 1972; Stow and Bowen, 1980).

Contorted muds, with silt laminae and silty clasts (e.g. Core 28; Figure 4-11), are likely produced from shearing of silt/mud laminae within fluid mud layers developed towards the tail of a decelerating turbidity current (Kneller and McCaffrey, 2003). Exactly when this shearing occurs (i.e. syn and/or post depositional) and how far the sheared facies have been transported from their original site of deposition is difficult to determine.

Structureless, ungraded mud (M) is produced from the clay-rich suspension left at the end of the flow. Here the clay flocculates and settles onto the bed via cohesive fluid mud layers (McCave and Jones, 1988).

4.5.2.7 Origin of grain-size breaks

Kneller and McCaffrey (2003) attributed grain-size breaks to longitudinal velocity and concentration gradients within the flow. Longitudinal fluctuations in these parameters change the capacity of the flow, generating periods of deposition followed by periods of bypass and reworking of existing deposits. Deposition recommences with a finer grain size, producing a deposit with a grain-size break from coarse sand to finer sand. Experiments have demonstrated that a constantly decelerating sand suspension experiences a hiatus in

deposition (Sumner et al., 2008). A depositional hiatus in a decelerating turbidity current would bypass certain grain sizes, and produce deposits with grain-size breaks between coarse sand to finer sand. The origins of grain-size breaks in turbidites is discussed further in Chapter 6.

4.5.3 How does bed shape record flow evolution?

Major controls on deposit shape are first outlined, and the implications for inferring flow evolution from the observed bed shapes are then discussed.

Experimental and numerical models commonly predict that a dissipating (spatially decelerating) turbidity current will produce a deposit that thins in a quasi-exponential fashion away from source (Middleton, 1993; Kneller and Buckee, 2000; Talling et al., 2007a) (Figure 4-19A). The term 'dilute flow models' is used here to refer to this type of dissipating flow. A number of factors can modify the character of the flows and change the shape of the resulting deposit.

4.5.3.1 Gradient

Experiments have demonstrated that increasing slope means that flows travel faster and are able to transport more of their sediment load further along the length of the flume tank. This produces deposits that extend further and maintain their thickness for longer along the length of the tank (Figure 4-19B; Gray et al., 2005).

4.5.3.2 Flow 'efficiency'

Increasing the proportion of fines within experimental turbidity currents enables them to transport their entire sediment load further, increasing their 'efficiency' (Mutti, 1992; Talling et al., 2007b). This is because finer-grained sediment is more easily transported than coarser-grained sediment yet still provides significant excess density to the flow, generating longer run-out distances and more tabular deposits (Figure 4-19C; Gladstone et al., 1998). Within longer lived particulate gravity currents finer-grained sediment will also be more easily resuspended from the bed, which will maintain the flow density (near-to-bed) and deposit thickness further down slope (Mutti, 1992; Talling et al., 2007b).

4.5.3.3 Flow thickness

Theoretically, flow thickness is a major control on bed shape, as it governs how long suspended grains will take to settle onto the bed. A turbidity current travelling down slope with particles settling vertically within it must transport those settling grains until they sediment onto the bed. Within a thicker flow grains will take longer to settle out and be transported further down slope than grains settling within a thinner flow. This will extend deposits further down slope and maintain their thickness for longer (Figure 4-19D).

4.5.3.4 Sediment concentration

Dissipating flows in numerical and experimental modelling are dilute (< 10 % sediment concentration) with non-cohesive particles supported via fluid turbulence (Middleton, 1993; Kneller and Buckee, 2000). With increased sediment concentrations (> 10 %) particles are supported via inter-particle interactions rather than fluid turbulence, particularly near to the bed (Lowe, 1982; Jha and Bombardelli, 2010). Inter-particle interactions within the flow

boundary zone will reduce the settling velocity of grains falling from the overriding suspension (hindered settling) (Davis and Gecol, 1994; Tomkins et al., 2005; Cuthbertson et al., 2008b). This allows grains that would otherwise be sedimented on the bed to be transported further down slope. The nature of a high-concentration suspension means when a critical velocity is reached, a flow will 'collapse' (rapidly deposit) its sediment load onto the bed, producing abrupt changes in bed thickness (Figure 4-19E).

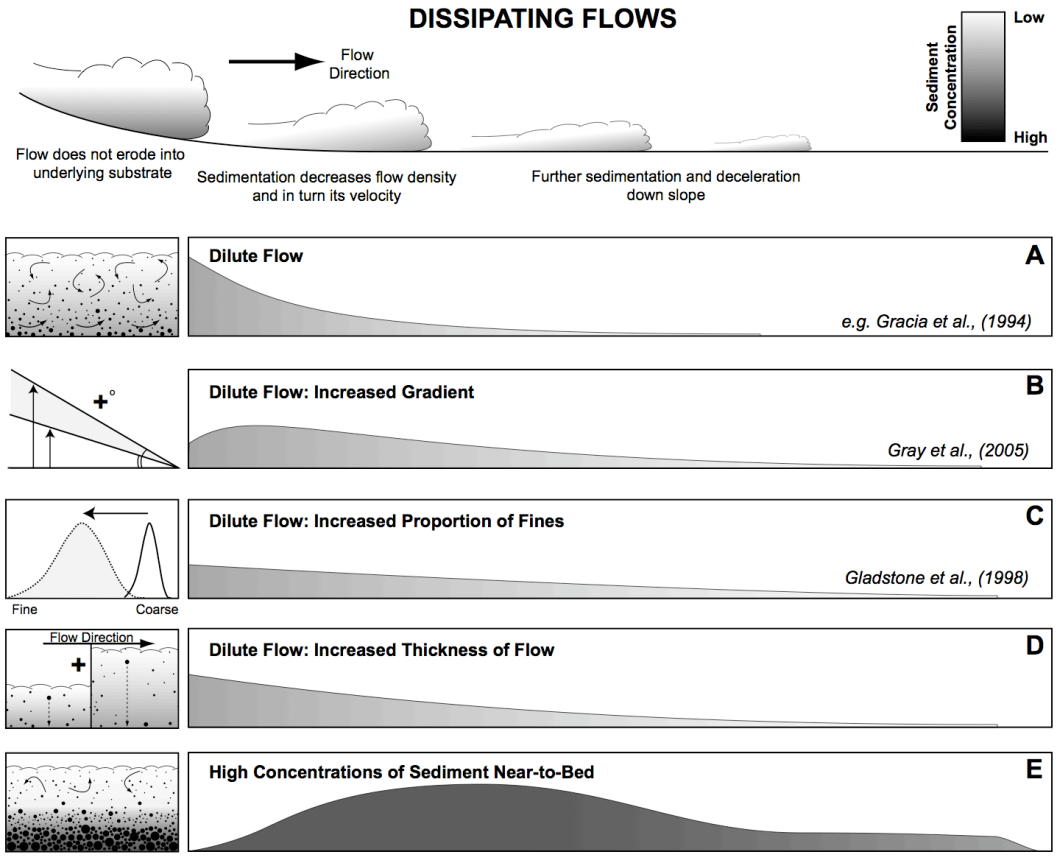

Figure 4-19: Cartoon illustrating a range of different bed shapes. (A) 'Typical', dissipating dilute-flow behaviour, producing a bed shape that thins in a quasi-exponential fashion down flow (e.g. Garcia, 1994). A number of factors can influence flow behaviour and the resulting bed shape: (B) Changes in slope (Gray et al., 2005), (C) Changes in the proportion of fines within the flow (Gladstone et al., 1998), (D) Differences in flow thickness, and (E) high-concentrations of sediment, particularly near-to-bed. These effects are discussed within the main text.

4.5.4 Evolution of flows in the Agadir Basin

Bed shapes, and distributions of lithofacies within the five beds, are now used to interpret the evolution of the parent flows across the Agadir Basin. Due to the significant differences between the beds, each bed is discussed separately (Table 4-2).

4.5.4.1 Bed 3 (Tabular and abruptly thinning)

The flow that deposited Bed 3 was relatively small-volume (~ 16 km^3) with very different thicknesses for the sandy basal flow (< 2 m) and the upper muddy part of the flow (> 24 m). The sandy basal part of the flow was initially high-concentration with high aggradation rates, because it deposited planar laminated sands overlain by upper structureless sands. The thin high-concentration layer did not dissipate, but abruptly ceased to be able to transport its sand load. This produced a tabular sand interval with an abrupt termination. The thicker, upper parts of the flow that were transporting the finer grain sizes were able to travel further down slope, and progressively deposited along the length of the basin.

4.5.4.2 Bed 11 (Abruptly thinning to quasi-exponential)

The flow that deposited Bed 11 was small-volume (~ 14 km^3) and relatively thin. The basal, sandy part of the flow was < 1 m thick, whilst the upper muddy part was < 5 m thick (Table 4-2). The flow was initially high concentration and rapidly deposited sand proximal to the mouth of the Agadir Canyon. Temporal fluctuations in high aggradation rates produced interbedded planar and structureless sands. Due to high aggradation rates the flow quickly dissipated and ultimately became dilute, depositing ripple cross-laminated sands more distally. The initial rapid thinning of Bed 11 is most likely due to the high-concentration nature of the flow. However, the bed then displays a quasi-exponential thinning, similar to

that predicted by dilute flow models. The finer grained parts of the flow were bypassed through proximal areas, and progressively deposited in the distal parts of the basin.

4.5.4.3 Bed 7 (Tabular)

The flow that deposited Bed 7 had a large sediment volume (~ 120 km^3). The sandy and muddy parts of the flow were > 24 m thick (Table 4-2). The flow was dilute as it progressed along the length of the Agadir Basin, as shown by the deposition of ripple cross-laminated sands. Near to the Agadir Canyon the flow was most likely dilute but fast enough to generate planar laminated sands. Lateral grading into ripple cross-laminated sands indicates the dilute flow must have decelerated. The unchanging grain size within the extensive ripple cross-laminated basal sands (Figure 4-11C) indicates that the near-bed flow changed little along the entire length of the basin, remaining dilute and maintaining a relatively constant velocity. A high proportion of fines in Bed 7 (Figure 4-11C) indicates that the parent flow was very efficient and therefore able to transport sediment much further down slope than would otherwise be predicted by 'dilute flow models'. Towards the rear of the turbidity current the flow waned sufficiently to deposit its fine-grained sediment load. It first deposited inter-laminated silts and muds, then with an increasingly clay-rich suspension, ungraded structureless mud. However, as fine-grained sediments were deposited along the basin margins they became unstable, and remobilized to flatter areas of the basin. This produced the complex contorted mud textures observed extending across flow from the basin margins (Figure 4-12).

4.5.4.4 Bed 12 (Thinning to tabular)

The flow that deposited Bed 12 had a large sediment volume (~ 220 km^3) that was mostly fine-grained mud and silt (~ 190 km^3; Frenz et al., 2008). It had different thicknesses for its lower sandy parts (< 5 m thick) and its upper muddy parts (< 14 m thick). The flow was

initially high-concentration, as shown by the deposition of structureless and planar laminated sands. Down slope the flow slowly dissipated into a dilute suspension with an elevated mud content, as shown by the progressive deposition of low-angle cross-laminated sand and then ripple cross-laminated sand. The lack of fining in basal sands within the distal parts of the basin suggests that the flow was able to maintain a relatively constant velocity once it became dilute. The quasi-steady flow enabled suspended sediment to slowly concentrate near-to-bed towards the rear of the turbidity current, such that sediment concentrations within the flow boundary layer increased near to the capacity of the flow. With decreased slope and hence flow velocity, turbulence within the hyperconcentrated zone collapsed and sand was deposited rapidly onto the bed, producing upper structureless sands in the distal parts of the basin. The essentially tabular shape of Bed 12 differs from the exponentially thinning shape of deposits from dilute flow models. Bed 12 shows a progressive increase in fine grain percentage along the basin (Figure 4-15C). An increase in fines within the parent flow would have increased its efficiency, enabling it to transport its sediment load further than would otherwise be predicted by dilute flow models. Eventually the flow waned sufficiently to deposit fine-grained sediment. It first deposited interlaminated silts and muds, then with an increasingly clay-rich suspension, ungraded structureless muds. However, due to the large volume of the flow most of the fines were bypassed ~ 700 km down slope into the Madeira Abyssal Plain (Wynn et al., 2002b).

4.5.4.5 Bed 5 (Tabular and abruptly thinning)

The flow that deposited Bed 5 had a large sediment volume (~ 160 km^3). It was relatively thin with both sand and mud being < 24 m thick. The parent flow was high-concentration, as shown by the deposition of basal structureless sands interbedded with planar laminated sands (Figure 4-9B). The flow maintained this high-concentration state for almost the entire length of the basin, as evidenced by the unchanging, basin-wide deposition of its facies. A lack of fining in these basal sands demonstrates the flow maintained its capacity for most of the length of the basin (Figure 4-9C). The high-concentration nature of the flow promoted hindered settling, resulting in an extensive, tabular bed shape, followed by an abrupt thinning. Toward the rear of the body of the flow increasing proportions of cohesive mud within the

suspension suppressed fluid turbulence, forming a laminar plug. Continued deceleration increased the thickness of the plug until it was able to freeze 'en masse', producing mud-rich structureless sand (i.e. linked-debrite) on flatter parts of the basin floor (Talling et al., 2007c; Wynn et al., 2010). Since dilute flow models do not simulate high sediment concentrations or cohesive effects, it is unsurprising that both clean sand (high-concentration turbidite) and mud-rich sand (cohesive debrite) geometries are not predicted by dilute flow models.

4.6 Discussion

4.6.1 What controls flow thickness?

Previous studies have suggested that flow thickness is a function of sediment grain size (Rouse, 1937; Bowen et al., 1984; Normark et al., 2009) and flow volume. For example, Bowen et al. (1984) constrained turbidity current thicknesses on the Navy Fan. They found that a turbidity current containing ~ 3 % sand was 15-75 m thick, whereas a turbidity current containing ~ 42 % sand was less than 10 m thick. Similarly, within confined submarine channel settings, deposits of sand abruptly pinch out laterally over small changes in elevation: < 27 m within the Redondo Fan, offshore California (Normark et al., 2009); and, < 39 m within the Congo Fan, offshore west Africa (Babonneau et al., 2010). In contrast, finer-grained sediment drapes hundreds of meters up topography often overspilling the confines of a channel, generating channel levees (Hiscott et al., 1997). However, in this study we find limited evidence for strong correlation between either sediment size or flow volume and flow thickness (Figure 4-20).

The finest grained turbidites (Beds A3 and A7), which contain 10 % sand, drape > 29 m up the basin margin, whereas the coarser grained turbidites (Beds A11 and A12), which contain 15 – 25 % sand, drape < 14 m up the basin margin (Figure 4-20A). However, the coarsest grained turbidite (Bed A5), which contains 40 % sand, drapes 24 – 33 m up the basin margin. If grain-size alone controls flow thickness then Bed A5 would be expected to be the thinnest flow.

The smallest volume turbidite (Bed A3) drapes > 29 m up the basin margin, whilst Bed A11 is a similar volume it only drapes < 6 m up the basin margin (Figure 4-20B). Large-volume Beds A5 and A7 drape 24 – 33 m and > 33 m up the basin margin respectively. However, the largest volume turbidite (Bed A12) only drapes < 14 m up the basin margins. If volume alone governed flow thickness then it would be expected that Bed A12 would be the thickest flow.

Flow volume may not be an important control on flow thickness in this system because the Agadir Basin is an open system, connected to the Madeira Abyssal plain at its distal end (Figure 4-1). This may result in large-volume flows bypassing much of their sediment load through the Agadir Basin and depositing it on the Madeira Abyssal plain.

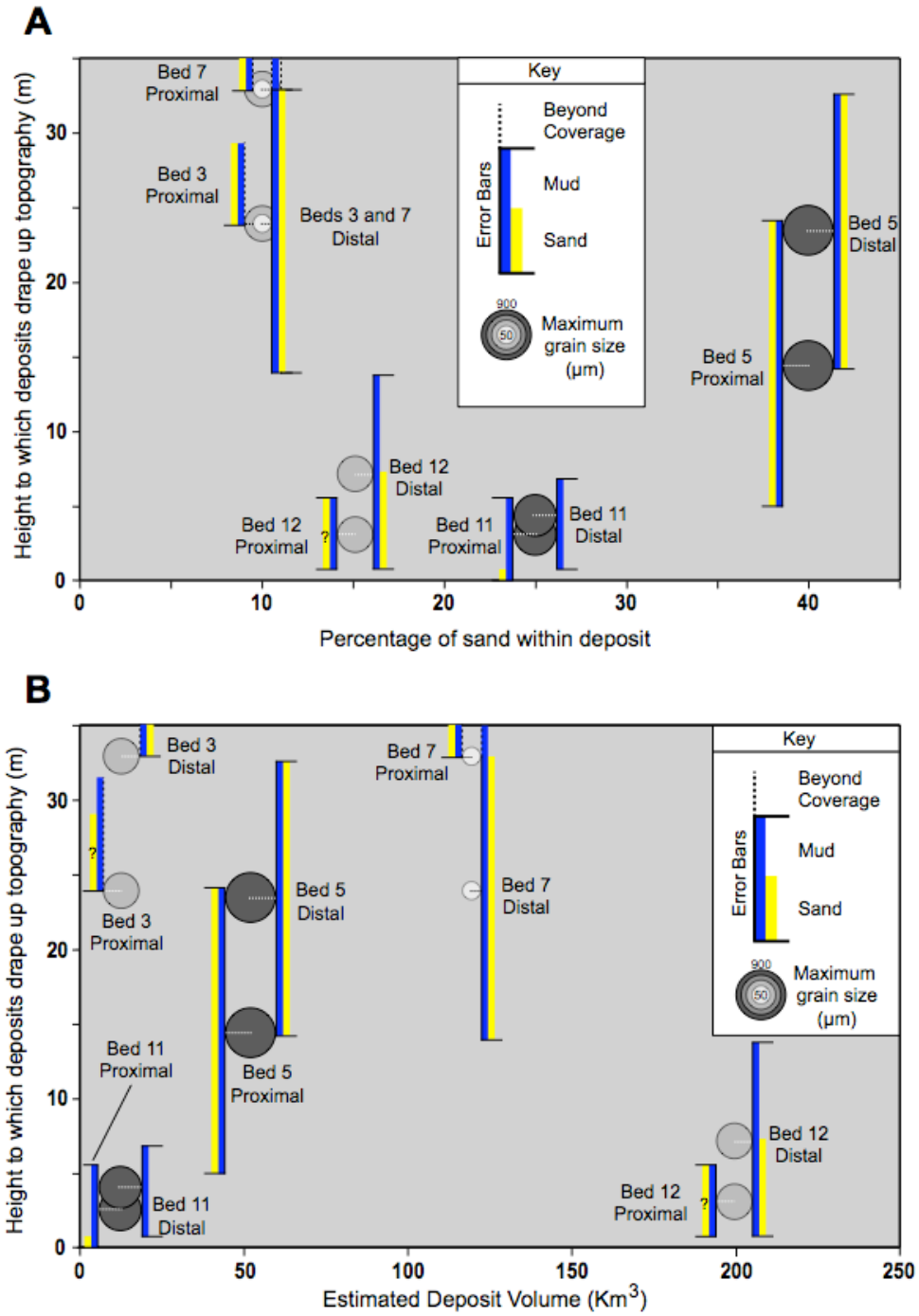

Figure 4-20: Graphs showing the height to which deposits drape up the southeast basin margin, interpreted to be a measure of flow thickness. Error bars (blue and yellow) show where deposits pinch out up topography, and are constrained by elevations between core sites. Mid-points within the error bars show maximum grain size measured in the bed (Table 4-2). White dashed lines connect error bars with the associated grain-size measurement for each bed. Height to which deposits drape up basin basin margin topography is plotted against: (A) Total sand fraction within bed (measured from the total estimated deposit volume), and (B) Total estimated deposit volume, including bed volumes from the Agadir Basin and Madeira Abyssal Plain (after Frenz et al., 2008). Note the poor correlation in both cases.

4.6.2 Modelling flow processes, sediment transport and erosion

This section attempts to understand how flows were able to run-out so far, producing beds that did not appreciably thin or fine for hundreds of kilometres down slope. First, the erosion threshold of the seafloor is calculated, providing an important constraint on near bed shear stresses beneath the flows (i.e. how fast flows could travel before eroding into the seafloor). Flow parameters derived from the field data are tested against this constraint, providing a means to validate the proposed models.

4.6.2.1 Calculating flow speeds required to erode the seafloor

The flows that deposited Beds A5, A7 and A12 were not erosive across the Agadir Basin, as determined by similar coccolith assemblages in their mud caps down slope (Weaver, 1994; Wynn et al., 2002b) and relatively uniform thicknesses of hemipelagic sediment underlying the beds (Figure 4-2). Therefore, calculating erosion thresholds for the hemipelagic (sea-floor) sediments provides estimates for maximum flow velocities for turbidity currents passing across the basin floor. Currently there are no in-situ measurements of erosion thresholds for deep-water hemipelagic sediments. Therefore, we assume that deep-water hemipelagic erosion thresholds are similar to those determined from in situ field measurements in muddy, shallow-water environments (e.g. Amos et al., 1997; Amos et al., 2010). We estimate the critical shear stress required to initiate seafloor erosion via:

$$U^* = \sqrt{\frac{T_o}{P_f}} \qquad \text{Eq. 1}$$

where, U^* is the critical shear stress for seafloor erosion (ms^{-1}), P_f is the bulk density of the flow, and T_o is the shear strength of the seafloor sediment. A range of values for P_f are shown in Table 4-3, ranging from relatively high-concentration values (12.5% sediment by volume) to low-concentration values (1.25% sediment by volume). For the purposes of our calculation a relatively low value for P_f is used (1100 kgm^{-3}) representing a dilute flow comprising ~6.25% sediment by volume. Using a low value for P_f produces a higher value for U* (Eqn. 1), meaning the calculated erosion threshold is high, i.e. representing an upper threshold. Flows with a higher bulk density will reduce this threshold. For example, it is likely that Bed A5 was deposited beneath a high-concentration flow (>10% sediment by volume). Therefore, P_f values of >1175 kgm^{-3} (~10% sediment by volume) may be more appropriate when estimating the seafloor erosion threshold beneath the flow that deposited Bed A5 (Table 4-3). The shear strength (T_o) of seafloor sediment has been related to a wide range of sediment properties such as water content, bulk density, cation exchange capacity, clay content, and organic content (Otsubo and Muraoka, 1988; Mehta et al., 1989; Amos et al., 2010). Here we use the empirical relationship between sediment bulk density and shear strength, as examined by Amos et al. (2010) in shallow-water muddy sediments, to calculate values of T_o for seafloor sediment across the Agadir Basin:

$$T_o = \left[5.44 \times 10^{-4} P_b\right] - 0.28 \qquad \text{Eq 2.}$$

where, P_b is the wet bulk density of the sea floor sediment (kgm^{-3}). Gamma-ray measurements of cores across the Agadir Basin show hemipelagic sediments within the uppermost parts of shallow piston cores to have densities of between ~ 1600 and 1700 kgm^{-3} (see multi-sensor core log data; Appendix). This corresponds to T_o values of 0.59 and 0.64 Pa respectively. Hence, from Eq. 1, assuming a P_f value of 1100 kgm^{-3}, a seafloor erosion threshold (U^*) is calculated between 0.023 and 0.024 ms^{-1}, depending on the bulk density of the hemipelagic sediment. For the purposes of length advection scale analysis (outlined below), these U^* values are converted to flow velocities of approximately 0.35-0.4 ms^{-1} (Table 4-3). However, for all other analyses U^* is used to avoid the uncertainty associated with the value of C_D (see Eq. 9 and related discussion below).

		Erosion threshold (U^* ms^{-1})		Erosion threshold (U ms^{-1})	
P_f (kgm^{-3})	Sediment concentration (volume %)	T_o from sediment bulk density (Pa)		C_D=0.004	
		(1600 kgm^{-3}) T_o=0.59	(1700 kgm^{-3}) T_o=0.64	(1600 kgm^{-3}) T_o=0.59	(1700 kgm^{-3}) T_o=0.64
1200	12.5	0.022	0.023	0.35	0.37
1175	10.9	0.022	0.023	0.35	0.37
1150	9.4	0.023	0.024	0.36	0.37
1125	7.8	0.023	0.024	0.36	0.38
1100	6.3	0.023	0.024	0.37	0.38
1075	4.7	0.023	0.024	0.37	0.39
1050	3.1	0.024	0.025	0.37	0.39
1025	1.6	0.024	0.025	0.38	0.40
1000	0	0.024	0.025	0.38	0.4

Table 4-3: Summary of calculated seafloor erosion thresholds. A range of bulk flow densities (P_f) are considered. The associated sediment concentration within the flow (Vol. %) is calculated assuming the sediment is the density of silica sand (2600 kgm^{-3}) and suspended in seawater with a density of 1000 kgm^{-3}. Erosion threshold is calculated as a critical shear stress (U^*). Values for T_o are discussed in the main text. Converting U^* to flow velocities (U) is achieved assuming a C_D value of 0.004. This is a crude approximation, which is only applied to the length scale analysis in Figure 4-21.

4.6.2.2 Simple dilute flow

A flow that is depositional will progressively decelerate as its sediment load (and its bulk density) decreases. Experiments have shown that dilute depositional turbidity currents progressively decelerate and produce deposits that thin and fine in a quasi-exponential fashion away from source (see reviews by Middleton, 1993; Kneller and Buckee, 2000; Talling et al., 2007a). However, the rate of thinning and fining within a turbidite deposit can be significantly reduced by the length advection scale of settling particles, making a bed more tabular with less fining in grain size down slope (Dade and Huppart, 1994; Straub et al., 2008). The advective length scale describes the average downstream distance a settling particle is transported before adhering to the bed, described by Lamb et al. (2010) as:

$$L_a = UT_S \qquad \text{Eq. 3}$$

where U is the average downstream velocity of the flow (ms^{-1}) and T_S is the time taken for a settling particle to settle onto the bed, defined as:

$$T_S = \frac{H_f}{W_S} \quad \text{Eq. 4}$$

where H_f is the flow thickness (m) and W_S is the settling velocity of the particle (ms^{-1}). This calculation uses individual flow thicknesses (H_f) inferred from the height to which deposits drape up the basin margins, as discussed earlier in the Chapter. W_S is calculated after Gibbs et al. (1971), assuming spherical particles settling within a stationary Newtonian fluid and no inter-particle interaction:

$$W_S = \frac{-3\eta + \sqrt{9\eta + gr^2 P_A (P_P - P_A)(0.015476 + 0.19841r)}}{W_S} \quad \text{Eq. 5}$$

where η is the dynamic viscosity of water (0.001 Pa), g is acceleration due to gravity (9.81 ms^{-2}), r is the radius of the settling particle (m), P_A is the density of seawater (1000 kgm^{-3}), and P_P is the density of the settling particle (assumed to be silica sand 2600 kgm^{-3}). Given the flow thicknesses inferred from deposits and assuming the settling grain is suspended within the uppermost parts of the flow, a maximum possible settling time can be estimated. If the advection length scale within the flows that deposited Beds 5, 7 and 12 was long enough, it could have produced the observed tabular bed shapes and uniform grain size distributions along the length of the Agadir Basin. Rearranging Equation 1 provides a means to calculate what flow speeds would be necessary if this were the case:

$$U = \frac{L_a}{T_S} \quad \text{Eq. 6}$$

where L_a is the advection length scale (m). The advection length is determined from the first and last instance of a particular grain size (D90) within the basal sands of each bed (Figure 4-21A). Hence, using T_S values from Equation 4, the flow velocity required to produce a

length advection scale, capable of generating the observed deposits, can be calculated (Figure 4-21B). Flow velocities required are: 632 ms^{-1} for Bed A5 (grains of 680µm and L_a of ~150km), 108 ms^{-1} for Bed 7 (grains of 150µm and L_a of 250km), and 1100 ms^{-1} for Bed 12 (grains of 180µm and L_a of 100km (Bed A12). Such high flow velocities are several orders of magnitude above the erosion threshold of the seafloor (~0.4 ms^{-1}; Figure 4-21B) and no significant erosion is observed. Therefore, it is not possible that flows were travelling at such speeds, which rules out advection length scale effects producing Beds A5, A7 and A12.

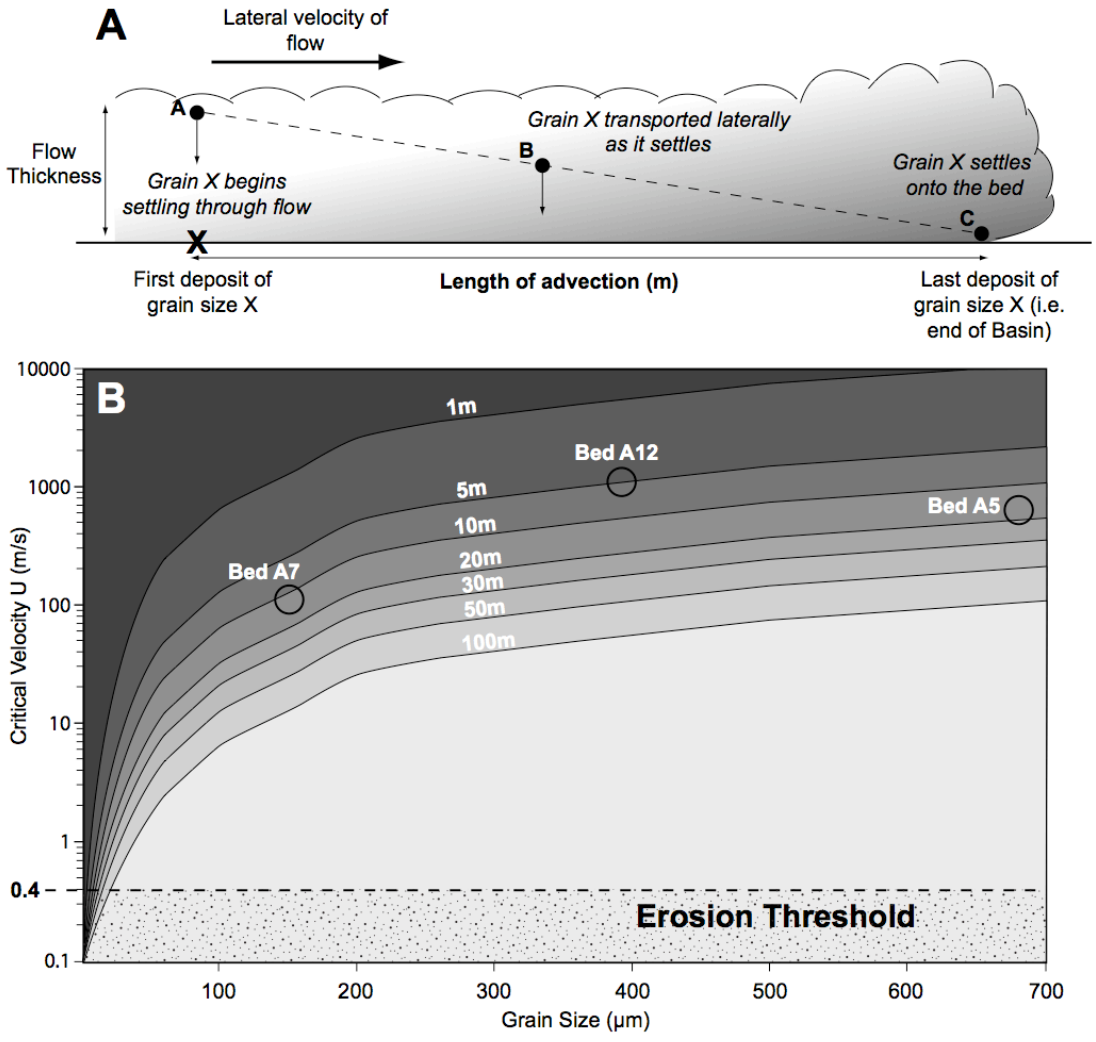

Figure 4-21: Cartoon illustrating a simple dilute flow model. (A) At the most proximal deposit containing a particular basal grain size, it is assumed the flow must be settling all grains of that size towards the bed. Given a certain flow thickness and assuming the settling grain is suspended within the uppermost parts of the flow, the maximum possible settling time can be estimated. (B) During this time the vertically settling grain is transported laterally (down slope) by the flow. (C) Until all the grains of that size are sedimented onto the bed, forming the most distal deposits of that grain size. Given the distance between the proximal and distal deposits (A – C) and the particle settling velocities, the flow speed (U) required to transport settling grains between A – C is plotted against grain size, assuming a range of flow thicknesses. The calculated sea-floor erosion threshold is marked with a dashed line at ~0.4 m/s. Beds A5, A7 and A12 are plotted onto the graph, predicting high U values.

4.6.2.3 Alternative Model – Autosuspending flows

The analysis above assumes turbidity currents behave in a similar manner to dilute experimental and numerical turbidity currents, where deposition causes the flow to decelerate, which in turn results in more deposition and further deceleration. The flow progressively decays, producing a bed that thins and fines in a quasi-exponential fashion away from source (see reviews by Middleton, 1993; Kneller and Buckee, 2000; Talling et al., 2007a). However, the length advection scale analysis above demonstrates that this model does not explain the observed architectures of Beds A5, A7, and A12. An alternative model is that flows were primarily autosuspending (bypassing), only depositing a small proportion of their total sediment load per square kilometre along their flow pathway. We now employ two sets of calculations to estimate the required flow shear stresses (U^*) for such a model to operate (Table 4-4). These shear stresses are compared to the erosion threshold of the seafloor (U^*), providing a means to validate the model.

Flow velocities required to autosuspend sand: Suspension threshold approach

To estimate how fast a flow must travel to autosuspend its entire sediment load, we assume that the coarse grain size (D90) within deposits is representative of the maximum shear stress,

which is related to the forward velocity of the flow (van Tassell, 1981; Bowen et al., 1984; Komar, 1985; van Tassell, 1986):

$$U^* = kW_S \qquad \text{Eq. 7}$$

where, U^* is the velocity shear stress beneath the flow (ms^{-1}), W_S is the settling velocity calculated from Equation 5 (ms^{-1}), and k is the flow condition (Wash load = 1; Suspended load = 1.25 and Bedload = 7-30). Previous values for k (suspended load) range from 1.0 to 1.25, representing the somewhat arbitrary distinction between suspended load and wash load sediment transport (Komar, 1985). It is assumed that bypassing sediment must be held aloft within the suspended load, such that k is between 1.0 and 1.25. Accounting for this range, Equation 7 estimates velocity shear stresses of 0.10-0.13 ms^{-1} for Bed A5 (680 μm grains), 0.020-0.025 ms^{-1} for Bed A7 (150 μm grain size), and 0.055-0.69 ms^{-1} for Bed A12 (180 μm grains). Almost all these calculated flow shear stresses exceed the calculated erosion threshold of the seafloor from Equation 1 (0.023 to 0.024 ms^{-1}). The exception is Bed A7, where a low value for k yields flow shear stresses that are within the seafloor erosional threshold. This calculation indicates that the parent flow of Bed A7 could have bypassed its sediment load without eroding into the seafloor.

Flow velocities required to autosuspend sand: Rouse approach

An alternative approach to estimate the velocity shear stress (U^*) required to suspend sediment is to relate the grain size to the Rouse Number (Rouse, 1937; Hiscott et al., 1997):

$$U^* = \frac{W_S}{ZBK_C} \qquad \text{Eq. 8}$$

where, B is a coefficient relating the sediment diffusion to the diffusion of turbulent energy ($B = 1$), K_C is the von Karman constant ($K_C = 0.4$ for a dilute flow; Straub et al., 2008), and Z is the Rouse Number. As with Equation 7 a somewhat arbitrary distinction between suspended and bedload sediment transport must be assigned. Here we consider Z values between 0.8 and 1.2 to represent 100% of a particular grain size being suspended within a flow (Table 4-4). Accounting for this range Equation 8 estimates velocity shear stresses of 0.21-0.31 ms^{-1} for Bed A5 (680µm grain size), 0.041-0.061 ms^{-1} for Bed A7 (150 µm grain size), and 0.11-0.17 ms^{-1} for Bed A12 (180 µm grain size). All of these calculated velocity shear stresses exceed the erosional threshold of the seafloor (0.023-0.024 ms^{-1}).

Estimates of flow velocity were calculated from the values of U^*:

$$U = \frac{U^*}{\sqrt{C_D}} \qquad \text{Eq. 9}$$

where U is the forward velocity of the flow, and C_D is the dimensionless friction coefficient. Importantly, values for C_D are derived from open surface flows. Indeed, it is debatable whether values for C_D, derived from free surface flows, are appropriate to apply to turbidity current modelling because entrainment of ambient fluid across the upper surface is likely to significantly affect the value of C_D at the base. These effects are yet to be resolved and remain an important parameter to constrain. This considered, a range of values for C_D have previously been employed to represent the friction coefficient beneath turbidity currents, from 0.0035 to 0.006 (Komar, 1969; Komar, 1971; van Tassell, 1981; Bowen et al., 1984). However, this range does not reflect the actual uncertainty within the parameter (Komar, 1985). Accounting for this range and for both approaches, flow speeds are calculated for Bed A5 (1.31-5.34 ms^{-1}), Bed A7 (0.25-1.04 ms^{-1}), and Bed A12 (0.71-2.90 ms^{-1}) and summarized in Table 4-4. We note that our estimated flow velocities, are similar to those determined from submarine cable breaks (~ 6 - 14 m/s; Heezen 1952; Krause, 1970), and directly from instrumentation (~ 1 – 4 m/s; Xu et al., 2004; Vangriesheim et al., 2009).

		Suspension threshold						Rouse					
Bed	Grain size (D90)	U^* (ms^{-1})		U ms^{-1} $= \frac{U*}{\sqrt{C_D}}$				U^*		U ms^{-1} $= \frac{U*}{\sqrt{C_D}}$			
		k=1.0	k=1.25	k=1.0		k=1.25		Z=0.8	Z=1.25	Z=0.8		Z=1.25	
				C_D=0.0035	C_D=0.006	C_D=0.0035	C_D=0.006			C_D=0.0035	C_D=0.006	C_D=0.0035	C_D=0.006
A5	680 µm	0.100	0.126	1.71	1.31	2.14	1.63	0.32	0.20	5.34	4.08	3.42	2.61
A7	150 µm	0.020	0.025	0.33	0.25	0.42	0.32	0.061	0.04	1.04	0.79	0.66	0.51
A12	180 µm	0.055	0.069	0.93	0.71	1.16	0.88	0.17	0.11	2.90	2.21	1.85	1.42

Table 4-4: Summary of calculated turbidity current shear stresses (U*) and flow speeds (U). Details of 'Suspension Threshold' and 'Rouse' calculations are discussed within the main text. Note the grey shaded cell in Bed A7, highlighting the only shear stress within the erosional threshold of the seafloor.

4.6.2.4 Autosuspension versus seafloor erosion

For the parent flows of Beds A5, A7 and A12 to autosuspend (i.e. bypass) their sediment loads Equations 7 and 8 require near bed shear stresses that exceed the erosional threshold of the seafloor. Two conceptual models are now proposed to explain how flows could be autosuspending yet non-erosive, as they passed across the Agadir Basin.

1. Slow moving autosuspending flows (Figure 4-22A)

The analysis above assumes particle settling velocities within turbidity currents can be approximated to those in clear still water. However, a number of factors can reduce the settling velocity of particles (discussed below). Reduced particle settling velocities would mean flows would require lower shear stresses to maintain grains in suspension. Hence, a flow with slow rates of particle settling would be able to travel relatively slowly yet still autosuspend (bypass) most of its sediment load (Figure 4-22A). In addition, reduced particle settling velocities would increase the length advection scale, maintaining the bulk density and velocity of the flow further down slope. Processes that can reduce the settling velocity of particles are now discussed.

Hindered settling in high concentration sediment suspensions

In the case of Bed A5, widespread deposition of structureless and parallel laminated sands indicate the parent flow was high-concentration throughout the Agadir Basin (Figure 4-9). The flow contained enough mud to deposit a linked-debrite (Talling et al., 2007c). At high sediment concentrations hindered settling can significantly reduce the settling velocity of particles (Richardson and Zaki, 1954; Batchelor, 1982; Tomkins et al., 2005; Cuthbertson et al., 2008).

Settling through a muddy suspension rather than clear fluid

The concentration and cohesive strength of mud within a particulate suspension can have a profound effect on fluid rheology. Relatively small amounts of mud within particulate suspensions can impart significant increases in yield strength and fluid viscosity (Coussot and Piau, 1994; Coussot and Boyer, 1995). Mud concentrations as low as 2 – 7 % by volume increase fluid viscosity and can develop yield strength, which hinders the settling of sand (Hampton, 1975; Amy et al., 2006). Determining exact mud concentrations within the parent flows of Beds A5 and A12 is problematic, because the behaviour of mud is governed by a number of factors acting individually or in concert, including clay type, proportion of cohesive versus non-cohesive particles, properties of the non-cohesive grains (shape, size and size-distribution), salinity of the fluid, and time (Cuthbertson et al., 2008). Within a submarine flow, these affects will also interact with shear stresses near to bed. The turbidites in this study are all mud-rich. In Beds A5 and A12, linked-debrite and low-angle cross-laminated facies indicate that elevated mud content within the parent flows was directly influencing non-cohesive sediment deposition (Baas et al., 2011; Sumner et al., 2012). Therefore, it is highly likely that mud was also reducing the particle settling velocities within the flows, enabling grains to be transported further than would otherwise be predicted.

2. Fast autosuspending flows that armour the seafloor (Figure 4-22B)

For the autosuspending model to work at relatively high near bed shear stresses (similar to those calculated above) without eroding, the seafloor erosion threshold must be significantly increased. A scenario in which this could be achieved is if the head of a flow was strongly depositional, and armoured the bed with sand before the faster moving (autosuspending) body eroded/reworked the bed (Figure 4-22B). High-concentration flows are able to rapidly deposit sediment at their heads, which could protect the underlying seafloor from erosion. However, dilute flows would not have the aggradation rates necessary to armour the seafloor before the flow eroded/reworked the bed.

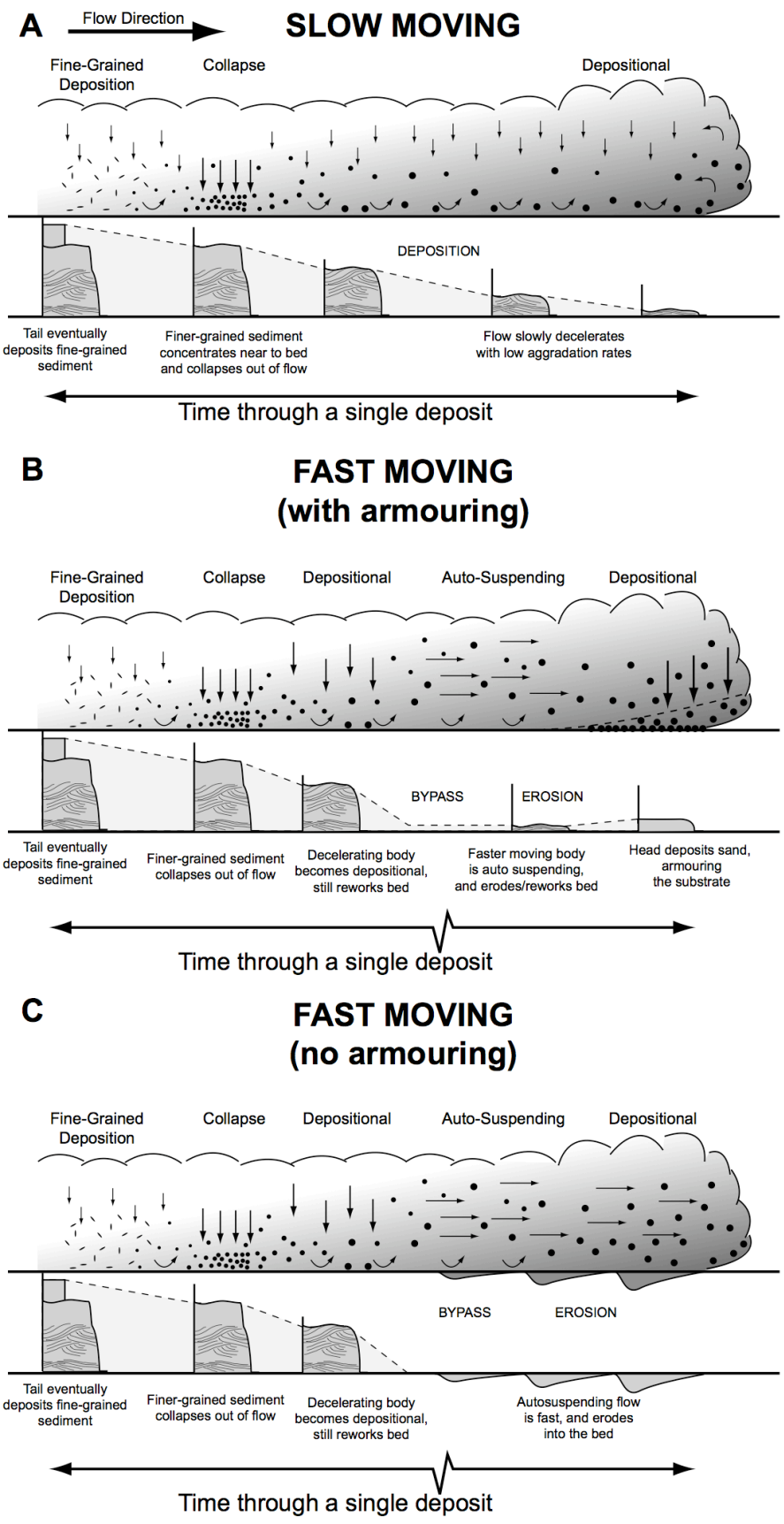
A
Flow Direction
SLOW MOVING
Fine-Grained Deposition
Collapse
Depositional
DEPOSITION
Tail eventually deposits fine-grained sediment
Finer-grained sediment concentrates near to bed and collapses out of flow
Flow slowly decelerates with low aggradation rates
Time through a single deposit
B
FAST MOVING (with armouring)
Fine-Grained Deposition
Collapse
Depositional
Auto-Suspending
Depositional
BYPASS
EROSION
Tail eventually deposits fine-grained sediment
Finer-grained sediment collapses out of flow
Decelerating body becomes depositional, still reworks bed
Faster moving body is auto suspending, and erodes/reworks bed
Head deposits sand, armouring the substrate
Time through a single deposit
C
FAST MOVING (no armouring)
Fine-Grained Deposition
Collapse
Depositional
Auto-Suspending
Depositional
BYPASS
EROSION
Tail eventually deposits fine-grained sediment
Finer-grained sediment collapses out of flow
Decelerating body becomes depositional, still reworks bed
Autosuspending flow is fast, and erodes into the bed
Time through a single deposit

Figure 4-22: Conceptual models of flow processes. (A) Flows are relatively slow, due to slow particle settling velocities. They maintain their density and dissipate very slowly down slope. Near-bed re-entrainment transports grains large distances down slope. Towards the rear of the flow the sediments concentrate near to the bed. The high-concentration suspension rapidly aggrades (collapses) onto the bed. Otherwise the deposits are built incrementally. (B) Flows are relatively fast with a complex longitudinal structure. First the head rapidly deposits sand onto the seafloor, armouring the bed. Next the autosuspending body passes over bypassing most of its sediment load, and erodes into and reworks the 'just deposited' sand. Eventually the flow decelerates enough to begin deposition, and follows similar processes towards the rear of the flow as (A). Deposition only begins towards the rear of the flow after significant flow bypass. (C) Shows an autosuspending flow that does not armour the bed, resulting in erosion of the underlying seafloor. This model does not work in the Agadir Basin.

4.6.2.5 Which model best explains turbidites in the Agadir Basin?

Autosuspending (bypassing) flows best explain the architectures of Beds A5, A7, and A12. The ability of the flows to autosuspend most of their sediment load, only depositing a small proportion per square kilometre along their flow pathway, was likely a product of two processes: 1) Reduced particle settling velocities induced by sediment concentration and cohesive mud effects, enabled the flows to travel slowly and not erode yet still autosuspend most of their sediment loads; and 2) Deposition at the head of the flows armoured the seafloor, increasing its erosion threshold, which enabled flows to travel faster without eroding into the seafloor and autosuspend most of their sediment loads. These two models represent end member scenarios and are not mutually exclusive. For example, Bed A5 has facies indicating both elevated mud content and high concentrations of sediment within the parent flow. Such a flow state would significantly reduce particle settling velocities, enabling the flow to travel much slower whilst maintaining much of its sediment load in suspension (Figure 4-22A). In addition, high sediment concentrations within the flow would also have enabled the head to rapidly deposit sediment and armour the bed, as it travelled across the Agadir Basin. With an armoured bed the flow could have travelled faster without eroding the seafloor and autosuspend its sediment load (Figure 4-22B). Proximally, Bed A12 comprises structureless and parallel laminated sands, indicating deposition beneath a high-concentration flow. Such a flow would have been able to armour the seafloor and travel fast whilst autosuspending its sediment load. In contrast, Bed A12 in the distal parts of the Agadir Basin comprises low-angle and ripple cross-laminated sands, indicating deposition beneath a dilute

flow with elevated mud contents. Here, mud most likely hindered the settling of grains, which enabled the flow to travel slowly (non-erosive) yet still autosuspend most of its sediment load (Figure 4-22A).

4.7 Conclusions

This contribution presents a field dataset that documents five individual turbidite beds, in unprecedented detail, across the Agadir Basin, in both down flow and across flow directions. Three aspects of the beds were examined: (1) The height to which deposits draped up basin margin topography, which is interpreted to be a measure of flow thickness; (2) The vertical and spatial distribution of facies and grain size, used to interpret the character of the parent flows and how they evolved through time and space; and (3) the shape of the beds down flow.

Most of the beds were deposited by flows inferred to have been relatively thin (< 5 – 24 m thick). Each turbidite that was examined had significantly different patterns of facies, grain size and bed shape. This indicates that the parent flows were also different and evolved differently from the mouth of the Agadir Canyon to the end of the Agadir Basin (~ 250 km to the SE). Three of the beds (A5, A7 and A12) record tabular bed geometries with no significant fining for over 150 km down slope.

Quantitative analysis indicates the parent flows of Beds A5, A7 and A12 did not dissipate progressively along the Agadir Basin. Rather the flows were autosuspending (bypassing) most of their sediment loads, only depositing a small proportion per square kilometre along their flow pathways. Two conceptual models are proposed, whereby flows were able to autosuspend their sediment loads yet not erode into the seafloor. First, reduced particle settling velocities induced by sediment concentration and cohesive mud effects, enabled the flows to travel slowly and not erode yet still autosuspend most of their sediment load. Second, deposition at the head of the flows armoured the seafloor, increasing its erosion

threshold, which enabled flows to travel faster without eroding into the seafloor and autosuspend most of their sediment load. These two models represent end member scenarios and the beds examined in this study were most likely a combination of both these processes.

Despite the topographically simple basin-plain setting, and similar flow pathways and compositions, detailed examination of Beds A3, A5, A11 and A12 reveals remarkable complexity in individual flow processes and major differences between turbidite beds. Subtle differences in flow properties (volume, velocity, density, suspended grain size and volume of mud within the flow) fundamentally affected how the flows behaved and evolved as they progressed across the basin. Factors such as including hindered settling, effects of mud concentration, near-bed processes, and fluid turbulence are shown to be important in governing the transport and deposition of sediment from submarine flows. Although important, these factors are poorly understood within submarine flows and present a significant challenge to include in future experimental and numerical simulations.

5 The flows that left no trace: Very large-volume turbidity currents that bypassed sediment through submarine channels without eroding the seafloor

Stevenson, C.J., Talling, P.J., Wynn, R.B., Masson, D.G., Hunt, J.E., Frenz, M., Akhmetzhanhov, A., and Cronin, B.T.

5.1 Abstract

Turbidity currents are an important process for transporting sediment from the continental shelf to the deep ocean. Submarine channels are often conduits for these flows, exerting a first order control on turbidity current flow processes and resulting deposit geometries. Here we present a detailed examination of the Madeira Channel System, offshore northwest Africa, using shallow seismic profiles, swath bathymetric data and a suite of sediment cores. This shallow (< 20 m deep) channel system is unusual because it was fed infrequently, on average once every 10, 000 years, by very large volume (> 100 km^3) turbidity currents. It therefore differs markedly from most submarine channels which have well developed levees, formed by much more frequent flows. A northern and a southern channel comprise the Madeira Channel System, and channel initiation is associated with subtle but distinct increases in sea-floor gradient from 0.02º to 0.06º. Most of the turbidity currents passing through the northern channel deposited laterally extensive (> 5 km), thin (5 to 10 cm) ripple cross-laminated sands along the channel margins, but deposited no sand or mud in the channel axis. Moreover, these flows failed to erode sediment in the channel axis, despite being powerful enough to efficiently bypass sediment in very large volumes. The flows were able to reach an equilibrium state (autosuspension) whereby they efficiently bypassed their sediment loads down slope, leaving no trace of their passing.

5.2 Introduction

Turbidity currents are one of the most important flow processes for moving sediment across the surface of the Earth. Individual events, such as those described in this study, can be extremely large volume, transporting over ten times the annual sediment flux for all the world's rivers (Mulder and Syvitski, 1995). Submarine channels are often conduits for these flows, exerting a first order control on turbidity current flow processes and resulting deposit geometries. Much of our understanding of submarine channel morphology comes from a number of intensely studied modern deep-water fans (Wynn et al., 2007). The channels found across these fans are generally sinuous (> 1.2) and are connected to larger feeder canyons, which cut back into the continental shelf. Within the upper parts of the fans the channels are relatively deep (100 s meters) and narrow (2-20 km), becoming progressively shallower (tens of meters) and broader (tens of km) as they progress distally down the fan (Wynn et al., 2007). In terms of depositional architecture, submarine channels and their flanking levees are commonly referred to as channel-levee systems. Such systems broadly comprises a coarse-grained channel fill, such as massive sands and gravels (Wynn et al., 2007; Babonneau et al., 2010; Bernhardt et al., 2011), and fine-grained levee deposits that thin and fine away from the axis of the channel (Kane et al., 2007). Channel depth may be maintained via a combination of erosion along the channel floor and/or from construction of levees along the channel margins. However, many channels are also net aggradational both in the channel axis and across the levees (Wynn et al., 2007). Channel-levee architecture is pervasive across most modern fan systems and has been interpreted in numerous ancient channel systems (Normark, 1978; Normark et al., 1979; Wynn et al., 2007; Babonneau et al., 2010; Bernhardt et al., 2011; McHargue et al., 2011).

However, not all channel systems fit the deep-water fan model. For example, the Northwest Atlantic Mid-Ocean Channel (NAMOC) consists of a major "basin draining" trunk channel supplied by numerous tributary and satellite channels that are linked up with the continental slope (Hesse et al., 1987a; Hesse, 1989; Hesse et al., 1990; Hesse and Rakofsky, 1992; Klaucke et al., 1998; Hesse et al., 2001). Proximally the system is dominated by sandy braid-plains with relatively shallow relief channels (10 s meters). Little variation in grain size

occurs between braided channel and levee elements, with channel axes and levees being sand-rich. As the NAMOC progresses distally (extending over 4000 km) it develops into a deep single channel with a coarse-grained channel fill and thinner, fine-grained channel levees (Chough and Hesse, 1976; Hesse et al., 1987a; Hesse et al., 1987b; Hesse, 1989; Hesse et al., 1990; Hesse and Rakofsky, 1992; Klaucke et al., 1997; Klaucke et al., 1998; Hesse et al., 2001).

Flow processes operating within submarine channels are complex, involving erosive, bypassing and depositional phases (Peakall et al., 2000). These processes are governed by sea floor/channel morphology and the properties of the flows passing through the channels (e.g. flow thickness, grain size, density and velocity). Specifically, gradient has been shown to be a fundamental control on the ability of turbidity currents to erode, transport and deposit sediment (Mulder and Alexander, 2001; Wynn et al., in press). Therefore, changes in sea-floor gradient down flow can exert a strong control on channel architecture, particularly in complex slope settings (Adeogba et al., 2003; Ferry et al., 2005). However, there have been very few direct measurements of active flows passing through submarine channels (Kripounoff et al., 2003; Xu et al., 2004; Vangriesheim et al., 2009), and sediment concentrations have never been measured in any channel in the deep ocean. This ensures that major questions remain concerning submarine flow dynamics. Thus our understanding rests on analysis of flow deposits in submarine channels. However, the highly complex, often discontinuous nature of deposition within channels (Di Celma et al., 2011) means our understanding of how individual flows actually behave is limited. A novel aspect of this study is that the deposits of individual flows can be correlated between basins that lie upslope and downslope of the channel system. This correlation enables the number, grain size and volume of flows that passed through the intervening channels to be well constrained. Hence, the depositional architectures of individual turbidites within the channels themselves can be placed in context and the flow processes can be better understood. This study aims to:

(1) Document a poorly studied modern channel system and show how it differs from previously described channel-levee models

(2) Document in detail the deposits of individual flows across the channels

(3) Discuss how differences in flow properties can affect depositional architecture across the channels

(4) Discuss the effects of sea-floor gradient on individual flow behaviour (e.g. erosion, bypass and deposition) and the resulting channel architecture

5.2.1 The Moroccan Turbidite System

Over the past 200 ka the Moroccan Turbidite System, situated offshore northwest Africa, has been host to some of the largest turbidity currents ever recorded on Earth with volumes exceeding 150 km^3 (Wynn et al., 2002b; Talling et al., 2007c; Frenz et al., 2008; Wynn et al., 2010). The system spans ~2000 km comprising three interconnected sub basins (Figure 5-1A): the Seine Abyssal Plain to the north east, the Agadir Basin situated centrally and the Madeira Abyssal Plain forming the western most extent of the system. Entering the system from three sources are: (1) organic-rich siliciclastic flows, sourced from the Moroccan Margin; (2) volcanoclastic flows, sourced from either the Canary Islands or Madeira and; (3) carbonate-rich flows, sourced from local seamount collapses (de Lange et al., 1987; Pearce and Jarvis, 1992; Weaver et al., 1992; Wynn et al., 2002b). Excellent core recovery throughout the system, coupled with a robust geochemical and chronostratigraphic framework, has enabled individual turbidite beds to be correlated between all three sub-basins (Wynn et al., 2002b). A complex series of channels cross the lower continental rise, connecting the Agadir Basin with the Madeira Abyssal Plain. These channels, originally mapped by (Masson, 1994), are ~700 km long and comprise separate northern and southern channel systems. For clarity this study refers to the southern channel system and northern channel system, of (Masson, 1994), as the Canary Island Channel System and the Madeira Channel System respectively (Figure 5-1B). The Madeira Channel System itself comprises a northern channel and a southern channel that are initially separated by local seamounts before converging ~200 km down slope (Figure 5-1B). This study focuses on the proximal parts of the Madeira Channel System. Herein, the term Madeira Rise will be used to describe the

immediate area surrounding the Madeira Channels themselves and is restricted to the area of study as shown in Figure 5-1B, unless otherwise stated.

The Madeira Channel System is unusual in that it initiates far from the continental shelf, located at the distal end of the relatively flat Agadir Basin (Figure 5-1A). Turbidity currents entered the channels obliquely from the northeast, via the Agadir Basin, or perpendicular to the channels, from the Canary Islands to the south (Wynn et al., 2002b; Frenz et al., 2008). Turbidity currents passing into the Madeira Channels from the Agadir Basin were largely unconfined and able to spread across the width of the basin (Frenz et al., 2008). Turbidity currents from the Canary Islands were also unconfined and able to spread across the entire Madeira Rise (Hunt et al., 2011). This makes the Madeira Channels significantly different from most submarine fan channel systems that are directly fed by flows that are confined within large canyons that cut back into the shelf (Wynn et al., 2007).

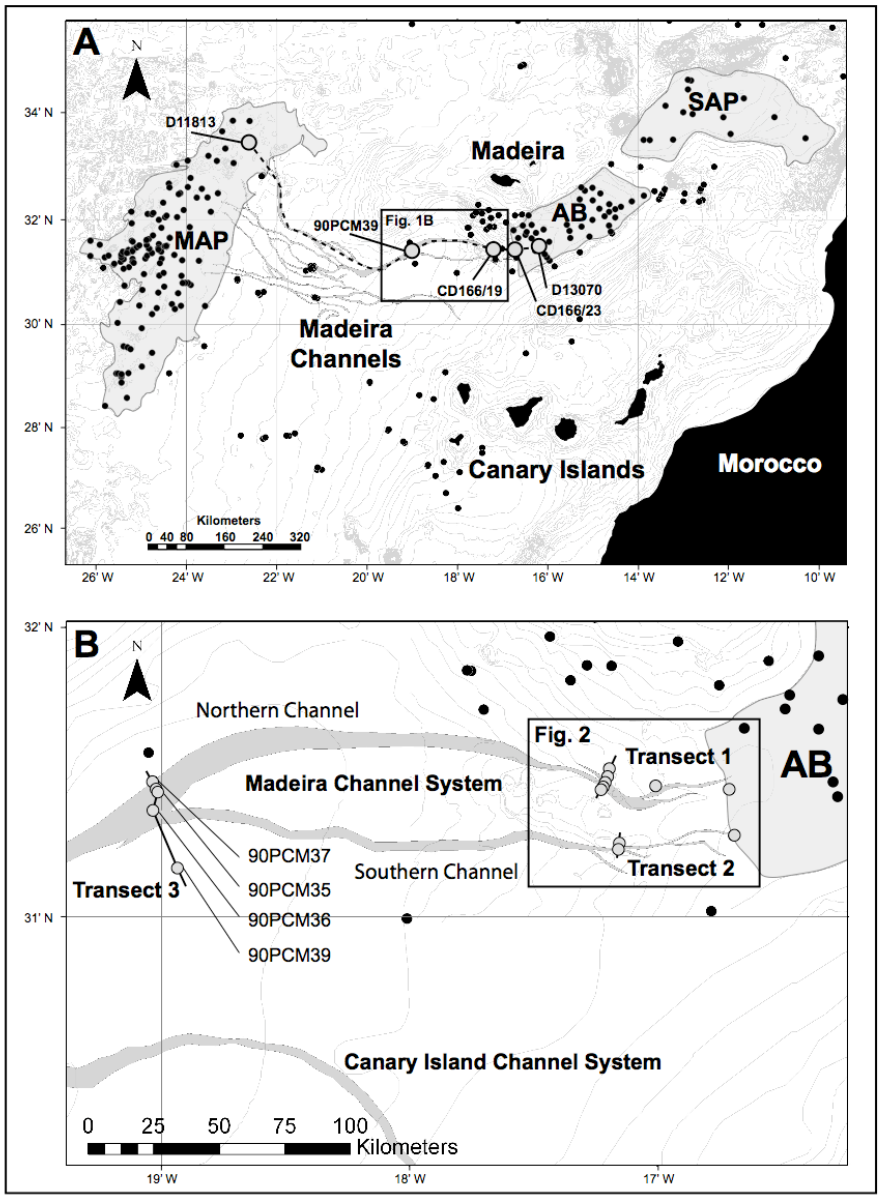

Figure 5-1: Map showing: (A) The Moroccan Turbidite System comprising the Seine Abyssal Plain (SAP), Agadir Basin (AB) and Madeira Abyssal Plain (MAP) highlighted in light grey. Morocco, Madeira and The Canary Islands are coloured black. Sediment cores are marked with black circles. The Madeira Channels connect the Agadir Basin to the Madeira Abyssal Plain and are shaded in light grey. Core sites used to correlate individual beds across the length of the channel system are highlighted with large grey circles and labelled (see Figure 5-7). (B) Shows the Canary Island and Madeira Channel Systems. The Madeira Channel System has two main channels, referred to as northern and southern in the text. Cores used in this study are marked with large grey circles and core transects 1-3 are labelled. The proximal Madeira Channel System, highlighted with a square box, is the focus for this study and illustrated in more detail in Figure 5-2 and Figure 5-3.

5.3 Methods

The geophysical data used in this study were collected during *'RRS Charles Darwin cruise CD166'*. A dense network of 3.5 kHz profiles and continuous EM12 multibeam bathymetry (Figure 5-2 and Figure 5-3) covers the eastern part of the Madeira Channel System. Shallow sediment cores collected from a number of cruises over the past 30 years, situated in three transects across the Madeira Channel System, are used to 'ground truth' the geophysical data (Figure 5-1B). Cores were analyzed using a number of methods. First, cores were subject to detailed visual logging. Deposits from turbidity currents were described and categorized into planar laminated sand, ripple cross-laminated sand and mud. Detailed grain size analysis was carried out on turbidite beds using a Malvern Mastersizer. Samples (1 cm^3) were taken from turbidites and disaggregated with 1% Calgon solution then shaken continuously for ~10 hours. This ensured that individual sediment grains, particularly clay particles, were not clumped together into larger flocs. Samples were then analyzed three times and the average grain size distribution calculated. Geochemical analysis was carried out on cores CD166/17 and 19 using an ITRAX XRF core scanner (Croudace et al., 2006; Rothwell et al., 2006). Elemental abundance was measured down core every 0.5 mm. Cores CD166/15, 16, 17, 18, 19, 23 and 90PCM36, 37 and 39 were subject to high-resolution coccolith biolithostratigraphic dating, following the method of Weaver and Kuijpers (1983). Smear slides were taken down core every 5-10 cm, although intervals that were considered likely to be eroded were subject to sampling every 1 cm. Approximately 300 coccoliths were counted per smear slide.

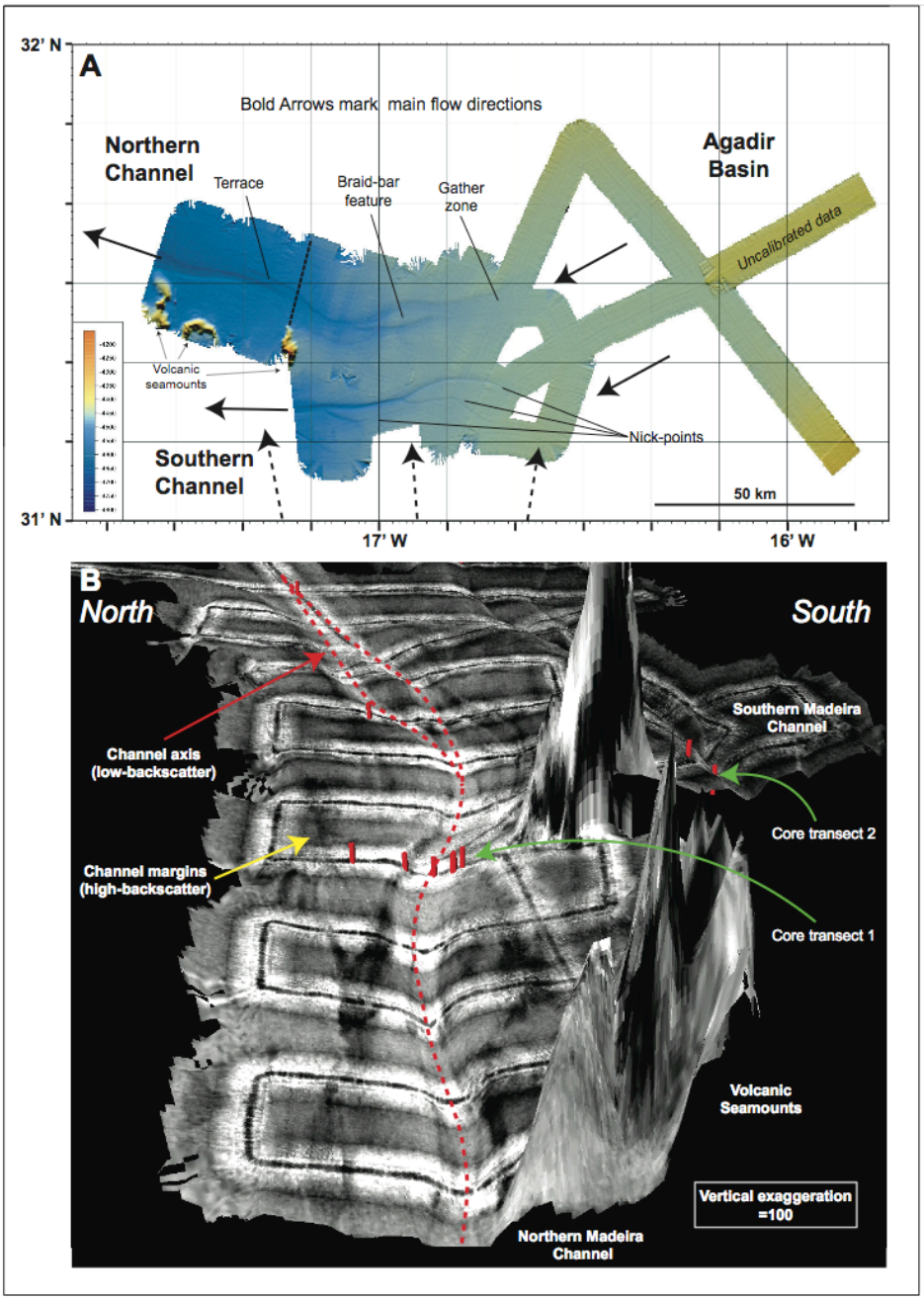

Figure 5-2: (A) EM12 multibeam bathymetric map over the southwest (distal) Agadir Basin and proximal northern Madeira Channels. Bold arrows show main flow pathways: organic-rich siliciclastic flows sourced from the Moroccan Margin passing through the Agadir Basin (solid arrows) and volcanoclastic flows originating from the Canary Islands (dashed arrows). (B) 3-D view of EM12 backscatter looking upstream along the northern channel towards the Agadir Basin. Lighter grey areas denote zones of low backscatter and darker grey/black areas denote zones of high backscatter. Core locations are marked with red bars. Note the low backscatter response within the northern channel axis (highlighted with a dashed red line) and the patchy high-backscatter response across the channel margins. The highest and most extensive backscatter response is seen in an area across the southern channel (top right of figure).

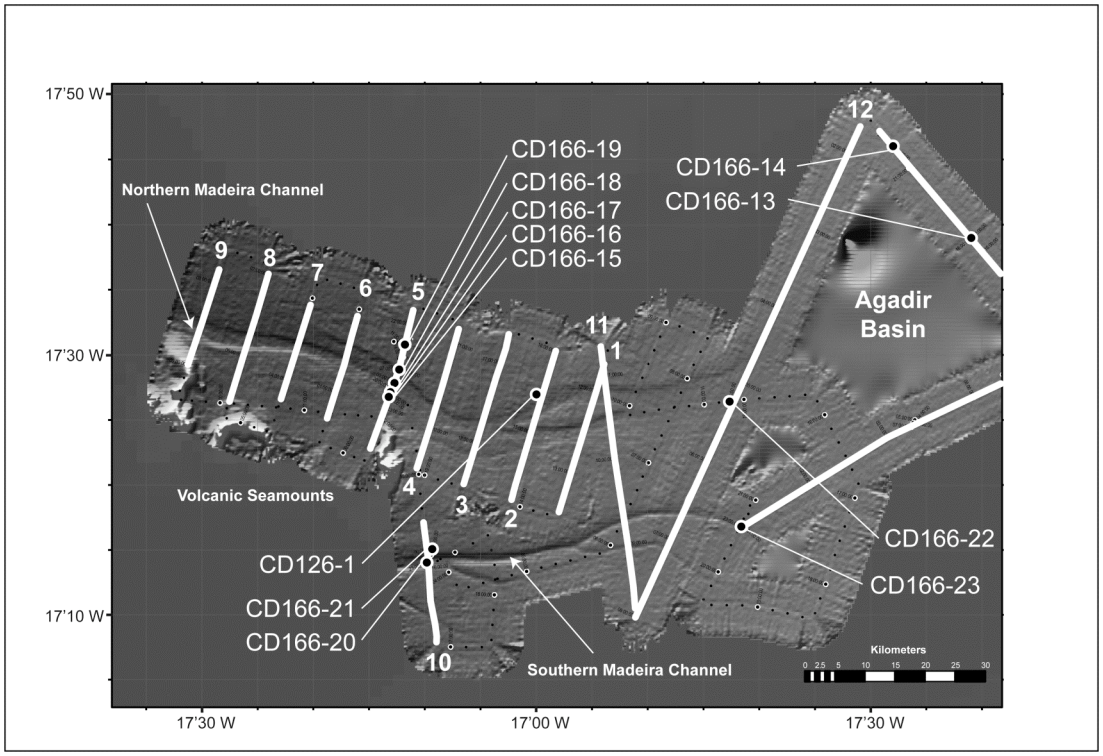

Figure 5-3: EM12 grey shaded bathymetry showing the position of 3.5 kHz profiles across the proximal Madeira Channel System. 3.5 kHz profiles are marked with thick white lines and labelled 1-12. Black circles denote locations of core sites.

5.4 Results

5.4.1 Morphology of the Madeira Channels

The Madeira Channels initiate on the southwest margin of the Agadir Basin (Figure 5-1B and Figure 5-2A). Two channels are identified, developed to the north and south of volcanic seamounts (herein referred to as the northern and southern channels, respectively). Both the northern and the southern channels are shallow (<30 m) and relatively narrow (<5 km) with low sinuosity (< 1.1). The northern channel initiates from a broad shallow gather zone ~5 km across and ~12 m deep, progressing into a more defined, flat-bottomed channel with braid bar like features down slope (Figure 5-2A). The more-defined segment of the northern channel maintains a depth of ~20 m and a width of ~5 km, up to ~100 km from the point of channel initiation. The southern channel initiates from a well-defined nick point, into a narrow (~1

km across), V-shaped channel up to 28 m deep (Figure 5-2A). A number of smaller tributary channels occur on the southern margin and converge with the main southern channel (Figure 5-2A and Figure 5-3).

The southern and northern channels converge approximately 180 km from the point of channel initiation (Figure 5-1B). At this confluence the channel is broad, shallow and poorly defined. GEBCO bathymetry and sea-floor gradient profiles, trending northwest to southeast across this zone, show an exceptionally low-relief channel, ~36 km across and ~20 m deep (Figure 5-4). This style of low-relief channel evolves down slope into steeper-walled narrower channels before debouching into the Madeira Abyssal Plain (Masson, 1994).

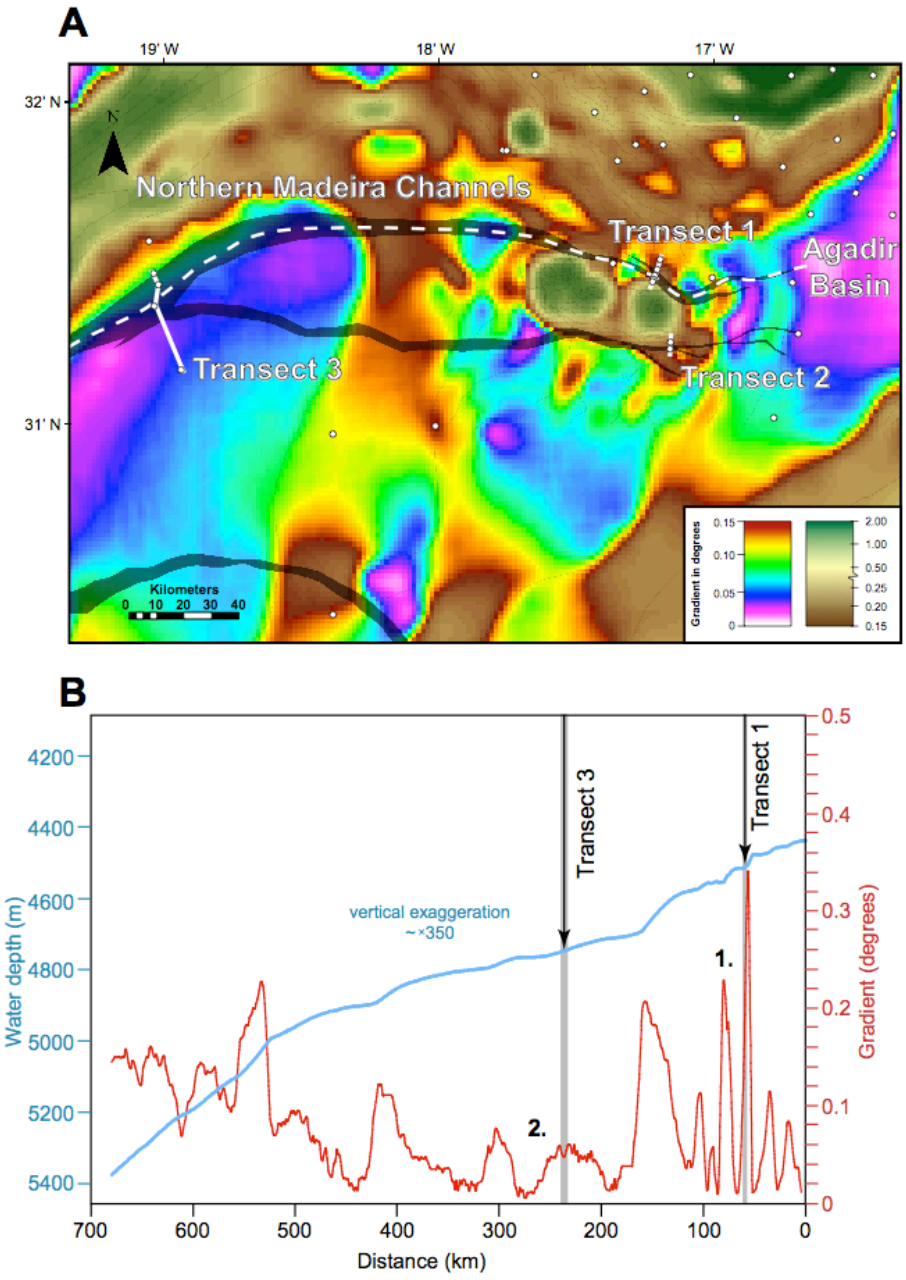

Figure 5-4: (A) Slope map of the proximal Madeira Channel System. Two scales are used representing the minor and larger magnitude changes in sea floor gradient. Gradients from 0º up to 0.15º range in colour from white to dark red, whilst gradients from 0.15º to 2º are shaded brown to dark green respectively. Note the change in scale within the second colour scheme. The channels are highlighted in black. The dashed white line shows the trace of the 2D sea floor profile in B. Core transects 1-3 are marked with solid white lines and are labelled. (B) 2D sea floor profile (blue line) and gradient (red line) following the axis of the northern Madeira Channel along its entire length (see Figure 5-1A), which passes through core transects 1 and 3. Note two distinct zones along the Madeira Channel System: (1) a relatively steep zone with high variability, showing gradients between 0.02º and 0.34º; (2) a flatter zone with less variability, showing gradients between 0.01º and 0.06º.

5.4.2 Character of Madeira Channels in seismic profiles

3.5 kHz shallow seismic profiles across the northern channel show two distinct acoustic signatures (Figure 5-5). The first occurs proximal to the site of channel initiation. The 3.5 kHz profiles show relatively high amplitude reflectors on the margins of the channel and lower amplitude reflectors in the channel axis (Figure 5-6A). Deeper acoustic penetration is observed in the channel floor compared with the surrounding high-amplitude margins. The second acoustic signature occurs more distally, where the character of the northern channel changes (Figure 5-6C). The axis of the channel is flat-bottomed with high-amplitude reflectors, similar in strength to those observed on the channel margins. The acoustic penetration is the same inside the channel as it is on the margins. The acoustic change is associated with steeper channel walls and a narrower channel floor. The 3.5 kHz profiles shown in Figure 5-6A and Figure 5-6C (and indeed lines 4-9, Figure 5-5) show the walls of the northern channel becoming progressively steeper through time. In contrast, the walls of the southern maintain a relatively constant morphology to the present day sea-floor (Figure 5-6D). 3.5 kHz profiles running across the southern channel show high-amplitude reflectors developed on the channel margins and within the axis of the channel itself (Figure 5-6D). Reflectors appear vertically stacked within the channel axis, maintaining relatively steep channel walls of similar gradients up to modern sea-floor morphology. The smaller tributaries show very similar acoustic character to the main channel. The axes of both the southern and the northern channels do not appear to migrate laterally.

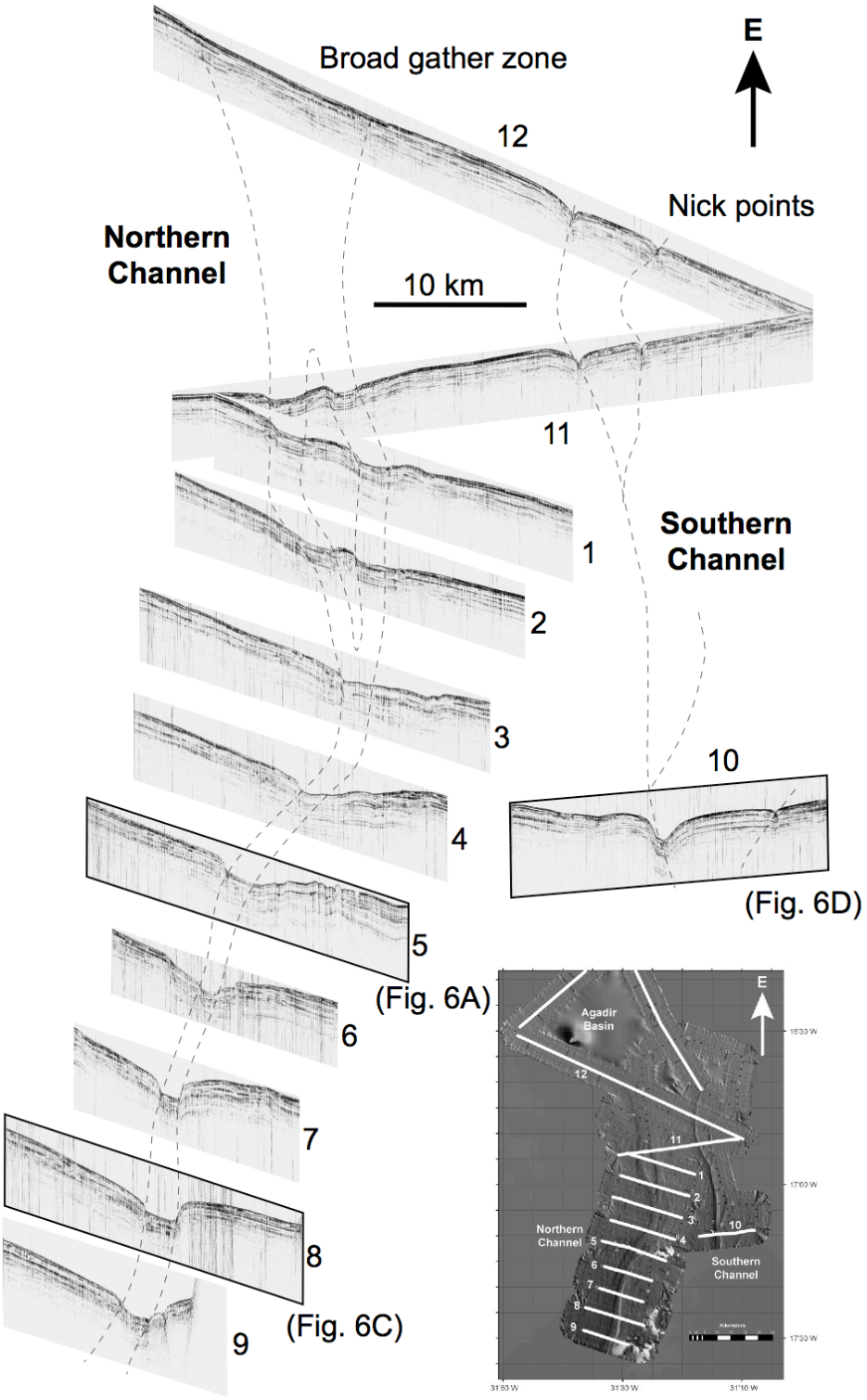

Figure 5-5: Consecutive 3.5 kHz profiles along the Madeira Channel System showing channel morphology and acoustic character of the channels (scale of 3.5 kHz lines is shown in Figure 5-6). Dashed black lines highlight the course of the channels. Detail of profile lines 5, 8 and 10 are shown in Figure 5-6A-D. An EM12 bathymetric map is included showing plan form channel morphology (bottom right).

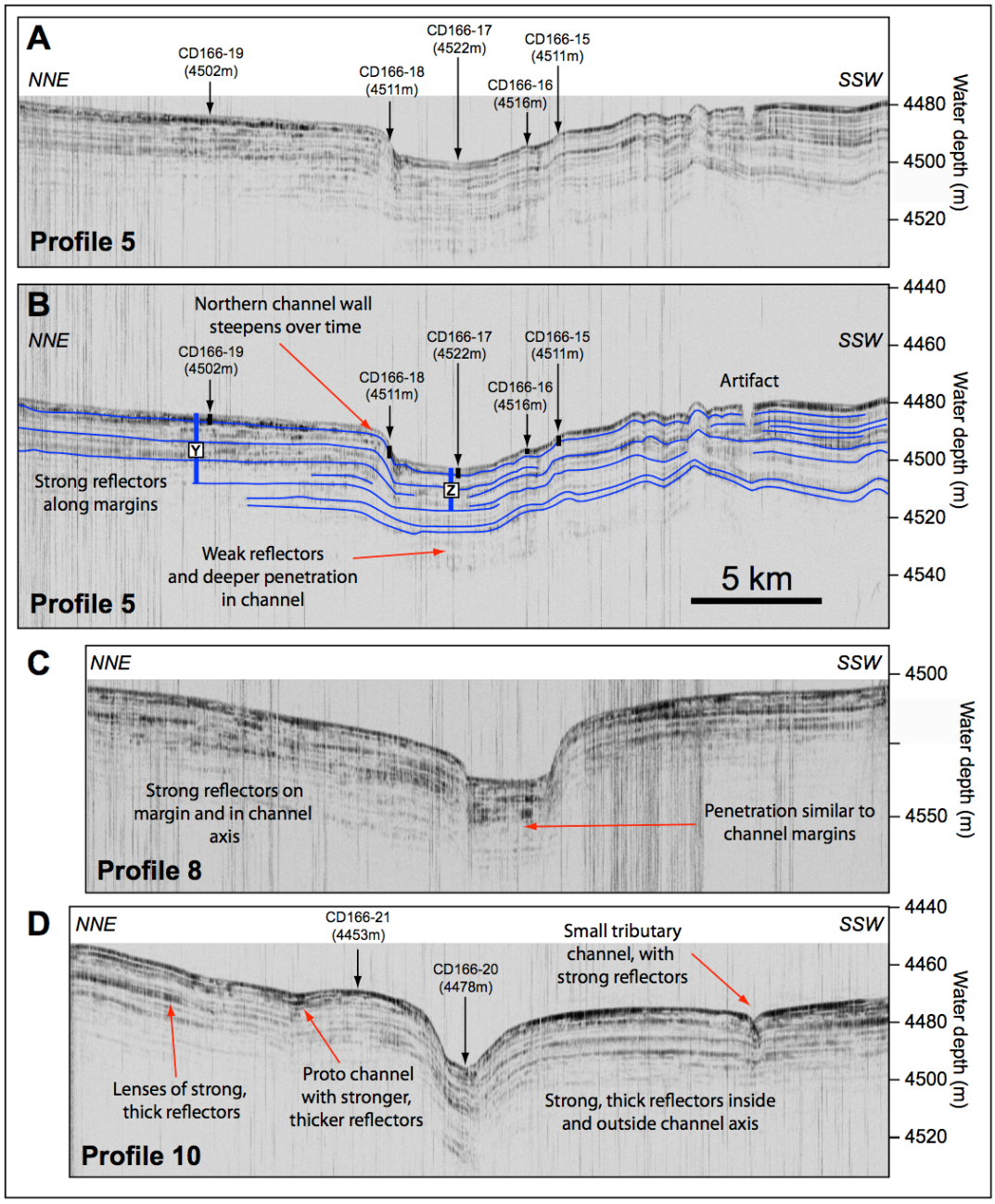

Figure 5-6: 3.5 kHz profiles across the northern (A-C) and southern (D) Madeira Channels. The horizontal scale is the same for all profile lines. Profile Line 5 (A and B) shows higher amplitude reflectors under the northern channel margin. The channel axis shows weaker sub-bottom reflectors and significantly deeper acoustic penetration than the margin. (B) Shows an interpretation of Profile Line 5 with reflectors manually correlated and estimates of core penetration under each core site (black pillars). Blue pillars Y and Z denote the thickness of the sedimentary sequence outside and inside the channel respectively. The thickness is measured from a continuous reflector to the present day sea floor. (C) Shows Profile Line 8 with high amplitude reflectors both inside and outside the northern channel axis. Note the change to a flat-bottomed channel with steeper channel walls. The southern channel (D) shown in Profile Line 10 has high relief, steep channel walls and shows high amplitude reflectors both inside and outside the channel axis. The southern channel also has several low-relief tributaries highlighted with strong reflectors along its margins.

5.4.3 Character of the Madeira Channels in backscatter images

The northern and southern channels are significantly different in terms of their backscatter response (Figure 5-2B). The northern channel shows patches of high (dark grey) backscatter along its northern margin and significantly lower backscatter (light grey) within the channel axis. The backscatter response does increase slightly within the channel axis between 3.5 kHz profile lines 7 and 9. The southern channel shows a high backscatter response both inside the channel axis and on the margins. Indeed, the area surrounding the southern channel shows larger, higher backscatter zones compared with the northern channel.

5.4.4 Bed correlations across the Madeira Channels

A robust geochemical and chronostratigraphic framework has been well established across the Moroccan Turbidite System. Within the Agadir Basin and Madeira Abyssal Plain this has been achieved from:

- High-resolution coccolith biolithostratigraphy of hemipelagic sediments, which provides an age model as far back as ~ 500 ka (Weaver and Kuijpers, 1983; Weaver and Rothwell, 1987; Weaver, 1991; Weaver et al., 1992).
- Detailed geochemical analysis of large volume volcanoclastic turbidites, which provides aerially extensive marker beds across the system (de Lange et al., 1987; Pearce and Jarvis, 1992; Pearce and Jarvis, 1995).
- Analysis of coccolith species within turbidite mud caps, which enables individual turbidite events and their erosional characteristics to be identified (Weaver and Thomson, 1993; Weaver, 1994; Wynn et al., 2002b).

Using the methods outlined above, the detailed individual bed correlations across the Agadir Basin and Madeira Abyssal Plain (Weaver and Rothwell, 1987; Jones et al., 1992; Rothwell et al., 1992; Weaver et al., 1992; Wynn et al., 2002b; Talling et al., 2007c; Frenz et al., 2008) are extended across the Madeira Channel System (Figure 5-7). Bed numbering from 1-14 follows the nomenclature of (Wynn et al., 2002b) as established for the Agadir Basin. Below bed 14, beds are numbered sequentially down core. The stratigraphy within the Madeira Channel System is penetrated down to ~ 400 ka and comprises 18 correlatable turbidite beds. Many of the large-volume turbidites (Wynn et al., 2002b) correlate continuously across the channel system (e.g. Beds 2, 5, 12 and 14) maintaining a relatively constant grain size. Turbidite deposits within the Madeira Channel System are generally thinner than those in the Agadir Basin or Madeira Abyssal Plain, indicating significant amounts of sediment bypass. Indeed, the silt and mud component of most beds is thickest in distal areas, where it is ponded into the Madeira Abyssal Plain (McCave and Jones, 1988; Jones et al., 1992; Rothwell et al., 1992).

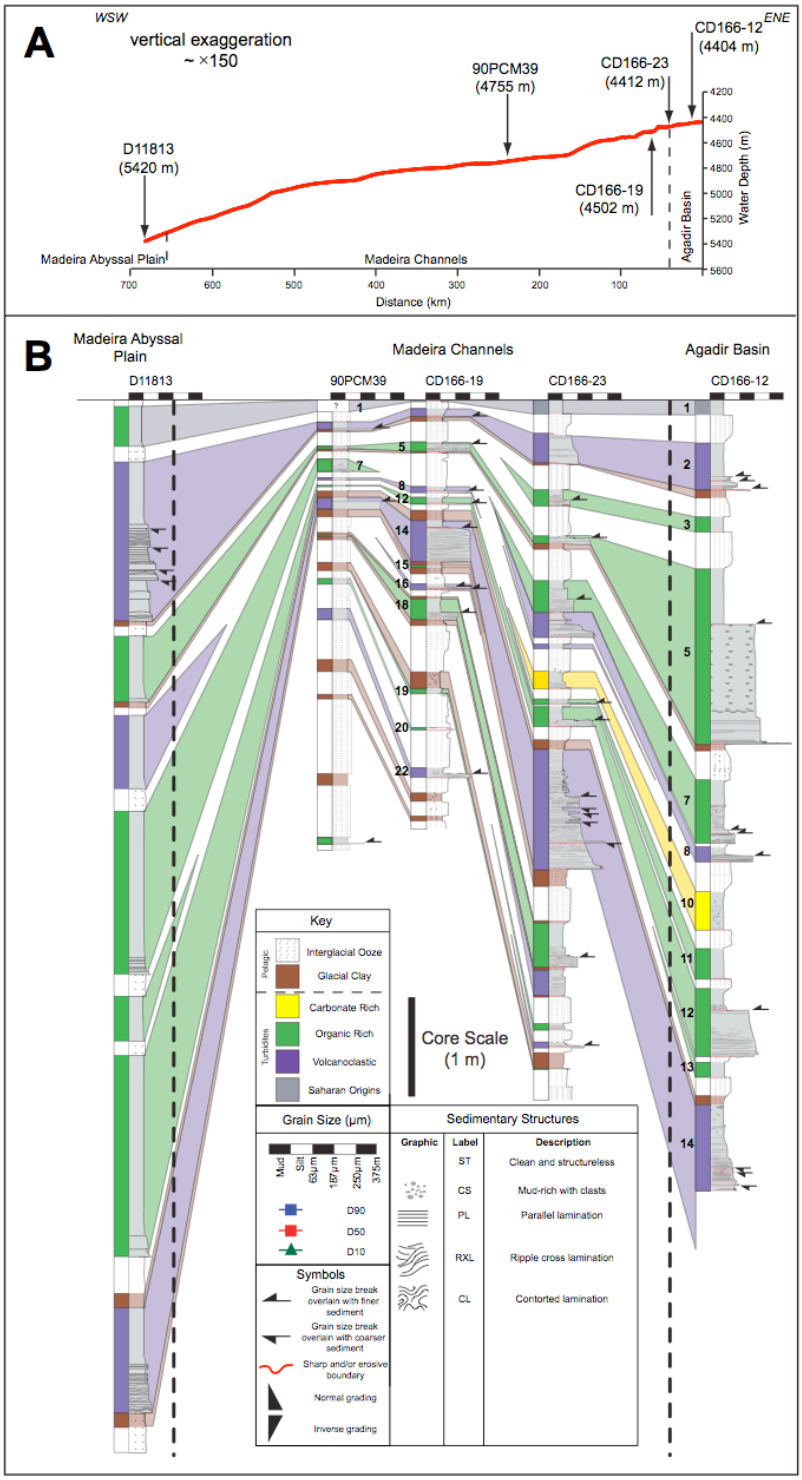

Figure 5-7: Core transect (located on Figure 5-1A) showing correlation of individual turbidite beds across the Madeira Channels. (A) Shows sea floor topography (red line) with core locations marked. (B) Shows turbidite bed correlations across the Agadir Basin, Madeira Channel System and the Madeira Abyssal Plain. Note the relatively condensed sequence found in the area of the Madeira Channels. Bold numbers (1-22) label turbidites that can be correlated across the Moroccan Turbidite System.

5.4.5 Sedimentary facies across the Madeira Channels

The cores comprise two distinct types of sediment: hemipelagic mud and turbidites. The hemipelagic mud has two end member lithologies: (1) Cream coloured carbonate ooze comprising abundant randomly distributed foraminifera tests and coccolithophores; (2) Dark red/brown mud mainly composed of terriginous clay. These lithologies have been related to changes in the dissolution of carbonate in the ocean bottom waters caused by climatic variations (Crowley, 1983). In interglacial periods dissolution of carbonate is relatively low and allows sedimentation of carbonate-rich ooze. During glacial periods dissolution of carbonate is increased, which produces smooth brick-red clay (Crowley, 1983). Turbidites are identified by a sharp base, often with a distinct change in grain size (i.e. from mud to sand), and changes in the colour of the sediment. Turbidites found within the Madeira Channel System and across the Madeira Rise are either: (1) organic-rich with a green colouration, sourced from the Moroccan Margin or; (2) volcanoclastic with a dark grey/black colouration, sourced from either the Canary Islands or Madeira (de Lange et al., 1987; Pearce and Jarvis, 1992; Weaver et al., 1992; Wynn et al., 2002b).

Turbidites primarily comprise thin (15 to 28 cm), ripple cross-laminated fine sands with modal grain sizes of between 63 and 250 μm (Figure 5-8B, 1-8D and 1-8F). Some turbidites have planar laminated sand at the base or occasionally throughout the deposit (Figure 5-8A). Contorted lamination occurs in the upper parts of the deposits, often underlain by planar laminated sand and overlain by ripple cross-laminated sand (Figure 5-8C, 5-8D and 5-8E). Proximal to the site of channel initiation, deposits have inversely graded bases overlain by an ungraded interval, which progresses into a normally graded top (Figure 5-8A-D). Inverse to normal vertical grading patterns are found but are less frequent in the more distal parts of the channel system. For the most part, turbidites found in the confluence zone typically have ungraded sandy bases overlain by normally graded sands (Figure 5-8E and Figure 5-8F). Both proximal and more distal sandy deposits are typically overlain by a sharp grain size break and in turn a thin (1 to 10 cm) turbidite mud cap with modal grain sizes between 8 and 24 μm. However, in a number of proximal core sites the turbidite beds have no mud cap at all (e.g. Figure 5-8A).

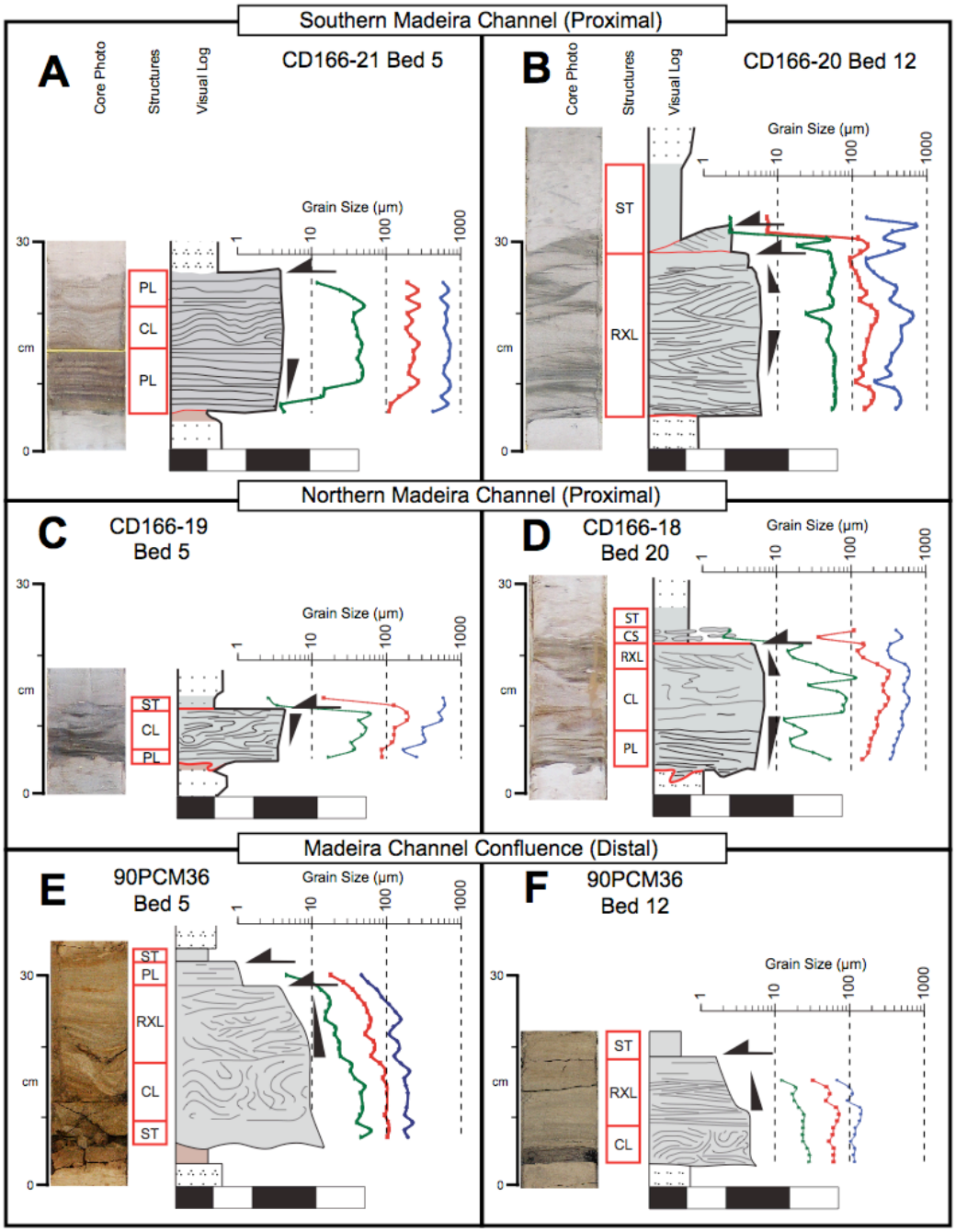

Figure 5-8: Photographs of turbidite deposits in core with accompanying logs and grain size profiles (see Figure 5-7 for key) showing examples of turbidite deposition from the southern channel (A and B), northern channel (C and D) and the confluence (E and F). Deposits are located on Figure 5-11, Figure 5-9, and Figure 5-12 respectively. Turbidites mainly comprise ripple-cross laminated and contorted sands. Proximally, subtle inverse grading can be seen in the base of the southern and northern channel deposits (Figures A-D) whilst those at the downstream confluence have normal grading (Figures E and F). Note that in all examples there is a sharp grain size break between sand and the overlying mud cap. Sand-to-mud grain size breaks of this nature are pervasive throughout the channel system. In the case of Figure E two grain size breaks are shown, the first has sand overlain by finer sand/silt, the second has sand overlain by mud.

5.4.6 Turbidites from the northern channel

Transect 1 comprises five cores across the northern channel located along 3.5 kHz profile line 5 (Figure 5-9). In this transect turbidite deposition primarily occurs outside the channel. Turbidites mainly comprise ungraded, thin (5 to 10 cm) ripple cross-laminated or planar laminated clean sands overlain by a sharp grain size break and very thin turbidite mud (1-2 cm). Deposits mostly thin and pinch out to the south, toward the channel. However, some turbidites (e.g. Beds 20, 21 and 23) are thickest on the northern channel margin, thinning both towards the south, toward the channel, and north, away from the channel. Within the channel axis itself almost no turbidite deposition is recorded. Turbidite Beds 5, 7 and 12 originating from the Moroccan Margin, passing across the Agadir Basin and into the Madeira Abyssal Plain (Wynn et al., 2002b; Frenz et al., 2008), show no deposition in the channel axis (Figure 5-9). The only deposition of turbidite sediments in the channel axis is that of Bed 14 originating from the Canary Islands, and Bed 10.5 from Madeira. In this case the deposits are only subtle traces of strongly bioturbated turbidite mud and are barely visible. These deposits are difficult to detect through grain size analysis or in down core magnetic susceptibility profiles. However, deposits of Bed 14 can be detected from elevated levels of titanium and potassium within the sediment (Figure 5-10B).

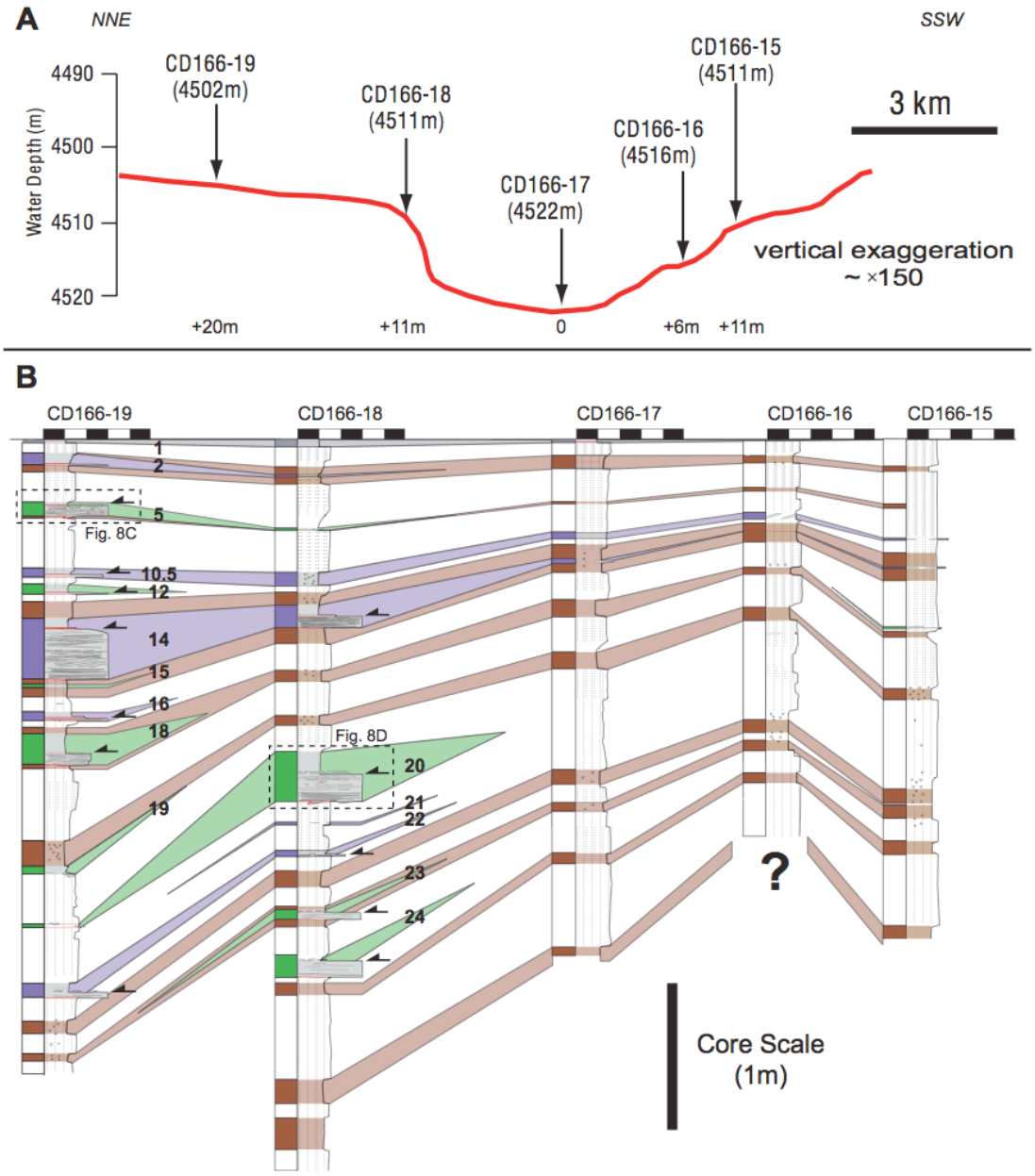

Figure 5-9 Core transect 1 across the proximal northern channel. (A) exaggerated sea floor topography across the channel (red line) with core locations marked. The difference in water depth between core sites is noted underneath the red line. (B) turbidite stratigraphy within the northern channel. Turbidite Beds are labelled after the established Agadir Basin stratigraphy (Wynn et al., 2002b). Below the base of the established Agadir Basin stratigraphy (Bed 14) turbidite beds are labelled sequentially down core. The core transect shows individual turbidite beds and glacial clay layers correlated across the channel axis (refer to Figure 5-7 for key). Note turbidite deposition is preferentially developed on the northern channel margin with almost no deposition occurring within the channel axis. Two distinct architectures of channel margin deposition can be seen; (1) Turbidites 1-19, which thin and fine towards the channel axis and; (2) Turbidites 20-23, which thin and fine towards and away from the channel axis.

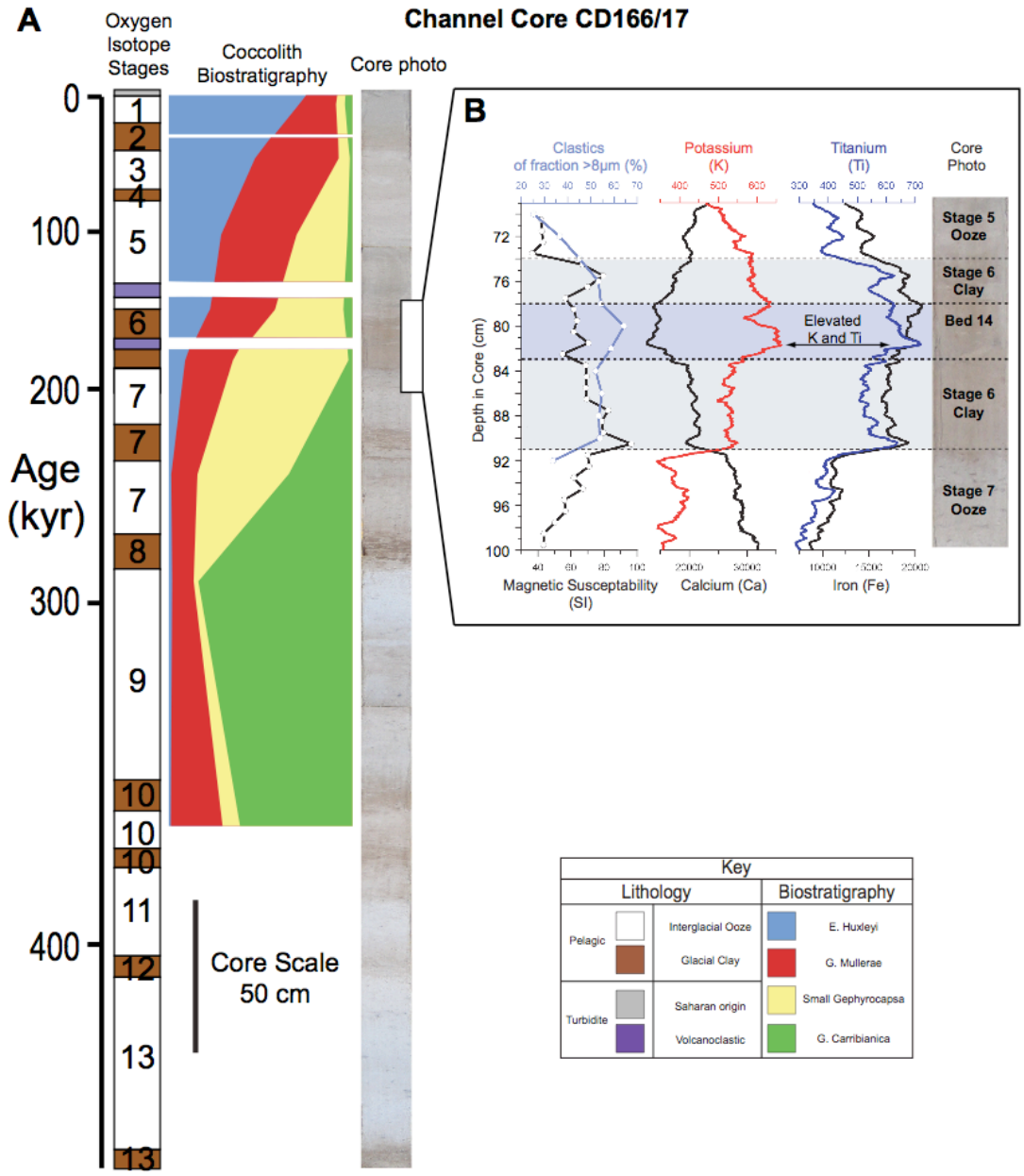

Figure 5-10: Detailed analysis of core CD166-17 illustrating the absence of most turbidites in the axis of the northern channel. (A) Core photograph with interpreted stratigraphy and coccolith biostratigraphy down to ~350 ka (after Weaver and Kuijpers, 1983). Note the lack of erosional hiatuses. (B) A suite of grain size and ITRAX data through the interval where Bed 14 should occur (i.e. the glacial clay of oxygen isotope stage 6). Grain size shows no significant change through the interval but Potassium (K) and Titanium (Ti) show increased levels where a grey bioturbated mud occurs. This is the only trace left behind from Bed 14.

5.4.7 Turbidites from the southern channel

Core Transect 2 cutting across the southern channel is limited in that it only has two core sites: one from the channel axis and the other from the channel margin (Figure 5-11). Turbidites are predominantly thick (22 to 46 cm) ripple cross-laminated clean sands overlain by a sharp grain size break and a thin mud. Some turbidites have planar laminated sands developed at their bases. In contrast to the northern channel, the southern channel shows turbidite deposition occurring both in the channel axis and on the margins. Volcanoclastic Beds 8 and 10.5, sourced from Madeira (Frenz et al., 2008), show deposition within the channel and thinning/pinching out up to the channel margin. Canary Island Turbidite 2 is thicker on the channel margins and thins significantly into the channel axis. Turbidity currents sourced from the Moroccan Margin, flowing southwest through the Agadir Basin, show a complex range of depositional architectures. These include: deposition located only on the channel margin with deposits pinching out into the channel axis (Bed 5); deposition occurring both inside and outside the channel axis with no significant thinning or fining of the deposits between core sites (Bed 7); and deposition localized within the channel axis (Bed 12).

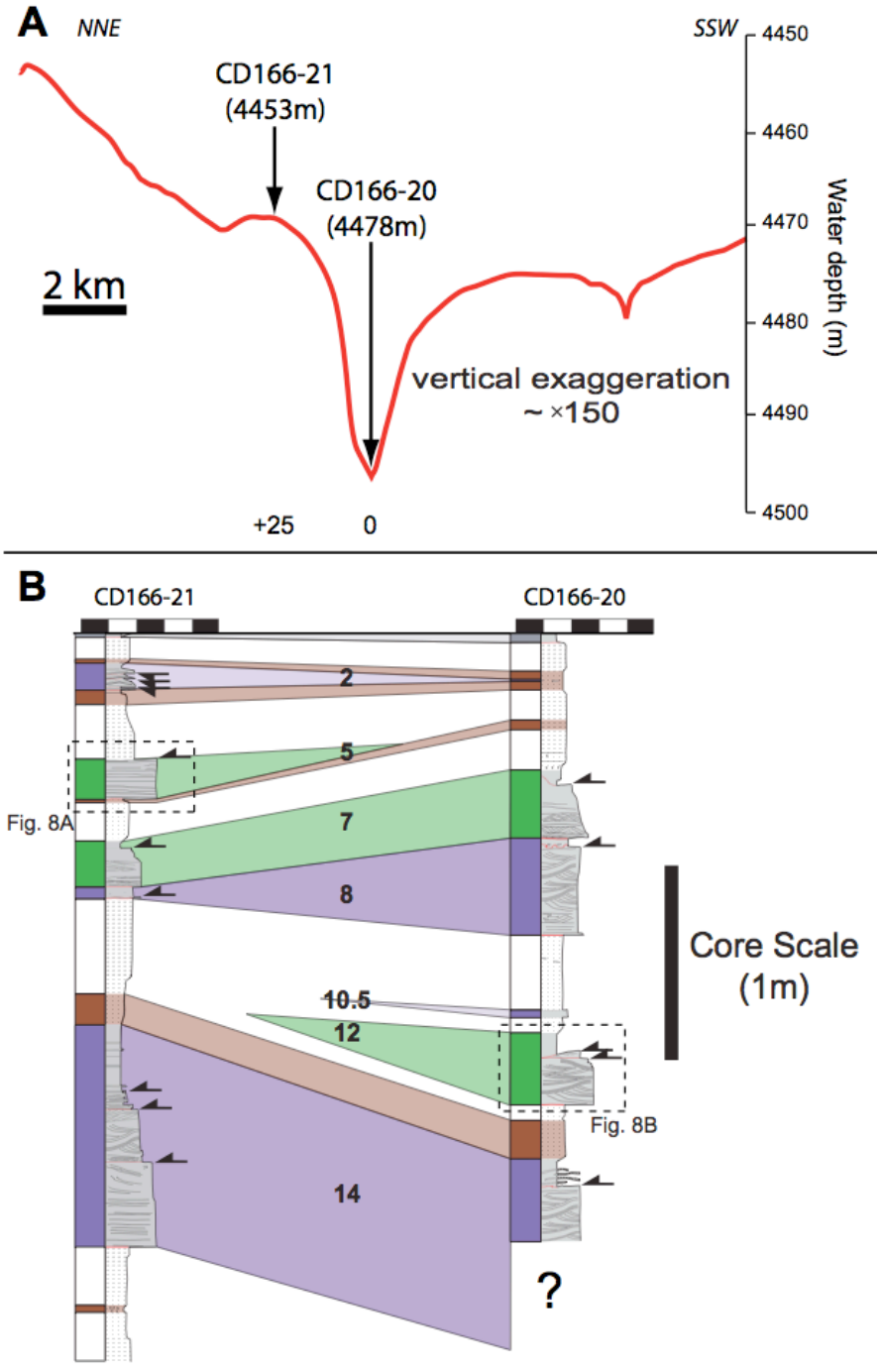

Figure 5-11: Core transect 2 across the proximal southern Madeira Channel. (A) Exaggerated sea floor topography across the channel (red line) with core locations marked. The difference in water depth between core sites is noted underneath the red line. (B) Turbidite stratigraphy for the southern Madeira Channel. Turbidite Beds are labelled after the established Agadir Basin stratigraphy (Wynn et al., 2002b). The core transect shows both turbidite beds and glacial clay layers correlated across the channel (refer to Figure 5-7B for key). Note the complex depositional heterogeneity from flows with the same flow pathway (i.e. through the Agadir Basin); Bed 5 deposits on channel margin and is non-depositional in channel axis; Bed 7 deposits across both channel axis and margin equally; Bed 12 deposition is restricted to the channel axis only.

5.4.8 Turbidites from the Madeira Channel confluence

Core Transect 3 (Figure 5-12) cuts across the wide, low-relief channel situated approximately 100 km down slope of Transects 1 and 2, where the northern and southern channels converge (Figure 5-4). Turbidite deposition within this transect is dominated by relatively thick (20 to 62 cm), normally graded, planar laminated and ripple cross-laminated sands overlain by a sharp grain size break and thin turbidite mud. Occasionally grain-size breaks occur between planar laminated and ripple cross-laminated sands. Deposits appear thickest within the deepest part of the channel axis and thin to the southeast. Turbidites in the southeastern part of the channel are much thinner (2 to 12 cm) and comprise only fine-grained turbidite silt and mud.

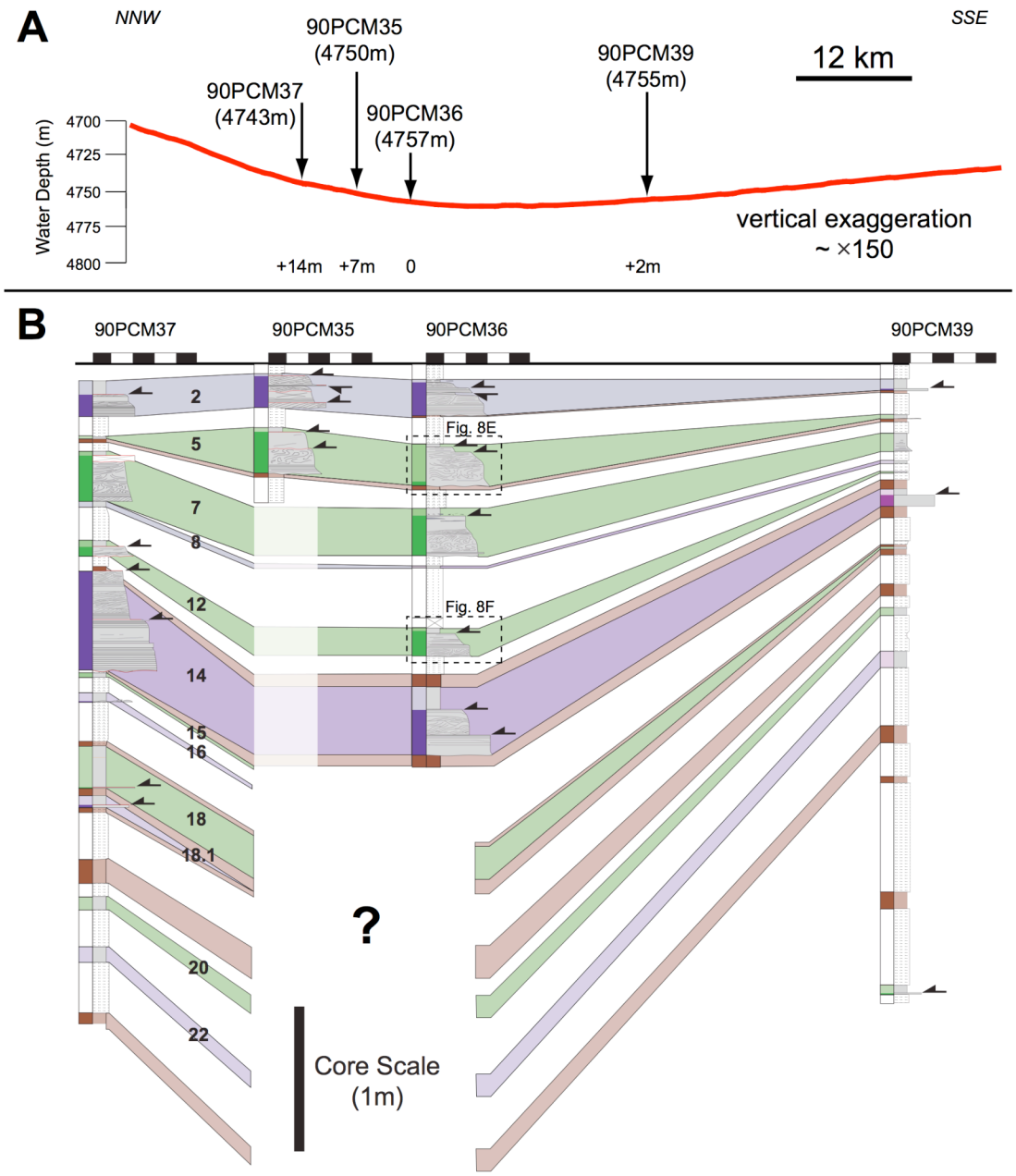

Figure 5-12: Core Transect 3 across the distal northern Madeira Channel System. (A) Exaggerated sea floor topography across the channel (red line) with core locations marked. The channel is extremely low relief at this point and its boundaries are difficult to distinguish. The difference in water depth between cores sites is noted underneath the red line. (B) Turbidite stratigraphy across the distal northern Madeira Channel System. Turbidite Beds are labelled after the established Agadir Basin Stratigraphy (Wynn et al., 2002b). The core transect shows both turbidite beds and glacial clay layers correlated across the channel (refer to Figure 5-7B for key). Note the rippled clean sands deposited within the channel axis and thinner finer deposition on the southwest margin.

5.4.9 Turbidites from the Madeira Abyssal Plain

The Madeira Abyssal Plain is situated at the end of the Madeira Channel System (Figure 5-1A) and records most of the turbidites found in the Madeira Channel System (Figure 5-7B). The turbidity currents that deposited Beds 1, 2, 5, 7, 12 and 14 deposited fine sandy lobes at the Madeira Channel terminuses (Wynn et al., 2000) then fine-grained silts and muds across the rest of the Madeira Abyssal Plain (McCave and Jones, 1988; Jones et al., 1992; Rothwell et al., 1992). These turbidites have estimated volumes within the Madeira Abyssal Plain of 30 km^3 (Bed 5), 110 km^3 (Bed 7), 190 km^3 (Bed 12) and 80 km^3 (Bed 14; (Frenz et al., 2008).

5.5 Discussion

The aim of this discussion is to explain the origin of the patterns of turbidite deposition seen in the geophysical and core data across the Madeira Rise and Madeira Channel System. What was the nature of the turbidity currents passing through the channels? Specifically why is it that turbidites are mostly absent within the northern channel?

5.5.1 Interpretation of 3.5 kHz seismic and EM12 backscatter with core transects

Criteria for recognizing areas of coarse sediment deposition from 3.5 kHz echograms and EM12 backscatter data have been established by a number of studies (Masson, 1994). Areas of low 3.5 kHz acoustic penetration, often associated with high amplitude reflectors, indicates sandy sediment deposition, interpreted here to be turbidites. Turbidite sands interbedded with hemipelagic muds also produce a high-backscatter response on EM12 imagery (Droz et al., 1996). These acoustic signatures are often irregular, reflecting non-uniform deposition of sand by turbidity currents. In this study, groundtruthing the geophysical data with a suite of shallow sediment cores allows confident interpretations to be

made regarding the depositional architectures of turbidites within the Madeira Channels. Core Transect 1 shows deposition of relatively thick turbidite sands on the northern channel margin (Figure 5-9), corresponding with a patchy high-backscatter response on the EM12 bathymetry (Figure 5-2B), and high amplitude reflectors with shallow acoustic penetration on the 3.5 kHz profile line 5 (Figure 5-6A). In contrast, Core Transect 1 shows no sand deposition within the channel axis, which is reflected in the low-backscatter EM12 response (Figure 5-2B) and weak reflectors with deeper penetration on 3.5 kHz profile line 5 (Figure 5-6A and Figure 5-6B). This pattern is pervasive along the northern channel up to ~80 km from the site of channel initiation. Beyond ~80 km, sandy turbidite deposition is shown in the channel axis from high-amplitude reflectors with reduced penetration in 3.5 kHz profiles (Figure 5-6C).

5.5.2 Northern Channel Architecture

The northern channel shows turbidites developed only on the margins of the channel. Almost no turbidite deposition is recorded in the channel axis itself. This could be a result of the turbidity currents not passing through the channels. However, individual turbidite beds are correlated across the Madeira Rise, both northern and southern channels, and across the Agadir Basin and Madeira Abyssal Plain. It seems highly unlikely that these turbidity currents would spread across such an area and not pass through the northern channel. Indeed, trace deposition from Bed 14 (Figure 5-10B) shows that this large-volume flow did pass through the channels yet left minimal trace of its passing. We suggest that the northern channel was able to confine the basal parts of turbidity currents, accelerating these flows enough for them to become non-depositional within the channel axis. This allowed parts of the flows to become more efficient, bypassing their sediment loads further down slope (core transect 3, Figure 5-12).

The thickness of turbidity currents passing across the Madeira Rise and through the northern channel will have a profound impact on the depositional architecture inside and outside the channel axes. Relatively thick flows will be largely unconfined and able to spread laterally

over the entire rise and deposit sediment across the channel margins. Parts of the flows will be confined within the channel and become non-depositional, bypassing their sediment load down slope. Due to the subtle nature of the channel relief, the amount of confinement (hence amount of flow bypass) will progressively increase from the channel margin towards the channel axis. This produces deposits that are thickest away from the channel and progressively thin and pinch out towards the channel axis (e.g. Beds 5, 12, 14, 18; Figure 5-9). Thinner turbidity currents extending only a few metres above the sea-floor will be less able to spread laterally and have a larger proportion of the flow confined by the channels. In this case most of the flow will be confined and becomes non-depositional within the channel, bypassing sediment down slope. In places the thickness of the flow is sufficient that the upper parts can overspill the channel and deposit sands. This produces deposits that thin and fine both away from the channel axis and toward the channel axis (e.g. Beds 20, 21 and 23; Figure 5-9).

5.5.3 Southern Channel Architecture

Turbidity currents with similar flow pathways between the Agadir Basin and Madeira Abyssal Plain (e.g. Beds 5, 7, 8 and 12) show different depositional architectures inside and outside the southern channel. All of these turbidites are found down slope within the Madeira Channel System (Figure 5-12) and across the Madeira Abyssal Plain (Wynn et al., 2002b). High-backscatter signatures (Figure 5-3B) and high amplitude reflectors on the 3.5 kHz profiles (Figure 5-6D) indicate turbidity currents deposited sands across the Madeira Rise and within the southern channel. Indeed, Core Transect 2 shows turbidite deposits located up to 25 m above the axis of the southern channel (Figure 5-11). Therefore, it is most likely that all the turbidity currents passed through the southern channel. Beds 2 and 5 show deposition only on the channel margins and non-deposition within the southern channel axis (Figure 5-11). This suggests a similar process to that operating in the northern channel with confined parts of the flows becoming non-depositional within the channel axis and bypassing sediment down slope. Beds 10.5 and 12 show deposits restricted to the channel axis only, indicating the flows were relatively thin and not able to drape above the height of the channel wall. Bed 8 has thickest deposits in the channel axis and then thinner, finer-grained deposits on the

channel margin. This indicates that the flow was thicker than for Beds 10.5 and 12 with the upper, finer-grained parts of the flow able to drape over the channel margins. Whether completely confined or mostly confined by the southern channel, these flows remained depositional within the channel axis rather than becoming non-depositional. The differences in depositional architectures between turbidites is probably related to differences in individual flow properties such as velocity, flow density, the suspended grain size population, and the thickness of the flows as they enter the channels.

5.5.4 What type of flows were depositing across the channels?

Using a combination of sedimentary structures and detailed vertical grain size profiles the nature of the flows passing through the Madeira Channels can be assessed. The dominance of ripple cross-laminated sands (Figure 5-8A-F) indicates the parent flows were dilute, and incrementally depositing via tractional reworking of sediment along the bed (Allen, 1982; Best and Bridge, 1992). The vertical profile of an incrementally aggraded deposit reflects the longitudinal (i.e. temporal) structure of the base of a flow as it passes over a fixed point (Kneller and Branney, 1995; Kneller and McCaffrey, 2003). Changes in the velocity of the flow, and thus the shear stresses near to the bed, will produce variations in grain size vertically through a deposit. Hence, a waxing (accelerating) depositional flow is capable of producing inversely graded deposits, whilst a waning (decelerating) depositional flow will produce normally graded deposits (Kneller and Branney, 1995; Kneller and McCaffrey, 2003). Proximal to the site of channel initiation, inverse-to-normal grading in turbidite sands indicates that the parent flows were initially accelerating then decelerating. Turbidity currents spilling into the Madeira Channels from the Agadir Basin were most likely accelerated by the break in slope from $< 0.02^{\circ}$ to $> 0.06^{\circ}$. Although subtle, the relative change is a significant three-fold increase in gradient. Intense ambient mixing at the head (Middleton), and reduced mixing in the body of turbidity currents (Stevenson and Peakall, 2010), enables the body of a flow to maintain its density and move up to 30-40 % faster than the head (Kneller and Buckee, 2000). The velocity increase from the head into the body of the flow most likely produced the inversely graded deposits found in the proximal Madeira Channels. Eventually

the flows lost enough sediment and decelerated, depositing progressively finer sediments, resulting in normally graded deposits.

5.5.5 How erosive were the flows?

Turbidity currents that are non-depositional must be in one of two states: (1) erosive, where the flow has sufficient velocity to entrain more sediment into the flow (Parker et al., 1986), or (2) bypassing, whereby the flow is in equilibrium and able to keep its entire sediment load in suspension, yet not powerful enough to entrain any more sediment into the flow (Sequeiros et al., 2009). Flows entering into the Moroccan Turbidite System can initially be highly erosive, producing large-scale scours and erosional hiatuses around the mouth of the Agadir Canyon (Wynn et al., 2002a; Huvenne et al., 2009; Macdonald et al., 2011). Proximal to the Canary Islands, in parts of the Canary Island Channel System, some turbidites are underlain by significant hiatuses representing several meters of erosion (Masson, 1994). However, erosion is limited to the mouth of the Agadir Canyon and parts of the Canary Island Channel System (Wynn et al., 2002a; Huvenne et al., 2009; Macdonald et al., 2011). Where turbidity currents enter the Madeira Channel System, either from the Agadir Basin or from the Canary Islands to the south, they are non-erosive and depositional (Weaver and Thomson, 1993; Weaver, 1994; Wynn et al., 2002b; Talling et al., 2007c).

Within the axis of the northern Madeira Channel high-resolution coccolith biolithostratigraphy shows no significant erosional hiatuses over the past ~ 400 ka (Figure 5-10A). Core Transect 1 (Figure 5-9) shows that even thin (5 cm) glacial clay layers, correlate from the northern margin, through the channel axis and onto the southern margin without changing thickness. Therefore, the glacial clay layers have not been affected by erosion. If any significant erosion had occurred along the flow path it would be expected that the distal Madeira Abyssal Plain would record a different mixture of coccolith species within the turbidite mud caps compared with the proximal Agadir Basin (Weaver and Thomson, 1993). However, no significant variation in coccolith mixtures is found (Wynn et al., 2002b), indicating a lack of significant erosion within the Madeira Channels. The non-erosive/non-

depositional nature of the flows can be seen in the 3.5 kHz profiles, which show a distinct lack of channel migration or lateral accretion surfaces within the channel axis (Figure 5-5 and Figure 5-6).

Turbidity currents passing into the Madeira Channels appear to reach a non-erosive, bypassing equilibrium state, which is stable enough to be maintained for ~ 80 km along the channel. Numerical and experimental modelling has suggested flows can become autosuspending, whereby the net deposition and entrainment of sediment from the flow is zero (Pantin, 1979; Parker et al., 1986; Sequeiros et al., 2009). Flows can become autosuspending if they are accelerated down a slope yet cannot entrain more sediment into the flow. With no change in flow density or slope gradient, autosuspending flows can run out indefinitely (Sequeiros et al., 2009). Autosuspension can only be maintained if the flow is powerful enough to suspend its entire sediment load, yet not powerful enough to erode sediment from the underlying substrate. Flows entering the Madeira Channels are texturally mature, having travelled > 250 km before reaching the channels. Most of the coarse grain sizes have been deposited further up slope leaving predominantly fine-grained sand and mud in suspension (Frenz et al., 2008). With only a fine grain size in suspension, flows would only need a marginal increase in velocity to fully re-suspend their entire sediment load. The break in slope (< 0.02º to > 0.06º) found at the distal end of the Agadir Basin into the Madeira Channels, coupled with confinement within the channel axes, most likely caused a marginal increase in velocity. Within the northern Madeira Channel a critical velocity was reached whereby the relatively fine grain size population within the flows was fully suspended, yet the flows were not fast enough to erode sediment from the underlying sea floor. Autosuspension might explain why turbidity currents bypassing through the northern Madeira Channel can do so for ~ 80 km, and this state only changing with another break in slope a few kilometres west of transect 1 (Figure 5-4A). The change in slope decelerates the flows and forces them to deposit within the channel axis (Figure 5-6C).

5.5.6 Channel evolution: are the channels maintained by deposition or erosion?

Core Transect 1 shows the sediment sequence on the northern channel margin to be ~1.7 times thicker than the equivalent sequence in the channel axis (Figure 5-9). The difference in thickness is the product of sands being deposited on the margin and flows bypassing their sediment load within the channel axis. A similar architecture is seen in the 3.5 kHz profile line 5, with the northern margin sequence 1.7 times thicker than the channel axis stratigraphy (Figure 5-6B). This suggests that the increased thickness of the northern margin sequence seen on the 3.5 kHz profile is also the product of flow bypass within the channel axis, and that this asymmetry of deposition has been occurring over a time period much longer than that sampled by the cores. Hence erosion is not required for the channel to be maintained.

The northern channel has no defined nick point (Figure 5-3A), no detectable erosive surfaces either in core (Figure 5-9) or the 3.5 kHz profiles (Figure 5-5 and Figure 5-6), and is maintained by constructive margins rather than erosion in the channel axis. Therefore it seems unlikely that erosion would have generated the channel originally. It is more plausible that existing sea-floor topography (i.e. an increase in gradient) caused turbidity currents spilling out of the Agadir Basin to begin bypassing sediment down slope whilst allowing some deposition at the margins of the flows. Over time the flow pathway became more defined, as consecutive flows constructed its margins and bypassed sediment in its axis, eventually creating the channel as seen today. Considering the northern channel as a purely constructive feature suggests that it is very old. Extrapolating a constant sedimentation rate of 1 cm per 1000 years (Weaver and Kuijpers, 1983) through an estimated 3.5 kHz penetration of ~20 m (Figure 5-6B) gives an age of at least 2 million years for the northern channel. This estimate will be conservative, as compaction will effectively decrease the apparent sedimentation rate with depth thus yielding an even older age for the channel.

5.5.7 Effect of gradient on channel architecture

Initiation of both the northern and southern Madeira Channels coincides with a marked increase in sea-floor gradient (Figure 5-4 and Figure 5-13). For the first ~80 km from the site of channel initiation the gradient fluctuates but overall remains relatively high in the northern channel (~0.06º; Figure 5-13). This section is characterized by efficient flow bypass. Beyond ~80 km the sea-floor flattens out (<0.06º) coinciding with deposition of turbidite sands both within the northern channel and along its margins. Moving ~100 km further down slope to Core Transect 3 the sea-floor gradient is even lower (~0.04º; Figure 5-4), and here turbidite sands are deposited in the channel and finer grained silts and muds on the margins. It appears that for the northern channel, 0.06º is the critical sea-floor gradient above which flows become bypassing. However, the absolute gradient may not be as important as the relative change from one gradient to another in controlling flow behaviour (Wynn et al., in press). In this case the gradient changes relative to the Agadir Basin slope are approximately three fold (~ 0.02º to > 0.06º).

The southern Madeira Channel has a similar slope profile to the northern channel but exhibits considerable depositional complexity, showing variation from the architectures seen in the northern Madeira Channel (Figure 5-11). Individual turbidites have a range of depositional architectures with both sand deposition in the channel axis only and sand deposition on the margins only, bypassing the channel axis. It is difficult to explain why turbidity currents with similar flow pathways (e.g. down the Agadir Basin) and similar grain size distributions (Figure 5-8) would generate very different depositional architectures across the southern channel. Comparing individual turbidite architectures between the northern and southern channels adds further complexity. Some turbidites deposit in a similar manner in both channels. For example Bed 5 exhibits bypass in both northern and southern channel axes. However, other turbidites display different depositional architectures in different channels. For example, Bed 12 shows bypass in the northern channel axis yet confined sandy deposition in the southern channel axis. The non-uniformity of depositional architecture from the same flows following similar sea-floor slope profiles suggests further controls are acting upon the turbidity currents as they pass into the channels. It is possible that flow properties

such as density, velocity, grain size and flow thickness could affect how a flow might respond to changes in sea-floor gradient. Perhaps subtle differences in these flow properties within different parts of the flows were enough to trigger fundamentally different responses to similar changes in sea-floor gradient.

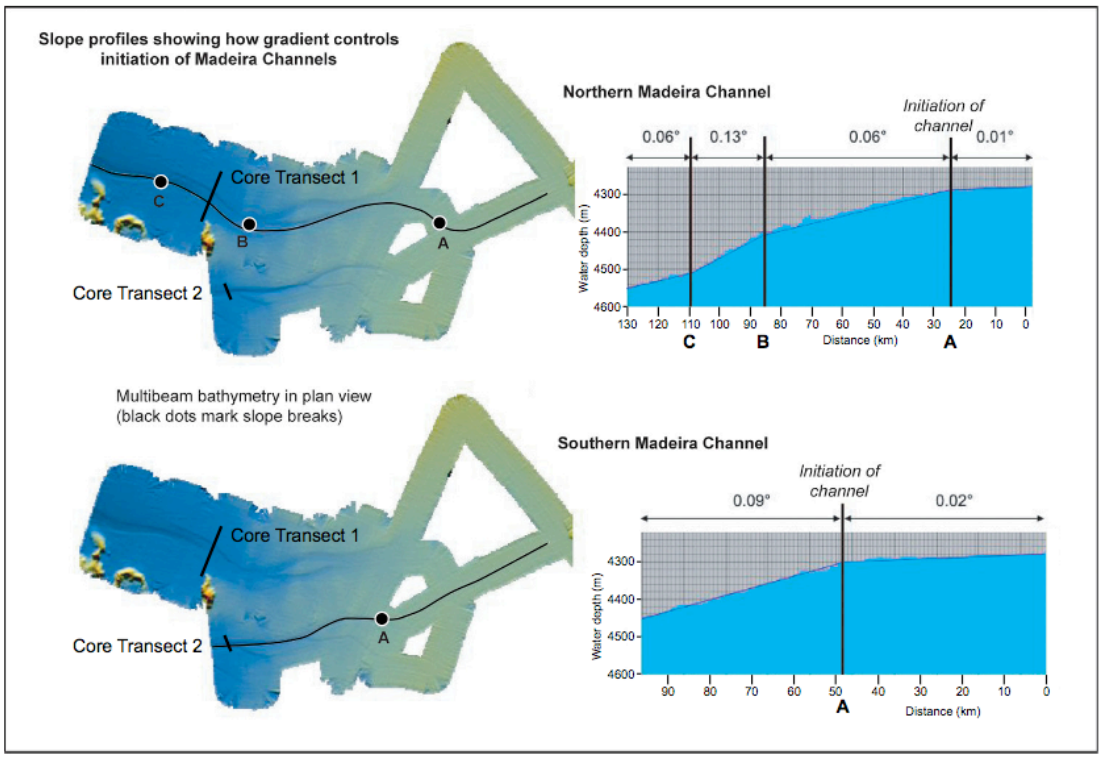

Figure 5-13: EM12 bathymetry with corresponding 2D sea-floor profiles showing gradient control on channel initiation. Averaged sea-floor gradient is labelled on the 2D profiles and significant breaks in slope are marked with black lines on the 2D profiles and black circles on the EM12 bathymetry maps (see Figure 5-4 for sea-floor gradients in plan view). Note that both channels initiate over the break in slope from the southwest (distal) Agadir Basin onto the Madeira Rise.

5.5.8 Comparison to other submarine channel deposits

The morphology and situation of the Madeira Channel System is significantly different compared to the large sinuous channels found within the Amazon, Bengal, Indus, Mississippi, Nile and Rhone fans. The channels that cross these fans are generally deeper

(hundreds of meters), narrower (1-3 km) and have higher sinuosities (Normark, 1978; Normark et al., 1979; Wynn et al., 2007) compared to the Madeira Channels. Fan channels are typically connected to larger feeder canyons, which means turbidity currents are already confined (channelized) by the canyon before they pass into the fan channels (Babonneau et al., 2002). Events passing through the channels are relatively frequent, in some cases occurring more than once a year (Heezen et al., 1964). The Madeira Channels are not directly connected with a feeder canyon. Instead, they are connected with the distal end of the Agadir Basin. This means that turbidity currents passing into the Madeira Channels via this flow pathway are largely unconfined, being as wide as the Agadir Basin (i.e. ~100 km across). Events that have sufficient volume to reach the channels are relatively infrequent, ~1 every 10, 000 years (Wynn et al., 2002b).

Typical channel-levee architectures are not observed in the Madeira Channels. Coarse-grained turbidite deposition is entirely lacking in the axis of the northern Madeira Channel whilst the axis of the southern Madeira Channel has a combination of thin sandy turbidites and flow bypass. Neither of the channel axes have any detectable lateral-accretion packages nor any erosive/cross cutting surfaces. Typically, channel levees are generated from the upper parts of turbidity currents periodically or continuously overspilling the confines of the channel walls as they pass along the channel axis (Peakall et al., 2000). Levees produced in this manner will thin and fine laterally, away from the channel axis (Kane et al., 2007; Kane et al., 2010; Kane and Hodgson, 2011). Most of the turbidites within the Madeira Channel System enter the Madeira Channel System as unconfined sheet flows resulting in deposition along the margins that progressively thickens away from the channel axis. Hence the channel margin deposits should not be referred to as channel levees, as the process for their formation (and depositional architecture) is quite different from channel overspill and crevasse splay type levee formation.

Some comparisons can be drawn with the smaller scale Brazos-Trinity Turbidite System, offshore Gulf of Mexico. Within this system submarine channels connect a series of mini-basins for ~ 60 km across the continental shelf (Badalni et al., 2000). Turbidity currents are interpreted to be channelized until they pass into the first mini-basin. Here they spread and

eventually spill over into the connecting channel system as unconfined flows, much wider than the channels. Due to the unconfined nature of the flows a number of nick points and smaller tributaries develop that coalesce into a main channel (Beaubouef and Friedmann, 2000). In terms of regional setting the Madeira Channels are a larger version of the Trinity-Brazos channels, connecting two basins over ~700 km. Indeed, turbidity currents passing into the Madeira Channels are also largely unconfined (> 100km wide). This is probably the reason why the southern Madeira Channel initiates from a number of well defined knick points that quickly converge into a main channel (Figure 5-2A). However, in terms of depositional architecture the Trinity-Brazos System is similar to other channel-levee systems with coarse-grained channel fill and fine-grained levees that thin away from the channel axis (Beaubouef and Friedmann, 2000). From detailed seismic profiles the channel axes show significant erosion cutting into underlying levee deposits and lateral channel migration (Beaubouef and Friedmann, 2000), whereas the Madeira Channels are purely constructional with no channel migration.

The NAMOC system found in the Labrador Sea, offshore Greenland has an extensive network of shallow (5-20 m deep) braided and 'yazoo type' channels that progressively converge into a main trunk channel (Chough and Hesse, 1976; Hesse et al., 1987a; Hesse et al., 1987b; Hesse, 1989; Hesse et al., 1990; Hesse and Rakofsky, 1992; Klaucke et al., 1997; Klaucke et al., 1998; Hesse et al., 2001). These shallow channels show little fractionation in grain size between channel fill and levee deposition with sandy levees developed along their margins. The sandy levees are interpreted to have formed by deposition from largely unconfined, sand-rich turbidity currents sourced from the continental shelf, travelling along the lowest points of the basin (Hesse et al., 1990; Hesse et al., 2001). This is similar to the depositional architecture of turbidites along the margins of the Madeira Channels. However, the NAMOC system has coarse-grained channel fill and records significant channel floor erosion, which contrasts with the bypass dominated, non-erosive Madeira Channels.

Exceptional exposures of deep-marine sediments within the Neoproterozoic Windermere Supergroup, western Canada, and in the Permian Lainsburg Formation, Karoo, South Africa, document 'poorly-' or 'weakly- confined' channel systems (Brunt et al., 2012; Arnott et al.,

in press). 'Poorly-confined' channel architectures are characterized by laterally extensive, rippled sands deposited across the channel margins. These architectures are interpreted to be the product of largely unconfined turbidity currents passing across low-sinuosity channels (Arnott et al., in press). The channel margin architectures observed across the Madeira Channels, albeit without any associated channel fill, are interpreted to the product of a similar process; largely unconfined flows passing across the low sinuosity channels.

5.5.9 Summary of turbidity current processes

As turbidity currents passed across the Madeira Rise through the Madeira Channel System, either from the Agadir Basin or the Canary Islands, their ability to transport and deposit sediment was fundamentally affected. The range of depositional architectures seen in the core transects and geophysical data are interpreted to be the product of three types of flow behaviour, categorized as: (1) Unconfined channel bypass, (2) Confined channel bypass and, (3) Confined channel deposition (Figure 5-14). Flow behaviour is primarily governed by changes in sea-floor gradient, and flow parameters such as: thickness, velocity and suspended grain size. These three types of flow behaviour are as follows: (1) Turbidity currents entering the channels were unconfined and large-volume relative to the channels. The flows were able to spread across the sea-floor largely unimpeded, depositing laterally extensive ripple cross-laminated sands across the Madeira Rise. The shallow (~20 m deep) channels confined only the lowermost parts of these turbidity currents. The confined parts of the flows were accelerated within the channel axis and bypassed sediment down slope. This state of 'unconfined channel bypass' dominates across the northern channel (e.g. Beds 2, 5, 12 and 14; Figure 5-9) but is also associated with turbidites in the southern channel (e.g. Beds 2 and 5; Figure 5-11). This state of 'unconfined channel bypass' can evolve into 'unconfined channel deposition' with changes in sea-floor gradient. Flatter areas of sea-floor decelerate both the confined and unconfined parts of the flows triggering deposition of ripple-cross laminated sands across the margins and within the axes of the channels. This depositional architecture is shown by one turbidite in the southern channel (Bed 7 in Core Transect 2; Figure 5-11) and acoustically across the more distal parts of the northern channel (Figure 5-5 and Figure 5-6C). (2) Thinner flows were more confined by the channels and are unable to spread as extensively. In this case a higher proportion of the flow was accelerated and

bypassed down slope. The uppermost parts of the flow were able to overspill the confines of the channel, which produced laterally restricted lenses of ripple cross-laminated sands along the channel margins. Examples of 'confined channel bypass' can be seen within the northern channel (e.g. Beds 20 and 23; Figure 5-9). (3) Some turbidity currents that were confined by the channels were not accelerated enough to become bypassing. In this case 'confined channel deposition' occurred with relatively thick ripple cross-laminated sands deposited in the channel axis and thinner, finer-grained sediment deposited on the channel margins (e.g. Bed 8; Figure 5-11). Indeed, Beds 10.5 and 12 in the southern channel demonstrate that some channelized flows were completely confined, and unable to deposit on the channel margins altogether (Figure 5-11). 'Confined channel deposition' also occurs with increasing distance from the site of channel initiation, across areas of flatter sea-floor. This indicates confined (channelized) parts of the flows were more efficient than the unconfined (lateral) parts of the flows and able to run out for much longer distances. These completely channelized turbidity currents deposited ripple cross-laminated sands within the axes of the channels and finer-grained silts and muds on the margins. This flow behaviour and depositional architecture dominates the distal parts of the channels (e.g. all Beds in Core Transect 3; Figure 5-12). Once channelized the flows were highly efficient, able to transport sediment for ~700 km down slope before eventually spreading and depositing across the Madeira Abyssal Plain (Figure 5-7).

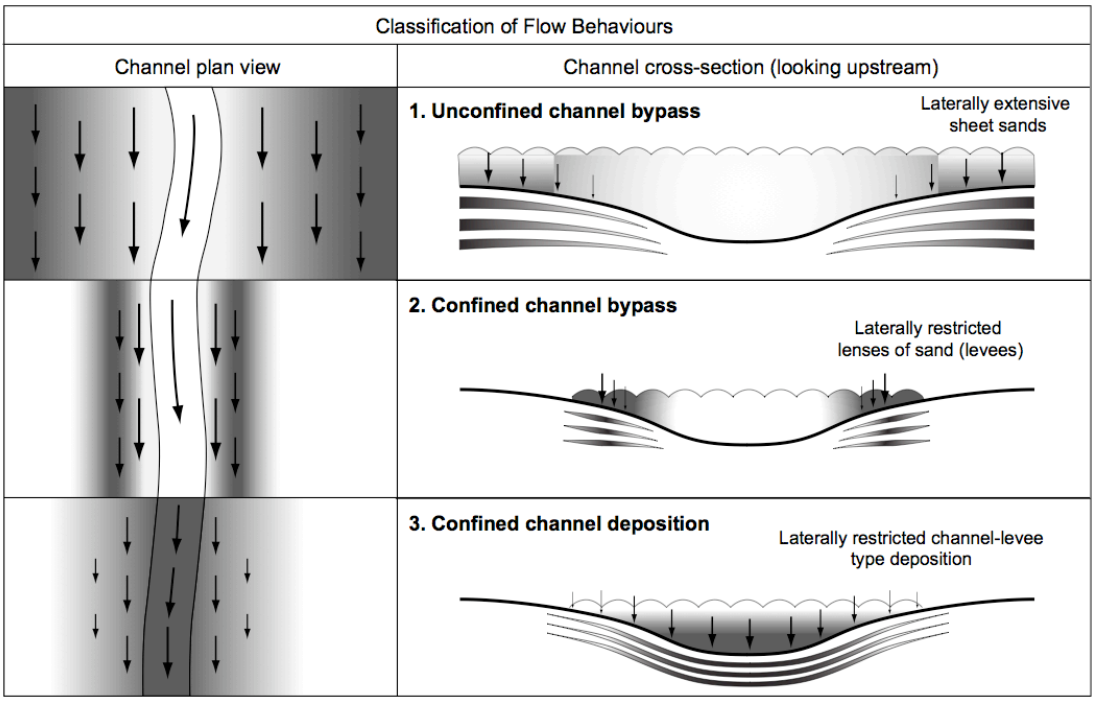

Figure 5-14: Simplified cartoon illustration summarizing the three main types of flow behavior and resulting depositional architectures across the Madeira Channel System. The left side shows a plan view of flows passing into the channel system. Arrows indicate flow direction and size of arrows shows flow velocity: the larger the arrow the faster the flow. Darker shading represents areas of turbidite deposition whilst lighter shading represents areas of non-deposition. The right side of the figure shows corresponding channel cross-sections with inferred flow behavior and associated depositional architectures (see main text for details). Downward pointing arrows indicate zones of deposition.

5.6 Conclusions

This contribution presents a detailed examination of the Madeira Channel System using EM12 bathymetric data, a dense network of 3.5 kHz profiles, and a suite of shallow sediment cores. This detailed data set provides insights into the response of large-volume turbidity currents entering a shallow (< 20 m) channel system. Specific conclusions are:

1. Although relatively shallow and low relief, the Madeira Channel System exerts a major influence on turbidity currents, generating complex across flow and down flow heterogeneities in turbidite deposition. The channel relief would be extremely difficult to detect in outcrop.

2. Subtle changes in sea-floor gradient (< 0.02º to 0.06º) can change turbidity current behaviour from deposition to efficient bypass of their sediment loads down slope. Relative change in slope (i.e. three fold) could be more important than the absolute slope change (i.e. ~ 0.04º). Currently these changes in sea-floor gradient would also be undetectable in outcrop or within the subsurface.

3. Extremely large-volume (> 100 km^3), aerially extensive turbidity currents can efficiently bypass sediment leaving no trace of their passing. Indeed, despite large volumes of bypass no discernable erosion occurred in the channels. This means that an absence of a turbidite (or associated erosion) in a channel axis does not necessarily mean an absence of a turbidity current passing through the channel.

4. Erosion is not required to build or maintain the Madeira Channels. Rather it is construction of the channel margins and bypass within the channel axes that builds and maintains channel relief.

6 The spatial and temporal distribution of grain-size breaks within five turbidite beds offshore NW Africa: The role of late-stage fluid mud layers

Stevenson, C.J., Talling, P.J., Masson, D.G., Sumner, E.J., Frenz, M., Wynn, R.B.

6.1 Abstract

Grain-size breaks are a sharp surface whereby an abrupt change in grain size occurs vertically within a deposit. Grain-size breaks are a common feature in turbidite deposits and have been documented in numerous locations around the world, including both ancient outcrops and modern cores. Despite their frequency and widespread occurrence, grain-size breaks have been regarded as exceptional, and not included within idealized models of turbidity current deposition. Understanding how grain-size breaks form is important because they are a significant departure from our current idealized models of turbidite deposition. This study uses a suite of ~ 100 shallow sediment cores, from the Moroccan Turbidite System, which coupled with a robust geochemical and chronostratigraphic framework, enables individual turbidite beds to be correlated across distances in excess of 2000 km. From these correlations we map out the vertical and spatial distributions of grain-size breaks within five turbidite beds. Five different types of grain-size break are found: *Type I* – occurred proximally between gravel and finer grained structureless sand, *Type II* – occurred proximally between inversely graded sand overlain by coarser sand, *Type III* – occurred proximally between sand overlain by ripple cross-laminated finer sand, *Type IV* – occurred almost everywhere between clean sand and mud, and *Type V* – occurred only in relatively distal areas between mud-rich (debrite) sand and mud. We interpret Types II and III as products of spatial/temporal fluctuations in flow capacity, whilst Types I and V are generated from sharp vertical concentration boundaries, controlled by total sediment and/or clay concentrations within the parent flows. *Type IV* grain-size breaks are interpreted to be the product of late-stage

development of fluid mud, which hinders the settling of non-cohesive grains and bypasses them down slope. Grain-size analysis of the individual beds proximally and distally (> 1500 km down slope) demonstrates the missing grain sizes are found down slope. Theoretically, a decelerating clay-rich suspension will always form a cohesive fluid mud layer near to the bed: resulting in a Type IV grain-size break. This may explain why Type IV grain-size breaks are widespread in all five turbidites examined here, and are commonplace within most turbidite sequences studied elsewhere. This considered, *Type IV* grain-size breaks should be regarded as the norm, not the exception, and understood as a typical feature within turbidite beds.

6.2 Introduction

Grain-size breaks are an abrupt change in grain size across a sharp surface. Grain-size breaks are a common phenomenon, documented in numerous turbidite systems from around the world (Bouma, 1962; Lebreiro et al., 1997; Gladstone and Sparks, 2002; Kneller and McCaffrey, 2003; Sinclair and Cowie, 2003; Kane et al., 2007; Eggenhuisen et al., 2011) and also occur within terrestrial gravity currents such as pyroclastic flows and ignimbrites (Gladstone and Sparks, 2002; Brown and Branney, 2004; Edmonds and Herd, 2005; Edmonds et al., 2006). Classic turbidite models predict sedimentation from a dilute waning flow to progressively fine upward (Bouma, 1962; Stow and Bowen, 1978; Stow and Shamugam, 1980; Lowe, 1982; Stow and Piper, 1984). Grain-size breaks are not included within the Bouma Sequence or other idealized facies schemes and are a significant departure from these models.

Previous work has offered a variety of explanations for the generation of grain-size breaks. These explanations can be grouped into five categories. First, grain-size breaks result from sharp internal discontinuities in concentration and grain size within the flow. Different types of discontinuity have been proposed that separate turbidity current and debris flow (Talling et al., 2004), or the body of a turbidity current from its overlying wake (Gladstone and Sparks, 2002). Second, grain-size breaks result from flow reflection (Pickering and Hiscott, 1985).

Third, grain-size breaks result from flow separation due to topographic obstacles, whereby the coarser-grained basal part of the flow is diverted to take a different path to the upper finer-grained part of the flow (Sinclair and Cowie, 2003). Fourth, grain-size breaks result from bypass of intermediate grain sizes for a period of time due to fluctuations in the flow's sediment carrying capacity (Kneller and McCaffrey, 2003). Fifth, grain-size breaks simply result from a strongly bimodal initial grain-size distribution within the flow (Bouma, 1962; Kneller and McCaffrey, 2003). A sixth mechanism is considered here. Grain-size breaks, from sand to mud, result from the development of cohesive fluid mud layers towards the rear of the flow (McCave and Jones, 1988; Jones et al., 1992). The missing grain sizes are supported within the fluid mud layer and transported significant distances down slope.

Many of the proposed mechanisms for the generation of grain-size breaks, are difficult to validate. For example, grain-size breaks are likely to develop beneath a flow with a strongly bimodal grain-size distribution (Bouma, 1962; Kneller and McCaffrey, 2003). However, to validate such a hypothesis, it is necessary to analyse the grain size of the entire deposit in order to establish whether the parent flow did or did not contain the range of grain sizes missing across the grain-size breaks. This requires detailed mapping of individual turbidite beds over their entire depositional extent, which commonly is not possible.

This contribution presents a detailed analysis of five turbidite beds, correlated across the Moroccan Turbidite System situated offshore NW Africa. These beds provide a rare opportunity to investigate how and why grain-size breaks form. The deposits are unconsolidated allowing detailed quantification of grain-size distribution. Analysis of deposits on the modern sea floor allows the relationships between grain-size breaks and changes in seafloor gradient to be established. The excellent core coverage coupled with a robust individual bed correlation framework enables turbidites to be documented over their entire depositional extent, both in down flow and across flow directions. This is arguably the most detailed and extensive correlative framework for individual flows in any turbidite system. The specific aims of this study are to:

1. Document the frequency, magnitude and spatial distribution of grain-size breaks within individual turbidite beds across the Moroccan Turbidite System.

2. Use spatially extensive grain-size analysis across the individual turbidites to estimate the total grain-size distributions within entire beds.

3. Relate the distribution of grain-size breaks to changes in sea-floor gradient.

4. Use these five turbidite beds to evaluate and develop proposed mechanisms for the formation of grain-size breaks.

6.2.1 The Moroccan Turbidite System

The Moroccan Turbidite System consists of three interconnected deep-water basins (Wynn et al., 2002b): the Seine Abyssal Plain in the northeast, the Agadir Basin situated in the central part of the system, and the Madeira Abyssal Plain in the west (Figure 6-1). The Seine Abyssal Plain and Agadir Basin are adjacent, only separated by a low relief ridge. The Agadir Basin and Madeira Abyssal Plain are connected via a series of ~ 20 m deep, ~ 700 km long distributary channels called the Madeira Channel System (Masson, 1994; Stevenson et al., 2012). Seafloor gradients across the basins are generally between ~ 0.01° and 0.05° with steeper gradients across the Madeira Channel System, ranging from 0.06° to 0.3° (Stevenson et al., 2012; Wynn et al., in press). Three main types of turbidite are found within the Moroccan Turbidite System: 1) organic-rich turbidites sourced from the Moroccan Margin, primarily composed of shallow water biogenic material, quartz and glauconite; 2) carbonate-rich turbidites sourced from local seamount collapses, composed almost exclusively of foraminifera and carbonate-rich ooze; and 3) volcanoclastic turbidites sourced from the Canary Islands, which are dominated by volcanic glass and mafic lithics (de Lange et al., 1987; Pearce and Jarvis, 1992; Weaver et al., 1992; Pearce and Jarvis, 1995; Wynn et al., 2002b; Hunt et al., 2011). The five turbidites examined in this study are organic-rich beds sourced from the Moroccan Margin. The main flow pathways for organic-rich flows are via the Agadir and El Jadida Canyons, which debouche directly into the Agadir Basin and Seine

Abyssal Plain (Figure 6-1). The Madeira Abyssal Plain is situated distally within the system, fed by flows with sufficient volume to run-out beyond the Agadir Basin and pass through the Madeira Channel System (Wynn et al., 2002b; Wynn et al., 2010; Stevenson et al., 2012).

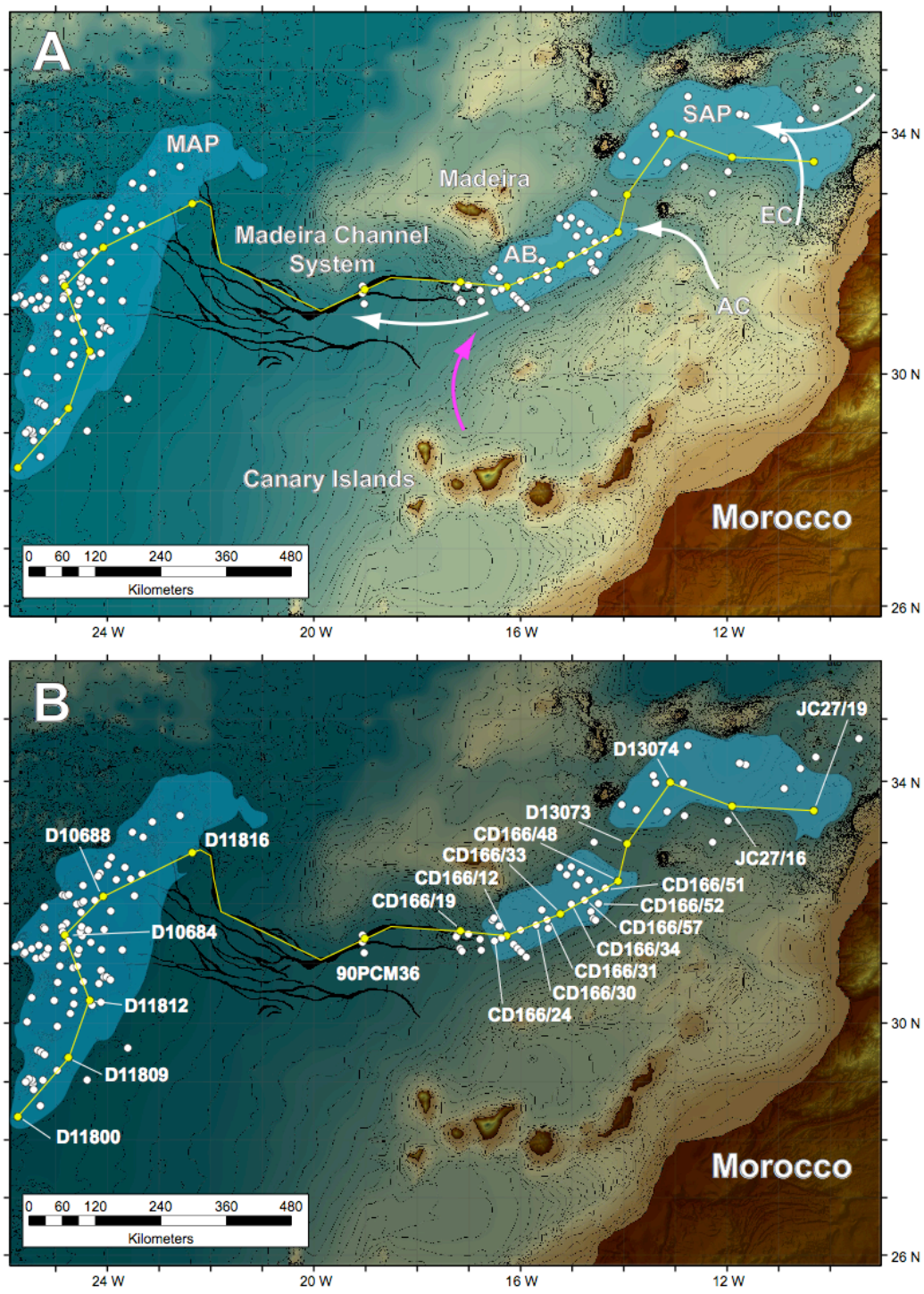

Figure 6-1: (A) Map of the Moroccan Turbidite System, comprising three interconnected basins: the Seine Abyssal Plain (SAP), the Agadir Basin (AB), and the Madeira Abyssal Plain (MAP). Marked in black are the Madeira Channels, which connect the Agadir Basin to the Madeira Abyssal Plain. Main flow pathways across the system are highlighted with organic-rich turbidites originating from the Moroccan margin (white arrows) and volcanoclastic turbidites originating from the Canary Islands (purple arrow). The Agadir Canyon (AC) and El Jadida Canyon (EC) are situated in the northeast parts of the system, and are conduits for flows originating from the Moroccan Margin. Cores used in this study are marked with white circles and labelled in (B). Highlighted in yellow are cores used in Core Transect 5 (Figure 6-2), which is a large-scale correlation of individual beds over the Moroccan Turbidite System.

6.3 Materials and methods

6.3.1 Sea floor bathymetry and gradient

Modern seafloor bathymetry is assumed to be similar to palaeobathymetry over the past 200 ka (see Chapter 2). GEBCO data provides bathymetry across the Seine Abyssal Plain and surrounding area with sufficiently high resolution to define large-scale topographic features such as canyons, seamounts and topographic low points within the Moroccan Turbidite System. Seafloor gradients are calculated from GEBCO bathymetry (see Chapter 2).

6.3.2 Cores

This study is based on ~100 shallow piston cores recovered over the last 30 years during a number of research cruises. Core sites are located throughout the Moroccan Turbidite System both in down flow and across flow directions (Figure 6-1). All cores were subject to detailed visual logging with particular attention focused on the turbidite beds. Grain size was initially established with a hand lens and comparison with a grain-size comparator card. The grain size of turbidite sediments was then analyzed using a Malvern Mastersizer 2000 (see Chapter 2).

6.4 Results

6.4.1 Sediments in cores

Cores collected from the Moroccan Turbidite System contain hemipelagic sediments punctuated by turbidite beds. Hemipelagic sediments deposited during interglacial (warm) periods are light greyish or brownish fine-grained carbonate-rich oozes, containing randomly dispersed foraminifera (Weaver and Kuijpers, 1983; Weaver and Rothwell, 1987; Weaver, 1991). In contrast, hemipelagic sediments deposited during glacial (cold) periods are reddish-brown clay with few forams (Weaver and Kuijpers, 1983). Turbidites have characteristically sharp bases with gradational bioturbated upper contacts with hemipelagic sediments. Foraminifera are absent from turbidite muds.

6.4.2 Bed Correlation

Over the past 30 years a robust geochemical and chronostratigraphic framework has been established across the Moroccan Turbidite System, enabling individual turbidite beds to be correlated: in both down flow and across flow directions (Weaver and Kuijpers, 1983; de Lange et al., 1987; Pearce and Jarvis, 1992; Rothwell et al., 1992; Weaver et al., 1992; Weaver and Thomson, 1993; Weaver, 1994; Pearce and Jarvis, 1995; Davies et al., 1997; Wynn et al., 2002b; Talling et al., 2007c). Exceptional core coverage has enabled individual turbidite beds to be correlated between basins, producing an inter-connected turbidite stratigraphy that extends across the entire Moroccan Turbidite System (Wynn et al., 2002b). Here we build upon this substantial body of work by incorporating a suite of ~ 70 cores into the established turbidite stratigraphy, recovered aboard ‘RRS Charles Darwin’ Cruise CD166 and ‘RRS James Cook’ Cruise JC27. The increased core control enables existing bed correlations to be extended from the base of the Moroccan Margin, across the Seine Abyssal Plain, through the Agadir Basin, into the Madeira Channel System and ultimately into the Madeira Abyssal Plain (Figure 6-2). Turbidites are numbered sequentially down core, using

the nomenclature adopted by Wynn et al., (2002b) for the Agadir Basin. Prefixes are used to denote in which part of the Moroccan Turbidite System the beds occur: 'S' for Seine Abyssal Plain, 'A' for the Agadir Basin and connecting Madeira Channel System, and 'M' for the Madeira Abyssal Plain. This study focuses on five turbidites: Beds 3, 5, 7, 11 and 12 (Figure 6-2).

Beds 5 and 12 are very large-volume events (> 160 km^3) and have impressive run-outs with deposits extending > 2000 km across the entire system. Bed 7 is also large-volume (~ 120 km^3) with deposits extending ~ 1500 km from the Agadir Basin to the Madeira Abyssal Plain. Beds 3 and 11 are relatively small-volume (~ 15 km^3) and are restricted to proximal parts of the system: the Seine Abyssal Plain and northeast parts of the Agadir Basin.

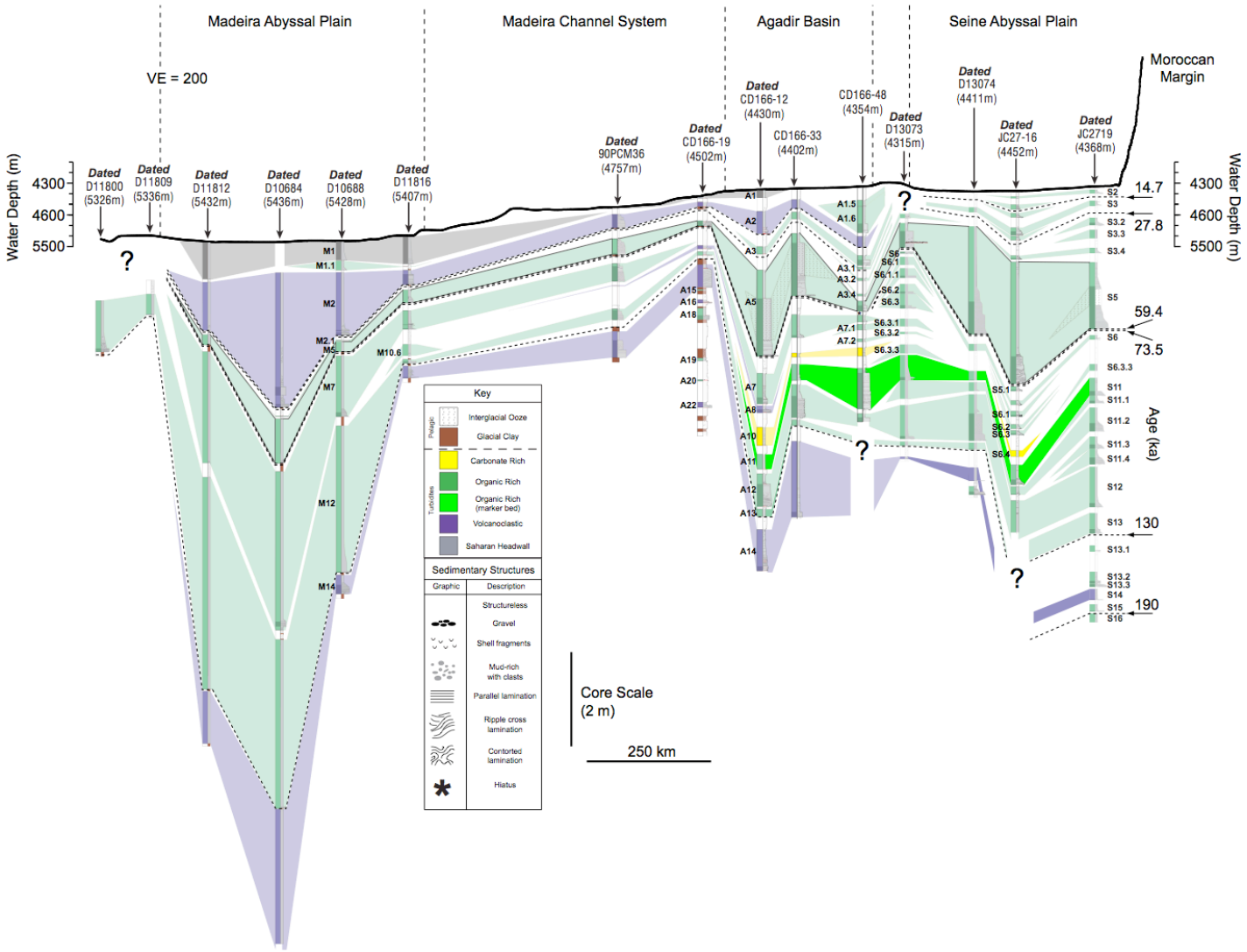
Madeira Abyssal Plain
Madeira Channel System
Agadir Basin
Seine Abyssal Plain
Moroccan Margin
VE = 200
Water Depth (m)
4300
4600
5500
Dated D11800 (5326m)
Dated D11809 (5336m)
Dated D11812 (5432m)
Dated D10684 (5436m)
Dated D10688 (5428m)
Dated D11816 (5407m)
Dated 90PCM36 (4757m)
Dated CD166-19 (4502m)
Dated CD166-12 (4430m)
CD166-33 (4402m)
CD166-48 (4354m)
Dated D13073 (4315m)
Dated D13074 (4411m)
Dated JC27-16 (4452m)
Dated JC2719 (4368m)
14.7
27.8
59.4
73.5
130
190
Age (ka)
Key
Pelagic
Interglacial Ooze
Glacial Clay
Turbidites
Carbonate Rich
Organic Rich
Organic Rich (marker bed)
Volcanoclastic
Saharan Headwall
Sedimentary Structures
Graphic
Description
Structureless
Gravel
Shell fragments
Mud-rich with clasts
Parallel lamination
Ripple cross lamination
Contorted lamination
Hiatus
Core Scale (2 m)
250 km

Figure 6-2: Turbidite correlation (Transect 1) extending from: the base of the Moroccan Margin, through the Seine Abyssal Plain, the Agadir Basin, the Madeira Channel System and across the Madeira Abyssal Plain (see Figure 6-1 for location of transect). Core sites selected for this transect are representative of local turbidite stratigraphy. However, selected core sites form a small proportion of the total core coverage across the system. More detailed, smaller-scale turbidite correlations (utilizing the full range of cores available) have been constructed separately for the Seine Abyssal Plain, Agadir Basin, Madeira Channel System, and Madeira Abyssal Plain (see main text for references). Cores are hung from exaggerated seafloor topography and comprise a lithological column and visual log. Datums are marked between cores with dashed black lines and dated cores are labelled. Key marker beds comprise: volcanoclastic Bed S14 (purple shading), mint-green organic-rich Bed S11 (bright green shading), and the largest volume event Bed S5 (heavy black outline). Note the increased thickness of turbidite muds within topographic low points, particularly within the Seine and Madeira Abyssal Plains.

6.4.3 Turbidite facies

Sedimentary textures found within turbidite beds are described within a facies scheme. Many of the facies described in this study are common to deep-water turbidite systems and have been thoroughly described elsewhere (Bouma, 1962; Lowe, 1982; Sumner et al., 2012). For clarity a brief description of each facies is provided below.

Structureless Clean Sand (ST; Bouma T_A)

Structureless clean sand comprises sand displaying no sedimentary structures with mud contents ≤ 20 %. The term 'clean' is used in a relative sense to distinguish this facies from mud-rich structureless sand, which has significantly higher mud contents.

Mud-Rich Structureless Sand (ST_D)

Distinctive intervals of mud-rich (30 – 40 % mud), structureless sand are found within Bed 5 across the Agadir Basin and eastern parts of the Seine Abyssal Plain. This facies can be ungraded or have weak normal grading (Talling et al., 2007c).

Laminated Sand (PL, RXL, CL; Bouma T_B and T_C)

Planar laminated sand (PL) is found in all the turbidites examined in this study, occurring towards the base of deposits. Laminae are relatively thin (< 2 mm thick) with low mud contents between 5 – 10 %. This facies can have a range of grading patterns including inverse, normal and ungraded. Ripple cross-laminated sand (RXL) occurs towards the upper parts of deposits, or at the base of relatively thin-bedded turbidites. This facies is normally graded and has low mud content (< 5 %). Contorted lamination (CL) within sand intervals is common through the basin. This facies typically occurs in the middle parts of the turbidite deposits and has a relatively low mud content (5 – 10 %). Contorted intervals can be inverse and/or normal graded.

Turbidite Mud (L, CM and, M; Bouma T_D and T_E)

Volumetrically turbidite mud is the most abundant type of sediment within the Moroccan Turbidite System. Often, basal parts of the mud cap have thin inter-laminated silts and muds (L). This facies normally grades into ungraded, structureless mud (M). Frequently, the basal parts of the mud cap, and/or higher up in the deposit, have intervals of contorted silty laminae, some with clasts of silt. These intervals can have multiple fining upward sequences.

6.4.4 Typical geometry of turbidite mud

Most of their mud, within the five beds examined, occurs as a relatively thin (10 – 20 cm) drape, overlying coarser sand deposits (e.g Agadir Basin; Figure 6-2). These thin muds are usually ungraded and structureless (M). However, large-volumes of mud are ponded in topographic low points within the system. Proximally, this occurs within the central and western parts of the Seine Abyssal Plain (see also Chapter 3). Distally, muds are ponded into the central parts of the Maderia Abyssal Plain (Figure 6-2). Ponded muds have silt-rich

normally graded bases, and within the Seine Abyssal Plain have contorted silty laminations and clasts.

6.4.5 Grain-size breaks

Grain-size breaks occur within all of the beds examined in this study and are also present in all other turbidites found across the Moroccan Turbidite System. Locally, five types of grain-size break are recognized (Figure 6-3; Table 6-1): *Type I grain-size breaks* occur between coarse-grained sand/gravel overlain by finer grained sand (Figure 6-3Ab). Suitable coarse material occurs within Beds 5 and 12. Within Bed 5 gravel-sized sediment occurs at the base of the bed along most of the length of the Agadir Basin. In Bed 12 very coarse-grained sediment only occurs in proximal areas of the Agadir Basin. *Type II grain-size breaks* comprise inversely graded sand overlain by finer grained sand. This type of grain-size break occurs in Beds 5 and 12 in proximal areas of the Agadir Basin, notably these are both large volume beds. *Type III grain-size breaks* are rare and comprise planar laminated sands overlain by structureless or contorted very-fine sands. This type of grain-size break is restricted to proximal localities within Bed 11. *Type IV grain-size breaks* comprise clean sand overlain by a relatively thin turbidite mud. They occur proximally, centrally and relatively distally within all five beds (Figure 6-3Ba and Figure 6-3Ca). Within the five beds examined, 82 % of grain-size transitions from sand into mud were Type IV grain-size breaks as opposed to a gradational transition from sand to mud. Type IV grain-size breaks can be overlain by a range of turbidite mud facies: a) mud with a normally graded base (occasionally with interlaminated silts), b) ungraded structureless mud, or c) mud with contorted silty laminations and/or silt clasts. However, where turbidite muds are ponded, Type IV grain-size breaks are generally absent with deposits grading from sand into contorted muds. *Type V grain-size breaks* comprise mud-rich structureless sand overlain by ungraded turbidite mud (Figure 6-3Aa). This type of grain-size break only occurs in Bed 5 and is restricted to relatively distal localities.

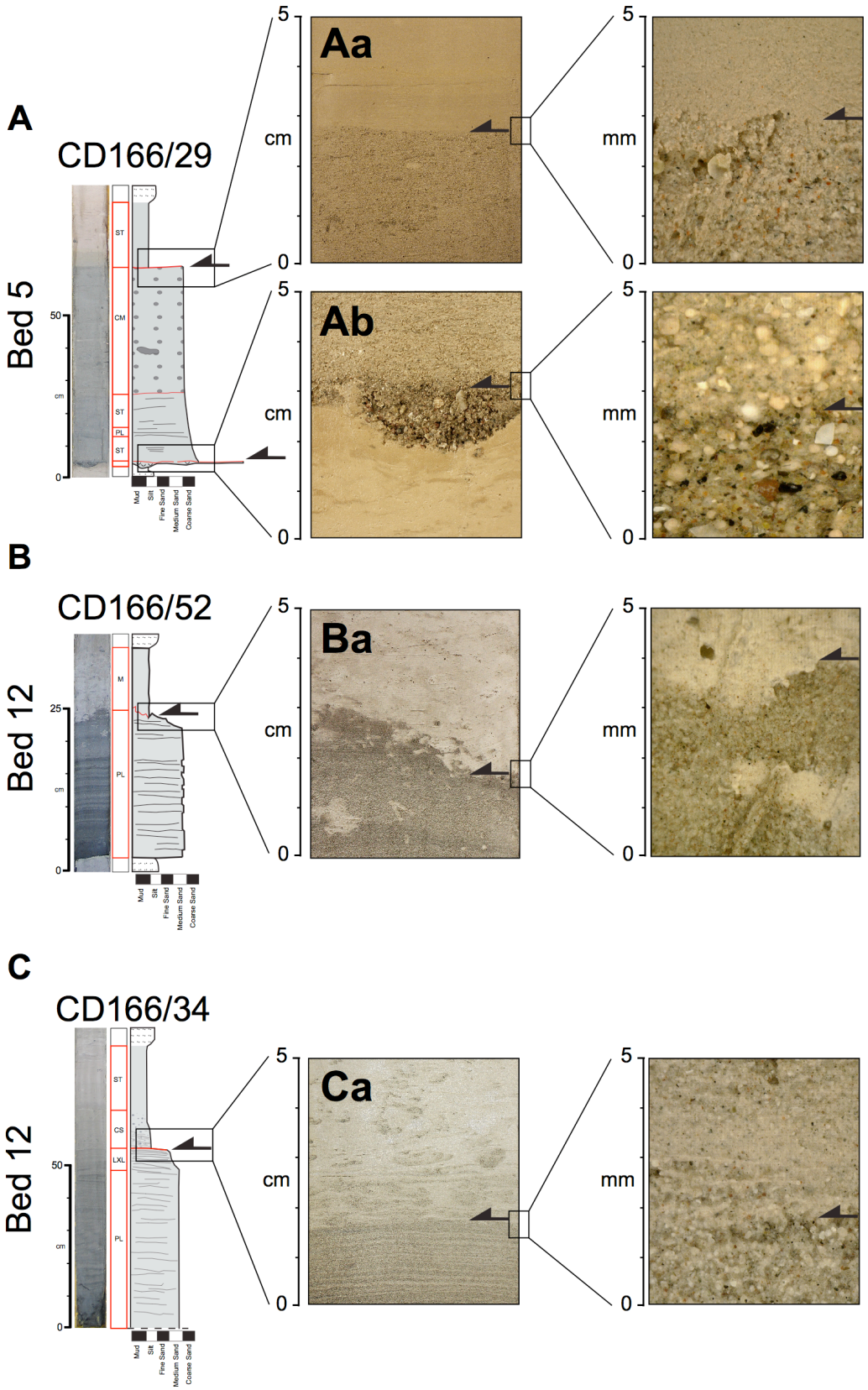
A
CD166/29
Bed 5
Aa
Ab
B
CD166/52
Bed 12
Ba
C
CD166/34
Bed 12
Ca
cm
mm
5
0
50
25
ST
CM
PL
M
CS
LXL
Mud
Silt
Fine Sand
Medium Sand
Coarse Sand

Figure 6-3: Examples of different types of grain-size break found within the Moroccan Turbidite System. Deposits of individual beds at specific core sites are shown, comprising a visual log, facies interpretation, and core photograph. Different types of grain-size break are highlighted within each deposit. (A) Mud-rich structureless sand overlain by ungraded structureless turbidite mud. (B) Coarse-grained gravel/sand overlain by finer grained structureless sand. Note the large grains overlying the grain-size break are foraminifera and have significantly lower settling velocities than the similar-sized underlying lithic fragments. (C) Clean structureless sand overlain by ungraded structureless turbidite mud. Note the ragged contact with clasts of mud and sand immediately underlying and overlying the grain-size break. (D) Clean laminated sand overlain by inter-laminated silt and mud, which is slightly contorted.

Bed	Position in deposit*	Number observed	Grading below break	Grading above break	Grain-size below break (D90)	Grain-size above break (D90)	Facies below break	Facies above break
Type I – Gravel overlain by finer sand								
5	Lower Proximal	11	Normal, Ungraded	Ungraded Normal Inverse	650 – >1000	300 – 650	ST (Gravel)	ST
12	Lower Proximal	1†	Ungraded	Inverse	400	200	ST	ST
Type II – Inversely graded sand overlain by finer sand								
5	Lower Proximal	2	Inverse	Normal	> 1000	600	ST	PL
12	Lower Proximal	1†	Inverse	Normal	700	300	ST	PL
Type III – Sand overlain by finer sand								
11	Lower Middle	5	Normal	Normal	90 – 100	60 – 70	PL	CL
Type IV – sand overlain by mud								
3	Upper Proximal Central	13	Normal	Ungraded Normal	100 – 200	10 – 30	ST	M

	Distal							
5	Upper Proximal Central Distal	34	Normal	Ungraded Normal	90 – 210	10 – 30	ST PL	M CM L
7	Upper Proximal Central Distal	22	Normal	Ungraded Normal	90 – 100	10 – 25	RXL	M CM L
11	Upper Proximal Central Distal	18	Normal	Ungraded Normal	90 – 180	10 – 30	PL CL	M CM L
12	Upper Proximal Central Distal	34	Normal	Ungraded Normal	70 – 90	7 – 20	PL CL ST	M CM L
Type V – Mud-rich sand overlain by mud								
5	Upper Distal	5	Ungraded Normal	Ungraded	100 – 210	20 – 30	ST_D	M CM

Table 6-1: Summarizing the five different types of grain-size break found within the Moroccan Turbidite System, in Beds 3, 5, 7, 11 and 12.
* Lower, middle and upper refer to the vertical position within the deposits. Proximal, central and distal refer to the distance deposits are located from source.
† A number of cores do not fully penetrate the proximal deposit

6.4.6 Grain-size distributions and grain-size breaks within individual beds

Vertical grain-size profiles and spatial distributions of all types of grain-size break are presented, in detail, for Beds 3, 5, 7, 11 and 12. In addition, total grain-size distributions are shown for each bed, which are the sum of all grain-size distributions measured within each bed (Figure 6-4). Total grain-size distributions are considered representative of the overall grain-size distribution of individual beds because: 1) grain-size measurements were analyzed as evenly distributed as possible, throughout the beds and throughout the system; 2) a substantial number of grain-size samples were analyzed (~ 1500).

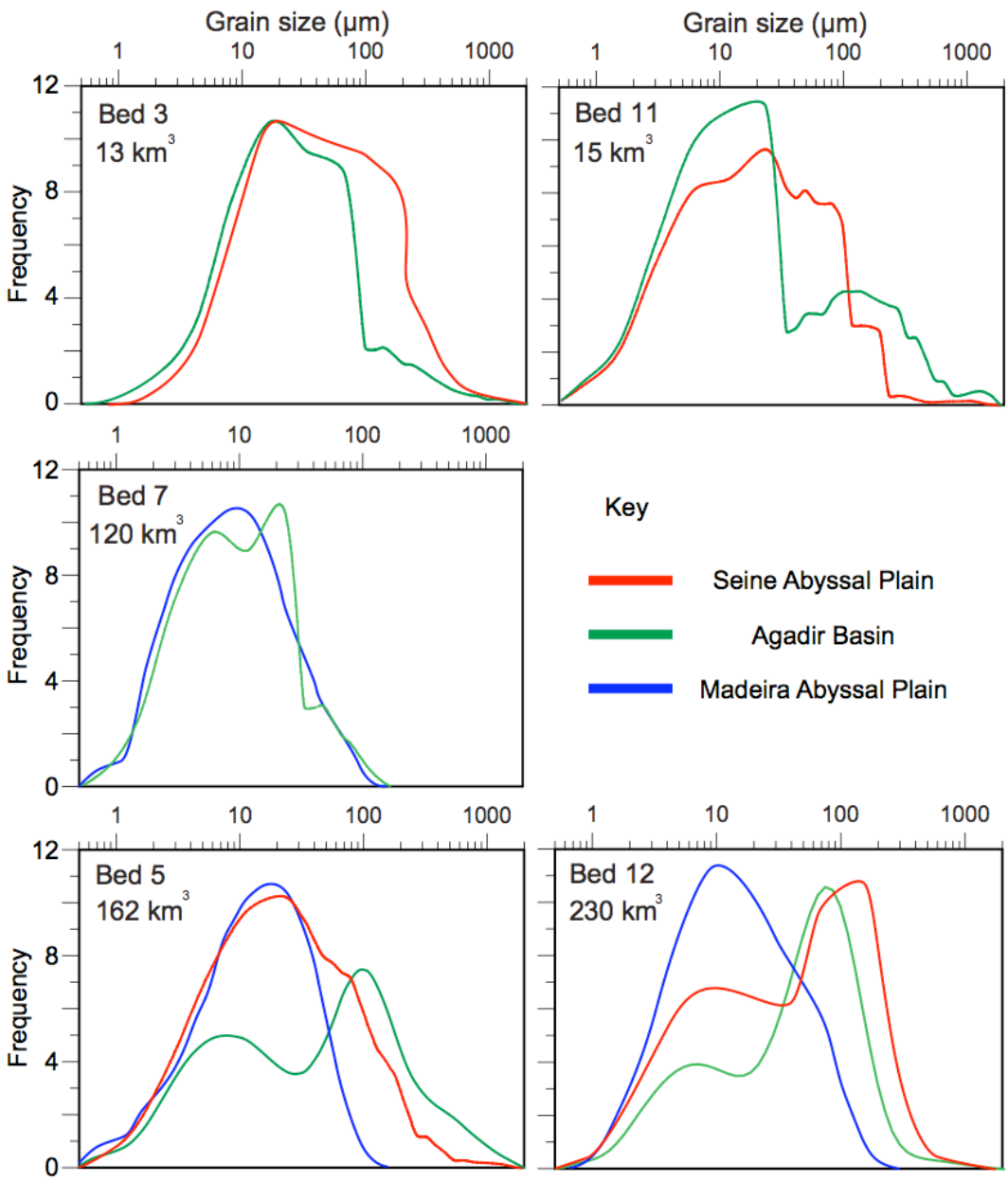

Figure 6-4: Total grain-size distributions for Beds 3, 5, 7, 11 and 12, in order of volume from top left to bottom right. Total grain-size distributions were calculated from all measured grain-size distributions sampled within each bed. This equates to ~ 1500 measured grain-size distributions within the large-volume beds and ~ 200 for the small-volume beds. Total grain-size distributions are shown for each basin within the Moroccan Turbidite System.

6.4.6.1 Bed 3

Bed 3 is a relatively small-volume turbidite (~ 13 km^3), which thins and fines rapidly from northeast to southwest along the Agadir Basin, yet extends throughout the Seine Abyssal Plain. Sand deposits are typically thin (< 12 cm) and are restricted to proximal areas of the system, particularly around the mouths of the Agadir and El Jadida Canyons (Frenz et al., 2008). Sand intervals are all normally graded across the Agadir Basin and Seine Abyssal Plain (Figure 6-5A).

Type IV grain-size breaks from sand to ungraded mud, primarily occur around the mouth of the Agadir Canyon and across the Safi Plateau (Figure 6-5B). Within some areas Type IV grain-size breaks are overlain by muds with normally graded bases. Normally graded transitions between sand and mud occur close to the margins of the Agadir Basin and Seine Abyssal Plain.

Total grain-size distributions calculated from deposits situated in the Agadir Basin and Seine Abyssal Plain are relatively similar (Figure 6-4). Bed 3 has a broadly unimodal grain-size distribution from ~ 20 μm to ~ 100 μm. The grain-size distribution within the Seine Abyssal Plain is slightly coarser, from ~ 20 μm to ~ 200 μm.

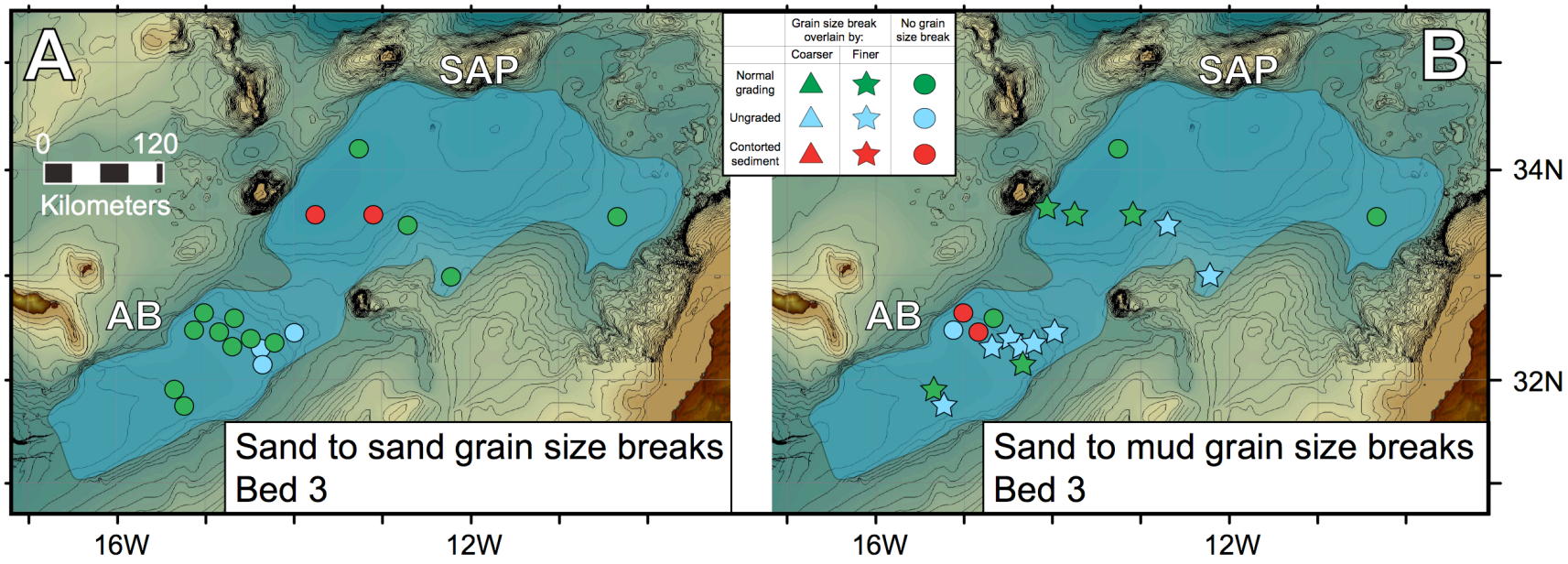

Figure 6-5: Maps showing the depositional extent of Bed 3 (light blue shading). Within this area deposits comprising sand overlain by fine-grained silt/mud are marked with coloured symbols. Symbols denote whether deposits are normally graded (circles) or have a grain-size break that is overlain by coarser sediment (triangles) or finer sediment (stars). Where deposits do not have a grain-size break, the colour of the circle indicates whether the bed is normally graded (green), ungraded (blue) or has contorted facies (red). Where deposits do have grain-size breaks, the colour of the symbol indicates the grading of the sediment immediately overlying the grain-size break: graded (green), ungraded (blue) and contorted (red). (A) shows sand to sand grain-size breaks, and (B) shows sand to mud grain-size breaks. MAP = Madeira Abyssal Plain, MCS = Madeira Channel System, AB = Agadir Basin and SAP = Seine Abyssal Plain.

6.4.6.2 Bed 5

This large-volume turbidite (> 160 km^3) is recorded in all three basins. Relatively thick (~ 40 – 120 cm), coarse-grained (up to ~ 1000 μm), structureless and parallel laminated, clean sands occur throughout the Seine Abyssal Plain and across most of the Agadir Basin (Talling et al., 2007c; Frenz et al., 2008; Wynn et al., 2010). Type I and II grain-size breaks are frequent in proximal localities (Figure 6-6A) occurring between coarse-grained gravel and inversely graded sands at the base of deposits (~ 900 – 1000 μm), overlain by finer ungraded clean sand (~ 100 – 200 μm; Figure 6-7 Core CD166/57). However, occasional thin deposits of gravel are found more distally, overlain by Type I grain-size breaks. Sand deposits found across the Madeira Channel System comprise thinner (~ 10 – 20 cm), finer (up to ~ 250 μm) parallel and ripple cross-laminated sands. Type III grain-size breaks are occasionally found in this area, occurring between normally graded ripple cross-laminated sands (~ 80 μm) overlain by finer grained parallel laminated sand (~ 60 μm; Stevenson et al., 2012). Across the Safi Plateau (south of the Seine Abyssal Plain) Type III grain-size breaks are found between very thin (~ 5 cm thick) structureless sands overlain by parallel laminated sands (Figure 6-6A).

Type IV grain-size breaks are found throughout the deposit (Figure 6-6B), occurring between inverse, normal and ungraded clean sands (~ 60 – 80 μm) overlain by ungraded, graded and contorted muds (~ 15 – 25 μm; Figure 6-7 Core D11938). Across the Agadir Basin overlying muds are relatively thin (10 – 20 cm). In contrast, turbidite muds found across the Seine Abyssal Plain are generally thicker (~ 10 – 250 cm). A single normally graded deposit (from sand to mud) is found in the central part of the basin (Figure 6-6B), which has thick (~ 250 cm) ponded mud cap with contorted laminations and silty clasts (see Chapter 3 for more detail). Contorted muds overlying Type IV grain-size breaks dominate across the other parts of the Seine Abyssal Plain (Figure 6-7 Core D11938). Mud-rich sand deposits found proximal to the mouths of the Agadir and El Jadida Canyons have normal grading between mud-rich sand and overlying turbidite mud (Figure 6-7 Cores CD166/57 and JC27/19). In contrast, every mud-rich sand deposit situated in the relatively distal, southeast part of the Agadir Basin is overlain by a Type V grain-size break, in turn overlain by ungraded mud (Figure 6-6B; Figure 6-7 Core CD166/12).

Deposits within the Madeira Abyssal Plain are mostly fine-grained with silt-rich normally graded bases overlain by ungraded turbidite mud (Figure 6-7 Core D11813) (McCave and Jones, 1988; Jones et al., 1992). Deposits are ponded into the central parts of the basin with thickness increasing from 30 cm to 100 cm (Figure 6-2). No sand or mud breaks are found in this part of the Moroccan Turbidite System (Figure 6-6A and Figure 6-6B).

Total grain-size distributions for Bed 5 within each of the three basins show significant variation (Figure 6-4). The Agadir Basin is bimodal with modes at ~ 10 μm and 100 μm and a deficiency of silt-sized sediment between ~ 30 – 40 μm. The Madeira Abyssal Plain is significantly finer grained compared to the Agadir Basin, and has a unimodal grain-size distribution comprising high frequencies between ~ 15 and 35 μm. The Seine Abyssal Plain has a broadly unimodal grain-size distribution that is negatively skewed to modal values of ~ 20 μm, albeit with significant abundances of grain sizes from ~ 100 – 200 μm.

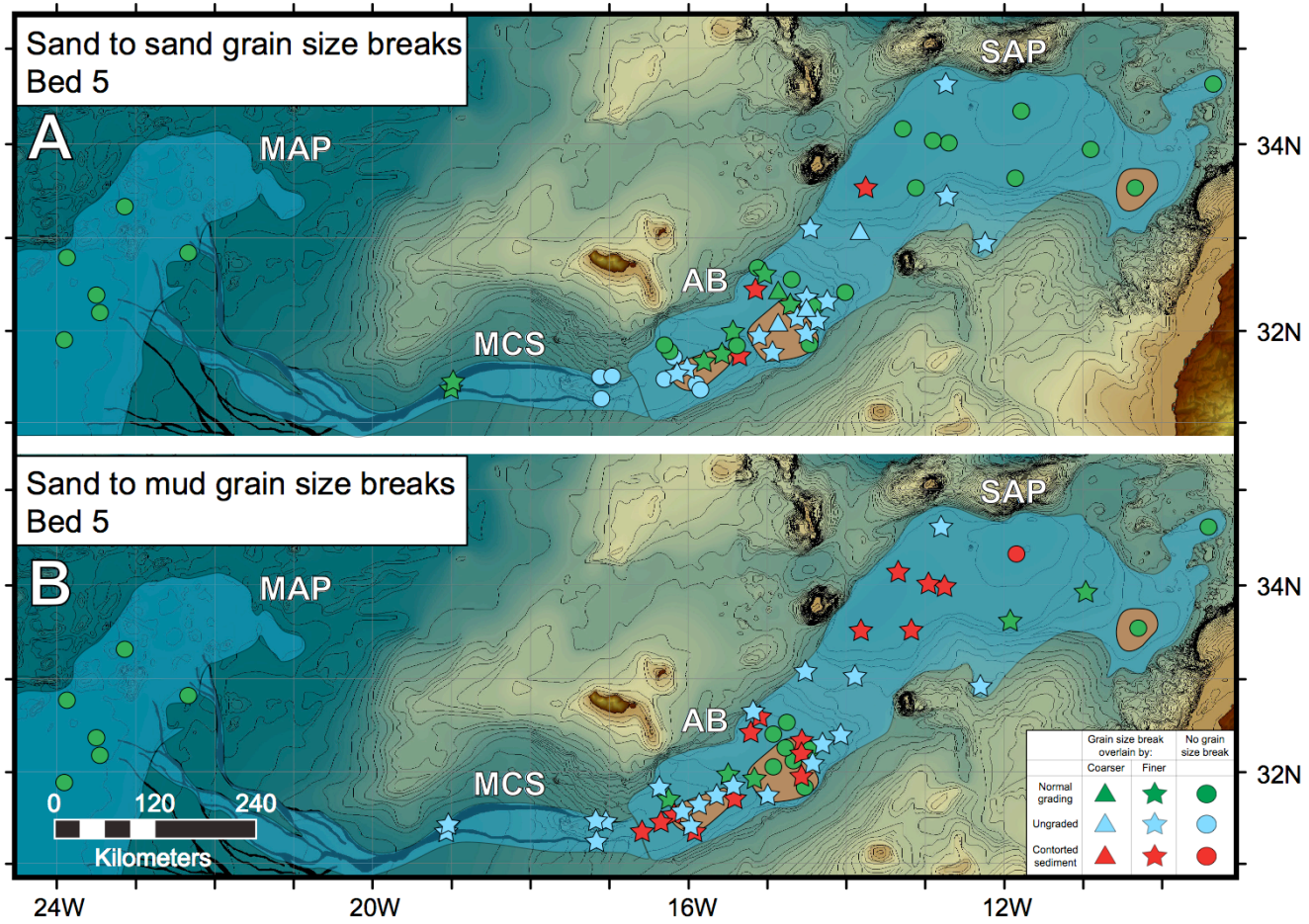
Sand to sand grain size breaks
Bed 5
A
MAP
SAP
AB
MCS
Sand to mud grain size breaks
Bed 5
B
MAP
SAP
AB
MCS
0
120
240
Kilometers
Grain size break overlain by:
Coarser
Finer
No grain size break
Normal grading
Ungraded
Contorted sediment
34N
32N
34N
32N
24W
20W
16W
12W

Figure 6-6: Maps showing the depositional extent of Bed 5 (light blue shading). Within this area deposits comprising sand overlain by fine-grained silt/mud are marked with coloured symbols. Note that mud-rich sand deposits overlain by silt/mud are highlighted with brown shading. Symbols denote whether deposits are normally graded (circles) or have a grain-size break that is overlain by coarser sediment (triangles) or finer sediment (stars). Where deposits do not have a grain-size break, the colour of the circle indicates whether the bed is normally graded (green), ungraded (blue) or has contorted facies (red). Where deposits do have grain-size breaks, the colour of the symbol indicates the grading of the sediment immediately overlying the grain-size break: graded (green), ungraded (blue) and contorted (red). (A) Shows sand to sand grain-size breaks, and (B) shows sand to mud grain-size breaks. MAP = Madeira Abyssal Plain, MCS = Madeira Channel System, AB = Agadir Basin and SAP = Seine Abyssal Plain.

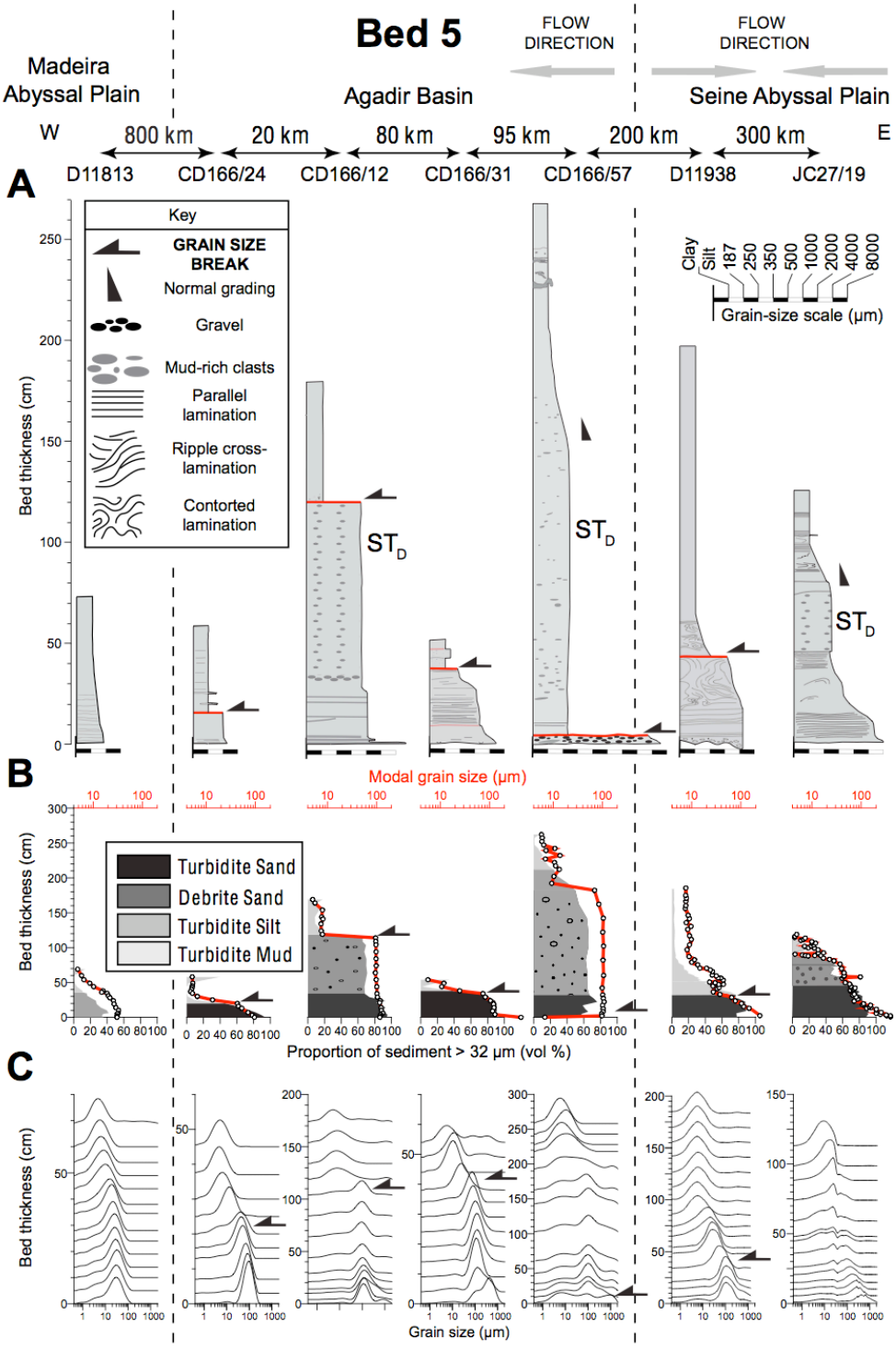

Figure 6-7: Examples of deposits found within Bed 5. (A) Visual logs illustrating the sequence of facies and grain-size trends vertically in each deposit. Grain-size breaks and normally graded transitions are marked. ST_D denotes mud-rich structureless sand, deposited 'en masse' as a linked-debrite within otherwise clean turbidite sands. Quantitative analysis of grain size is below the visual logs. (B) Shows the mode (red line) and proportion of sediment > 32 µm as a shaded area. (C) Shows the measured grain-size distributions.

6.4.6.3 Bed 7

This large-volume turbidite (~ 120 km^3) comprises relatively thin (~ 5 – 15 cm), fine-grained sands with modal values of between ~ 65 and 100 μm, which extend across the Agadir Basin, Madeira Channel System and Madeira Abyssal Plain (Figure 6-2)(Wynn et al., 2002b; Frenz et al., 2008; Stevenson et al., 2012). Almost all sand deposits are normally graded with no grain-size breaks (Figure 6-8A).

In contrast, Type IV grain-size breaks are common throughout Bed 7 (Figure 6-8B). Within the Agadir Basin they occur between normally graded, ripple cross-laminated sand with modal grain sizes of ~ 60 – 80 μm, overlain by relatively thick (~ 25 – 60 cm), graded, ungraded and contorted muds with modal values between ~ 10 and 20 μm. Within the southwest parts of the Agadir Basin contorted muds are the most common facies overlying type IV grain-size breaks (Figure 6-8B). Across the Madeira Abyssal Plain deposits are generally fine-grained (~ 60 – 80 μm) and thicken progressively into the central parts of the basin (Figure 6-2). No grain-size breaks are observed in this part of the Moroccan Turbidite System.

Total grain-size distributions for Bed 7 within the Agadir and Madeira Abyssal Plain are similar (Figure 6-4). The Madeira Abyssal Plain has a unimodal distribution with a modal value of ~ 10 μm. The Agadir Basin has a slightly bimodal distribution with modes of ~ 6 and 20 μm. Overall, Bed 7 is the finest-grained turbidite examined in this study.

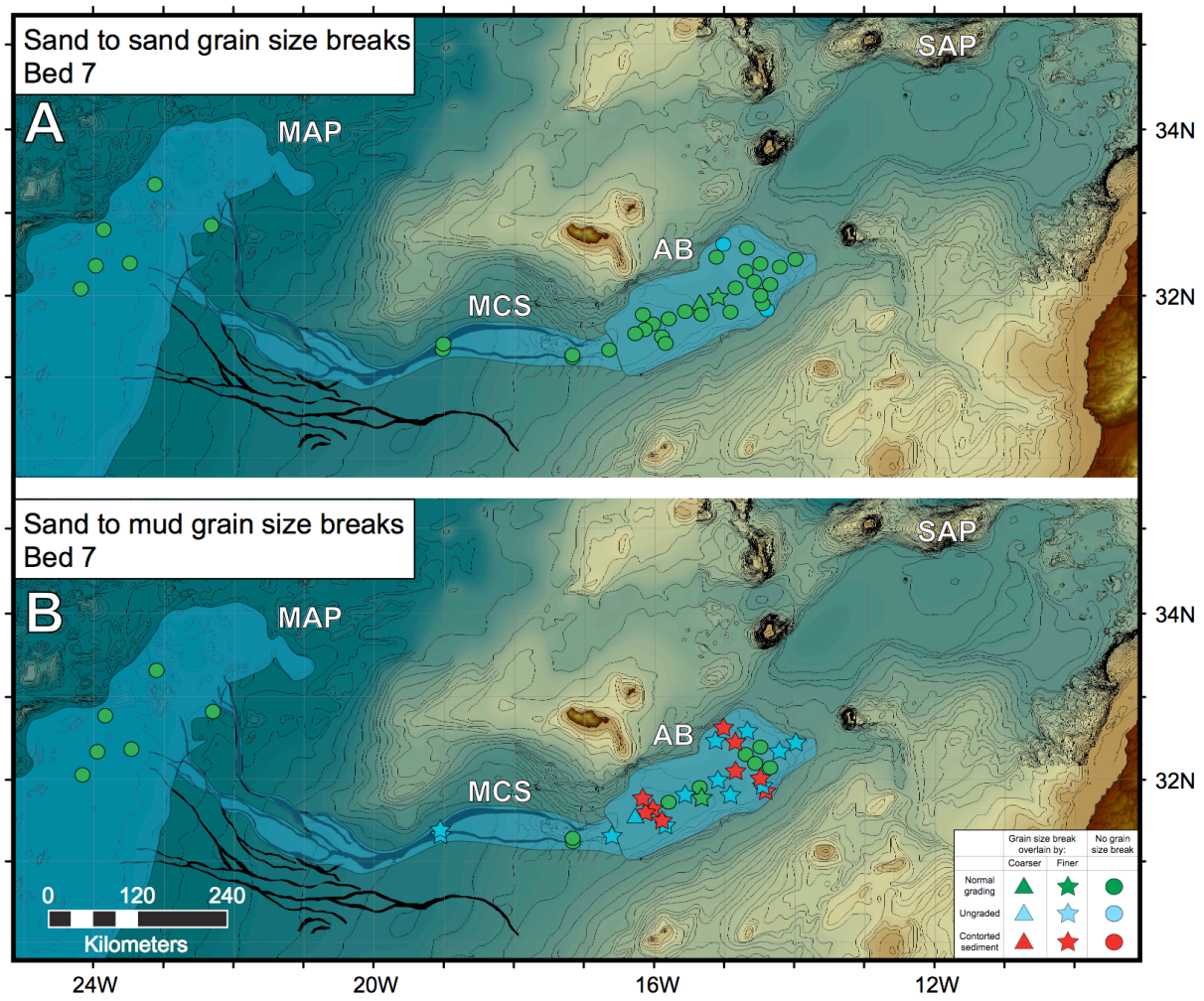
Sand to sand grain size breaks
Bed 7
A
MAP
SAP
AB
MCS
Sand to mud grain size breaks
Bed 7
B
MAP
SAP
AB
MCS
0
120
240
Kilometers
Grain size break overlain by:
Coarser
Finer
No grain size break
Normal grading
Ungraded
Contorted sediment
34N
32N
34N
32N
24W
20W
16W
12W

Figure 6-8: Maps showing the depositional extent of Bed 7 (light blue shading). Within this area deposits comprising sand overlain by fine-grained silt/mud are marked with coloured symbols. Symbols denote whether deposits are normally graded (circles) or have a grain-size break that is overlain by coarser sediment (triangles) or finer sediment (stars). Where deposits do not have a grain-size break, the colour of the circle indicates whether the bed is normally graded (green), ungraded (blue) or has contorted facies (red). Where deposits do have grain-size breaks, the colour of the symbol indicates the grading of the sediment immediately overlying the grain-size break: graded (green), ungraded (blue) and contorted (red). (A) Shows sand to sand grain-size breaks, and (B) shows sand to mud grain-size breaks. MAP = Madeira Abyssal Plain, MCS = Madeira Channel System, AB = Agadir Basin and SAP = Seine Abyssal Plain.

6.4.6.4 Bed 11

This relatively small-volume turbidite (~ 15 km^3) initially comprises a thick, structureless, parallel laminated, normally graded clean sand deposit (~ 80 cm thick) within the northeast Agadir Basin (Frenz et al., 2008). The bed rapidly thins to the southwest progressing into deposits composed of thin (~ 10 cm) clean sands, which ultimately pinch out leaving normally graded silt and mud deposits across most of the basin. Type III grain-size breaks are frequent within the upper parts of sand deposits but restricted to proximal localities (Figure 6-9A). They occur between parallel laminated sands with modal values between ~ 100 – 150 μm, overlain by structureless finer sand with modal values ~ 60 μm (Figure 6-10 Core CD166/51).

Type IV grain-size breaks occur almost throughout Bed 11, where there is a grain-size transition from sand into mud (Figure 6-9B). The majority of Type IV grain-size breaks found within Bed 11 are overlain by ungraded, structureless turbidite mud ~ 10 to 20 cm thick. However, in some deposits graded or contorted muds can overlie the grain-size break (Figure 6-10 Core D13073). Two deposits within the Seine Abyssal Plain have exceptionally thin sands (2 – 9 cm) that normally grade into silts and muds.

Total grain-size distributions for Bed 11 within the Agadir Basin and Seine Abyssal Plain are different (Figure 6-4). The Agadir Basin shows a bimodal distribution with modes of ~ 20

μm and 200 μm, and a deficiency in grain sizes between ~ 30 to 40 μm. The Seine Abyssal Plain has a broadly unimodal grain-size distribution, which has high frequencies from ~ 10 μm to 100 μm and a modal peak at ~ 25 μm.

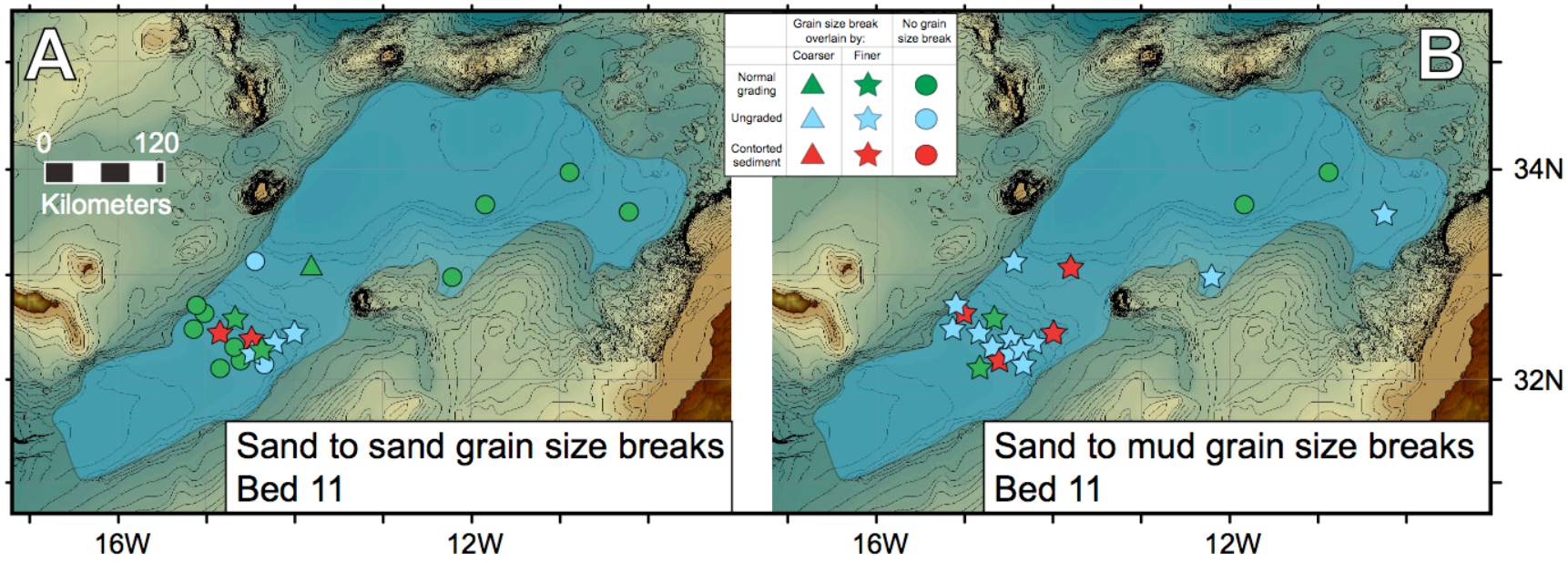

Figure 6-9: Maps showing the depositional extent of Bed 11 (light blue shading). Within this area deposits comprising sand overlain by fine-grained silt/mud are marked with coloured symbols. Symbols denote whether deposits are normally graded (circles) or have a grain-size break that is overlain by coarser sediment (triangles) or finer sediment (stars). Where deposits do not have a grain-size break, the colour of the circle indicates whether the bed is normally graded (green), ungraded (blue) or has contorted facies (red). Where deposits do have grain-size breaks, the colour of the symbol indicates the grading of the sediment immediately overlying the grain-size break: graded (green), ungraded (blue) and contorted (red). (A) Shows sand to sand grain-size breaks, and (B) shows sand to mud grain-size breaks. MAP = Madeira Abyssal Plain, MCS = Madeira Channel System, AB = Agadir Basin and SAP = Seine Abyssal Plain.

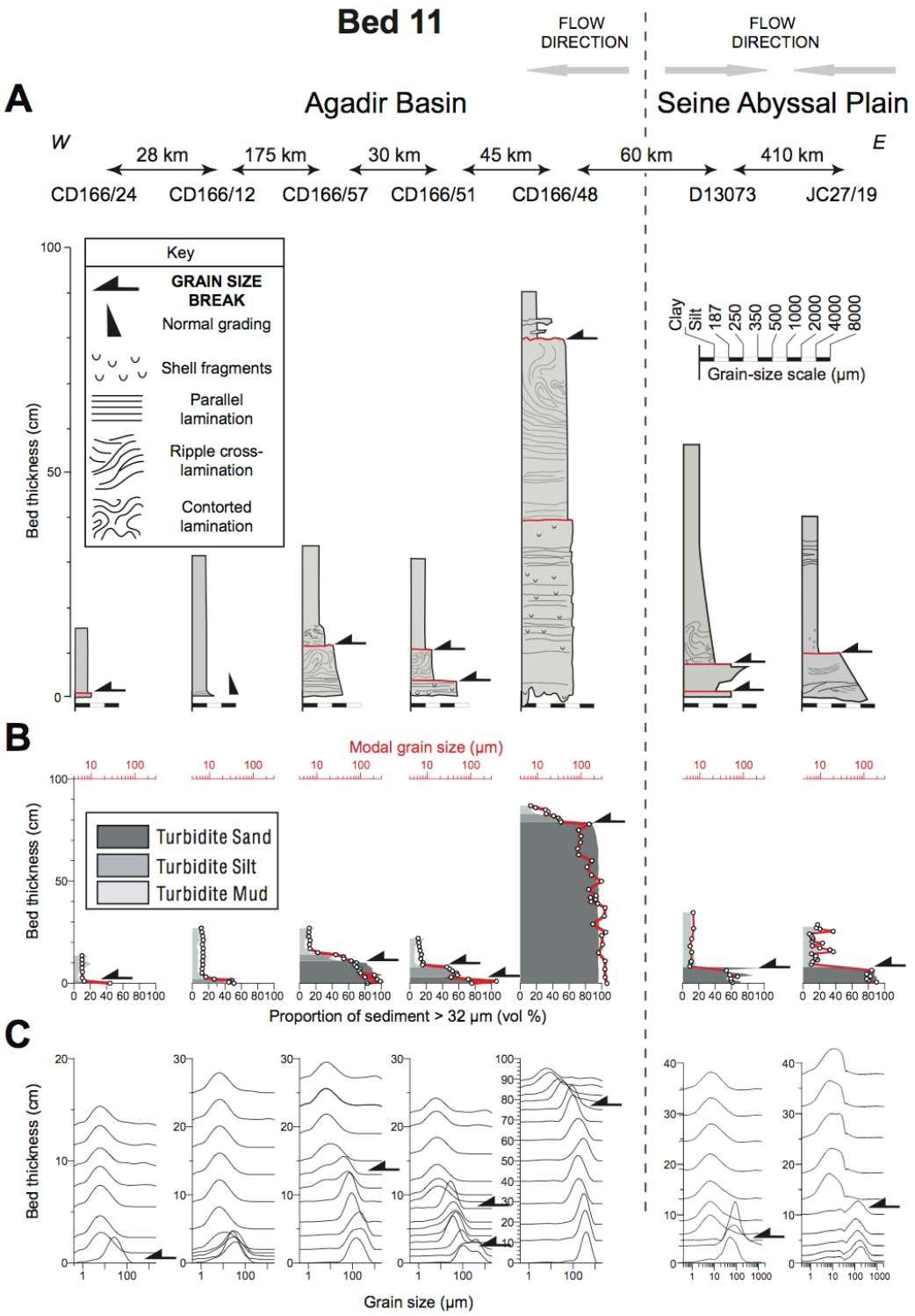

Figure 6-10: Examples of deposits found within Bed 11. (A) Visual logs illustrating the sequence of facies and grain-size trends vertically in each deposit. Grain-size breaks and normally graded transitions are marked. Quantitative analysis of grain-size is shown below the visual logs. (B) Shows the mode (red line) and proportion of sediment > 32 µm as a shaded area. (C) Shows the measured grain-size distributions.

6.4.6.5 Bed 12

This large-volume bed (> 180 km^3) is one of the biggest turbidites emplaced across the Moroccan Turbidite System over the past 200 ka (Wynn et al., 2002b; Frenz et al., 2008). It comprises relatively tabular, 60 – 120 cm thick, structureless, planar and ripple cross-laminated sheet sands that extend across the Seine Abyssal Plain, Agadir Basin, across the Madeira Channel System, and into the Madeira Abyssal Plain (Wynn et al., 2002b; Frenz et al., 2008; Stevenson et al., 2012). Type II grain-size breaks are occasionally found close to the mouth of the Agadir Canyon (Figure 6-11A) and occur between inversely graded sands with modal values of ~ 400 μm, overlain by ungraded finer sand with modal values of ~ 150 μm (Figure 6-12 Core CD166/51).

Type IV grain-size breaks are found almost throughout Bed 12 (Figure 6-11B). Across the Agadir Basin Type IV grain-size breaks occur between sand (~ 70 μm) overlain by a relatively thin (~ 10 to 15 cm), ungraded structureless mud (~ 10 – 15 μm; Figure 6-12 Core CD166/24). Within the Seine Abyssal Plain, Type IV grain-size breaks are overlain by thicker muds with graded and contorted bases (Figure 6-12 Core D13073). Deposits within the Madeira Abyssal Plain are normally graded, very fine-grained sands, silts and muds (Figure 6-12 Core D11813). Bed 12 develops from thin-bedded (5 – 10 cm) sands at the terminus of the Madeira Channel System in the northeast, to thick deposits (~ 200 – 500 cm) of ponded mud with silt-rich, normally graded bases within the central parts of the basin (Figure 6-2) (Jones et al., 1992; Rothwell et al., 1992; Weaver et al., 1992). Only four core sites, proximal to the mouth of the Madeira Channel System, record Type IV grain-size breaks, which are overlain by ungraded, graded or contorted mud (Figure 6-11B).

Total grain-size distributions for Bed 12 within the Seine Abyssal Plain, Agadir Basin and Madeira Abyssal Plain are different (Figure 6-4). Grain-size distributions within the Agadir Basin are bimodal with a weak mode of ~ 10 μm and a strong mode of ~ 90 μm, and a deficiency of grain sizes between ~20 to 30 μm. The Seine Abyssal Plain shows similar bimodal grain-size distributions with modal values of ~ 10 and 150 μm. The Madeira

Abyssal Plain has a negatively skewed unimodal grain-size distribution with a modal value of ~ 10 μm but with relatively high frequencies of grain sizes from ~ 6 to 40 μm.

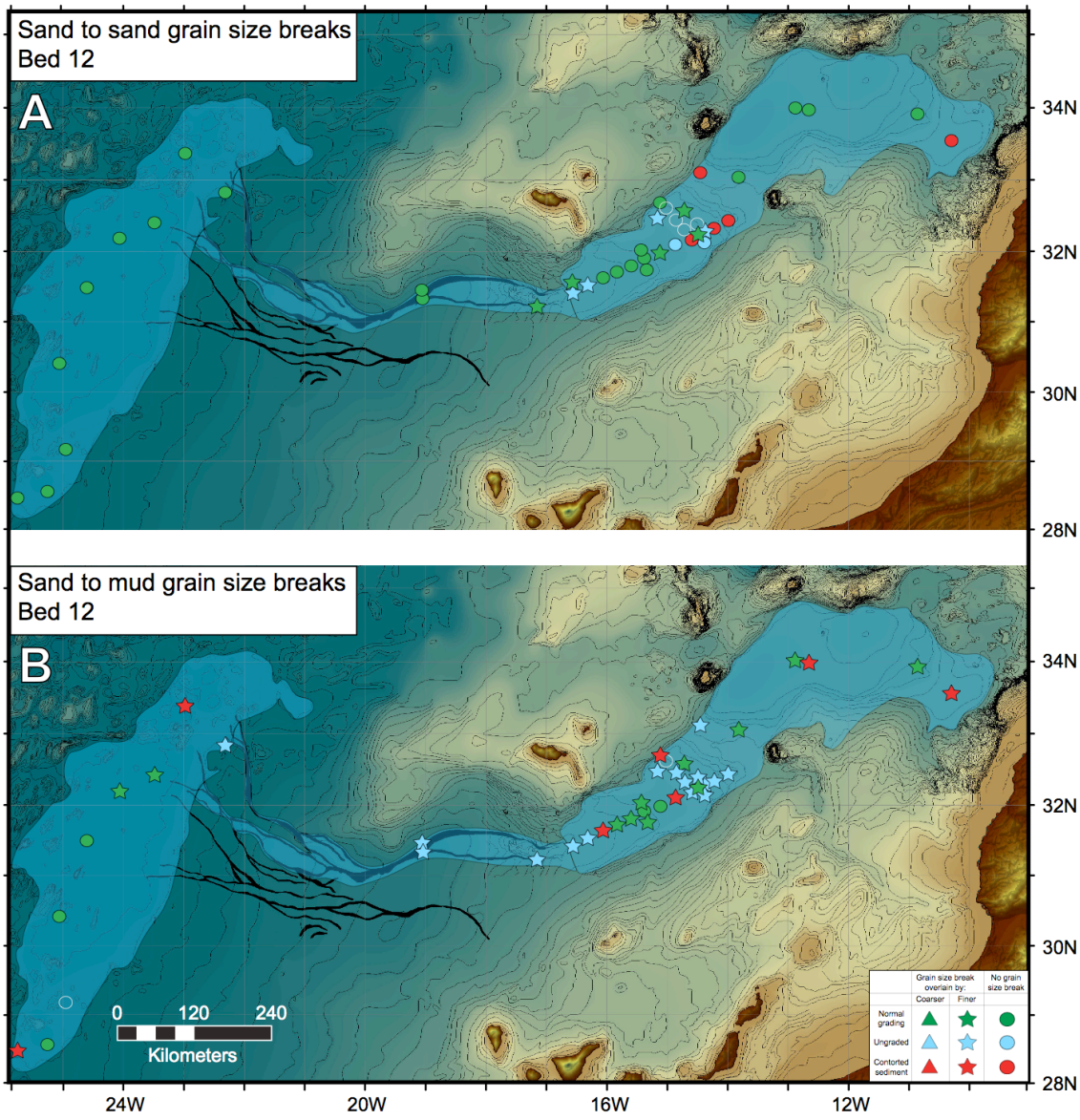

Figure 6-11: Maps showing the depositional extent of Bed 12 (light blue shading). Within this area deposits comprising sand overlain by fine-grained silt/mud are marked with coloured symbols. Symbols denote whether deposits are normally graded (circles) or have a grain-size break that is overlain by coarser sediment (triangles) or finer sediment (stars). Where deposits do not have a grain-size break, the colour of the circle indicates whether the bed is normally graded (green), ungraded (blue) or has contorted facies (red). Where deposits do have grain-size breaks, the colour of the symbol indicates the grading of the sediment immediately overlying the grain-size break: graded (green), ungraded (blue) and contorted (red). Hollow symbols represent deposits that are not fully penetrated by the core. (A) Shows sand to sand grain-size breaks, and (B) shows sand to mud grain-size breaks. MAP = Madeira Abyssal Plain, MCS = Madeira Channel System, AB = Agadir Basin and SAP = Seine Abyssal Plain.

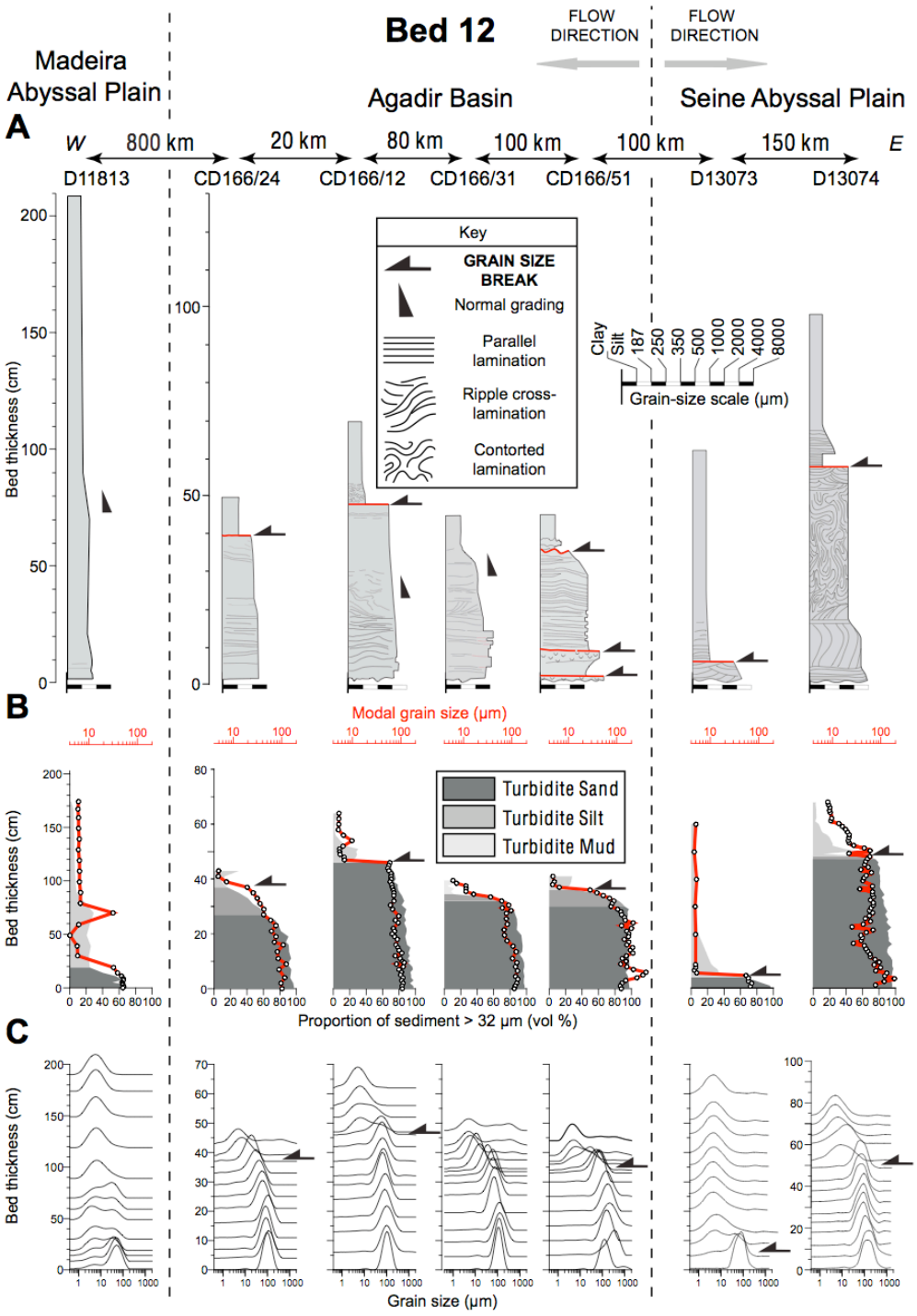

Figure 6-12: Examples of deposits found within Bed 12. (A) Visual logs illustrating the sequence of facies and grain-size trends vertically in each deposit. Grain-size breaks and normally graded transitions are marked. Quantitative analysis of grain size is shown below the visual logs. (B) Shows the mode (red line) and proportion of sediment > 32 µm as a shaded area. (C) Shows the measured grain-size distributions.

6.5 Discussion

In this section the different mechanisms by which grain-size breaks form are discussed and evaluated for the grain-size breaks observed in the Moroccan Turbidite System.

6.5.1 Bimodal grain-size distribution within flows

An ideal turbidite deposit comprises coarse sediment at the base that progressively fines upwards, i.e. from sand, to silt and then mud (Bouma, 1962). Flows that produce these beds must contain the full range of coarse to fine grain sizes. Flows with strongly bimodal grain-size distributions, in which the intermediate grain sizes are entirely absent (or in very low abundance), will produce deposits that have sharp vertical transitions in grain size, i.e. grain-size breaks (Figure 6-13A) (Bouma, 1962; Kneller and McCaffrey, 2003). Grain-size breaks produced in this manner would form across grain sizes that are absent (or in low abundance) from the flow.

Type I and II grain-size breaks are found in Beds 5 and 12 within the Agadir Basin (Figure 6-6A and Figure 6-11A). They occur between coarse sand/gravel (~ 900 – 1000 μm) overlain by finer grained structureless sand (~ 100 – 200 μm). Total grain-size distributions for Beds 5 and 12 within the Agadir Basin show that both beds have smoothly increasing abundances of grain sizes from ~ 1000 to 200 μm. Therefore, grain-size breaks were not formed by a low abundance of grain sizes between ~ 1000 and 200 μm within the parent flow. Type IV grain-size breaks are in every bed, occurring between sand with modal values of ~ 100 – 70 μm, overlain by mud with modal values of ~ 10 – 20 μm. Beds 3, 7 and 11 have unimodal distributions that include significant abundances of grain sizes between ~ 10 – 20 μm (Figure 6-4). Beds 5 and 12 have bimodal distributions with deficiencies of grain sizes between ~ 10 – 20 μm within the Agadir Basin. However, the missing grain sizes are found ~ 1000 km down slope within the Madeira Abyssal Plain (Figure 6-4). Therefore, Type IV grain-size

breaks were not produced from grain sizes between 20 and 70 μm being in low abundance within the parent flows.

6.5.2 Flow reflection

Grain-size breaks can be caused by reflection of turbidity currents at basin margins or at other obstacles (Figure 6-13B) (Pickering and Hiscott, 1985; Kneller et al., 1991; Kneller and McCaffrey, 1999). Laboratory experiments illustrate how reflected solitary waves or wave trains are generated by interactions with topography (Kneller et al., 1991; Edwards et al., 1994; Kneller and McCaffrey, 1999). These experiments show that weak reflected waves can propagate along density interfaces within the incoming flow, whilst stronger reflected waves may undercut the incoming flow.

In general terms the Moroccan Turbidite System is comprised of large basins that are > 100 km across (Wynn et al., 2002b), with shallow seafloor gradients (Weaver et al., 1992; Talling et al., 2007c; Wynn et al., in press) and low gradient basin margins; not a setting where turbidites would be expected to reflect. Indeed, sedimentary structures within Beds 5, 11 and 12 provide no evidence for flow reflection, e.g. there are no intervals of cross lamination indicating reversal of flow direction or patterns of stacked sub units (Figure 6-13B). Flow reflection can produce grain-size breaks overlain by coarser sediment, as the reflected flow component is more energetic than the rear of the incoming flow. Multiple reflections of this type would generate a series of normally graded sub-units, whose thickness and basal grain size decreases upwards (Rothwell et al., 1992; Haughton, 1994; Remacha et al., 2005). This mechanism does not explain how it is possible for a reflected flow to generate a single abrupt grain-size break overlain by much finer sediment. To do this, the reflected flow must be finer grained, with weaker turbulence and less density than the incoming flow (Pickering and Hiscott, 1985). Such a weak reflected flow is likely to form a series of waves along a density interface well above the bed (Figure 6-13B) (Edwards et al., 1994). These internal waves may generate ripples at a high angle to the incoming flow direction (Kneller et al., 1991; Kneller et al., 1997; Kneller and McCaffrey, 1999), but not an abrupt decrease in the size of sediment

being deposited. Deposition of intermediate grain sizes from the original incoming flow must be suddenly suppressed in order to form a grain-size break overlain by much finer sediment. A physical mechanism is not apparent by which the reflected flow 'switches off' deposition from the original incoming flow. For these reasons, the grain-size breaks in Beds 3, 5, 7, 11 and 12 were not formed by flow reflection.

6.5.3 Flow separation due to topographic obstacles

Sinclair and Cowie (2003) proposed that grain-size breaks could form when a turbidity current encounters a topographic barrier that diverts only the lower part of the flow (Figure 6-13C). The upper and finer-grained part of the flow thus follows a different path to the coarser-grained lower part of the flow. The Moroccan Turbidite System lacks suitable topographic barriers for this process to operate, with deposition occurring on low-gradient open slopes or basin plains. This mechanism did not form the grain-size breaks in the Moroccan System turbidites.

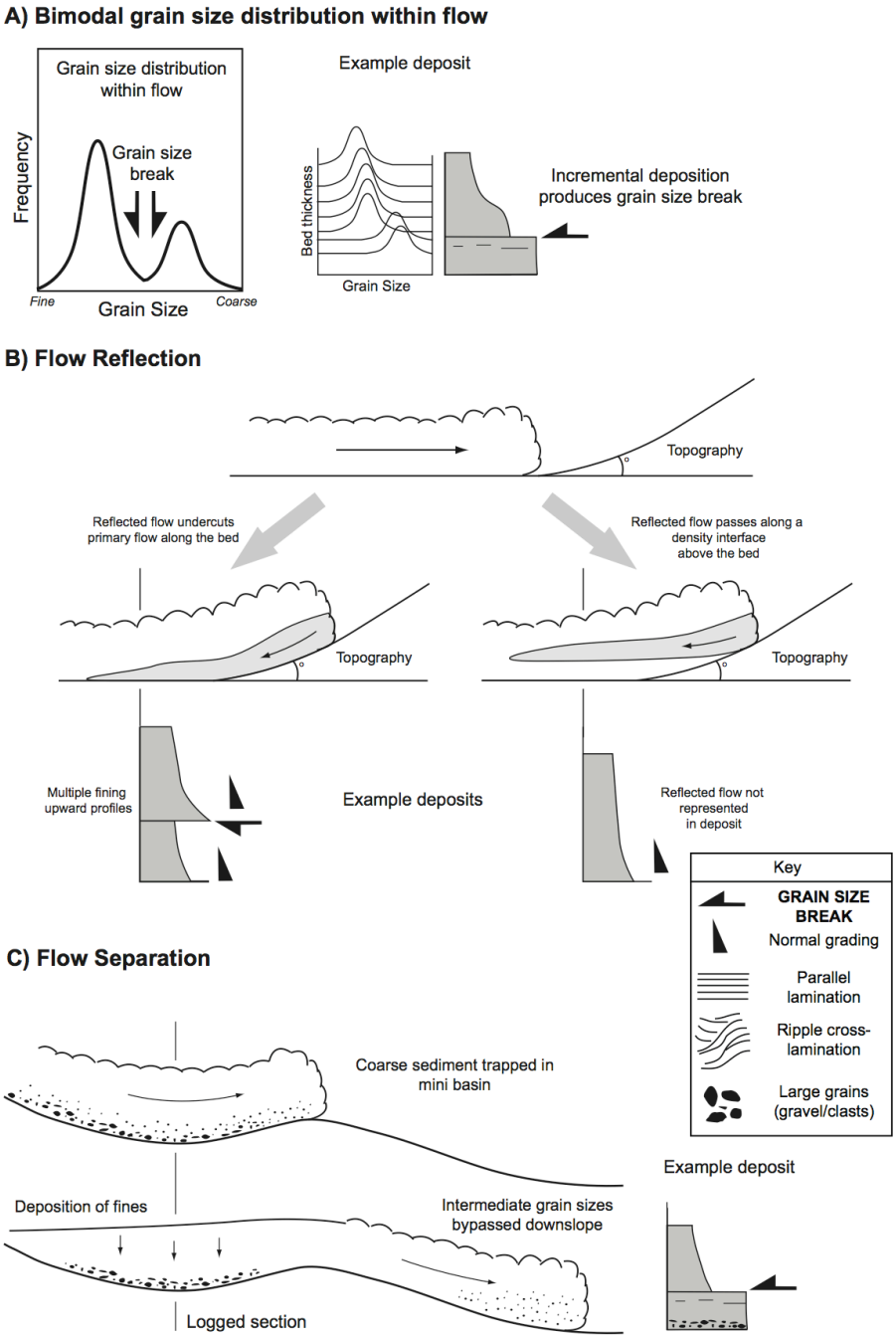

Figure 6-13: Models proposed for the generation of grain-size breaks within turbidites. (A) Bimodal grain-size distribution within the parent flow. Grain sizes in low abundance produce a grain-size break. (B) Flow reflection. Two scenarios are illustrated whereby: a strong reflected flow is more dense than the primary flow and undercuts, depositing sediment along the bed; a weak reflected flow is less dense than the primary flow and is reflected as an internal wave along a density interface within the flow. A weak reflected flow does not produce a grain-size break. (C) Flow separation due to topography. Here sediment transported within the lower parts of the flow is trapped or diverted, whilst the finer grained sediment transported higher in the flow is able to surmount the topography and bypass down slope. The grain-size break is produced because topography is controlling where certain grain sizes are deposited.

6.5.4 Internal grain size and concentration boundary within a flow

Gladstone and Sparks (2002) attributed grain-size breaks in turbidites to deposition from a flow comprising two distinct layers: a body and an overlying wake (Figure 6-14A). In their model, both body and wake are relatively dilute and fully turbulent. They inferred that a sharp discontinuity in grain size occurred within the flow at the boundary between body and wake. The grain-size break within the deposit was attributed to an abrupt change from deposition by the body to deposition from the wake. There are two significant problems with this type of explanation for grain-size breaks.

First, unless the flow 'freezes' abruptly or deposits 'en masse', the vertical structure of the flow will not be preserved as the vertical structure of the deposit. A deposit that builds up incrementally will preserve the longitudinal (front to tail) structure of the flow (Kneller and Branney, 1995). Grain-size breaks within incrementally aggraded deposit result from abrupt longitudinal boundaries within the flow, rather than the flow's vertical structure (Mutti et al., 2002; Kneller and McCaffrey, 2003). Type IV grain-size breaks are immediately underlain by normally graded sands with a range of sedimentary structures including parallel and ripple cross-lamination. These facies were most likely deposited incrementally beneath a waning flow (Best and Bridge, 1992; Kneller and Branney, 1995; Sumner et al., 2008; Baas et al., 2011). Therefore, Type IV grain-size breaks overlying these sands were not produced from a sharp vertical concentration boundary within the parent flows.

Second, Gladstone and Sparks (2002) based their hypothesis that a flow with relatively low sediment concentration may develop a sharp internal boundary on visual observations of saline density currents (Britter and Simpson, 1978; Hallworth et al., 1996). Experimental analyses of dilute particle-laden density flows have not observed such sharp vertical boundaries in grain size and concentration (Kneller and Buckee, 2000; Felix, 2002; Kneller and McCaffrey, 2003; Choux et al., 2005; Felix et al., 2005). In these experiments turbulent mixing tends to produce gradational changes in grain size and concentration vertically within flows, albeit that more rapid changes can occur near to the bed. However, sharp vertical

changes in grain size and sediment concentration have been observed in laboratory experiments involving relatively high sediment concentration flow phases (Marr et al., 2001; Mohrig and Marr, 2003; Ilstad et al., 2004; Felix et al., 2005). In these experiments, a sharp density interface develops between an overlying dilute, finer grained turbulent suspension and a high-concentration basal flow in which turbulence is suppressed. High-concentration flows (including debris flows) can deposit 'en masse' rather than incrementally. Thus, deposits that were produced by high-concentration parts of a flow could have grain-size breaks generated via sharp vertical concentration boundaries (Figure 6-14A).

Type I grain-size breaks are found wherever poorly sorted, gravel-sized sediment is deposited (e.g. Figure 6-7 and Figure 6-12; Beds 5 and 12 respectively). Such coarse-grained sediment is likely to be transported as a very high-concentration traction carpet at the base of the flow, whereby the grains are supported by inter-grain interactions rather than fluid turbulence (Lowe, 1982). Deposition from this traction carpet will occur 'en masse' via frictional freezing to the bed (Lowe, 1982), which will preserve the vertical structure of the flow. Therefore, Type I grain-size breaks occurring between gravel overlain by finer grained structureless sand are likely produced from a sharp concentration boundary near to the bed; separating a very high-concentration traction carpet (*sensu* Lowe, 1982) and an overlying lower concentration suspension.

Mud-rich sands found in Bed 5 are interpreted to be linked-debrites deposited from a high-concentration turbidity current, which transformed into a debris flow, and deposited 'en masse' across the Agadir Basin (Talling et al., 2007c; Wynn et al., 2010). Type V grain-size breaks occurring between mud-rich structureless sand overlain by turbidite mud were most likely generated from a sharp concentration boundary within the parent flow. With time and distance from source, flow stratification will become stronger (McCaffrey et al., 2003; Choux et al., 2005; Felix et al., 2005), which is more likely to produce sharper and more frequent grain-size breaks. This explains why Type V grain-size breaks are rare in relatively proximal linked-debrites yet exclusively overlie relatively distal linked-debrites (Figure 6-7B).

6.5.5 Fluctuations in flow capacity

Kneller and McCaffrey (2003) attributed grain-size breaks to longitudinal velocity and concentration gradients within the parent flow (Figure 6-14B). Proximally, a flow is relatively disorganized (unsteady) with strong variations in velocity, concentration and grain size along its length. Theoretical analysis and experimental results show that capacity (the amount of particles that can be supported in a flow) increases with higher shear velocities and turbulence intensities, and within flows transporting finer grain sizes (Hiscott, 1994; Huppert et al., 1995; Orlins and Gulliver, 2003). Therefore, as the flow passes over a fixed point its capacity will temporally fluctuate relative to its sediment load. This can produce periods of deposition followed by periods of bypass and/or erosion of pre-existing deposits, at which point a grain-size break is produced (Kneller and McCaffrey, 2003). This mechanism is now discussed in terms of temporal and spatial changes in flow capacity.

6.5.5.1 Temporal changes in flow capacity and sediment load

Temporal changes in flow capacity require flows to be unsteady, either waxing or waning. Temporal changes in flow capacity will be manifested within incrementally aggraded deposits as inversely graded sands for waxing flows and normally graded sands for waning flows (Kneller and Branney, 1995). Theoretically, unsteadiness will decrease with distance from source because the flow organizes itself longitudinally, with faster moving parts of the flow overtaking slower moving parts of the flow (Kneller and McCaffrey, 2003). Hence, relatively distal turbidites generally have normally graded vertical profiles, whereas more proximal turbidites can show complex inverse-to-normal vertical grading profiles.

Within this study, Type II grain-size breaks occur between inversely graded sands overlain by coarser sand, and are only found close to the mouth of the Agadir Canyon. Their association with inversely graded sands indicates these grain-size breaks were most likely

generated from waxing flows, which became sufficiently energetic to erode the pre-existing deposit, before recommencing deposition with a coarser grain size (Talling et al., 2007a; Sumner et al., 2012).

The experiments of Sumner et al. (2008) have observed depositional hiatuses within flows temporally decelerated at a constant rate (waning). Initially, aggradation rates were relatively high with deposition of structureless and planar laminated sands. This was followed by a period of non-deposition and sometimes erosion/reworking of the pre-existing deposit. Deposition recommenced under much lower aggradation rates, forming a strongly graded deposit (Sumner et al., 2008). The change in aggradation rate across the hiatus may relate to the amount of hindered settling particles experience during deposition, or a change in settling regime from capacity to competence, i.e. the largest particle size that can be transported by the flow (Kneller and McCaffrey, 2003).

Type III grain-size breaks occur between parallel laminated sands overlain by better-sorted sands with strong normal grading (Figure 6-10 Core CD166/51). Facies overlying and underlying the grain-size break is similar to that observed by Sumner et al. (2008). Therefore, we interpret Type III grain-size breaks as a product of a depositional hiatus beneath a constantly waning flow.

6.5.5.2 Spatial changes in flow capacity and sediment load

Deposition of sediment, entrainment of ambient fluid, erosion, and changes in slope will determine how a flow evolves (spatially), as it travels across the seafloor. Spatial changes in capacity and sediment load within the flow may generate grain-size breaks, even when the flow is temporally steady along its entire length (Kneller and McCaffrey, 2003). In this scenario, the front of the flow must be oversaturated with sediment and depositional, whilst the body of the flow must be undersaturated with sediment and bypassing. This longitudinal

flow organisation is most likely to occur near to source, before the flow has time to equilibrate its velocity (i.e. capacity) with its sediment load (Kneller and Buckee, 2000; Kneller and McCaffrey, 2003; McCaffrey et al., 2003; Choux et al., 2005). Spatial changes in flow capacity and sediment load is a plausible mechanism by which grain-size breaks can form within an incrementally aggrading sand deposit. If gravel deposits found in Beds 5 and 12 were deposited incrementally, it is most likely Type I grain-size breaks were produced via this mechanism.

Type IV grain-size breaks comprising clean sand overlain by a range of turbidite mud facies, occur throughout most of the Moroccan Turbidite System. Normal grading immediately underlying the grain-size breaks indicates the parent flows were waning (Kneller and Branney, 1995). Potentially, these grain-size breaks were produced by spatial and/or temporal fluctuations in flow capacity as outlined above. However, the mechanism does not explain why mud breaks occur so consistently between fine sand with modal grain sizes of ~ 70 – 100 μm, overlain by mud with modal grain sizes of ~ 10 – 20 μm, irrespective of their proximity to source. Rather, it would be expected that higher flow velocities, proximal to source and on steeper areas of seafloor, would produce Type IV grain-size breaks between coarser sands and finer grained muds compared with slower moving parts of the flow, in more distal and/or flatter areas of seafloor. Indeed, the opposite trend is found within Bed 12, where sharp mud breaks occur across flatter areas of the Agadir basin, whilst normally graded deposits occur across the steeper areas (Figure 6-15). For these reasons both spatial and temporal fluctuations in capacity could not generate the mud grain-size breaks observed in the Moroccan Turbidite System.

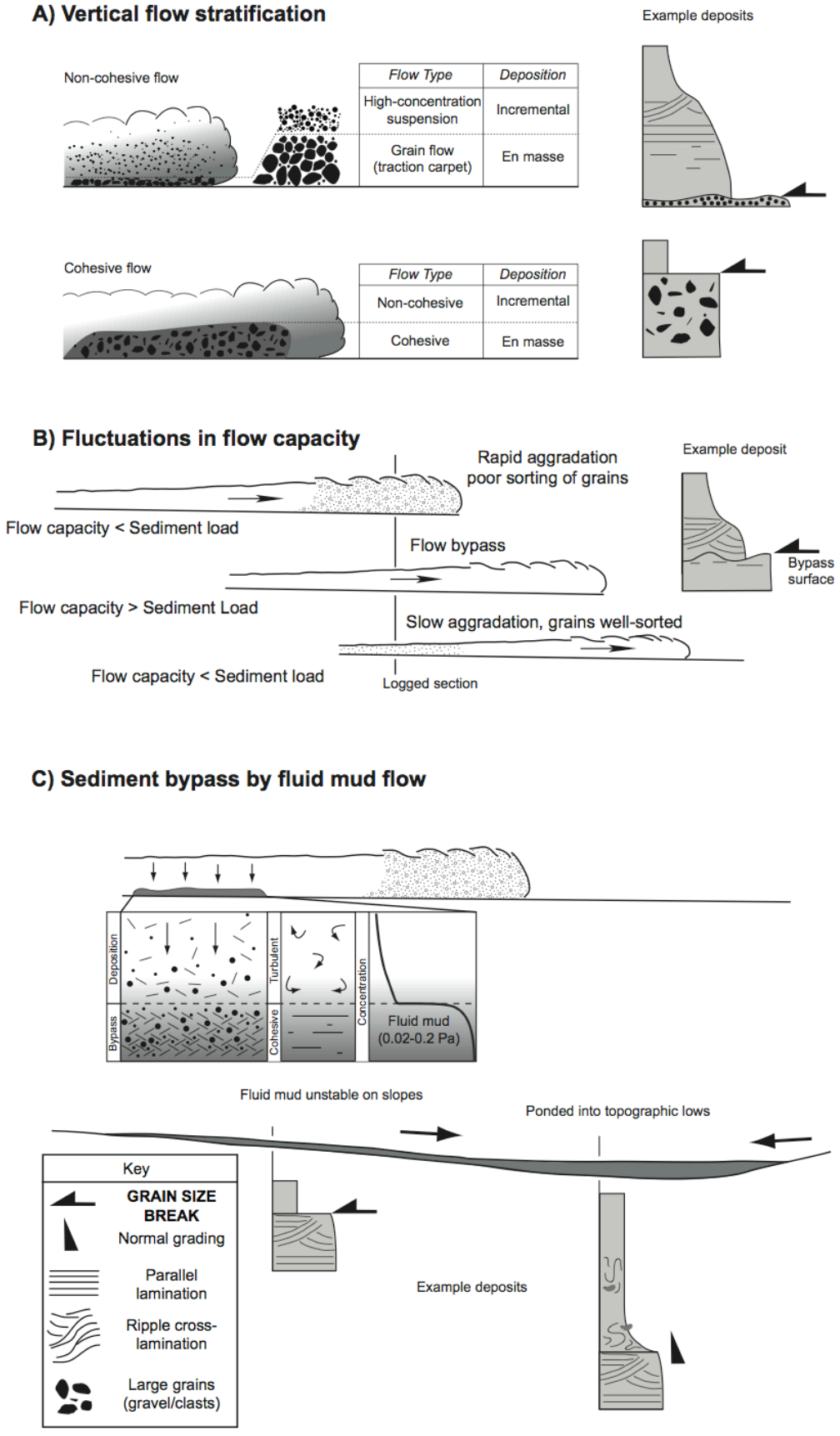
A) Vertical flow stratification
Example deposits
Non-cohesive flow
Flow Type
Deposition
High-concentration suspension
Incremental
Grain flow (traction carpet)
En masse
Cohesive flow
Flow Type
Deposition
Non-cohesive
Incremental
Cohesive
En masse
B) Fluctuations in flow capacity
Example deposit
Rapid aggradation poor sorting of grains
Flow capacity < Sediment load
Flow bypass
Bypass surface
Flow capacity > Sediment Load
Slow aggradation, grains well-sorted
Flow capacity < Sediment load
Logged section
C) Sediment bypass by fluid mud flow
Deposition
Bypass
Turbulent
Cohesive
Concentration
Fluid mud (0.02-0.2 Pa)
Fluid mud unstable on slopes
Ponded into topographic lows
Key
GRAIN SIZE BREAK
Normal grading
Parallel lamination
Ripple cross-lamination
Large grains (gravel/clasts)
Example deposits

Figure 6-14: Models proposed for the generation of grain-size breaks in turbidites. (A) A sharp vertical concentration boundary within the flow. For grain-size breaks to be generated from the vertical structure of the flow, deposition must occur 'en masse'. Two flow types are illustrated that can deposit sediment 'en masse': 1) non-cohesive flow with very high sediment concentrations near to the bed, where grains are supported by inter-particle interactions rather than fluid turbulence; and 2) cohesive (debris) flow with sufficient clay content to have yield strength, which can support grains within it. (B) Fluctuations in flow capacity. Incrementally aggraded deposits preserve the longitudinal profile of the flow. Therefore, fluctuations in the ability of the flow to transport its sediment load can result in complex vertical profiles in deposits. Illustrated is an initially depositional flow, which becomes bypassing, before recommencing deposition. The grain-size break is produced because of the flow bypass.

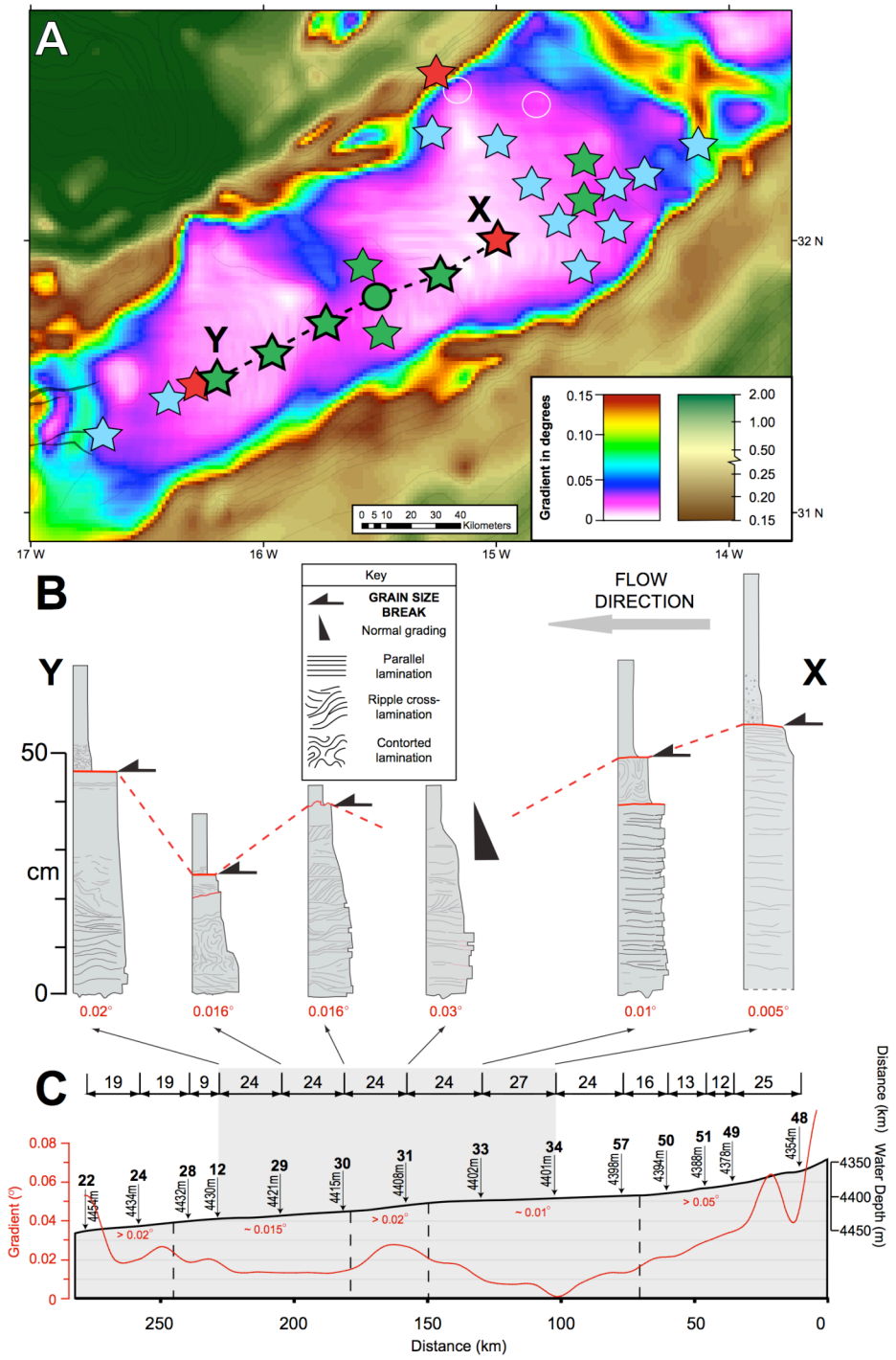

Figure 6-15: Shows the relationship between Type III grain-size breaks (sand overlain by mud) and seafloor gradient within Bed 12, across the Agadir basin. (A) Plots the spatial distribution of Type III grain-size breaks on a gradient map of the Agadir Basin. Note the two areas of flatter seafloor, proximal and distal from the mouth of the Agadir Canyon. (B) Visual logs of the deposits along the axis of the basin. Note the only normally graded deposit sits on the steeper gradient. (C) Topographic profile down the axis of the Agadir Basin with seafloor gradient marked with a red line.

6.5.6 Development of Fluid Mud Layers

This section first describes a conceptual model by which cohesive fluid mud layers can produce Type IV grain-size breaks from a turbidity current. Second, the structure of fluid mud and the controls on its rheology are discussed, which are then related to vertical grading profiles within turbidite muds. Finally, the depositional architecture of fluid muds and Type IV grain-size breaks is discussed in relation to changes in slope.

Towards the rear of a turbidity current, mud concentrations are relatively high and shear velocities at a minimum, allowing fine-grained silt and mud particles to settle out from suspension (Figure 6-14C). Due to flocculation of clay particles, silt and mud may initially settle towards the bed at similar shear velocities (Whitehouse et al., 2000). Continued settling of mud flocs from the overlying suspension increases the clay concentration near to the bed. At sufficiently high concentrations ($> \sim 10$ g l^{-1}) the flocs suppress turbulence and develop a yield strength, similar to fluid muds observed in estuarine and coastal settings (McAnally et al., 2007a; McAnally et al., 2007b). The fluid mud layer hinders the settling of both mud flocs and non-cohesive silt grains, settling from the overlying suspension. The fluid mud layer is able to support grains that would otherwise settle out from a turbulent flow and bypasses these grains down slope (Figure 6-14C). Ultimately, continued deceleration from the flow allows the fluid mud layer to deposit 'en masse' via frictional freezing onto the bed, which produces deposits of ungraded, structureless turbidite mud (McCave and Jones, 1988; Jones et al., 1992).

Type IV grain-size breaks are interpreted to be generated by this process. In theory when a suspension containing a sufficient proportion of clay settles towards the bed, it will always produce a cohesive mud layer. This may explain the widespread occurrence of Type IV grain-size breaks across the Moroccan Turbidite System.

6.5.6.1 Competence of fluid mud layers

Fluid mud layers occur when mud concentrations exceed ~10 g/l and interactions between cohesive particles lead to hindered settling. Fluid muds measured in shallow marine settings can exceed concentrations of ~ 4 % or ~ 100 g/l (Trowbridge and Kineke, 1994; Kineke and Sternberg, 1995; Wright et al., 2001; McAnally et al., 2007b) and can contain 20 to 60 % of silt-sized particles, and occasionally support a few percent of fine sand (McAnally et al., 2007b). A fluid mud yield strength of ~ 0.2 to 0.02 Pa would be sufficient to support non-cohesive quartz grains with diameters between 10 μm and 100 μm (Hampton, 1975; Amy et al., 2006). Mud suspensions achieve these yield strengths at volume concentrations of ~ 3 to 11 % (Berlamont et al., 1993; Coussot and Piau, 1994; Coussot, 1995; McAnally et al., 2007b). Therefore, it is reasonable a fluid mud layer could have sufficient yield strength to prevent deposition of the grain sizes (~10 μm to ~100 μm) missing across Type IV grain-size breaks within the Moroccan Turbidite System.

6.5.6.2 Vertical structure of a fluid mud layer

Baas et al. (2009) constructed a phase diagram for turbulent, transitional and laminar clay-laden open channel flows. Their experiments demonstrated the vertical turbulence structure within the flow was determined by shear velocity and clay concentration (Figure 6-16). Increasing the proportion of clay in a flow led to five different flow types: 1) turbulent flow, which is turbulent throughout its depth; 2) turbulence-enhanced flow; 3) lower transitional plug flow, comprising a lower turbulent region and a thinner overlying laminar plug; 4) upper transitional plug flow, which has a thin turbulent underlayer overlain by a thicker laminar plug; and 5) quasi-laminar plug flow, comprising a laminar plug that moves on a thin shear layer (Baas et al., 2009). Here we consider the experiments of Baas et al. (2009) as analogous to conditions experienced by a fluid mud developed toward the rear of a decelerating turbidity current: increasing clay content and decreasing shear stresses near to the bed. The five flow types of Baas et al. (2009) are used to interpret the range of vertical grading profiles

found within turbidite muds overlying mud breaks across the Moroccan Turbidite System (Figure 6-16). Quasi-laminar plug flows will produce structureless, ungraded deposits. Upper transitional plug flows will produce deposits with a thin graded base, overlain by ungraded structureless mud. Lower transitional plug flows will produce a thicker graded zone at the base of the deposit, overlain by ungraded structureless mud. Turbulent and turbulence-enhanced flows will produce deposits that are graded, potentially with sedimentary structures throughout.

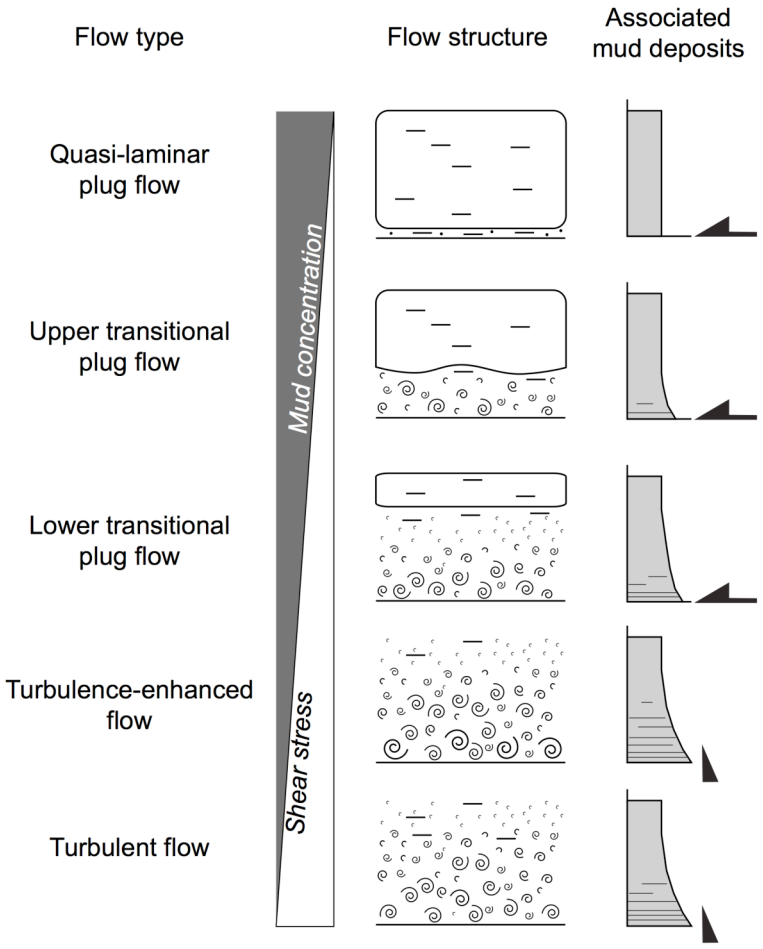

Figure 6-16: Cartoon cross-sections representing the vertical turbulence structure within a fluid mud layer (adapted from the experiments of Baas et al., 2009). The type of flow within a fluid mud is determined by the amount of clay within the flow relative to the shear stresses near to the bed. With relatively high clay content cohesive forces dominate forming a quasi-laminar plug flow. This hinders settling of non-cohesive grains and ultimately deposits 'en masse' producing an ungraded structureless turbidite mud. With relatively low clay content shear stresses dominate, which generates a fully turbulent flow. Deposition occurs incrementally producing graded deposits, potentially with sedimentary structures.

6.5.6.3 Spatial variability in fluid mud

Once a fluid mud layer has formed, toward the rear of a turbidity current, the balance of cohesive and turbulent forces is likely to be affected by changes in seafloor gradient. Increases in slope will increase flow velocity and near bed shear stresses, which will promote a more turbulent flow type. Decreases in slope will have the opposite affect, promoting a more cohesive (laminar) flow type.

An association between slope and Type IV grain-size breaks is found in the deposits of Bed 12 along the axis of the Agadir Basin (Figure 6-15). Initially, mud breaks overlain by ungraded structureless mud are found across the relatively flat northeast parts of the Agadir Basin. Progressing southwest along the axis of the basin (i.e. distally) there is a significant increase in slope from ~ 0.01º to 0.03º. Although subtle, the relative change in slope is significant (double). Here, a single core site shows Bed 12 to have a deposit that is normally graded between sand and mud. Continuing southwest the slope decreases to ~ 0.016º, where Type IV grain-size breaks are found overlain by turbidite mud with normally graded and contorted bases. This down flow pattern of mud breaks is interpreted to be the product of quasi-laminar fluid mud hindering the settling of non-cohesive grains and bypassing them down slope. As the fluid mud accelerated over the increased slope it transformed into a turbulent flow that could not support the non-cohesive grains within it, enabling them to deposit onto the bed. As the fluid mud travelled further down slope onto flatter seafloor, a laminar plug flow could re-establish, which hindered the settling of non-cohesive grains.

6.5.6.4 Silt and mud settling

Another hypothesis to consider is the behaviour of settling mud flocs with silt grade sediment. As the mud-rich flow decelerates, individual clay particles flocculate. Mud flocs have a similar settling velocity (0.1 to 1 mm/s) to that of silt-sized particles (Whitehouse et al., 2000). If we consider the turbidity current to deposit mud and silt within a dilute flow,

rather than a fluid mud layer, then this mechanism ensures that both mud flocs and silt grains will settle together. This mechanism could produce ungraded, structureless deposits of turbidite mud. However, although physically possible, experimental studies examining the settling behaviour of sand/mud mixtures show that as mud flocculates it hinders the settling of the non-cohesive grains (Berlamont et al., 1993; Torfs et al., 1996; Cuthbertson et al., 2008; Dankers et al., 2008). With increased flocculation the non-cohesive grains are suspended within the consolidating cohesive matrix. Considering this process it is most likely that the time window in which silt grains and mud flocs could settle together, without being hindered by cohesive forces, would be relatively small. Furthermore, if increasing sand content within a sand/mud mixture serves to increase settling velocities (Torfs et al., 1996), then the same would be expected of silt/mud mixtures. Exactly how cohesive forces and settling velocities are balanced within silt/mud mixtures is not known and requires settling tube experiments to substantiate theoretical arguments and comparison with sand/mud mixtures.

6.5.7 Models for the generation of grain-size breaks

Considering the above discussion, a range of potential processes can act within a flow to produce grain-size breaks. Each process will evolve with time and distance from source. Here we present a spatial and temporal framework describing the generation of grain-size breaks within an individual bed (Figure 6-17A). The model illustrates an idealized flow that produces each type of grain-size break found with the Moroccan Turbidite System. Type I grain-size breaks are produced first from ‘en masse’ deposition of a high-concentration traction carpet (*sensu* Lowe, 1982). Next Type II and III grain-size breaks are produced whilst the flow is waxing/waning and its capacity equilibrating with its sediment load. These types of grain-size break are absent distally as the flow organizes itself with distance from source. Finally, Type IV grain-size breaks are produced by fluid mud bypassing grains down slope. This type of grain-size break occurs almost everywhere representing widespread generation of late-stage fluid mud layers.

Type V grain-size breaks are produced via ‘en masse’ deposition from a cohesive flow (Figure 6-17B). This type of grain-size break is found distally because vertical stratification within the flow increases away from source, which generates a sharper concentration profile (McCaffrey et al., 2003; Choux et al., 2005; Felix et al., 2005). With increasing yield strength a cohesive flow is likely to develop stronger (and sharper) internal concentration boundaries (Marr et al., 2001; Mohrig and Marr, 2003; Ilstad et al., 2004). Therefore, Type V grain-size breaks are likely to be more frequent and occur more proximally within higher yield strength flows.

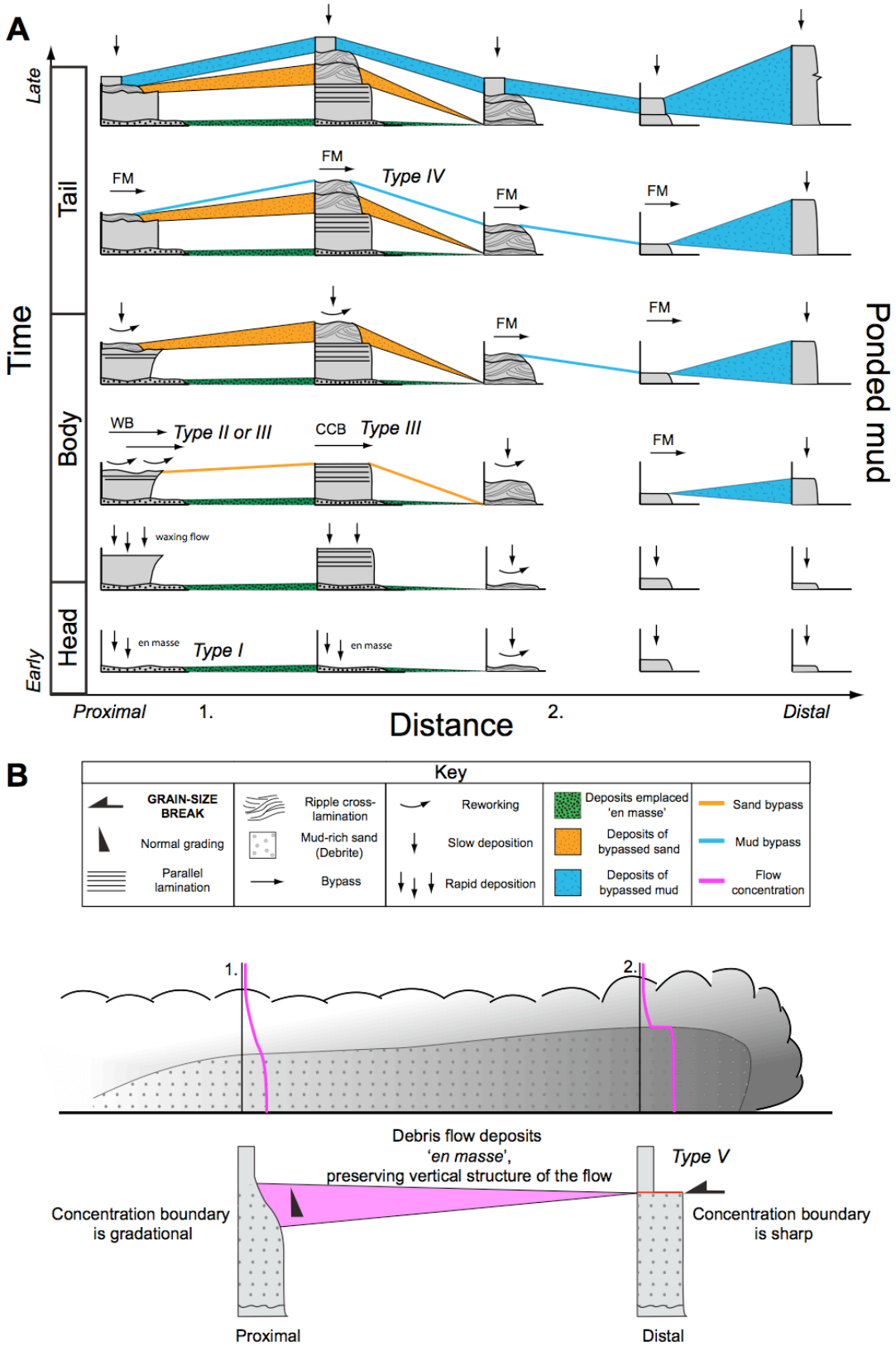
A
Late
Tail
Body
Head
Early
Time
FM
Type IV
FM
FM
FM
FM
WB
Type II or III
CCB
Type III
FM
waxing flow
en masse
Type I
en masse
Ponded mud
Proximal
1.
Distance
2.
Distal
B
Key
GRAIN-SIZE BREAK
Normal grading
Parallel lamination
Ripple cross-lamination
Mud-rich sand (Debrite)
Bypass
Reworking
Slow deposition
Rapid deposition
Deposits emplaced 'en masse'
Deposits of bypassed sand
Deposits of bypassed mud
Sand bypass
Mud bypass
Flow concentration
1.
2.
Debris flow deposits 'en masse', preserving vertical structure of the flow
Type V
Concentration boundary is gradational
Concentration boundary is sharp
Proximal
Distal

Figure 6-17: Conceptual model for the generation of grain-size breaks within turbidites. (A) Idealized deposits from an individual (non-cohesive) flow are illustrated with distance away from source. Individual deposits are illustrated through time as the flow passes over fixed geographical points. Different types of grain-size break are shown occurring at different points within this spatial/temporal framework. Type I grain-size breaks, generated by 'en masse' deposition of thin traction carpets, will occur at an early stage in the deposit and only extend to relatively proximal areas. Type II and III grain-size breaks, generated by waxing flow conditions (Trowbridge and Kineke) and/or capacity- to competence-induced deposition (CCB), occur next and are also restricted to relatively proximal areas (orange line). Type IV grain-size breaks, generated by fluid mud bypassing grains down slope (FM), are produced at a late-stage and occur everywhere across the turbidite (blue line). (B) Cohesive flows (including debris flows) will develop sharp vertical concentration boundaries with distance from source. Therefore, Type V grain-size breaks are more likely to be found distally with normal grading found proximally.

6.5.8 Grain-size breaks in other turbidite sequences

6.5.8.1 Modern turbidite systems

Lebreiro et al. (1997) provide a detailed analysis of grain-size trends within Quaternary turbidites in the Horseshoe Abyssal Plain offshore from the Iberian Margin. Grain-size breaks between fine sand and mud are found throughout the basin (Lebreiro et al., 1997). However, the magnitude of the grain-size breaks (10 to 30 μm) is somewhat less than that seen in Type IV grain-size breaks within the Moroccan Turbidite System (10 to 100 μm). This is probably due to a lack of coarse-grained sediment within Horseshoe Abyssal Plain turbidites, which are composed primarily of silt and mud (Lebreiro et al., 1997).

Migeon et al. (2001) identified two types of grain-size break in recent turbidites on the southern levee of the Var Fan in the Mediterranean Sea. The first type of grain-size break occurred between normally graded ripple cross-laminated sand, overlain by ungraded structureless turbidite mud (their facies I and II). The change in modal grain size across these grain-size breaks is ~ 10 – 100 μm; similar to Type IV grain-size breaks found across the Moroccan Turbidite System. Migeon et al. (2001) interpret this type of grain-size break as localized flow acceleration over the crest of sediment waves. However, similar (Type IV) grain-size breaks found in the Moroccan Turbidite System occur within relatively flat basin-plain settings that do not have sediment wave fields. Therefore, we propose grain-size breaks

between clean sand and ungraded turbidite mud within the Var Fan could be a product of fluid mud bypassing sediment down slope, as interpreted for the Moroccan Turbidite System. The second type of grain-size break Migeon et al. (2001) recognized occurred between mud-rich sand with mud clasts, overlain by ungraded structureless turbidite mud (their facies IV). These are similar to Type V grain-size breaks found in the Moroccan Turbidite System, occurring between mud-rich sand overlain by ungraded turbidite mud. We concur with Migeon et al. (2001) that this type of grain-size break is generated by a strong vertical concentration profile within a cohesive flow, which deposits 'en masse' (i.e. a debris flow).

6.5.8.2 Ancient turbidite systems

Two types of grain-size break have been recognised in basin-plain turbidites within the older part of the Marnoso Arenacea Formation: 1) those occurring between normally graded sand (Bouma T_A, T_B) overlain by finer grained, rippled cross laminated sand (Bouma T_C) and; 2) those occurring between fine sand/silt (Bouma T_C) and mud (Bouma T_E)(Gladstone and Sparks, 2002; Amy and Talling, 2006; Talling et al., 2007a; Talling et al., 2007b; Sumner et al., 2012). The first type of grain-size break found in the Maronoso Arenacea Formation only occurs in relatively proximal localities (Sumner et al., 2012). Type III grain-size breaks found within the Moroccan Turbidite System are associated with similar facies and area also restricted to relatively proximal localities. These similarities suggest that grain-size breaks between sand overlain by finer sand, within the Marnoso Arenacea Formation, are probably analogous to Type III grain-size breaks found in the Moroccan Turbidite System. The second type of grain-size break found in the Marnoso Arenacea Formation, between (clean and mud-rich) sand and ungraded structureless turbidite mud, occurs almost everywhere. Although gradational boundaries are found more frequently in the distal most parts of the system because silt bypassed proximally can deposit in distal localities (Sumner et al., 2012). These grain-size breaks are similar to Type IV and V grain-size breaks found within the Moroccan Turbidite System.

Grain-size breaks between sand and turbidite mud are a common (if not a dominant) feature in: the Aberystwyth Grit Formation and Windermere Super Group, UK (Gladstone and Sparks, 2002), the Eocene-Oligocence Tavezyannaz Sandstone, SE France (Sinclair and Cowie, 2003), and the Eocene Hecho Group in the Spanish Pyrenees (Remacha et al., 2005). Lateral correlation of turbidites in the Eocene Hecho Group, Spanish Pyrenees, and within the Marnoso Arenacea Formation, demonstrates that the missing grain sizes were bypassed and deposited down slope (Remacha et al., 2005; Sumner et al., 2012). This is similar to the Moroccan Turbidite System, whereby the missing grain sizes are also found hundreds of kilometres down slope (Figure 6-4).

6.6 CONCLUSIONS

This study examines in detail the vertical and spatial distribution of grain-size breaks within five turbidites found across the Moroccan Turbidite System. Five types of grain-size break were found: *Type I* – occurred proximally between gravel and finer grained structureless sand, *Type II* – occurred in proximally between inversely graded sand overlain by coarser sand, *Type III* – occurred proximally between sand overlain by ripple cross-laminated finer sand, *Type IV* – occurred almost everywhere between clean sand and mud and, *Type V* – occurred only in relatively distal areas between mud-rich (debrite) sand and mud.

We interpret *Type I* grain-size breaks as a product of 'en masse' deposition from a thin, high-concentration traction carpet (*sensu* Lowe, 1982). *Types II* and *III* are interpreted as a product of spatial and temporal fluctuations in flow capacity, and/or flows switching from capacity-induced to competence-induced deposition. Indeed, the absence of these types of grain-size break distally supports the notion that flows organize themselves longitudinally with distance from source (Kneller and McCaffrey, 2003). *Type IV* grain-size breaks are interpreted to be the product of late-stage development of fluid mud, which hinders the settling of non-cohesive grains and bypasses them down slope. Grain-size analysis of the individual beds proximally and distally (up to > 1500 km down slope) demonstrates the missing grain sizes are found down slope, situated within thick ponded mud caps. Finally, *Type V* grain-size

breaks are interpreted to be a product of a sharp vertical concentration boundary within the parent flow. *Type V* grain-size breaks are only found in distal linked-debrite deposits, whereas proximal linked-debrite deposits are normally graded.

It is important to understand that late-stage settling of fines toward the rear of a decelerating turbidity current should always result in the generation a cohesive fluid mud layer near to the bed, unless there is insufficient clay to generate a cohesive fluid. Therefore, Type IV grain-size breaks should form a typical component of turbidite deposits, rather than occurring as an exception. A number of existing studies support this notion, reporting most turbidites to have Type IV grain-size breaks.

7 Conclusions

7.1 Large-scale individual bed correlations

Exceptional core coverage across the entire Moroccan Turbidite System coupled with a robust geochemical and chronostratigraphic framework has enabled individual turbidite beds to be examined across their depositional extent: both in down flow and across flow directions. Revised estimates of bed volumes and run-out distances are impressive with some events being extremely large-volume (> 200 km^3) with deposits extending for more than 2,000 km across the seafloor.

It is rare to be able to document beds over these distances. Such data is extremely valuable because our current understanding of submarine flow processes relies on idealized models, derived from laterally restricted field data and, experimental and theoretical evidence. Without large-scale individual bed correlations it is difficult to validate these models.

7.2 Complex flow pathways

Chapter 3 examines turbidites within the most proximal part of the system, the Seine Abyssal Plain. Fining patterns in grain size within turbidites indicate that some of the beds were produced by synchronous flows passing into the basin from multiple disparate entry points.

Similar patterns of deposition have been interpreted in other parts of the world as evidence of earthquake triggered events (Adams, 1990; Gorsline et al., 2000; Shiki et al., 2000; Goldfinger et al., 2003; Gracia et al., 2010; Goldfinger, 2011; Masson et al., 2011). However, careful analysis of the sedimentological evidence shows that it is not possible to categorically

determine whether the synchronous flows originated from a single slope failure that was subsequently split along its pathway into the basin, or multiple simultaneous slope failures caused synchronous flows. The distinction is important because simultaneous disparate slope failures require a regional trigger, i.e. an earthquake; whilst a single slope failure could be triggered by a range of mechanisms (including earthquakes).

This chapter highlights the difficulties faced by the application of turbidite palaeoseismology beyond the historical earthquake record.

7.3 Thin and slow: autosuspending flows with a difference

Chapter 4 focuses on flow processes operating across the Agadir Basin, whilst Chapter 5 analyzes flow behaviour through the Madeira Channel System. Careful analysis of depositional architecture in relation to seafloor topography shows that flows must have been relatively thin (tens of meters). For example, sandy deposits from Bed 12 (the largest volume event at ~ 230 km^3) only drape < 5 m up basin margin topography in across flow directions, indicating the parent flow was < 5 m thick. Just beyond the distal end of the Agadir Basin, Bed 12 is found completely confined within the 2 km wide, ~ 20 m deep Southern Madeira Channel. This supports the interpretation made within the Agadir Basin that the parent flow was indeed relatively thin (< 5 thick).

Analysis of hemipelagic intervals immediately underlying turbidite beds coupled with analysis of nannofossil assemblages within the turbidite mud caps shows the flows were not erosive across the Agadir Canyon, nor within the Madeira Channels. For flows not to be eroding the seafloor they must have been travelling relatively slowly (< 0.6 m/s).

Despite being relatively thin and slow, flows were able to run-out for exceptional distances. Indeed, Bed 12 within the Agadir Basin extends ~ 150 km down slope without appreciably thinning or fining. To produce such uniform beds the parent flows must have been primarily autosuspending: Only depositing a small proportion of their sediment load per square kilometre along their flow pathway across the basin (Chapter 4). Chapter 5 supports this model, demonstrating that when subject to a subtle increase in slope and increased confinement (within the Madeira Channel System), these flows became completely autosuspending and bypassed large-volumes of sediment down slope.

Idealized facies models predict bed architecture (Bouma, 1962; Stow and Shamugam, 1980; Lowe, 1982), theoretical and experimental models predict flow dynamics (Pantin, 1979; Parker, 1982; Parker et al., 1986; Parker et al., 1987; Garcia and Parker, 1991; Kneller and Buckee, 2000; Pantin, 2001; Naruse et al., 2008; Sequeiros et al., 2009; Pantin and Franklin, 2011). Currently, these models are widely accepted to be representative of natural submarine flow dynamics and their deposits. However, these models cannot explain how thin and slow flows could autosuspend most of their sediment loads, depositing uniform sheet sands across the Agadir Basin. Reproducing the key field observations found in Chapters 4 and 5 will be a challenge for future modelling.

7.4 Submarine channels built by deposition not erosion

In general, submarine channels are thought to initiate and be maintained via erosion through the channel axis and deposition of levees along their margins (Normark, 1978; Normark et al., 1979; Peakall et al., 2000; Wynn et al., 2007). Indeed, it is argued that submarine channels must have erosion to initiate (Fildani et al., 2012).

Chapter 5 examines the Madeira Channel System and concludes that erosion is not required for channel initiation or maintenance. Analysis of hemipelagic sediments across event horizons reveals no erosion within the channel axes. Deposition occurs along the channel

margins, which builds the channel relief. Seismic profiles that penetrate deeper than the cores show no erosion in the channel axes, indicating that purely constructional processes have been operating for a long time, and probably created the channel morphology found today.

7.5 Grain-size breaks: the norm not the exception

Chapter 6 documents the vertical and spatial distribution of grain size breaks within turbidites across the Moroccan Turbidite System. With individual beds documented both down flow and across flow over their depositional extent, it enables conceptual models of grain size break formation to be validated.

All beds had grain size breaks. Most of the grain size breaks occurred between sand overlain by coarser or finer sand. This type of grain size break was restricted to relatively proximal localities. They are attributed to spatial/temporal fluctuations in flow capacity and competence proximal to source. With time and distance from source, the flows progressively equilibriated their capacity and sediment load. This produced deposition of normally graded sands and an absence of grain size breaks between sand and sand in distal localities.

Grain size breaks between sand overlain by mud were almost everywhere. Chapter 6 proposes a new model, whereby as the fines settle out toward the rear of a decelerating turbidity current increased clay concentration near to the bed produces a cohesive fluid mud layer. This fluid mud layer hinders settling of grains and bypasses sediment down slope.

With sufficient clay content a decelerating flow should always form fluid mud layers. This may explain why this type of grain-size break is found throughout the Moroccan Turbidite System and is a typical (if not dominant) feature within most turbidite beds around the world (Bouma, 1962; Migeon et al., 2001; Gladstone and Sparks, 2002; Kneller and McCaffrey,

2003; Remacha et al., 2005; Sumner et al., in press). Therefore, grain-size breaks from sand overlain by mud should be recognized as the norm not the exception.

7.6 Summary

This thesis presents, arguably, the most detailed and extensive correlative framework for individual flows in any turbidite system. This level of detail demonstrates remarkable complexity in bed architectures and flow pathways across the seafloor. It is shown that flow behaviour may differ from established models, suggesting there is still much to learn about the dynamics of submarine flows. This demonstrates how important such field data is, which should be used to validate and underpin the predictive models widely used to understand submarine flows.

8 Future Work

- More cores that penetrate deeper sediments are needed across the Seine Abyssal Plain to better constrain the flow pathways and turbidite frequencies in older sediments (> 150 ka). Integrating more cores will allow more confident assertions to be made regarding the flow pathways into the basin and the correlation between turbidite frequency and sea-level. Understanding the controls on turbidite frequency is important for the assessment of geohazards across the seafloor.

- Distinguishing whether beds emplaced across the Seine Abyssal Plain from multiple entry points are the product of multiple slope failures or a single slope failure is a key question. If Beds S3, S5 and S11 did originate from single slope failures, the slope failures were most likely situated on similar areas of seafloor. Repeated slope failures across a small area would produce an identifiable landslide scar. The area of seafloor highlighted in Chapter 3 should have identifiable landslide scars. Fortuitously, this area has been investigated by the 'Meteor' Cruise M58-2. The cruise report states "A slump in the upper part of core GeoB 8603-3 may have eroded an uncertain amount of sediment at this location". Analysis of parasound profiles and cores collected aboard this cruise will show whether such a scar exists and, in turn, help determine the origins of Beds S3, S5 and S11. I am currently organizing a trip to Bremen to view the cores, and collaborating with Dr. Sebastian Krastel to access the parasound profiles from this cruise.

- The Madeira Channels are a new type of submarine channel system, a purely constructional feature. However, are the processes operating within this channel system applicable elsewhere? Are other submarine channels subject to large-volume flow bypass? More work is required comparing the architecture and processes operating within a range of submarine channels.

- Initial results shown in Chapters 3 and 6 show muds are ponded into topographic low points. More work needs to be done examining bed thicknesses and distribution of facies within turbidite mud caps. This work will show how differently mud behaves as it is transported and deposited across the seafloor.

- This thesis highlights that hindered settling within submarine flows is an important mechanism by which sediment is transported. Mud likely plays an important role hindering settling grains and affecting bedform development. Current numerical and experimental models do not account for hindered settling effects nor for the potential effects of mud within a flow. Collaboration is required between numerical modellers and field geologists to generate models that reproduce the key field observations presented in this thesis (and where other beds have been mapped out across their depositional extent). Revising numerical models is the next step in a better understanding of flow processes operating within submarine flows.

- In a similar vein, there is a paucity of laboratory experiments that have investigated how mixtures of sand/silt and mud settle out from suspension. What are the settling laws that govern sand/silt and mud settling out from a mixed suspension? What effect does total sediment concentration and/or mud content have on the rates of particle settling. Within a submarine flow these settling processes will also be affected by shear stresses near to the bed. More laboratory experiments are needed that investigate these controls. Such experiments are important if we are to better understand how natural particulate suspensions behave.

9 Bibliography

ADAMS, J. (1990) PALEOSEISMICITY OF THE CASCADIA SUBDUCTION ZONE - EVIDENCE FROM TURBIDITES OFF THE OREGON-WASHINGTON MARGIN. *Tectonics,* 9**,** 569-583.

ADEOGBA, A., MCHARGUE, T. R. & GRAHAM, S. A. (2003) Influence of slope gradient on the distribution and architecture of deep-water channels and fans inferred from near-surface 3-D seismic data, Niger Delta slope, Nigeria. *AAPG Annual Meeting extended abstracts, Salt Lake City, US***,** 2.

ALLEN, J. R. L. (1977) The possible mechanics of convolute lamination in graded sand beds. *Geological Society of London,* 134**,** 19-31.

ALLEN, J. R. L. (1982) Sedimentary structures: their character and physical basis, Volume 1. *Amsterdam, Elsevier*.

AMOS, C. L., FEENEY, T., SUTHERLAND, T. F. & LUTERNAUER, J. L. (1997) The stability of fine-grained sediments from the Fraser River delta. *Estuarine Coastal and Shelf Science,* 45**,** 507-524.

AMOS, C. L., UMGIESSER, G., FERRARIN, C., THOMPSON, C. E. L., WHITEHOUSE, R. J. S., SUTHERLAND, T. F. & BERGAMASCO, A. (2010) The erosion rates of cohesive sediments in Venice lagoon, Italy. *Continental Shelf Research,* 30**,** 859-870.

AMY, L. A. & TALLING, P. J. (2006) Anatomy of turbidites and linked debrites based on long distance (120 x 30 km) bed correlation, Marnoso Arenacea Formation, Northern Apennines, Italy. *Sedimentology,* 53**,** 161-212.

AMY, L. A., TALLING, P. J., EDMONDS, V. O., SUMNER, E. J. & LESUEUR, A. (2006) An experimental investigation of sand-mud suspension settling behaviour: implications for bimodal mud contents of submarine flow deposits. *Sedimentology,* 53**,** 1411-1434.

ARGUS, D. F., GORDON, R. G., DEMETS, C. & STEIN, S. (1989) CLOSURE OF THE AFRICA EURASIA NORTH AMERICA PLATE MOTION CIRCUIT AND TECTONICS OF THE GLORIA FAULT. *Journal of Geophysical Research-Solid Earth and Planets,* 94**,** 5585-5602.

ARNOTT, R. W. C., NAVARRO, L. & KHAN, Z. A. (in press) Contrasting the stratal architecture of highly-confined and poorly confined deep-marine sinuous channels systems - An outcrop perspective. *Marine and Petroleum Geology*.

BAAS, J. H., BEST, J. L. & PEAKALL, J. (2011) Depositional processes, bedform development and hybrid bed formation in rapidly decelerated cohesive (mud-sand) sediment flows. *Sedimentology,* 58**,** 1953-1987.

BAAS, J. H., BEST, J. L., PEAKALL, J. & WANG, M. (2009) A PHASE DIAGRAM FOR TURBULENT, TRANSITIONAL, AND LAMINAR CLAY SUSPENSION FLOWS. *Journal of Sedimentary Research,* 79**,** 162-183.

BABONNEAU, N., SAVOYE, B., CREMER, M. & BEZ, M. (2010) Sedimentary architecture in meanders of a submarine channel: detailed study of the present Congo Turbidite Channel (ZAIANGO Project). *Journal of Sedimentary Research,* 80**,** 852-866.

BABONNEAU, N., SAVOYE, B., CREMER, M. & KLEIN, B. (2002) Morphology and architecture of the present canyon and channel system of the Zaire deep-sea fan. *Marine and Petroleum Geology,* 19**,** 445-467.

BADALNI, G., KNELLER, B. & WINKER, C. D. (2000) Architecture and Processes in the Late Pleistocene Brazos-Trinity Turbidite System, Gulf of Mexico Continental Slope. *In: Weimer, P. et al., (eds), Deep-Water Reservoirs of the World. Gulf Coast Society SEPM.*

BATCHELOR, G. K. (1982) SEDIMENTATION IN A DILUTE POLYDISPERSE SYSTEM OF INTERACTING SPHERES .1. GENERAL-THEORY. *Journal of Fluid Mechanics,* 119**,** 379-408.

BEAUBOUEF, R. T. & FRIEDMANN, S. J. (2000) High resolution seismic/sequence stratigraphic framework for the evolution of Pleistocene intra slope basins, Western Gulf of Mexico: depositional models and reservoir analogs. *In: Weimer, P. et al., (eds), Deep-Water Reservoirs of the World. Gulf Coast Society SEPM.*

BERLAMONT, J., OCKENDEN, M., TOORMAN, E. & WINTERWERP, J. (1993) THE CHARACTERIZATION OF COHESIVE SEDIMENT PROPERTIES. *Coastal Engineering,* 21**,** 105-128.

BERNHARDT, A., JOBE, Z. R. & LOWE, D. R. (2011) Stratigraphic evolution of a submarine channel-lobe complex system in a narrow fairway within the Magallanes foreland basin, Cerro Toro Formation, southern Chile. *Marine and Petroleum Geology,* 28**,** 785-806.

BEST, J. & BRIDGE, J. (1992) The morphology and dynamics of low amplitude bedwaves upon upper stage plane beds and the preservation of planar laminae. *Sedimentology,* 39**,** 737-752.

BLANCHETTE, F., STRAUSS, M., MEIBURG, E., KNELLER, B. & GLINSKY, M. E. (2005) High-resolution numerical simulations of resuspending gravity currents: Conditions for self-sustainment. *Journal of Geophysical Research-Oceans,* 110.

BONNECAZE, R. T., HUPPERT, H. E. & LISTER, J. R. (1996) Patterns of sedimentation from polydispersed turbidity currents. *Proceedings of the Royal Society of London Series a-Mathematical Physical and Engineering Sciences,* 452**,** 2247-2261.

BOUMA, A. H. (1962) Sedimentology of some Flysch Deposits: A Graphic Approach to Facies Interpretation. *Elsevier.*

BOWEN, A. J., NORMARK, W. R. & PIPER, D. J. W. (1984) Modelling of turbidity currents on Navy Submarine Fan, California Continental Borderland. *Sedimentology,* 31**,** 169-185.

BRITTER, R. E. & SIMPSON, J. E. (1978) EXPERIMENTS ON DYNAMICS OF A GRAVITY CURRENT HEAD. *Journal of Fluid Mechanics,* 88**,** 223-&.

BROWN, R. J. & BRANNEY, M. (2004) Bypassing and diachronous deposition from density currents: Evidence from a giant regressive bed form in the Poris ignimbrite, Tenerife, Canary Islands. *Geology,* 32**,** 445-448.

BRUNT, R. L., HODGSON, D. M., FLINT, S. S., PRINGLE, J. K., DI CELMA, C., PR√©LAT, A. & GRECULA, M. (2012) Confined to unconfined: Anatomy of a base of slope succession, Karoo Basin, South Africa. *Marine and Petroleum Geology,* doi: 10.1016/j.marpetgeo.2012.02.007.

CANTERO, M. I., CANTELLI, A., PIRMEZ, C., BALACHANDAR, S., MOHRIG, D., HICKSON, T. A., YEH, T., NARUSE, H. & PARKER, G. (2012) Emplacement of massive turbidites linked to extinction of turbulence in turbidity currents. *Nature Geoscience,* 5**,** 42-45.

CHOUGH, S. & HESSE, R. (1976) SUBMARINE MEANDERING THALWEG AND TURBIDITY CURRENTS FLOWING FOR 4,000 KM IN NORTHWEST ATLANTIC MID-OCEAN CHANNEL, LABRADOR SEA. *Geology,* 4**,** 529-533.

CHOUX, C. M. A., BAAS, J. H., MCCAFFREY, W. D. & HAUGHTON, P. D. W. (2005) Comparison of spatio-temporal evolution of experimental particulate gravity flows at two different initial concentrations, based on velocity, grain size and density data. *Sedimentary Geology,* 179**,** 49-69.

CLEARY, P. W. (2010) DEM prediction of industrial and geophysical particle flows. *Particuology,* 8**,** 106-118.

COLEMAN, J. M., PRIOR, D. B. & LINDSAY, J. F. (1983) Deltaic influences on shelfedge instability processes. *In: Stanley, D.J., Moore, G.T. (Eds), The Shelfbreak: Critical Interface on Continental Margins. SEPM Special Publication,* 33**,** 121-138.

COUSSOT, P. (1995) STRUCTURAL SIMILARITY AND TRANSITION FROM NEWTONIAN TO NON-NEWTONIAN BEHAVIOR FOR CLAY-WATER SUSPENSIONS. *Physical Review Letters,* 74**,** 3971-3974.

COUSSOT, P. & BOYER, S. (1995) Determination of yield stress fluid behaviour from inclined plane test. *Rheologica Acta,* 34**,** 534-543.

COUSSOT, P. & PIAU, J. M. (1994) ON THE BEHAVIOR OF FINE MUD SUSPENSIONS. *Rheologica Acta,* 33**,** 175-184.

CROUDACE, I. W., RINDBY, A. & ROTHWELL, R. G. (2006) ITRAX: description and evaluation of a new multi-function X-ray core scanner. *In: Rothwell RG (ed) New techniques in sediment core analysis. Geological Society London, Special Publication,* 267**,** 51-63.

COVAULT, J. A. & GRAHAM, S. A. (2010) Submarine fans at all sea-level stands: Tectono-morphologic and climatic controls on terrigenous sediment delivery to the deep sea. *Geology,* 38**,** 939-942.

COVAULT, J. A., NORMARK, W. R., ROMANS, B. W. & GRAHAM, S. A. (2007) Highstand fans in the California borderland: The overlooked deep-water depositional systems. *Geology,* 35**,** 783-786.

CROWLEY, T. J. (1983) Depth dependent carbonate dissolution changes in the eastern North-Atlantic during the last 170, 000 years. *Marine Geology,* 54**,** M25-M31.

CUTHBERTSON, A., DONG, P., KING, S. & DAVIES, P. (2008) Hindered settling velocity of cohesive/non-cohesive sediment mixtures. *Coastal Engineering,* 55**,** 1197-1208.

DADE, W. B. & HUPPERT, H. E. (1994) PREDICTING THE GEOMETRY OF CHANNELIZED DEEP-SEA TURBIDITES. *Geology,* 22**,** 645-648.

DANKERS, P. J., SILLS, G. C. & WINTERWERP, J. C. (2008) On the hindered settling of highly concentrated mud-sand mixtures. *Sediment and Ecohydraulics - INTERCOH,* 9**,** 255-274.

DAVIES, T. L., VANNIEL, B., KIDD, R. B. & WEAVER, P. P. E. (1997) High-resolution stratigraphy and turbidite processes in the Seine Abyssal Plain, northwest Africa. *Geo-Marine Letters,* 17**,** 147-153.

DAVISON, I. (2005) Central Atlantic margin basins of North West Africa: Geology and hydrocarbon potential (Morocco to Guinea). *Journal of African Earth Sciences,* 43**,** 254-274.

DAVIS, R. H. & GECOL, H. (1994) HINDERED SETTLING FUNCTION WITH NO EMPIRICAL PARAMETERS FOR POLYDISPERSE SUSPENSIONS. *Aiche Journal,* 40**,** 570-575.

DE LANGE, G. J., JARVIS, I. & KUIJPERS, A. (1987) Geochemical characteristics and provenance of late Quaternary sediments from the Madeira Abyssal Plain, N. Atlantic. *In: Weaver, P.P.E., Thomson, J. (Eds.), Geology and Geochemistry of Abyssal Plains. Geol. Soc. Spec. Publ.,* 31**,** 147-165.

DI CELMA, C., BRUNT, R. L., HODGSON, D. M., FLINT, S. S. & KAVANAGH, J. P. (2011) Spatial and Temporal Evolution of a Permian Submarine Slope Channel-Levee System, Karoo Basin, South Africa. *Journal of Sedimentary Research,* 81**,** 579-599.

DROZ, L., RIGAUT, F., COCHONAT, P. & TOFANI, R. (1996) Morphology and recent evolution of the Zaire turbidite system (Gulf of Guinea). *Geological Society of America Bulletin,* 108**,** 253-269.

DUITT, T. H., CALDER, E. S., COLE, P. D., HOBLITT, R. P., LOUGHLIN, S. C., NORTON, G. E., RITCHIE, L. J., SPARKS, R. S. J. & VOIGHT, B. (2002) Small-volume, highly mobile pyroclastic flows formed by rapid sedimentation from pyrclastic surges at Soufriere Hills Volcano, Monserrat: an important volcanic hazard. *In (eds. Druitt, T. H. and Kokelaar, B. P.) The eruption of Soufriere Hills Volcano, Monserrat, from 1995 to 1999. Geological Society Memoirs.,* 21**,** 263-279.

DURANTI, D. & HURST, A. (2004) Fluidization and injection in the deep-water sandstones of the Eocene Alba Formation (UK North Sea). *Sedimentology,* 51**,** 503-529.

EDMONDS, M. & HERD, R. A. (2005) Inland-directed base surge generated by the explosive interaction of pyroclastic flows and seawater at Soufriere Hills volcano, Montserrat. *Geology,* 33**,** 245-248.

EDMONDS, M., HERD, R. A. & STRUTT, M. H. (2006) Tephra deposits associated with a large lava dome collapse, Soufriere Hills Volcano, Montserrat, 12-15 July 2003. *Journal of Volcanology and Geothermal Research,* 153**,** 313-330.

EDWARDS, D. A., LEEDER, M. R., BEST, J. L. & PANTIN, H. M. (1994) On experimental reflected density currents and the interpretation of certain turbidites. *Sedimentology,* 41**,** 437-461.

EGGENHUISEN, J. T., MCCAFFREY, W. D., HAUGHTON, P. D. W. & BUTLER, R. W. H. (2011) Shallow erosion beneath turbidity currents and its impact on the architectural development of turbidite sheet systems. *Sedimentology,* 58**,** 936-959.

EIDSVIK, K. J. & BRORS, B. (1989) Self-accelerated turbidity current prediction based upon Kappa-Epsilon turbulence. *Continental Shelf Research,* 9**,** 617-627.

FAIRBANKS, R. G., MORTLOCK, R. A., CHIU, T. C., CAO, L., KAPLAN, A., GUILDERSON, T. P., FAIRBANKS, T. W., BLOOM, A. L., GROOTES, P. M. & NADEAU, M. J. (2005) Radiocarbon calibration curve spanning 0 to 50,000 years BP based on paired Th-230/U-234/U-238 and C-14 dates on pristine corals. *Quaternary Science Reviews,* 24**,** 1781-1796.

FELIX, M. (2002) Flow structure of turbidity currents. *Sedimentology,* 49**,** 397-419.

FELIX, M., STURTON, S. & PEAKALL, J. (2005) Combined measurements of velocity and concentration in experimental turbidity currents. *Sedimentary Geology,* 179**,** 31-47.

FERRY, J.-N., MULDER, T., PARIZE, O. & RAILLARD, S. (2005) Concept of equilibrium profile in deep-water turbidite systems: effects of local physiographic changes on the nature of sedimentary process and the geometries of deposits *In Hodgson, D.M. and Flint, S.S. (Eds), Submarine slope systems: processes and products. Geological Society, London, Special Publications,* 244**,** 181-193.

FILDANI, A., HUBBARD, S. M., COVAULT, J. A., MAIER, K. L., ROMANS, B. W., TRAER, M. & ROWLAND, J. C. (2012) Erosion at inception of deep-sea channels. *Marine and Petroleum Geology,* doi: 10.1016/j.marpetgeo.2012.03.006.

FOLK, R. L. & WARD, W. (1957) Brazos River bar: a study in the significance of grain size parameters *Sedimentary Petrology,* 27**,** 3-26.

FRENZ, M., WYNN, R. B., GEORGIOPOULOU, A., BENDER, V. B., HOUGH, G., MASSON, D. G., TALLING, P. J. & CRONIN, B. T. (2008) Provenance and pathways of late Quaternary turbidites in the deep-water Agadir Basin, northwest African margin. *International Journal of Earth Sciences,* 98**,** 721-733.

FUKUSHIMA, Y. & PARKER, G. (1990) Numerical-simulation of powder-snow avalanches. *Journal of Glaciology,* 36**,** 229-237.

GARCIA, M. & PARKER, G. (1991) Entrainment of bed sediment into suspension. *Journal of Hydraulic Engineering-Asce,* 117**,** 414-435.

GARCIA, M. & PARKER, G. (1993) Experiments on the entrainment of sediment into suspension by a dense bottom current. *Journal of Geophysical Research-Oceans,* 98**,** 4793-4807.

GARCIA, M. H. (1994) Depositional turbidity currents laden with poorly sorted sediment. *Journal of Hydraulic Engineering-Asce,* 120**,** 1240-1263.

GIBBS, R. J., MATTHEWS, M. D. & LINK, D. A. (1971) RELATIONSHIP BETWEEN SPHERE SIZE AND SETTLING VELOCITY. *Journal of Sedimentary Petrology,* 41**,** 7-&.

GLADSTONE, C., PHILLIPS, J. C. & SPARKS, R. S. J. (1998) Experiments on bidisperse, constant-volume gravity currents: propagation and sediment deposition. *Sedimentology,* 45**,** 833-843.

GLADSTONE, C. & SPARKS, R. S. J. (2002) The significance of grain size breaks in turbidites and pyroclastic density current deposits. *Journal of Sedimentary Research,* 72**,** 182-191.

GOLDFINGER, C. (2011) Submarine Paleoseismology Based on Turbidite Records. IN CARLSON, C. A. & GIOVANNONI, S. J. (Eds.) *Annual Review of Marine Science, Vol 3.* Palo Alto, Annual Reviews.

GOLDFINGER, C., NELSON, C. H., JOHNSON, J. E. & SHIPBOARD SCI, P. (2003) Holocene earthquake records from the Cascadia subduction zone and northern San Andreas Fault based on precise dating of offshore turbidites. *Annual Review of Earth and Planetary Sciences,* 31**,** 555-577.

GORSLINE, D. S., DE DIEGO, T. & NAVA-SANCHEZ, E. H. (2000) Seismically triggered turbidites in small margin basins: Alfonso Basin, Western Gulf of California and Santa Monica Basin, California Borderland. *Sedimentary Geology,* 135**,** 21-35.

GRACIA, E., VIZCAINO, A., ESCUTIA, C., ASIOLI, A., RODES, A., PALLAS, R., GARCIA-ORELLANA, J., LEBREIRO, S. & GOLDFINGER, C. (2010) Holocene earthquake record offshore Portugal (SW Iberia): testing turbidite paleoseismology in a slow-convergence margin. *Quaternary Science Reviews,* 29**,** 1156-1172.

GRAY, T. E., ALEXANDER, J. & LEEDER, M. R. (2005) Quantifying velocity and turbulence structure in depositing sustained turbidity currents across breaks in slope. *Sedimentology,* 52**,** 467-488.

HALLWORTH, M. A., HUPPERT, H. E., PHILLIPS, J. C. & SPARKS, R. S. J. (1996) Entrainment into two-dimensional and axisymmetric turbulent gravity currents. *Journal of Fluid Mechanics,* 308**,** 289-311.

HAMPTON, M. A. (1975) COMPETENCE OF FINE-GRAINED DEBRIS FLOWS. *Journal of Sedimentary Petrology,* 45**,** 834-844.

HARRIS, T. C., HOGG, A. J. & HUPPERT, H. E. (2002) Polydisperse particle-driven gravity currents. *Journal of Fluid Mechanics,* 472**,** 333-371.

HAUGHTON, P., DAVIS, C., MCCAFFREY, W. & BARKER, S. (2009) Hybrid sediment gravity flow deposits - Classification, origin and significance. *Marine and Petroleum Geology,* 26**,** 1900-1918.

HAUGHTON, P. D. W. (1994) DEPOSITS OF DEFLECTED AND PONDED TURBIDITY ENTS, CURRENTS, SORBAS BASIN, SOUTHEAST SPAIN. *Journal of Sedimentary Research Section a-Sedimentary Petrology and Processes,* 64**,** 233-246.

HAUGHTON, P. D. W., BARKER, S. P. & MCCAFFREY, W. D. (2003) 'Linked' debrites in sand-rich turbidite systems - origin and significance. *Sedimentology,* 50**,** 459-482.

HAY, A. E. (1987) Turbidity Currents and Submarine Channel Formation in Rupert Inlet, Bristish Columbia 2. The roles of continuous and surge-type flow. *Journal of Geophysical Research,* 92**,** 2883-2900.

HEESE, R., CHOUGH, S. & RAKOFSKY, A. (1987) The Northwest Atlantic Mid-Ocean Channel of the Labrador Sea. V. Sedimentology of a giant deep-sea channel. *Canadian Journal of Earth Sciences,* 24**,** 1595-1624.

HEESE, R. & RAKOFSKY, A. (1992) Deep-Sea Channels/Submarine-Yazoo System of the Labrador Sea: A New Deep-Water Facies Model. *AAPG Bulletin,* 76**,** 680-707.

HEEZEN, B. C. & EWING, M. (1952) Turbidity currents and submarine slumps and the 1929 Grand Banks earthquake. *American Journal of Science,* 250**,** 849-873.

HEEZEN, B. C., EWING, M. & MENZIES, R. J. (1955) The influence of submarine turbidity currents on abyssal productivity. *Oikos,* 6**,** 170-182.

HEEZEN, B. C., MENZIES, R. J., SCHNEIDER, E. D., EWING, W. M. & GRANELLI, N. C. L. (1964) Congo Submarine Canyon. *Bull Amer Ass Petrol Geol,* 48**,** 1126-1149.

HESSE, R. (1989) Drainage systems associated with mid-ocean channels and submarine yazoos - Alternative to submarine fan depositional systems. *Geology,* 17**,** 1148-1151.

HESSE, R., CHOUGH, S. K. & RAKOFSKY, A. (1987) The northwest Atlantic mid-ocean channel of the Labrador Sea. 5. Sedimentology of a giant deep-sea channel. *Canadian Journal of Earth Sciences,* 24**,** 1595-1624.

HESSE, R., KLAUCKE, I., KHODABAKHSH, S., PIPER, D. J. W., RYAN, W. B. F. & GRP, N. S. (2001) Sandy submarine braid plains: Potential deep-water reservoirs. *Aapg Bulletin,* 85**,** 1499-1521.

HESSE, R., RAKOFSKY, A. & CHOUGH, S. K. (1990) The Central Labrador Sea: facies and dispersal patterns of clastic sediments in a small ocean basin. *Marine and Petroleum Geology,* 7**,** 13-28.

HISCOTT, R. N. (1994) Loss of capacity, not competence, as the fundamental process governing deposition from turbidity currents. *Journal of Sedimentary Research Section a-Sedimentary Petrology and Processes,* 64**,** 209-214.

HISCOTT, R. N., HALL, F. R. & PIRMEZ, C. (1997) Turbidity current overspill from the Amazon Channel: Texture of the silt/sand load, paleoflow from anisotropy of magnetic susceptibility and implications for flow processes. *In: Flood, R.D., Piper, D.J.W., Klaus, A., Peterson, L.C. (Eds.), Proceedings of the Ocean Drilling Program Scientific Results,* 155**,** 53-78.

HSU, S. K., KUO, J., LO, C. L., TSAI, C. H., DOO, W. B., KU, C. Y. & SIBUET, J. C. (2008) Turbidity currents, submarine landslides and the 2006 Pingtung earthquake off SW Taiwan. *Terrestrial Atmospheric and Oceanic Sciences,* 19**,** 767-772.

HUGHEN, K. A., BAILLIE, M. G. L., BARD, E., BECK, J. W., BERTRAND, C. J. H., BLACKWELL, P. G., BUCK, C. E., BURR, G. S., CUTLER, K. B., DAMON, P. E., EDWARDS, R. L., FAIRBANKS, R. G., FRIEDRICH, M., GUILDERSON, T. P., KROMER, B., MCCORMAC, G., MANNING, S., RAMSEY, C. B., REIMER, P. J., REIMER, R. W., REMMELE, S., SOUTHON, J. R., STUIVER, M., TALAMO, S., TAYLOR, F. W., VAN DER PLICHT, J. & WEYHENMEYER, C. E. (2004) Marine04 marine radiocarbon age calibration, 0-26 cal kyr BP. *Radiocarbon,* 46**,** 1059-1086.

HUNT, J. E., WYNN, R. B., MASSON, D. G., TALLING, P. J. & TEAGLE, D. A. H. (2011) Sedimentological and geochemical evidence for multistage failure of volcanic island landslides: A case study from Icod landslide on north Tenerife, Canary Islands. *Geochemistry Geophysics Geosystems,* 12**,** 1-36.

HUPPERT, H. E., TURNER, J. S. & HALLWORTH, M. A. (1995) SEDIMENTATION AND ENTRAINMENT IN DENSE LAYERS OF SUSPENDED PARTICLES STIRRED BY AN OSCILLATING-GRID. *Journal of Fluid Mechanics,* 289**,** 263-293.

HUVENNE, V. A. I., MCPHAIL, S. D., WYNN, R. B., FURLONG, M. & STEVENSON, P. (2009) Mapping giant scours in the deep ocean. *Eos,* 90**,** 274-275.

ILSTAD, T., ELVERHOI, A., ISSLER, D. & MARR, J. G. (2004) Subaqueous debris flow behaviour and its dependence on the sand/clay ratio: a laboratory study using particle tracking. *Marine Geology,* 213**,** 415-438.

JHA, S. K. & BOMBARDELLI, F. A. (2010) Toward two-phase flow modeling of nondilute sediment transport in open channels. *Journal of Geophysical Research-Earth Surface,* 115**,** 27.

JOHANSSON, M., BRAAKENBURG, N. E., STOW, D. A. V. & FAUGERES, J. C. (1998) Deep-water massive sands: facies, processes and channel geometry in the Numidian Flysch, Sicily. *Sedimentary Geology,* 115**,** 233-265.

JONES, K. P. N., MCCAVE, I. N. & WEAVER, P. P. E. (1992) Textural and dispersal patterns of thick mud turbidites from the Madeira Abyssal Plain. *Marine Geology,* 107**,** 149-173.

KANE, I. A. & HODGSON, D. M. (2011) Sedimentological criteria to differentiate submarine channel levee subenvironments: Exhumed examples from the Rosario Fm. (Upper Cretaceous) of Baja California, Mexico, and the Fort Brown Fm. (Permian), Karoo Basin, S. Africa. *Marine and Petroleum Geology,* 28**,** 807-823.

KANE, I. A., KNELLER, B. C., DYKSTRA, M., KASSEM, A. & MCCAFFREY, W. D. (2007) Anatomy of a submarine channel-levee: An example from Upper Cretaceous slope sediments, Rosario Formation, Baja California, Mexico. *Marine and Petroleum Geology,* 24**,** 540-563.

KANE, I. A., MCCAFFREY, B., PEAKALL, J. & KNELLER, B. (2010) Submarine channel levee shape and sediment waves from physical experiments. *Sedimentary Geology,* 223**,** 75-85.

KINEKE, G. C. & STERNBERG, R. W. (1995) DISTRIBUTION OF FLUID MUDS ON THE AMAZON CONTINENTAL-SHELF. *Marine Geology,* 125**,** 193-233.

KLAUCKE, I., HESSE, R. & RYAN, W. B. F. (1997) Flow parameters of turbidity currents in a low-sinuosity giant deep-sea channel. *Sedimentology,* 44**,** 1093-1102.

KLAUCKE, I., HESSE, R. & RYAN, W. B. F. (1998) Seismic stratigraphy of the Northwest Atlantic Mid-Ocean Channel: growth pattern of a mid-ocean channel-levee complex. *Marine and Petroleum Geology,* 15**,** 575-585.

KNELLER, B. & BUCKEE, C. (2000) The structure and fluid mechanics of turbidity currents: a review of some recent studies and their geological implications. *Sedimentology,* 47**,** 62-94.

KNELLER, B., EDWARDS, D., MCCAFFREY, W. & MOORE, R. (1991) Oblique reflection of turbidity currents. *Geology,* 19**,** 250-252.

KNELLER, B. C., BENNETT, S. J. & MCCAFFREY, W. D. (1997) Velocity and turbulence structure of density currents and internal solitary waves: potential sediment transport and the formation of wave ripples in deep water. *Sedimentary Geology,* 112**,** 235-250.

KNELLER, B. C., BENNETT, S. J. & MCCAFFREY, W. D. (1999) Velocity structure, turbulence and fluid stresses in experimental gravity currents. *Journal of Geophysical Research-Oceans,* 104**,** 5381-5391.

KNELLER, B. C. & BRANNEY, M. J. (1995) Sustained high-density turbity currents and the deposition of thick massive sands. *Sedimentology,* 42**,** 607-616.

KNELLER, B. C. & MCCAFFREY, W. D. (1999) Depositional effects of flow non-uniformity and stratification within turbidity currents approaching a bounding slope: deflection, reflection and facies variation. *Journal of Sedimentary Research,* 69**,** 980-991.

KNELLER, B. C. & MCCAFFREY, W. D. (2003) The interpretation of vertical sequences in turbidite beds: The influence of longitudinal flow structure. *Journal of Sedimentary Research,* 73**,** 706-713.

KOMAR, P. D. (1969) Channelized Flow of Turbidity Currents with

Application to Monterey Deep-Sea Fan Channel. *Journal of Geophysical Research,* 74**,** 4544-4553.

KOMAR, P. D. (1971) Hydraulic jumps in turbidity currents. *Geological Society of America Bulletin,* 82**,** 1477-1488.

KOMAR, P. D. (1985) THE HYDRAULIC INTERPRETATION OF TURBIDITES FROM THEIR GRAIN SIZES AND SEDIMENTARY STRUCTURES. *Sedimentology,* 32**,** 395-407.

KRAUSE, D. C., WHITE, W. C., PIPER, D. J. W. & HEEZEN, B. C. (1970) TURBIDITY CURRENTS AND CABLE BREAKS IN WESTERN NEW-BRITAIN-TRENCH. *Geological Society of America Bulletin,* 81**,** 2153-&.

KRIPOUNOFF, A., VANGRIESHEIM, A., BABONNEAU, N., CRASSOUS, P., DENNIELOU, B. & SAVOYE, B. (2003) Direct observation of intense turbidity current activity in the Zaire submarine valley at 4000 m water depth. *Marine Geology,* 194**,** 151-158.

KUBO, Y. (2004) Experimental and numerical study of topographic effects on deposition from two-dimensional, particle-driven density currents. *Sedimentary Geology,* 164**,** 311-326.

KUENEN, P. H. (1966) Experimental turbidite lamination in a circular flume. *Journal of Geology,* 74**,** 523-545.

KUENEN, P. H. & MIGLIORINI, C. I. (1950) Turbidity currents as a cause of graded bedding. *Journal of Geology,* 58**,** 91-127.

LAMB, M. P., MCELROY, B., KOPRIVA, B., SHAW, J. & MOHRIG, D. (2010) Linking river-flood dynamics to hyperpycnal-plume deposits: Experiments, theory, and geological implications. *Geological Society of America Bulletin,* 122**,** 1389-1400.

LEBREIRO, S. M., MCCAVE, I. N. & WEAVER, P. P. E. (1997) Late Quaternary turbidite emplacement on the Horseshoe abyssal plain (Iberian margin). *Journal of Sedimentary Research,* 67**,** 856-870.

LISIECKI, L. E. & RAYMO, M. E. (2005) A Pliocene-Pleistocene stack of 57 globally distributed benthic delta O-18 records. *Paleoceanography,* 20**,** 17.

LOWE, D. R. (1982) Sediment gravity flows .2. Depositional models with special reference to the deposits of high-density turbidity currents. *Journal of Sedimentary Petrology,* 52**,** 279-298.

MACDONALD, H. A., WYNN, R. B., HUVENNE, V. A. I., PEAKALL, J., MASSON, D. G., WEAVER, P. P. E. & MCPHAIL, S. D. (2011) New insights into the morphology, fill, and remarkable longevity (>0.2 m.y.) of modern deep-water erosional scours along the northeast Atlantic margin. *Geosphere,* 7**,** 845-867.

MARR, J. G., HARFF, P. A., SHANMUGAM, G. & PARKER, G. (2001) Experiments on subaqueous sandy gravity flows: The role of clay and water content in flow dynamics and depositional structures. *Geological Society of America Bulletin,* 113**,** 1377-1386.

MARTI, J., MITJAVILA, J. & ARANA, V. (1994) STRATIGRAPHY, STRUCTURE AND GEOCHRONOLOGY OF THE LAS CANADA CALDERA (TENERIFE, CANARY-ISLANDS). *Geological Magazine,* 131**,** 715-727.

MASSON, D. G. (1994) Late Quaternary turbidity current pathways to the Madeira Abyssal Plain and some constraints on turbidity current mechanisms. *Basin Research,* 6**,** 17-33.

MASSON, D. G., ARZOLA, R. G., WYNN, R. B., HUNT, J. E. & WEAVER, P. P. E. (2011) Seismic triggering of landslides and turbidity currents offshore Portugal. *Geochemistry Geophysics Geosystems,* 12**,** 19.

MASSON, D. G., WYNN, R. B. & TALLING, P. J. (2010) Large Landslides on Passive Continental Margins: Processes, Hypotheses and Outstanding Questions. IN MOSHER, D. C., SHIPP, R. C., MOSCARDELLI, L., CHAYTOR, J. D., BAXTER, C. D. P., LEE, H. J. & URGELES, R. (Eds.) *Submarine Mass Movements and Their Consequences*. Dordrecht, Springer.

MCANALLY, W. H., FRIEDRICHS, C., HAMILTON, D., HAYTER, E., SHRESTHA, P., RODRIGUEZ, H., SHEREMET, A., TEETER, A. & FLU, A. T. C. M. (2007a) Management of fluid mud in estuaries, bays, and lakes. I: Present state of understanding on character and behavior. *Journal of Hydraulic Engineering-Asce,* 133**,** 9-22.

MCANALLY, W. H., TEETER, A., SCHOELLHAMER, D., FRIEDRICHS, C., HAMILTON, D., HAYTER, E., SHRESTHA, P., RODRIGUEZ, H., SHEREMET, A., KIRBY, R. & FL, A. T. C. M.

(2007b) Management of fluid mud in estuaries, bays, and lakes. II: Measurement, modeling, and management. *Journal of Hydraulic Engineering-Asce,* 133**,** 23-38.

MCCAFFREY, W. D., CHOUX, C. M., BAAS, J. H. & HAUGHTON, P. D. W. (2003) Spatio-temporal evolution of velocity structure, concentration and grainsize stratification within experimental particulate gravity currents. *Marine and Petroleum Geology,* 20**,** 851-860.

MCCAVE, I. N. & JONES, K. P. N. (1988) Deposition of ungraded muds from high-density non-turbulent turbidity currents. *Nature,* 333**,** 250-252.

MCHARGUE, T., PYRCZ, M. J., SULLIVAN, M. D., CLARK, J. D., FILDANI, A., ROMANS, B. W., COVAULT, J. A., LEVY, M., POSAMENTIER, H. W. & DRINKWATER, N. J. (2011) Architecture of turbidite channel systems on the continental slope: Patterns and predictions. *Marine and Petroleum Geology,* 28**,** 728-743.

MCMASTER, R. L. & LACHANCE, T. P. (1969) Northwestern African Continental Shelf Sediments. *Marine Geology,* 7**,** 57-67.

MEDIALDEA, T., VEGAS, R., SOMOZA, L., VAZQUEZ, J. T., MALDONADO, A., DIAZ-DEL-RIO, V., MAESTRO, A., CORDOBA, D. & FERNANDEZ-PUGA, M. C. (2004) Structure and evolution of the "Olistostrome" complex of the Gibraltar Arc in the Gulf of Cadiz (eastern Central Atlantic): evidence from two long seismic cross-sections. *Marine Geology,* 209**,** 173.

MEHTA, A. J., HAYTER, E. J., PARKER, W. R., KRONE, R. B. & TEETER, A. M. (1989) COHESIVE SEDIMENT TRANSPORT .1. PROCESS DESCRIPTION. *Journal of Hydraulic Engineering-Asce,* 115**,** 1076-1093.

MIDDLETON, G. V. (1993) Sediment deposition from turbidity currents. *Annual Reviews Earth and Planetary Sciences,* 21**,** 89-114.

MIGEON, S., SAVOYE, B., ZANELLA, E., MULDER, T., FAUGERES, J. C. & WEBER, O. (2001) Detailed seismic-reflection and sedimentary study of turbidite sediment waves on the Var Sedimentary Ridge (SE France): significance for sediment transport and deposition and for the mechanisms of sediment-wave construction. *Marine and Petroleum Geology,* 18**,** 179-208.

MOHRIG, D. & MARR, J. G. (2003) Constraining the efficiency of turbidity current generation from submarine debris flows and slides using laboratory experiments. *Marine and Petroleum Geology,* 20**,** 883-899.

MOORE, D. W., YOUNG, L. E., MODENE, J. S. & PLAHUTA, J. T. (1986) Geologic setting a genesis of the Red Dog zinc-lead-silver deposit, Western Brookes range, Alaska. *Economic Geology,* 81**,** 696-727.

MOSHER, D. C., MOSCARDELLI, L., SHIPP, R. C., CHAYTOR, J. D., BAXTER, C. D. P., LEE, H. J. & URGELES, R. (2010) *Submarine Mass Movements and Their Consequences,* Dordrecht, Springer.

MULDER, T. & ALEXANDER, J. (2001a) Abrupt change in slope causes variation in the deposit thickness of concentrated particle-driven density currents. *Marine Geology,* 175**,** 221-235.

MULDER, T. & ALEXANDER, J. (2001b) The physical character of subaqueous sedimentary density flows and their deposits. *Sedimentology,* 48**,** 269-299.

MULDER, T. & SYVITSKI, J. P. M. (1995) Turbidity currents generated at river mouths during exceptional discharges into the world oceans. *Journal of Geology,* 103**,** 285-299.

MUTTI, E. (1992) Turbidite Sandstones. *San Donato, Milanese, Parma, Agip***,** 275.

MUTTI, E., LUCCHI, F. & ROVERI, M. (2002) Revisiting turbidites of the Marnoso Arenacea Formation and their Basin-Margin equivalents: Problems with classic models. *Excursion Guidebook, 64th EAGE Conferene and Exhibition***,** 52.

NARUSE, H., SEQUEIROS, O., GARCIA, M. H., PARKER, G., ENDO, N., KATAOKA, K. S., YOKOKAWA, M. & MUTO, T. (2008) Self-accelerating turbidity currents at laboratory scale. *River, Coastal and Estuarine Morphodynamics: Rcem 2007, Vols 1 and 2***,** 473-476.

NORMARK, W. R. (1978) Fan Valleys, Channels, and Depositional Lobes on Modern Submarine Fans - characters for recognition of sandy turbidite environments. *Aapg Bulletin-American Association of Petroleum Geologists,* 62**,** 912-931.

NORMARK, W. R., PAULL, C. K., CARESS, D. W., USSLER, W. & SLITER, R. (2009) Fine-scale relief related to Late Holocene channel shifting within the floor of the upper Redondo Fan, offshore Southern California. *Sedimentology,* 56**,** 1690-1704.

NORMARK, W. R., PIPER, D. J. W. & HESS, G. R. (1979) Distributary channels, sand lobes, and meso-topography of Navy Submarine Fanm California Borderland, with applications to ancient fan sediments. *Sedimentology,* 26**,** 749-774.

ORLINS, J. J. & GULLIVER, J. S. (2003) Turbulence quantification and sediment resuspension in an oscillating grid chamber. *Experiments in Fluids,* 34**,** 662-677.

OTSUBO, K. & MURAOKA, K. (1988) CRITICAL SHEAR-STRESS OF COHESIVE BOTTOM SEDIMENTS. *Journal of Hydraulic Engineering-Asce,* 114**,** 1241-1256.

PANTIN, H. M. (1979) Interaction between velocity and effective density in turbidity flow-phase-plane analysis, with criteria for autosuspension. *Marine Geology,* 31**,** 59-99.

PANTIN, H. M. (2001) Experimental evidence for autosuspension. IN MCCAFFREY, W., KNELLER, B. & PEAKALL, J. (Eds.) *Particulate Gravity Currents*. Oxford, Blackwell Science Publ.

PANTIN, H. M. & FRANKLIN, M. C. (2011) Improved experimental evidence for autosuspension. *Sedimentary Geology,* 237**,** 46-54.

PARKER, G. (1982) Conditions for the ignition of catastrophically erosive turbidity currents. *Marine Geology,* 46**,** 307-327.

PARKER, G., FUKUSHIMA, Y. & PANTIN, H. M. (1986) Self-accelerating turbidity currents. *Journal of Fluid Mechanics,* 171**,** 145-181.

PARKER, G., GARCIA, M., FUKUSHIMA, Y. & YU, W. (1987) Experiments on turbidity currents over an erodible bed. *Journal of Hydraulic Research,* 25**,** 123-147.

PEAKALL, J., MCCAFFREY, B. & KNELLER, B. (2000) A process model for the evolution, morphology, and architecture of sinuous submarine channels. *Journal of Sedimentary Research,* 70**,** 434-448.

PEARCE, T. J. & JARVIS, I. (1992) Composition and provenance of turbidite sands - Late Quaternary, Madeira Abyssal Plain. *Marine Geology,* 109**,** 21-51.

PEARCE, T. J. & JARVIS, I. (1995) High-resolution chemostratigraphy of Quaternary distal turbidites: a case study of new methods for the analysis and correlation of barre sequences. *In: Dunay,*

R.E., Hailwood, E.A. (Eds.), Non-Biostratigraphical Methods of Dating and Correlation. Geol. Soc. Spec. Publ. , 89**,** 107-143.

PICKERING, K. T. & HISCOTT, R. N. (1985) Contained (reflected) turbidity currents from the Middle Ordivician Cloridorme Formation, Quebec, Canada - An alternative to the antidune hypothesis. *Sedimentology,* 32**,** 373-394.

PIPER, D. J. W. (1972) Turbidite origin of some laminated mudstones. *Geological Magazine,* 109**,** 115-&.

PIPER, D. J. W. (1978) Turbidite muds and silts on deepsea fans and abyssal plains. *In (eds. Stanley, D. J. and Kelling, G.) Sedimentation in submarine canyons, fans and trenches, Dowden, Hutchinsion and Ross***,** 163-176.

PIPER, D. J. W., COCCHONAT, P. & MORRISON, M. L. (1999) The sequence of events around the epicentre of the 1929 Grand Banks earthquake: initiation of debris flows and turbidity current inferred from sidescan sonar. *Sedimentology,* 46**,** 79-97.

PIPER, D. J. W. & SAVOYE, B. (1993) Processes of Late Quaternary turbidity-current flow and deposition on the Var deep-sea fan, North-west Mediterranean Sea. *Sedimentology,* 40**,** 557-582.

PIRMEZ, C. & IMRAN, J. (2003) Reconstruction of turbidity currents in Amazon Channel. *Marine and Petroleum Geology,* 20**,** 823-849.

REIMER, P. J., BAILLIE, M. G. L., BARD, E., BAYLISS, A., BECK, J. W., BERTRAND, C. J. H., BLACKWELL, P. G., BUCK, C. E., BURR, G. S., CUTLER, K. B., DAMON, P. E., EDWARDS, R. L., FAIRBANKS, R. G., FRIEDRICH, M., GUILDERSON, T. P., HOGG, A. G., HUGHEN, K. A., KROMER, B., MCCORMAC, G., MANNING, S., RAMSEY, C. B., REIMER, R. W., REMMELE, S., SOUTHON, J. R., STUIVER, M., TALAMO, S., TAYLOR, F. W., VAN DER PLICHT, J. & WEYHENMEYER, C. E. (2004) IntCal04 terrestrial radiocarbon age calibration, 0-26 cal kyr BP. *Radiocarbon,* 46**,** 1029-1058.

REMACHA, E., FERNANDEZ, L. P. & MAESTRO, E. (2005) The transition between sheet-like lobe and basin-plain turbidites in the Hecho basin (South-Central Pyrenees, Spain). *Journal of Sedimentary Research,* 75**,** 798-819.

RICHARDSON, J. F. & ZAKI, W. N. (1954) Sedimentation and fluidization: Part 1. *Transactions of the Institute of Chemical Engineers,* 32**,** 35-53.

ROCA, A., IZQUIERDO, A., SOUSA-OLIVEIRA, C. & MARTINEZ-SOLARES, J. M. (2004) An outline of earthquake catalogues, databases and studies of historical seismicity in the Iberian Peninsula. *Annals of Geophysics,* 47**,** 561-570.

ROHLING, E. J., GRANT, K., BOLSHAW, M., ROBERTS, A. P., SIDDALL, M., HEMLEBEN, C. & KUCERA, M. (2009) Antarctic temperature and global sea level closely coupled over the past five glacial cycles. *Nature Geoscience,* 2**,** 500-504.

ROTHWELL, R. G., HOOGAKKER, B., THOMSON, J., CROUDACE, I. W. & FRENZ, M. (2006) Turbidite emplacement on the southern Balearic Abyssal Plain (Western Mediterranean Sea) during Marine Isotope Stages 1–3: an application of ITRAX XRF scanning of sediment cores to lithostratigraphic analysis. *In: Rothwell RG (ed) New techniques in sediment core analysis. Geological Society London, Special Publication,* 267**,** 79-89.

ROTHWELL, R. G., PEARCE, T. J. & WEAVER, P. P. E. (1992) Late Quaternary Evolution of the Madeira Abyssal Plain, Canary Basin, NE Atlantic. *Basin Research,* 4**,** 103-131.

ROUSE, H. (1937) Modern conceptions of the mechanics of fluid turbulence. *Transactions of the American Society of Civil Engineers,* 102**,** 463-543.

SALAHELDIN, T. M., IMRAN, J., CHAUDHRY, M. H. & REED, C. (2000) Role of fine-grained sediment in turbidity current flow dynamics and resulting deposits. *Marine Geology,* 171**,** 21-38.

SEQUEIROS, O. E., NARUSE, H., ENDO, N., GARCIA, M. H. & PARKER, G. (2009) Experimental study on self-accelerating turbidity currents. *Journal of Geophysical Research-Oceans,* 114.

SHANMUGAM, G. (1996) High-density turbidity currents: Are they sandy debris flows? *Journal of Sedimentary Research,* 66**,** 2-10.

SHANMUGAM, G. (2000) 50 years of the turbidite paradigm (1950s-1990s): deep-water processes and facies models - a critical perspective. *Marine and Petroleum Geology,* 17**,** 285-342.

SHIKI, T., KUMON, F., INOUCHI, Y., KONTANI, Y., SAKAMOTO, T., TATEISHI, M., MATSUBARA, H. & FUKUYAMA, K. (2000) Sedimentary features of the seismo-turbidites, Lake Biwa, Japan. *Sedimentary Geology,* 135**,** 37-50.

SINCLAIR, H. D. & COWIE, P. A. (2003) Basin-floor topography and the scaling of turbidites. *Journal of Geology,* 111**,** 277-299.

SPARKS, R. S. J., BONNECAZE, R. T., HUPPERT, H. E., LISTER, J. R., HALLWORTH, M. A., MADER, H. & PHILLIPS, J. (1993) SEDIMENT-LADEN GRAVITY CURRENTS WITH REVERSING BUOYANCY. *Earth and Planetary Science Letters,* 114**,** 243-257.

STEVENSON, C. J. & PEAKALL, J. (2010) Effects of topography on lofting gravity flows: Implications for the deposition of deep-water massive sands. *Marine and Petroleum Geology,* 27**,** 1366-1378.

STEVENSON, C. J., TALLING, P. J., WYNN, R. B., MASSON, D. G., HUNT, J. E., FRENZ, M., AKHMETZHANOV, A. & CRONIN, B. T. (2012) The flows that left no trace: very large-volume turbidity currents that bypassed sediment through submarine channels without eroding the seafloor. *Marine and Petroleum Geology***,** In Press.

STOW, D. A. & SHAMUGAM, G. (1980) Sequence of structures in fine-grained turbidites: Comparison of recent deep-sea and ancient flysch sediments. *Sedimentary Geology,* 25**,** 23-42.

STOW, D. A. V. & BOWEN, A. J. (1978) ORIGIN OF LAMINATION IN DEEP-SEA, FINE-GRAINED SEDIMENTS. *Nature,* 274**,** 324-328.

STOW, D. A. V. & BOWEN, A. J. (1980) A physical model for the transport and sorting of fine-grained sediment by turbidity currents. *Sedimentology,* 27**,** 31-46.

STOW, D. A. V. & MAYALL, M. (2000) Deep-water sedimentary systems: New models for the 21st century. *Marine and Petroleum Geology,* 17**,** 125-135.

STOW, D. A. V. & PIPER, D. J. W. (1984) Deep-water fine-grained sediments: facies models. *In: Stow, D. A. V. and Piper, D. J. W. (eds), Fine-grained sediments: Deep-water processes and facies. The Geological Society***,** 611-646.

STRAUB, K. M. & MOHRIG, D. (2008) Quantifying the morphology and growth of levees in aggrading submarine channels. *Journal of Geophysical Research-Earth Surface,* 113**,** 20.

SUMMERHAYES, C. P., MILLIMAN, J. D., BRIGGS, S. R., BEE, A. G. & HOGAN, C. (1976) NORTHWEST AFRICAN SHELF SEDIMENTS - INFLUENCE OF CLIMATE AND SEDIMENTARY PROCESSES. *Journal of Geology,* 84**,** 277-300.

SUMMERHAYES, C. P., NUTTER, A. H. & TOOMS, J. S. (1972) The distribution and origin of phosphate in sediments off northwest africa. *Sedimentary Geology,* 8**,** 3-28.

SUMNER, E. J., AMY, L. A. & TALLING, P. J. (2008) Deposit structure and processes of sand deposition from decelerating sediment suspensions. *Journal of Sedimentary Research,* 78**,** 529-547.

SUMNER, E. J., TALLING, P. J., AMY, L., WYNN, R. B., STEVENSON, C. J. & FRENZ, M. (2012) Facies architecture of individual basin-plain turbidites: Comparison to existing models and implications for flow processes. *Sedimentology,* DOI: 10.1111/j.1365-3091.2012.01329.x.

SUMNER, E. J., TALLING, P. J. & AMY, L. A. (2009) Deposits of flows transitional between turbidity current and debris flow. *Geology,* 37**,** 991-994.

SYVITSKI, J. P. M. (2003) Supply and flux of sediment along hydrological pathways: research for the 21st century. *Global and Planetary Change,* 39**,** 1-11.

SYVITSKI, J. P. M., PECKHAM, S. D., HILBERMAN, R. & MULDER, T. (2003) Predicting the terrestrial flux of sediment to the global ocean: a planetary perspective. *Sedimentary Geology,* 162**,** 5-24.

TALLING, P. J., AMY, L. A. & WYNN, R. B. (2007a) New insight into the evolution of large-volume turbidity currents: comparison of turbidite shape and previous modelling results. *Sedimentology,* 54**,** 737-769.

TALLING, P. J., AMY, L. A., WYNN, R. B., BLACKBOURN, G. & GIBSON, O. (2007b) Evolution of turbidity currents deduced from extensive thin turbidites: Marnoso Arenacea Formation (Miocene), Italian Apennines. *Journal of Sedimentary Research,* 77**,** 172-196.

TALLING, P. J., AMY, L. A., WYNN, R. B., PEAKALL, J. & ROBINSON, M. (2004) Beds comprising debrite sandwiched within co-genetic turbidite: origin and widespread occurrence in distal depositional environments. *Sedimentology,* 51**,** 163-194.

TALLING, P. J., MASSON, D. G., SUMNER, E. J. & MALGESINI, G. (in press) Subaqueous sediment density flows: Depositional Processes and Deposit types. *Sedimentology*.

TALLING, P. J., WYNN, R. B., MASSON, D. G., FRENZ, M., CRONIN, B. T., SCHIEBEL, R., AKHMETZHANOV, A. M., DALLMEIER-TIESSEN, S., BENETTI, S., WEAVER, P. P. E., GEORGIOPOULOU, A., ZUHLSDORFF, C. & AMY, L. A. (2007c) Onset of submarine debris flow deposition far from original giant landslide. *Nature,* 450**,** 541-544.

TOMKINS, M. R., BALDOCK, T. E. & NIELSEN, P. (2005) Hindered settling of sand grains. *Sedimentology,* 52**,** 1425-1432.

TORFS, H., MITCHENER, H., HUYSENTRUYT, H. & TOORMAN, E. (1996) Settling and consolidation of mud/sand mixtures. *Coastal Engineering,* 27-45**,** 27-45.

TROWBRIDGE, J. H. & KINEKE, G. C. (1994) STRUCTURE AND DYNAMICS OF FLUID MUDS ON THE AMAZON CONTINENTAL-SHELF. *Journal of Geophysical Research-Oceans,* 99**,** 865-874.

VAIL, P. R., MITCHUM, R. M. & THOMPSON, S. (1977) Seismic stratigraphy and global changes in sea level, Part 4, Global cycles of relative changes in sea level. *In (Ed. Payton, C.E.) Seismic stratigraphy-Applications to hydrocarbon exploration, American Association of Petroleum Geologists Memoir,* 26**,** 83-97.

VAN TASSELL, J. (1981) SILVER ABYSSAL-PLAIN CARBONATE TURBIDITE - FLOW CHARACTERISTICS. *Journal of Geology,* 89**,** 317-333.

VAN TASSELL, J. (1986) THE HYDRAULIC INTERPRETATION OF TURBIDITES FROM THEIR GRAIN SIZES AND SEDIMENTARY STRUCTURES. *Sedimentology,* 33**,** 437-438.

VANGRIESHEIM, A., KHRIPOUNOFF, A. & CRASSOUS, P. (2009) Turbidity events observed in situ along the Congo submarine channel. *Deep-Sea Research Part Ii-Topical Studies in Oceanography,* 56**,** 2208-2222.

VROLIJIK, P. J. & SOUTHARD, J. B. (1997) Experiments on rapid deposition of sand from high-velocity flows *Geoscience Canada,* 24**,** 45-54.

WATTS, A. B. & MASSON, D. G. (1995) A giant landslide on the north flank of Tenerife, Canary Islands. *Journal of Geophysical Research-Solid Earth,* 100**,** 24487-24498.

WEAVER, P. P. E. (1991) Quaternary high-resolution stratigraphy and its application in studies of the Canary Basin. *Aapg Bulletin-American Association of Petroleum Geologists,* 75**,** 1424-1424.

WEAVER, P. P. E. (1994) Determination of turbidity current erosional characteristics from reworked coccolith assemblages, Canary Basinm northeast Atlantic. *Sedimentology,* 41**,** 1025-1038.

WEAVER, P. P. E., CHAPMAN, M. R., EGLINTON, G., ZHAO, M., RUTLEDGE, D. & READ, G. (1999) Combined coccolith, foraminiferal, and biomarker reconstruction of paleoceanographic conditions over the past 120 kyr in the northern North Atlantic (59 degrees N, 23 degrees W). *Paleoceanography,* 14**,** 336-349.

WEAVER, P. P. E. & KUIJPERS, A. (1983) Climatic control of turbidite deposition on the Madeira Abyssal Plain. *Nature,* 306**,** 360-363.

WEAVER, P. P. E. & KUIJPERS, A. (1986) Turbidite deposition and the origin of the Madeira Abyssal Plain. . *In: Summerhayes, C.P., Shackleton, N.J. (Eds.), North Atlantic Paleoceanography. Geol. Soc. Spec. Publ. ,* 21**,** 131-143.

WEAVER, P. P. E. & ROTHWELL, R. G. (1987) Sedimentation on the Madeira Abyssal Plain over the last 300,000 years. . *In: Weaver, P.P.E., Thomson, J. (Eds.), Geology and Geochemistry of Abyssal Plains. Geol. Soc. Spec. Publ. No. 31, pp. 71–86.,* 31**,** 71-86.

WEAVER, P. P. E., ROTHWELL, R. G., EBBING, J., GUNN, D. & HUNTER, P. M. (1992) Correlation, frequentcy of emplacement and source directions of megaturbidites on the Madeira Abyssal Plain. *Marine Geology,* 109**,** 1-20.

WEAVER, P. P. E. & THOMSON, J. (1993) Calculating erosion by deep-sea turbidity currents during initiation and flow. *Nature,* 364**,** 136-138.

WEAVER, P. P. E., WYNN, R. B., KENYON, N. H. & EVAN, J. (2000) Continental margin sedimentation, with special reference to the north-east Atlantic margin. *Sedimentology,* 47**,** 239-256.

WHITEHOUSE, R., SOULSBY, R., ROBERTS, W. & MITCHENER, H. (2000) Dynamics of Estuarine Muds. . *HR Wallingford and Thomas Telford, London***,** 210.

WOODS, A. W., BURSIK, M. I. & KURBATOV, A. V. (1998) The interaction of ash flows with ridges. *Bulletin of Volcanology,* 60**,** 38-51.

WRIGHT, L. D. (1985) River Deltas. *In: Davies Jr., R.A. (Ed.) Coastal Sedimentary Environments, 2nd edition. Sptinger, New York***,** 1-76.

WRIGHT, L. D., FRIEDRICHS, C. T., KIM, S. C. & SCULLY, M. E. (2001) Effects of ambient currents and waves on gravity-driven sediment transport on continental shelves. *Marine Geology,* 175**,** 25-45.

WYNN, R. B., CRONIN, B. T. & PEAKALL, J. (2007) Sinuous deep-water channels: Genesis, geometry and architecture. *Marine and Petroleum Geology,* 24**,** 341-387.

WYNN, R. B., KENYON, N. H., MASSON, D. G., STOW, D. A. V. & WEAVER, P. P. E. (2002a) Characterization and recognition of deep-water channel-lobe transition zones. *Aapg Bulletin,* 86**,** 1441-1462.

WYNN, R. B., MASSON, D. G., STOW, D. A. V. & WEAVER, P. P. E. (2000) The Northwest African slope apron: a modern analogue for deep-water systems with complex seafloor topography. *Marine and Petroleum Geology,* 17**,** 253-265.

WYNN, R. B., TALLING, P. J., MASSON, D. G., LE BAS, T. P., CRONIN, B. T. & STEVENSON, C. J. (in press) The influence of subtle gradient changes on deep-water gravity flows: a case study from the Moroccan Turbidite system. *SEPM Special Publication*.

WYNN, R. B., TALLING, P. J., MASSON, D. G., STEVENSON, C. J., CRONIN, B. T. & LE BAS, T. P. (2010) Investigating the Timing, Processes and Deposits of One of the World's Largest Submarine Gravity Flows: The 'Bed 5 Event' Off Northwest Africa. IN MOSHER, D. C., SHIPP, R. C., MOSCARDELLI, L., CHAYTOR, J. D., BAXTER, C. D. P., LEE, H. J. & URGELES, R. (Eds.) *Submarine Mass Movements and Their Consequences*. Dordrecht, Springer.

WYNN, R. B., WEAVER, P. P. E., MASSON, D. G. & STOW, D. A. V. (2002b) Turbidite depositional architecture across three interconnected deep-water basins on the north-west African margin. *Sedimentology,* 49**,** 669-695.

XU, J. P., NOBLE, M. A. & ROSENFELD, L. K. (2004) In-situ measurements of velocity structure within turbidity currents. *Geophysical Research Letters,* 31**,** 4 pp.-4 pp.4 pp.

ZAKERI, A. (2008) A potentially devastating offshore geohazard - submarine debris flow impact on piplines. *Exploration and Production Oil and Gas Review,* 6**,** 118 - 121.

ZENG, J. J. & LOWE, D. R. (1997) Numerical simulation of turbidity current flow and sedimentation .2. Results and geological applications. *Sedimentology,* 44**,** 85-104.

10 Appendix

This appendix contains additional grain size data collected from deposits in the Agadir Basin. This data was used to construct the vertical grain-size profiles for Beds A3, A5, A7, A11 and A12 within the Agadir Basin (Chapter 4). Also included in the appendix is down core multi-sensor core log data, comprising: P-wave velocity, gamma-ray density and magnetic susceptibility. Micha Frenz carried out the multi-sensor core log analyses. Gamma-ray density is used to estimate the bulk density of surface hemipelagic sediments across the Agadir Basin. In turn this is used to calculate erosion thresholds for the hemipelagic sediments (Chapter 4).

10.1 Grain-size data for Beds 3, 5, 7, 11 and 12

10.1.1 Bed 3

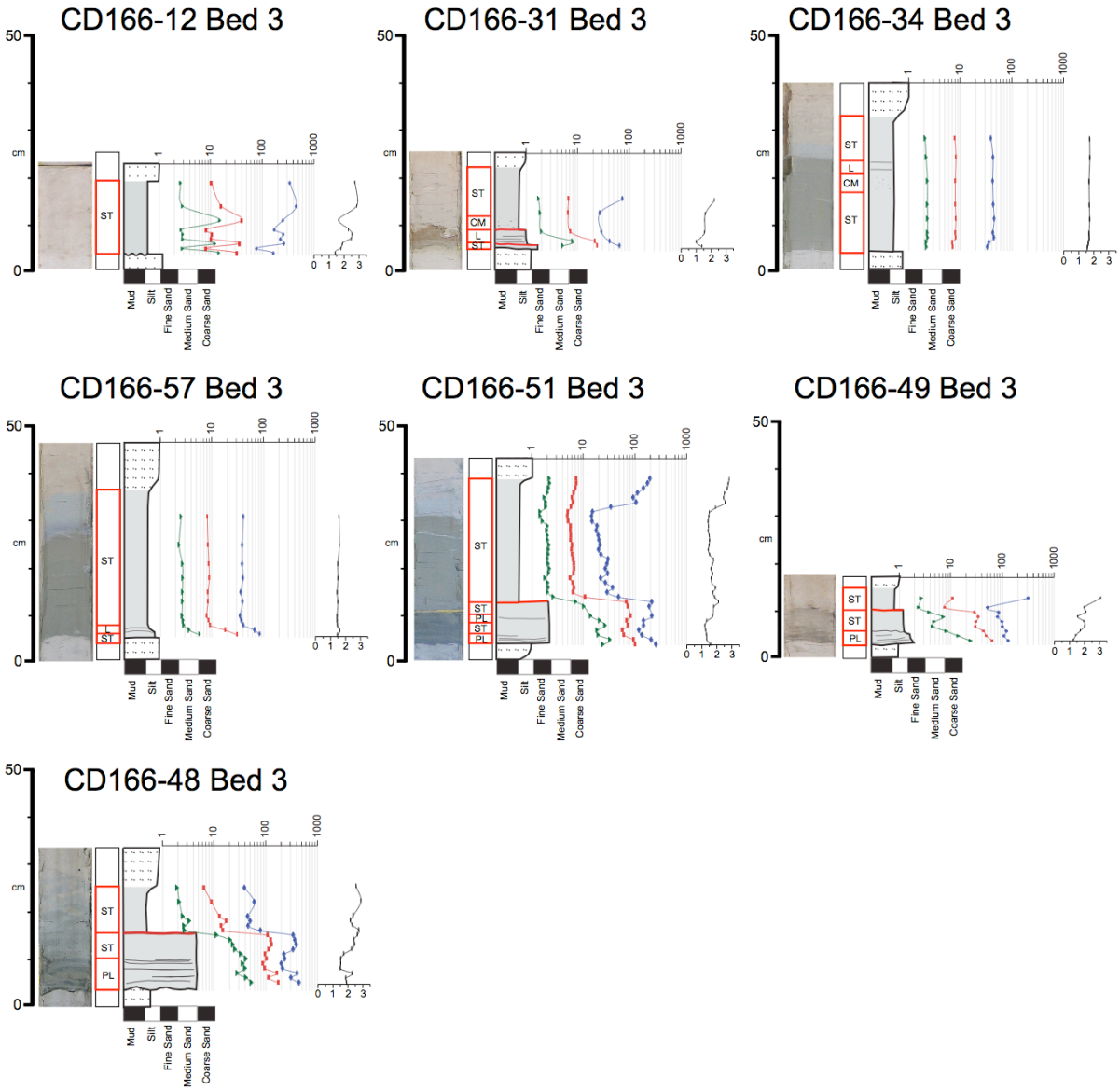

10.1.2 Bed 5

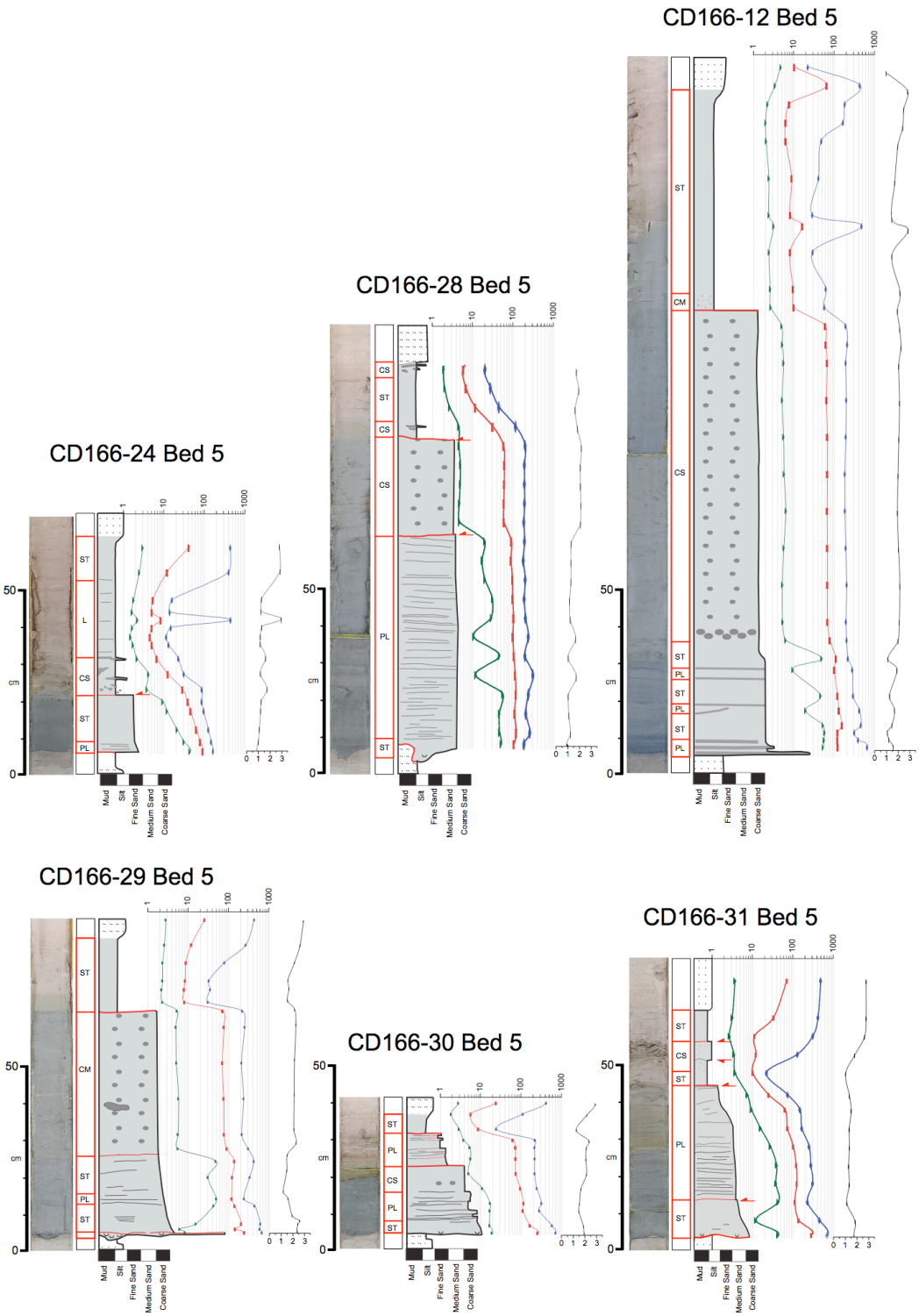
CD166-12 Bed 5
CD166-28 Bed 5
CD166-24 Bed 5
CD166-29 Bed 5
CD166-31 Bed 5
CD166-30 Bed 5
cm
Mud
Silt
Fine Sand
Medium Sand
Coarse Sand

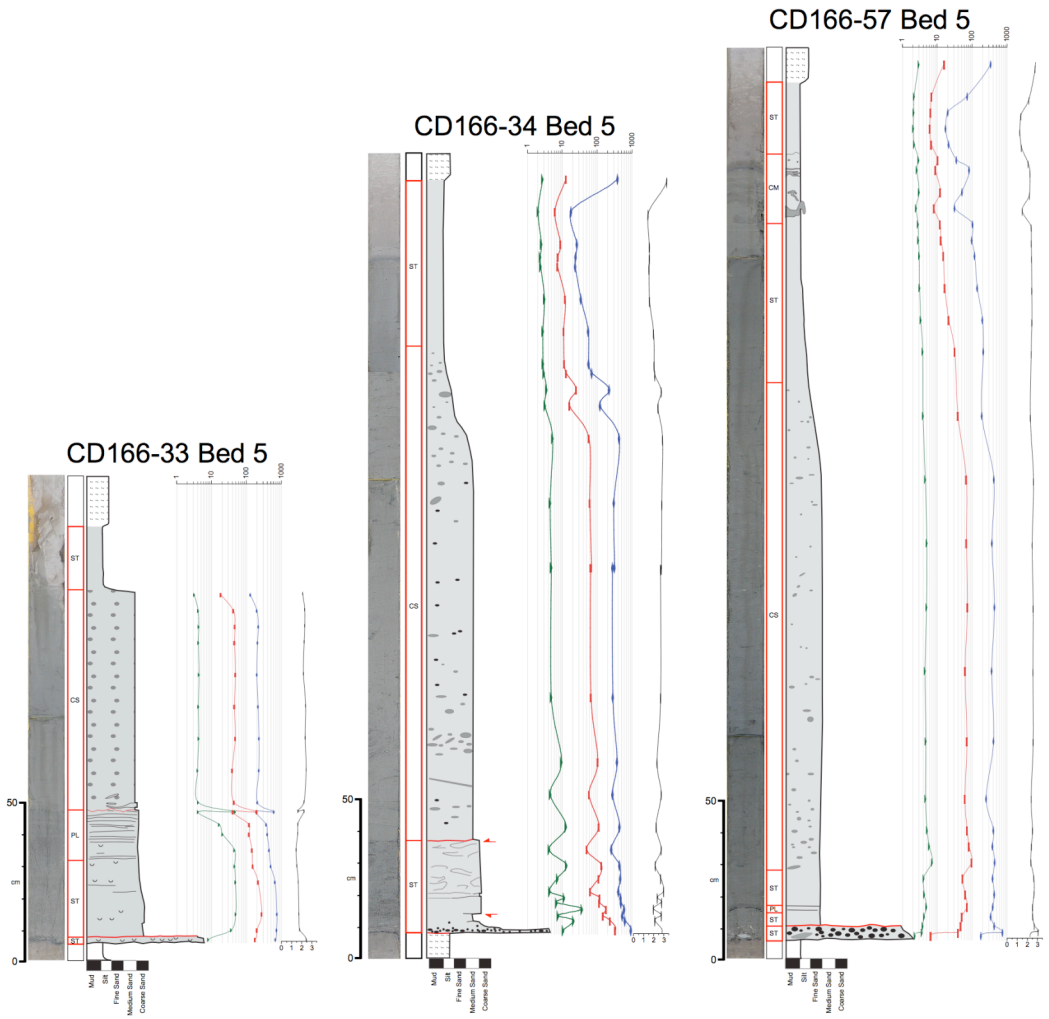
CD166-57 Bed 5
CD166-34 Bed 5
CD166-33 Bed 5
CD166-50 Bed 5
CD166-51 Bed 5
CD166-48 Bed 5

10.1.3 Bed 7

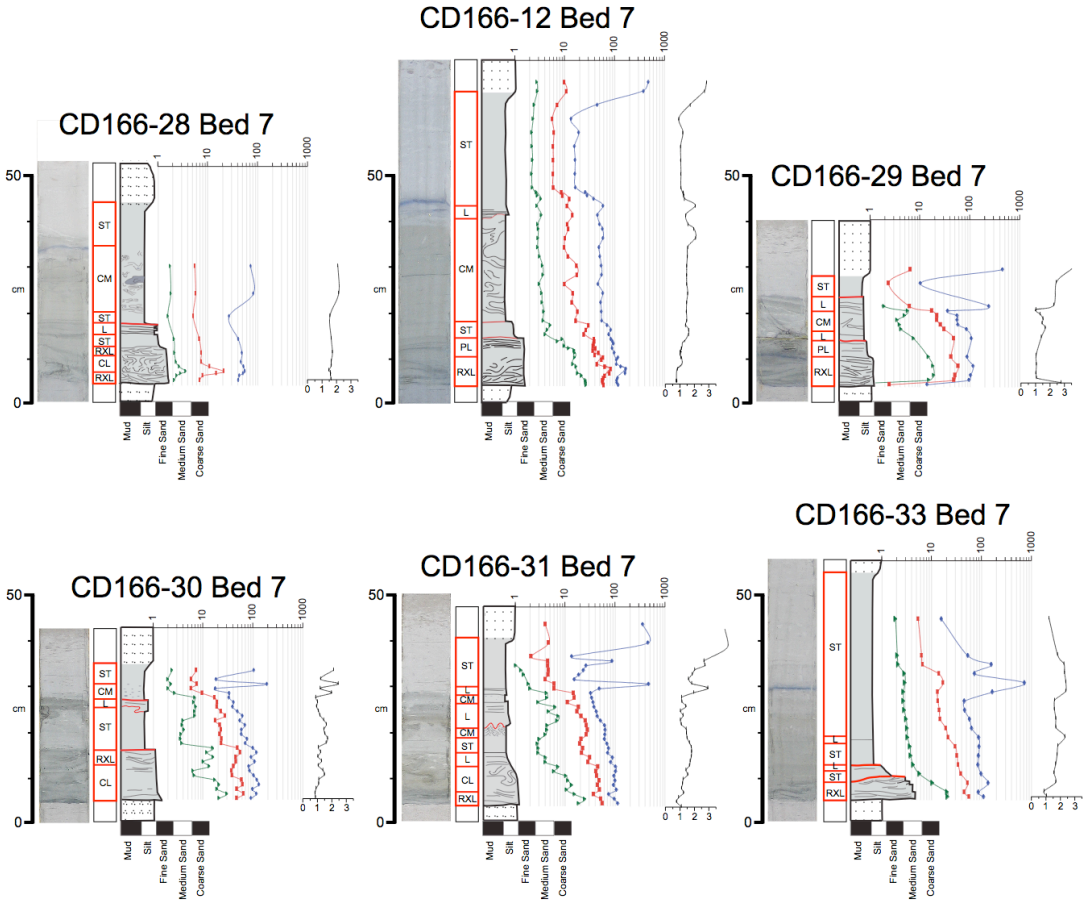
CD166-28 Bed 7
CD166-12 Bed 7
CD166-29 Bed 7
CD166-30 Bed 7
CD166-31 Bed 7
CD166-33 Bed 7
cm
50
0
Mud
Silt
Fine Sand
Medium Sand
Coarse Sand

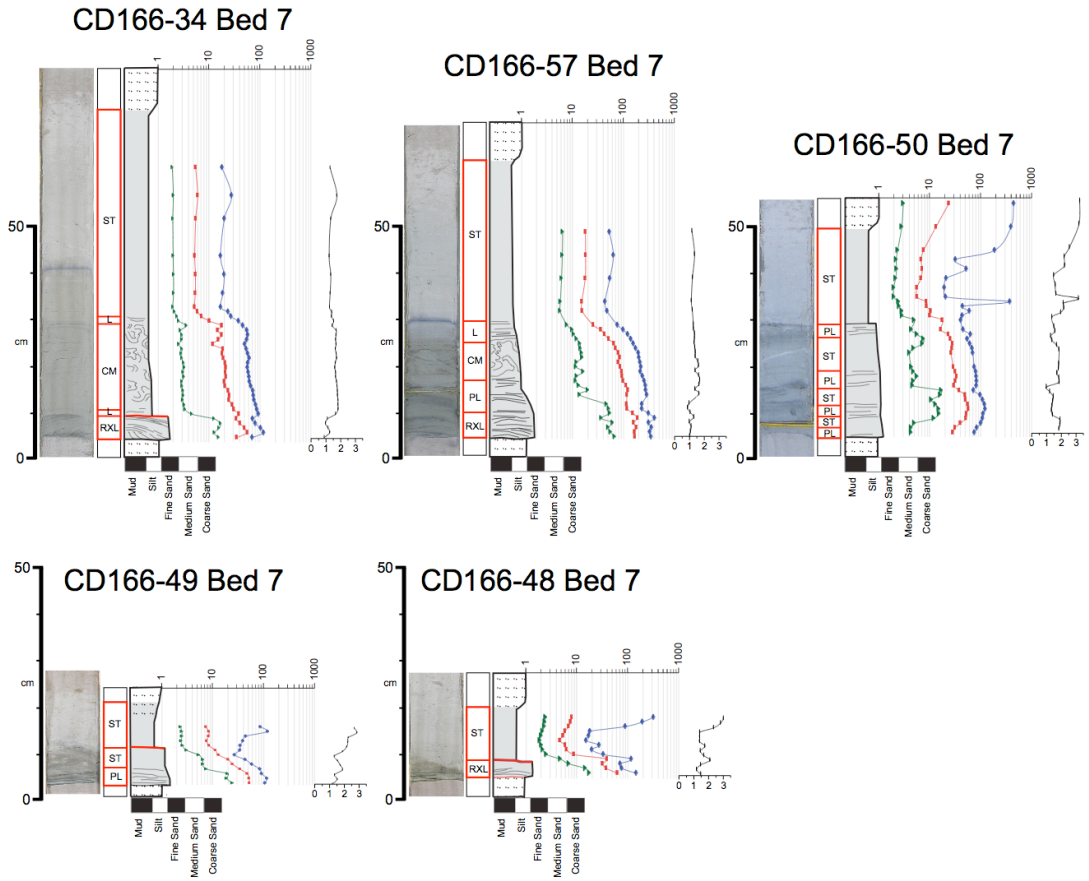
CD166-34 Bed 7
CD166-57 Bed 7
CD166-50 Bed 7
CD166-49 Bed 7
CD166-48 Bed 7
50
cm
0
ST
L
CM
PL
RXL
1
10
100
1000
0 1 2 3
Mud
Silt
Fine Sand
Medium Sand
Coarse Sand

10.1.4 Bed 11

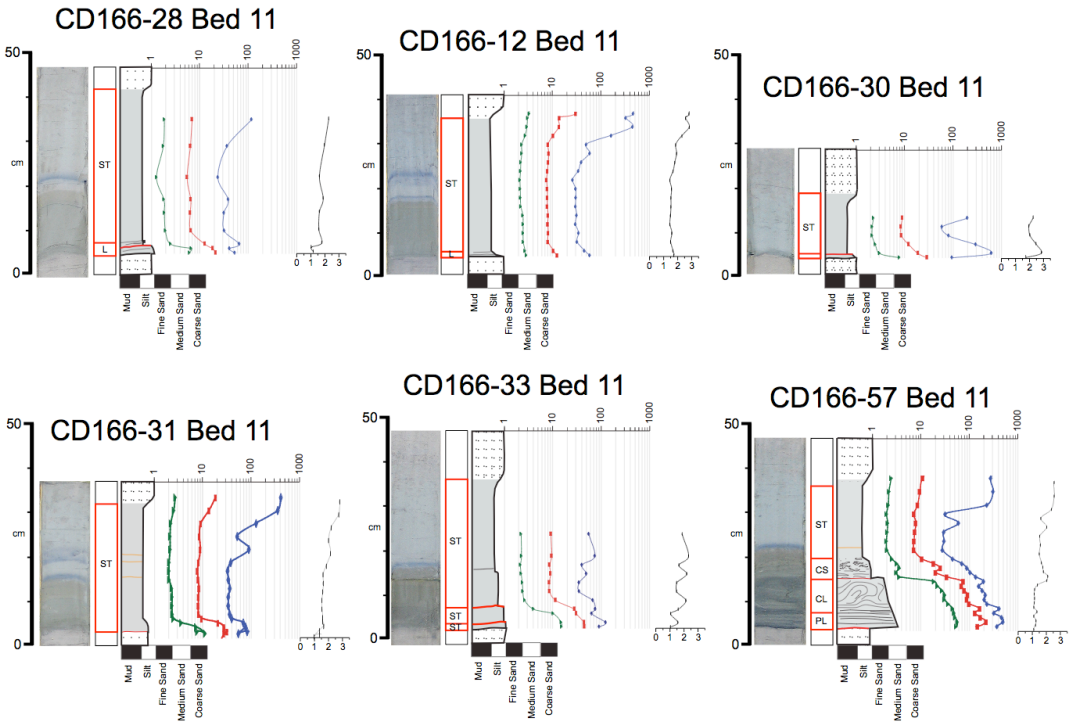
CD166-28 Bed 11
CD166-12 Bed 11
CD166-30 Bed 11
CD166-31 Bed 11
CD166-33 Bed 11
CD166-57 Bed 11
cm
ST
CS
CL
PL
Mud
Silt
Fine Sand
Medium Sand
Coarse Sand

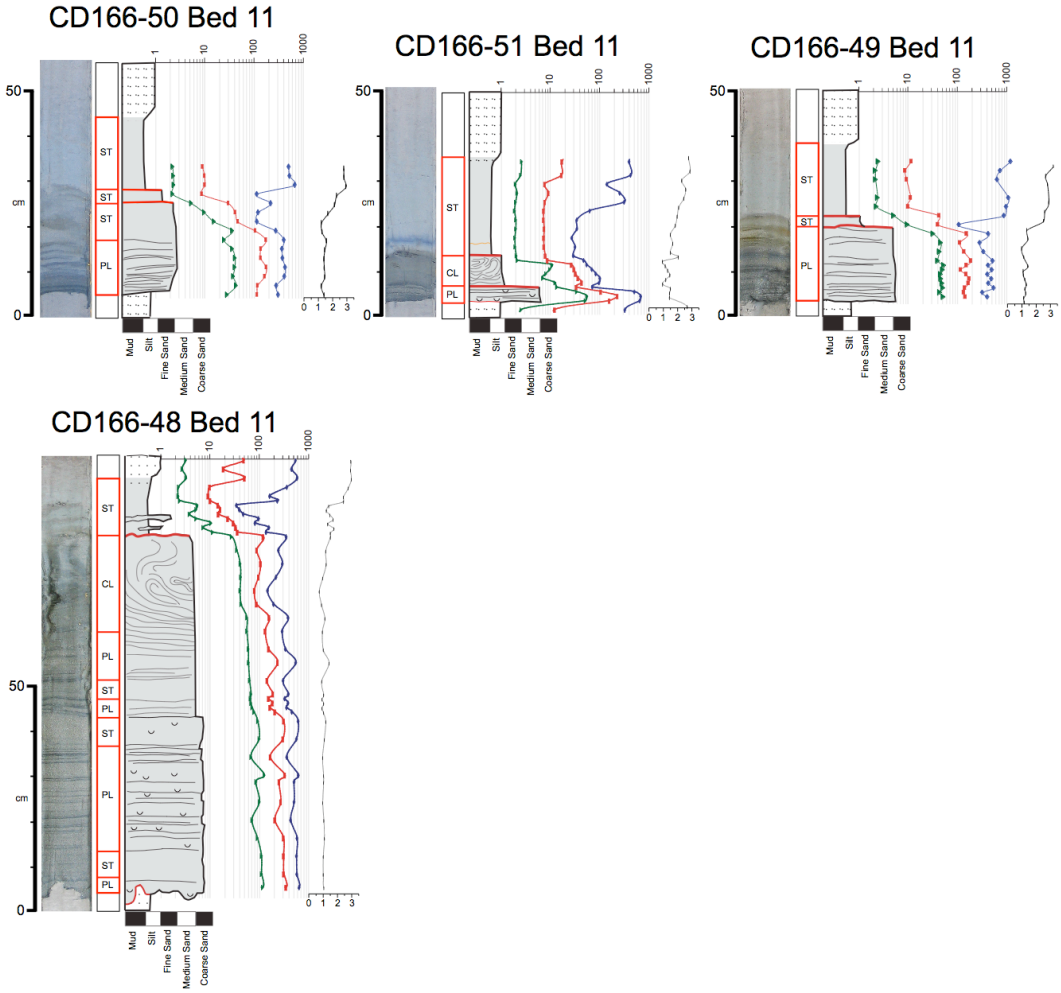
CD166-50 Bed 11
CD166-51 Bed 11
CD166-49 Bed 11
CD166-48 Bed 11
50
0
cm
ST
CL
PL
1
10
100
1000
0 1 2 3
Mud
Silt
Fine Sand
Medium Sand
Coarse Sand

10.1.5 Bed 12

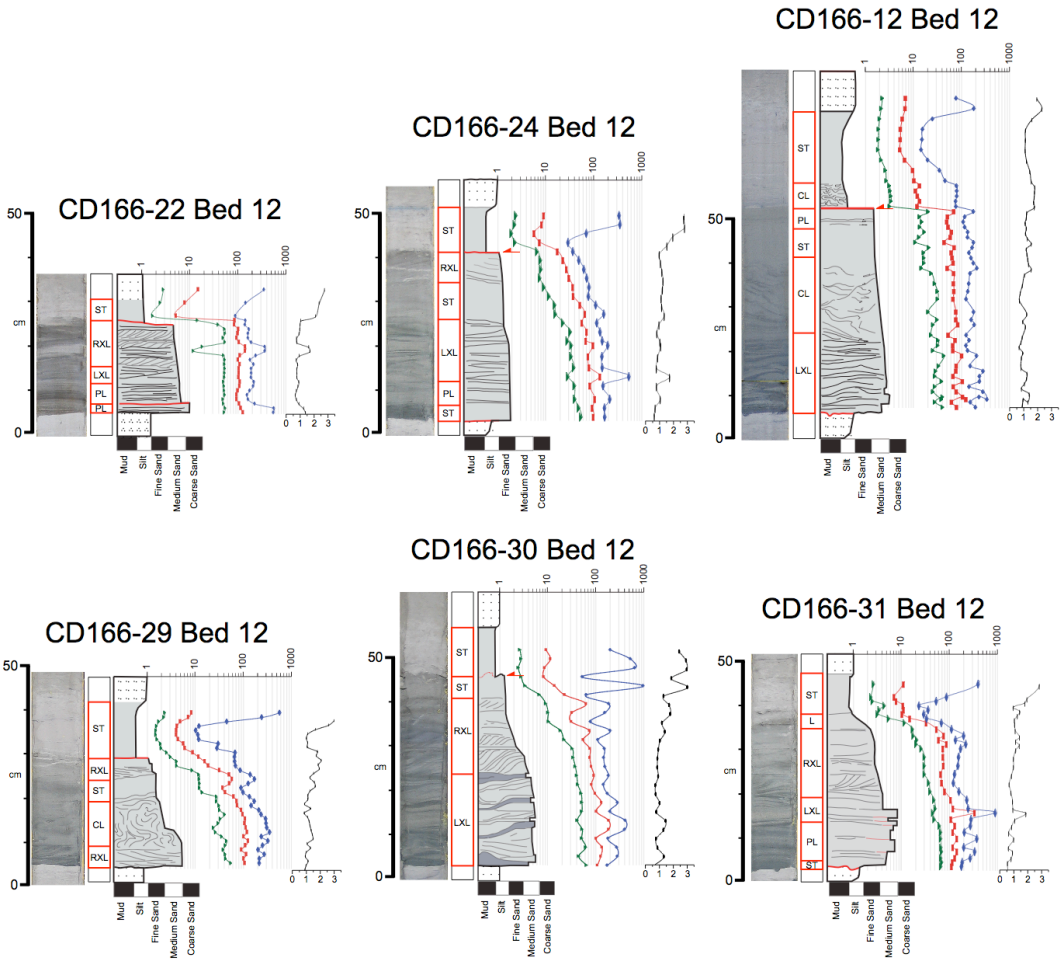
CD166-22 Bed 12
CD166-24 Bed 12
CD166-12 Bed 12
CD166-29 Bed 12
CD166-30 Bed 12
CD166-31 Bed 12
cm
Mud
Silt
Fine Sand
Medium Sand
Coarse Sand

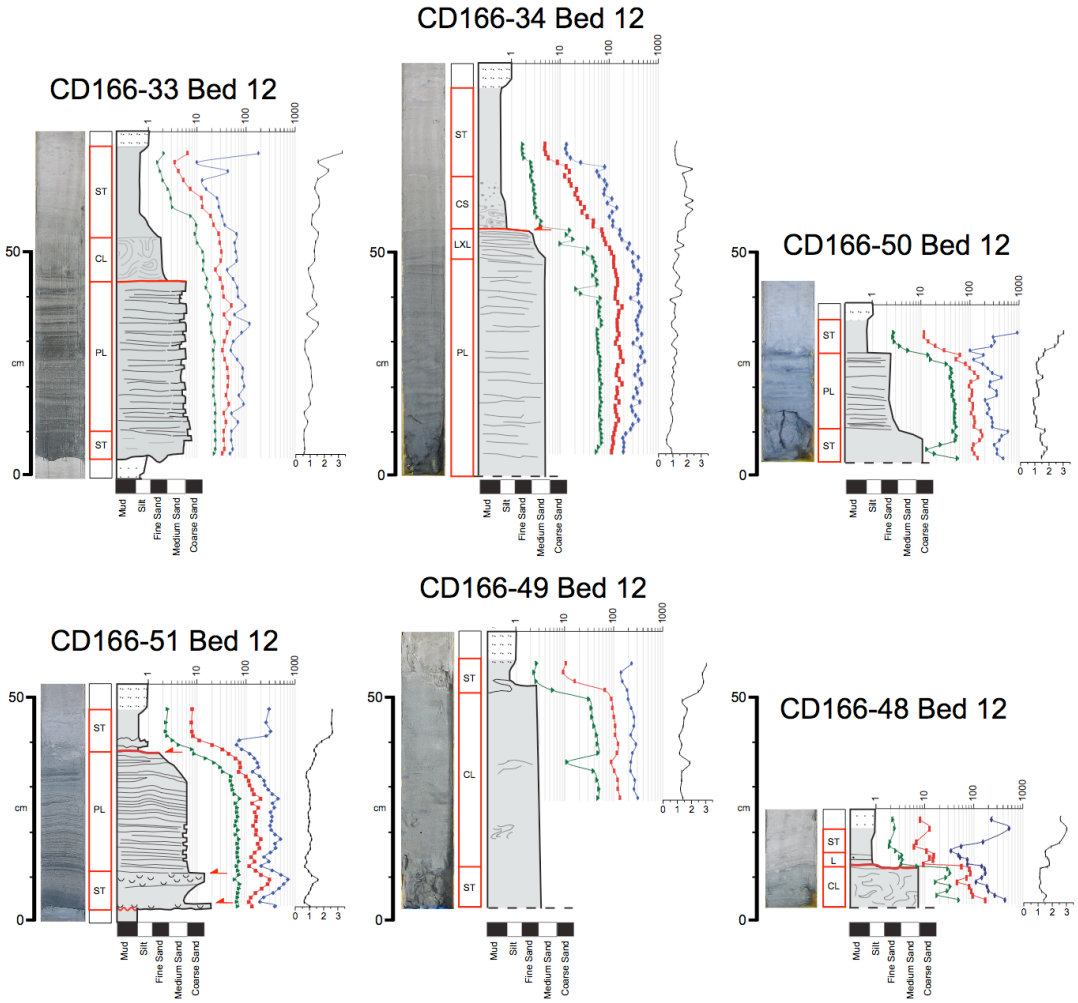
CD166-33 Bed 12
CD166-34 Bed 12
CD166-50 Bed 12
CD166-51 Bed 12
CD166-49 Bed 12
CD166-48 Bed 12
cm
Mud
Silt
Fine Sand
Medium Sand
Coarse Sand

10.2 Multi-sensor core log data

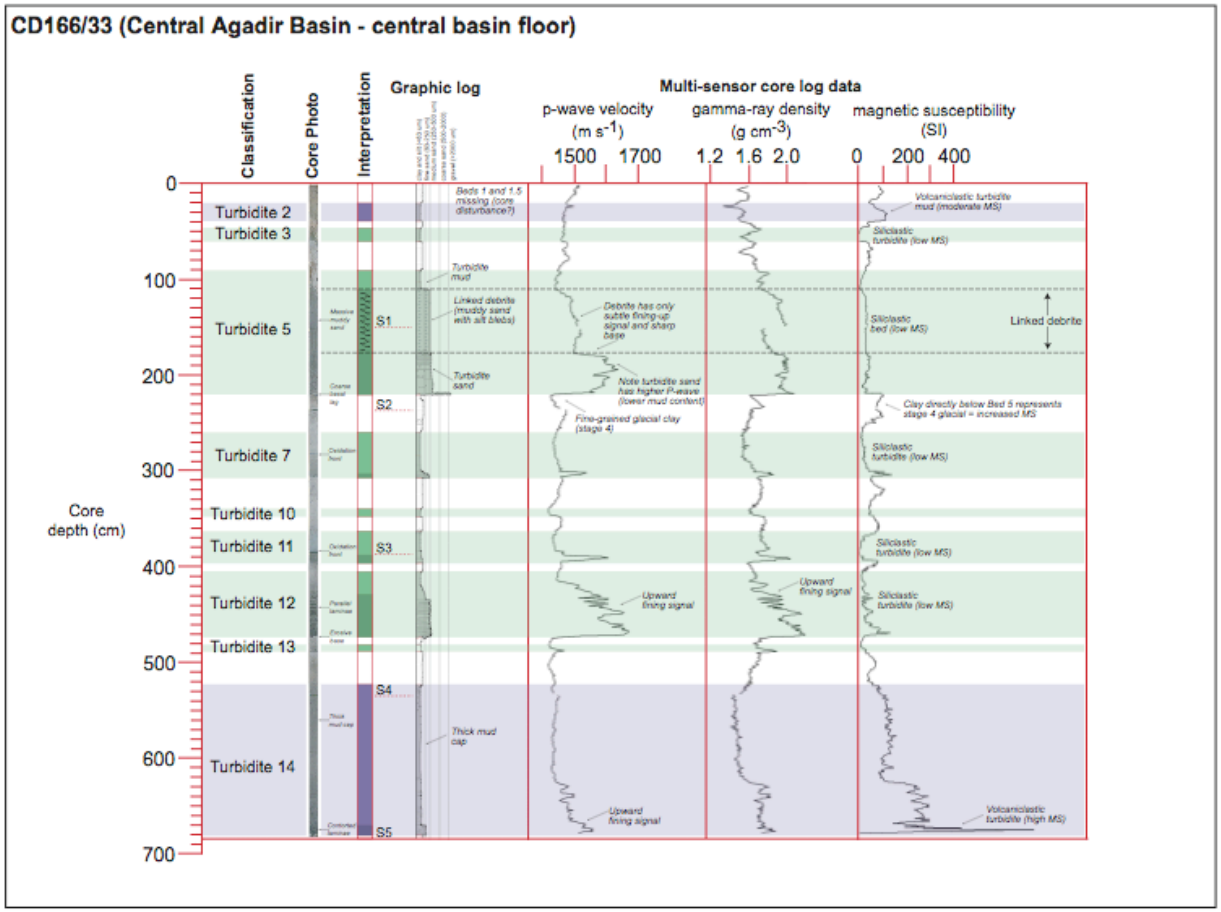

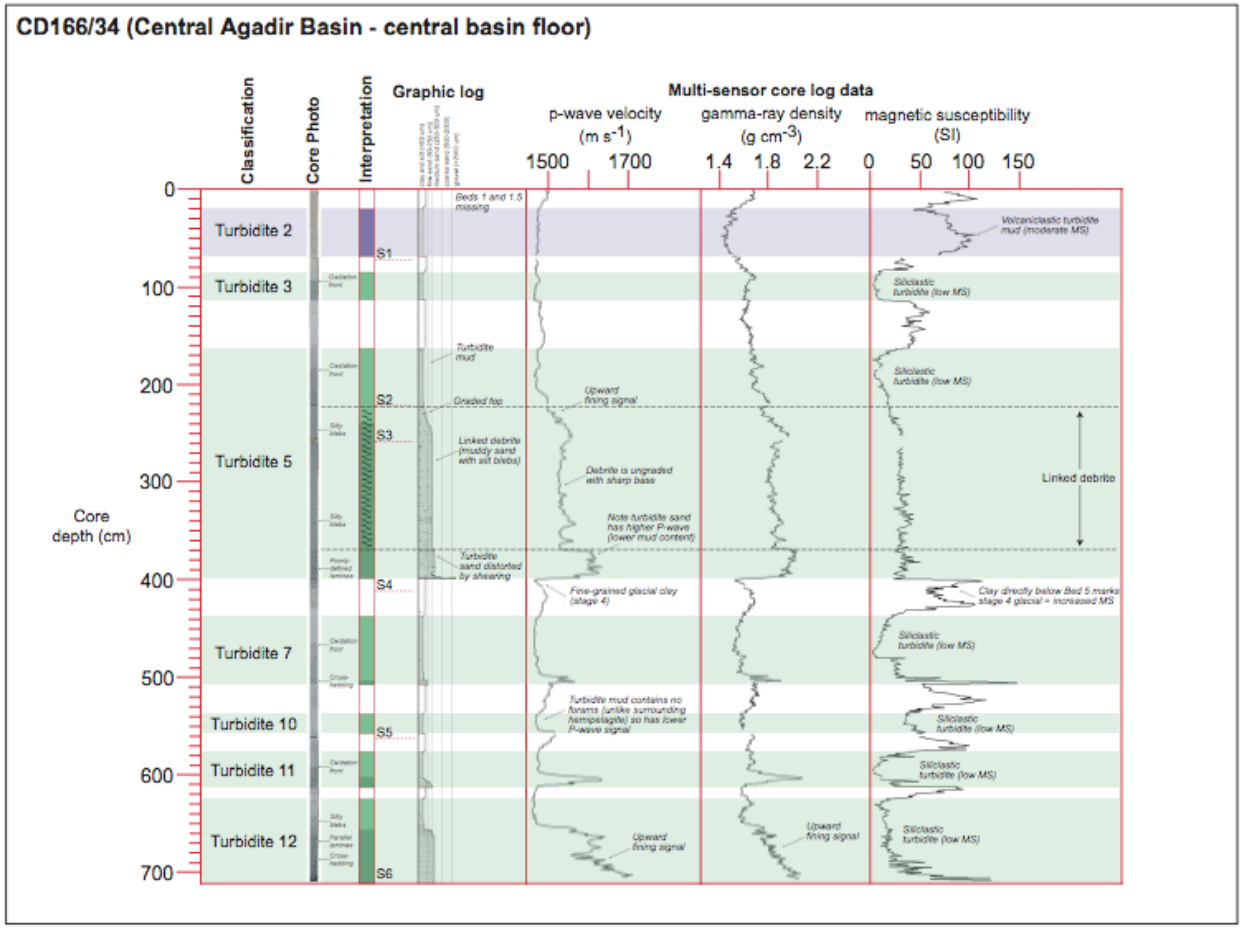
CD166/34 (Central Agadir Basin - central basin floor)
Classification
Core Photo
Interpretation
Graphic log
Multi-sensor core log data
p-wave velocity (m s-1)
gamma-ray density (g cm-3)
magnetic susceptibility (SI)
1500
1700
1.4
1.8
2.2
0
50
100
150
Core depth (cm)
0
100
200
300
400
500
600
700
Turbidite 2
Turbidite 3
Turbidite 5
Turbidite 7
Turbidite 10
Turbidite 11
Turbidite 12
S1
S2
S3
S4
S5
S6
Beds 1 and 1.5 missing
Turbidite mud
Graded top
Linked debrite (muddy sand with silt blebs)
Turbidite sand distorted by sheaning
Upward fining signal
Debrite is ungraded with sharp base
Note turbidite sand has higher P-wave (lower mud content)
Fine-grained glacial clay (stage 4)
Turbidite mud contains no foram (unlike surrounding hemipelagite) so has lower P-wave signal
Upward fining signal
Volcaniclastic turbidite mud (moderate MS)
Siliciastic turbidite (low MS)
Siliciastic turbidite (low MS)
Linked debrite
Clay directly below Bed 5 marks stage 4 glacial = increased MS
Siliciastic turbidite (low MS)
Siliciastic turbidite (low MS)
Siliciastic turbidite (low MS)
Siliciastic turbidite (low MS)

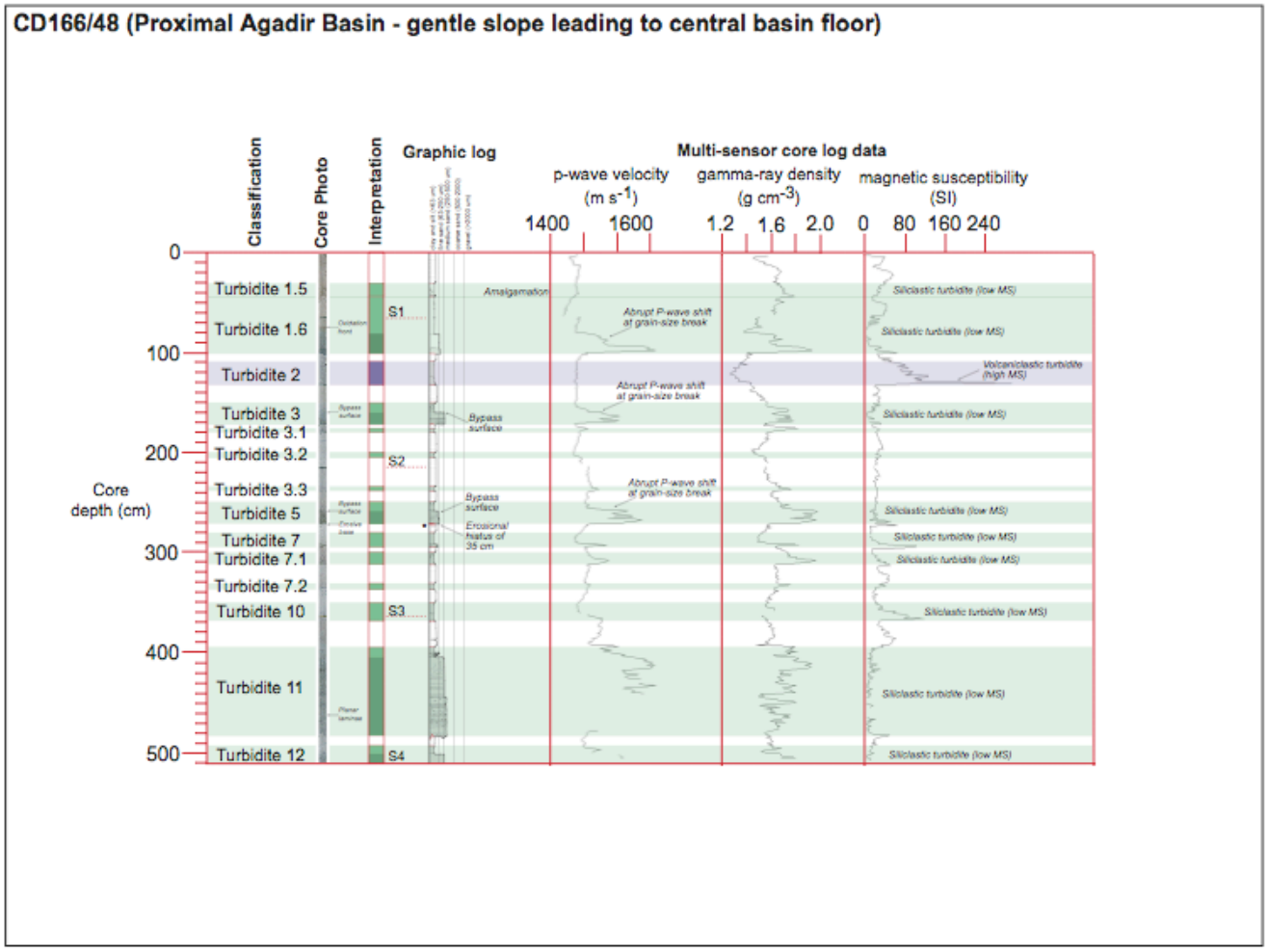
CD166/48 (Proximal Agadir Basin - gentle slope leading to central basin floor)
Classification
Core Photo
Interpretation
Graphic log
Multi-sensor core log data
p-wave velocity (m s-1)
gamma-ray density (g cm-3)
magnetic susceptibility (SI)
1400
1600
1.2
1.6
2.0
0
80
160
240
Core depth (cm)
0
100
200
300
400
500
Turbidite 1.5
Turbidite 1.6
Turbidite 2
Turbidite 3
Turbidite 3.1
Turbidite 3.2
Turbidite 3.3
Turbidite 5
Turbidite 7
Turbidite 7.1
Turbidite 7.2
Turbidite 10
Turbidite 11
Turbidite 12
S1
S2
S3
S4
Amalgamation
Abrupt P-wave shift at grain-size break
Bypass surface
Erosional hiatus of 35 cm
Siliclastic turbidite (low MS)
Volcaniclastic turbidite (high MS)